

**BEHAVIOUR OF FIBRE REINFORCED POLYMER
COMPOSITE PILES: EXPERIMENTAL AND
NUMERICAL STUDY**

A thesis submitted to The University of Manchester for the Degree of
Doctor Philosophy
in the Faculty of Engineering and Physical Sciences

2013

Hussein A. Shaia

School of Mechanical, Aerospace and Civil Engineering

TABLE OF CONTENTS

TABLE OF CONTENTS.....1

LIST OF FIGURES8

LIST OF TABLES14

LIST OF ABBREVIATIONS15

NOMENCLATURE16

ABSTRACT17

DECLARATION.....19

COPYRIGHT STATEMENT20

ACKNOWLEDGEMENTS.....21

PUBLICATIONS22

1. CHAPTER ONE: INTRODUCTION23

 1.1 Introduction23

 1.2 Statement of the Problem23

 1.3 Objectives and Scope25

 1.4 Thesis Organization26

2 CHAPTER TWO: BACKGROUND AND LITERATURE REVIEW28

 2.1 Introduction28

 2.2 FRP Composite Structure.....29

 2.3 FRP Composite Laminates.....30

 2.4 Types of Fibre Reinforcements.....32

 2.4.1 Carbon Fibre Reinforced Polymer (CFRP)..... 32

 2.4.2 Glass Fibre Reinforced Polymer (GFRP) 32

 2.4.3 Aramid Fibre Reinforced Polymer (AFRP) 33

 2.5 Resins33

 2.5.1 Epoxy Resin 34

 2.5.2 Polyester Resin 34

 2.5.3 Vinly Ester Resin..... 34

 2.6 FRP/Matrix Mechanism34

2.7	FRP Composite Applications	35
2.7.1	FRP in Aerospace Engineering	36
2.7.2	FRP in Civil Engineering	38
2.8	Advantages of FRP	40
2.8.1	High Specific Strength and Stiffness	40
2.8.2	Corrosion and Degradation Resistance	42
2.8.3	Quick and Easy Transport	43
2.8.4	Aesthetics and Dimensional Stability	44
2.8.5	Electromagnetic Transparency	44
2.9	Disadvantages of FRP Material	45
2.9.1	Higher Costs	45
2.9.2	Lack of Durability	46
2.9.3	Low Fire Resistance	46
2.9.4	Lack of Design Standards	46
2.10	Traditional and FRP Piling Foundations	47
2.10.1	Timber piles	47
2.10.2	Concrete Piles	48
2.10.3	Steel piles	49
2.10.4	FRP Composite Piles	49
2.10.4.1	Steel Core Piles	51
2.10.4.2	Reinforced Plastic Piles (RPP)	51
2.10.4.3	FRP-Confined Concrete Piles	51
2.10.4.4	Fibreglass Pultruded Piles	52
2.10.4.5	Plastic Lumber Piles	52
2.11	Rules of FRP Composites	53
2.12	Stress-Strain Relation for Orthotropic Materials	55
2.13	Structural Behaviour of FRP Piles	58
2.13.1	Behaviour under Axial Load	58
2.13.2	Mechanics of FRP Confinement	60
2.13.3	Behaviour under Flexural Load	64
2.14	Geotechnical Behaviour of FRP Piles	67
2.14.1	FRP Pile Response to Axial Loads	67
2.14.2	FRP Pile Response to Lateral Loads	69
2.15	FRP Surface Characterization	73
2.15.1	Description of FRP Surface Roughness	73

2.15.2	Surface Roughness Parameters.....	75
2.15.3	Profile Roughness Device	77
2.15.4	Hardness Tests	78
2.16	FRP/Soil Interface Mechanism	79
2.17	Interface Test Apparatus	81
2.18	Soil Particle Shape	87
2.19	Mean Grain Size (D_{50})	89
2.20	Soil Density.....	90
2.21	Long-Term Study.....	91
2.22	Numerical Studies.....	92
2.23	Summary.....	93

3 CHAPTER THREE: STRUCTURE BEHAVIOUR OF FRP TUBES

3	CHAPTER THREE: STRUCTURE BEHAVIOUR OF FRP TUBES	
	CONFINED CONCRETE.....	95
3.1	Introduction.....	95
3.2	Experimental Program	96
3.2.1	Tested Materials	96
3.2.1.1	FRP Tubes	96
3.2.1.2	FRP Hoop Testing.....	97
3.2.2	Concrete Mixtures	103
3.2.2.1	Preparation of Specimens.....	104
3.2.2.2	Instrumentation	105
3.2.2.3	Testing of Control Specimens	106
3.2.3	Experimental Results and Discussion	106
3.2.4	Behaviour of FRP-Tube Confined Concrete Specimens.....	110
3.2.4.1	Failure Mode.....	110
3.2.4.2	Compressive Strength	111
3.2.4.3	Stress-Strain Response	114
3.2.5	Confinement Modelling.....	116
3.2.5.1	Ultimate Compressive Strength	116
3.2.5.2	Ultimate Compressive Strain	117
3.3	Results in Relation to Previous Tests.....	118
3.4	FRP-confined Concrete Strength Enhancement.....	122
3.5	Flexural Behaviour.....	127
3.5.1	Control Specimen Behaviour.....	127

3.5.2	Long-Term Specimen Behaviour.....	131
3.6	Summary	136
4	CHAPTER FOUR: INTTERFACE CHARACTERISTICS OF FRP/SAND	
	137	
4.1	Introduction	137
4.2	Tested materials	138
4.2.1	Granular Materials.....	138
4.2.2	Direct Shear Tests.....	143
4.3	Counterface Materials	154
4.3.1	FRP Materials.....	154
4.3.2	Mild Steel	154
4.4	Measurement of Surface Roughness.....	154
4.5	Hardness Tests	155
4.6	Interface Shear Tests	157
4.6.1	Specimen preparation	157
4.6.2	Testing Procedure	158
4.6.3	Interface Shear Tests	159
4.6.4	Discussion of Results.....	166
4.6.4.1	Mean particle size (D_{50})	166
4.6.4.2	Surface Roughness (R_t).....	168
4.6.4.3	Sand relative density	171
4.7	Effect of Driving Process on the FRP surface	172
4.7.1	Shear Induced Surface Roughness Changes	173
4.7.2	Evolution of the Interface Shear Coefficient.....	175
4.8	Summary	181
5	CHAPTER FIVE: LONG-TERM INTERFACE BETWEEN FRP/SAND	
	183	
5.1	Introduction	183
5.2	Tested Materials	184
5.3	Test Procedures	184
5.4	Long-Term Interface Shear Tests (LTIST)	187
5.5	Behaviour of GFRP and CFRP in LTIST	187
5.6	Discussion of Results	190

5.6.1	Aging Effects on R_t and HV	190
5.6.2	Aging Effects on FRP-granular Interface Shear Coefficient	192
5.7	Summary	197
6	CHAPTER SIX: EFFECT OF SURFACE ROUGHNESS AND HARDNESS ON THE INTERFACE SHEAR STRENGTH	198
6.1	Introduction	198
6.2	Constitutive interface shear surface (CISS)	198
6.2.1	Experimental Results	199
6.2.2	Test Results and Discussion	201
6.2.3	Conceptual explanation of the proposed CISS	205
6.2.4	Qualitative Interpretation for the different Results in the Literature	207
6.3	Summary	210
7	CHAPTER SEVEN: FRP PILEING BEHAVIOUR UNDER LOADING 211	
7.1	Introduction	211
7.1.1	Test Setup	212
7.1.2	Pressure Chamber	214
7.1.3	Tested Materials	215
7.1.4	FRP pile/sand Preparation	219
7.1.5	Loading System	219
7.2	Experimental program.....	223
7.3	Discussion of Results	226
7.3.1	Axial Load Results	226
7.3.1.1	Influence of Pile Surface Roughness.....	226
7.3.1.2	Rate of Axial Loading	230
7.3.1.3	Vertical Pressure	231
7.3.1.4	Relative Density of Sand.....	232
7.3.2	Lateral Load Results	233
7.3.2.1	Influence of FRP Pile Type.....	234
7.3.2.2	Influence of FRP Pile Diameter	235
7.3.3	Influence of Ageing Environment	236
7.3.4	Model Scale Size	240
7.3.5	Slenderness Ratio	240
7.4	Summary	241

8	CHAPTER EIGHT: NUMERICAL SIMULATION OF FRP PILE/SAND	242
8.1	Introduction	242
8.2	Pile/Soil Analysis Using FEM	242
8.3	FE Commercial Code ABAQUS	243
8.4	Constitutive Model of Materials:	244
8.5	FEM Model	245
8.6	Model Characteristics.....	246
8.7	Validation of Axial Load Results.....	249
8.8	Influence of Important Parameters on FRP Pile Response Subjected to Axial Load.....	251
8.8.1	Effect of FRP Tube Configuration.....	251
8.8.2	Effect of Vertical Pressure	253
8.8.3	Effect of Sand Dilatation Angle	254
8.9	Lateral Load Modelling.....	255
8.10	Validation of Lateral Load Results	256
8.11	Influence of Important Parameters on FRP Pile Response Subjected to Lateral Load	258
8.11.1	Effect of FRP Pile/Soil Interface	258
8.11.2	Influence of Vertical Pressure	259
8.11.3	Influence of Young's Modulus of the Sand	260
8.12	Influence of FRP tube configuration.....	261
8.13	Comparison between FRP and Traditional Piles	264
8.14	Summary	265
9	CHAPTER NINE: SUMMARY AND CONCLUSIONS	266
9.1	Introduction	266
9.2	Activities Summary and Conclusions	269
9.2.1	Literature Review	269
9.2.2	Structural Behaviour of FRP-Tubes Confined Concrete Study	269
9.2.3	Interface Characteristics of FRP/granular Materials Study	270
9.2.4	Long-Term Interface between FRP/granular Materials Study	270
9.2.5	Effect of Surface Roughness and Hardness on the Interface Shear Strength	271
9.2.6	Performance of FRP Piles under Different Loading	271

9.2.7 Simulation FRP Piles Using ABAQUS Package 272

9.3 Conclusions and Final Remarks.....273

9.4 Recommendations for Future Works275

9.4.1 Experimental Study 275

9.4.2 Numerical Study 275

REFERENCES277

APPENDIX290

LIST OF FIGURES

Figure 1.1: Degradation of conventional piles	24
Figure 2.1: Phases of FRP Composite Materials (Daniel and Ishai, 1994).....	30
Figure 2.2: Lamina and principal coordinate axes	31
Figure 2.3: Load transfer between fibre and resin	35
Figure 2.4: Boeing 777 commercial aircraft	37
Figure 2.5: Different configuration of FRP tube confined with concrete (Fam and Rizkalla, 2002).....	38
Figure 2.6: Different structural applications of concrete filled FRP tubes	39
Figure 2.7: Second-level bridge in Moscow (http://www.apatech.ru/).....	41
Figure 2.8: FRP deck systems (http://www.compositesworld.com/).....	41
Figure 2.9: Comparison of the performance of FRP composite channel (left) and reinforced concrete channel (right) (Bernard Potyrala, 2011)	42
Figure 2.10: FRP composite pedestrian walkway in Russia	43
Figure 2.11: General view of the Lleida footbridge (Spain) (Bernard Potyrala, 2011)	45
Figure 2.12: Common piles shapes	47
Figure 2.13: Common types of composite piles (Iskander and Hassan, 1998).....	50
Figure 2.14: Deformation of a composite element under axial tensile stress	53
Figure 2.15: Simplified stress-strain curves of FRP tube confined concrete (Saafi et al., 1999).....	59
Figure 2.16: Confining action of fibre-reinforced polymer	60
Figure 2.17: Tests set up for bending tests on FR pile (Fam and Rizkalla, 2003).....	65
Figure 2.18: Test setup (Mohamed and Masmoudi, 2012)	66
Figure 2.19: Test pile instrumentation (Fam et al., 2003).....	68
Figure 2.20: Pile displacement-axial static load (Fam et al., 2003).....	69
Figure 2.21: Definition of (a) short and (b) long piles in terms of lateral loading.....	70
Figure 2.22: FRP composite and prestressed piles (Fam et al., 2003).....	72
Figure 2.23: Lateral load-displacement response of pile (Fam et al., 2003).....	72
Figure 2.24: Terminology used to describe topography used by (Dove et al., 1996)	74
Figure 2.25: Surface roughness parameters	75

Figure 2.26: Definition of R_t and R_n (Kishida and Uesugi, 1987)	76
Figure 2.27: Schematic Diagram of Stylus Instrument	77
Figure 2.28: Schematic Diagram of Stylus instrument used in present study	78
Figure 2.29: Examples of Geotechnical Interfaces	80
Figure 2.30: Typical plot of shear stress-displacement.....	82
Figure 2.31: Simple shear apparatus used by (Kishida and Uesugi, 1987).....	86
Figure 2.32: Strength Envelopes from interface shear tests on peak interface shear response between particulate materials and smooth geomembranes (Dove and Frost, 1999)	88
Figure 2.33: Influence of (D_{50}) on μ_p (Frost and Han, 1999).....	89
Figure 2.34: Relationship between interface friction angle and relative density (Frost and Han, 1999).....	90
Figure 3.1: Details of tube specimen and strain gauges locations	97
Figure 3.2: Split-ring fixture	99
Figure 3.3: Hoop tensile test	100
Figure 3.4: Load-displacement and stress-strain relationships for spilt-disk test	101
Figure 3.5: FRP failure modes	102
Figure 3.6: FRP's tubes confined concrete and control specimens	104
Figure 3.7: Layout of instrumentation of FRP tubes confined concrete and unconfined cylinders	105
Figure 3.8: FRP-Tube Confined Concrete testing set-up.....	107
Figure 3.9: Failure mode of FRP-tube confined concrete.....	110
Figure 3.10: Effect of batch strength on FRP-tube confined concrete.....	112
Figure 3.11: Relationship between strength gain and confinement ratio.....	113
Figure 3.12: Stress-strain behaviour of FRP specimens.	115
Figure 3.13: Relationship between strength gain and confinement ratio.....	117
Figure 3.14: Relationship between strain gain and confinement ratio.....	118
Figure 3.15: Comparison between the experimental model and nine previous models	121
Figure 3.16: Comparison between the experimental results with the nearest two models	121
Figure 3.17: Comparison of f_c' predictions by various models	122
Figure 3.18: FRP confined concrete strength based on f_c range	123

Figure 3.19: Effect of unconfined concrete strength on FRP strength enhancement	124
Figure 3.20: Representation of the entire data base in the form of contours	125
Figure 3.21: Contour lines of the data base after curve fitting.....	126
Figure 3.22: Schematic of test setup for FRP piles.....	127
Figure 3.23: CFRP and GFRP confined mortar tubes under loading system	128
Figure 3.24: Load-deflection behaviour of CFRP and GFRP piles	130
Figure 3.25: Load-axial strain behaviour of CFRP and GFRP piles.....	130
Figure 3.26: Oven used for acceleration process	131
Figure 3.27: Load-deflection behaviour of GFRP piles at long-term	134
Figure 3.28: Long-term effect on flexural behaviour at different pH level	135
Figure 3.29: GFRP rod section immersed on alkaline solution at different time (Katsuki, 1995).....	135
Figure 4.1: Pile's side friction (skin friction) and end bearing	137
Figure 4.2: Microscopic photos showing the tested sands.....	139
Figure 4.3: Microscopic photos showing the glass beads sands	140
Figure 4.4: Grain size curves of tested sands and glass beads	141
Figure 4.5: Schematic view of the: a) Sand Raining Frame. b) Sand preparation...	144
Figure 4.6: Density Index of viruses drop height.....	145
Figure 4.7: Direct shear test results for Leighton Sand A (Average Id = 87 %).....	146
Figure 4.8: Direct shear test results for Leighton Sand B (Average Id = 90 %).....	147
Figure 4.9: Direct shear test results for Mersey Sand (Average Id = 90 %)	148
Figure 4.10: Direct shear test results for Congleton sand (Average Id = 91 %).....	149
Figure 4.11: Direct shear test results for Glass Beads A (Average Id = 87 %)	150
Figure 4.12: Direct shear test results for Glass beads B (Average Id = 88 %)	151
Figure 4.13: Direct shear test results for Glass beads C (Average Id = 91 %)	152
Figure 4.14: Gage length ($L=D_{50}$).....	154
Figure 4.15: Surface roughness parameter R_t with gauge length $L=D_{50}$ for counterface material	155
Figure 4.16: Vicker hardness scheme	156
Figure 4.17: GFRP plate glued to the timber block	157
Figure 4.18: Details of modified Interface shear apparatus	158
Figure 4.19: Influenced of D_{50} coefficient interface friction at $\sigma_n=97.3$ kPa	167

Figure 4.20: Influence of R_t on coefficient interface friction at $\sigma_n=97.3$ kPa.....	169
Figure 4.21: Influenced of R_n on coefficient interface friction at $\sigma_n=97.3$ kPa	170
Figure 4.22: Relationship (I_d) and peak coefficient of interface friction	171
Figure 4.23: Evolution of normal and shear stress at a specific area element on the pile shaft during the driving process	172
Figure 4.24: Evolution of surface roughness as the normal stress increases	174
Figure 4.25: Evolution of the peak interface shear coefficient as the normal stress increases	176
Figure 4.26: Evolution of the peak interface shear coefficient under loading/unloading normal stress path.....	178
Figure 4.27: Interface shear induced striation.....	179
Figure 4.28: Schematic conceptual explanation for the effect of the different proposed mechanisms on the change of the interface shear coefficient as the normal stress increases	180
Figure 5.1: pH and temperature measurements.....	186
Figure 5.2: Variation in pH with time of the acidified and alkaline solution during acceleration period	186
Figure 5.3: Shear Stress–displacement curves at different pH values at various temperatures	189
Figure 5.4: Ageing induced changes in HV and R_t of FRP testing materials.....	190
Figure 5.5: The effect of ageing induced changes in HV and R_t of FRP testing materials on peak interface shear coefficient, (μ_p)	194
Figure 5.6: Effect of R_n and HV on μ_p	196
Figure 6.1: Schematic representation for the design methodology of the experimental program	199
Figure 6.2: Interface shear test results.....	202
Figure 6.3: Relation between HV and μ_p at $R_n=0.1$	203
Figure 6.4: Schematic idealization for the effect of R_n on HV- μ_p relation	204
Figure 6.5: Schematic representation of the proposed CISS in zones 1&2	204
Figure 6.6: Interpretation of HV- μ_p relation, at constant R_n , using the concept of the available and the mobilized ploughing resistances	206

Figure 6.7: Schematic explanation for the different test results in the literature using the proposed	209
Figure 6.8: Effect of R_n and HV on μ_p	210
Figure 7.1: Description of FRP-pile/soil chamber test.....	213
Figure 7.2: Top plates description.....	214
Figure 7.3: GFRP, CFRP and Mild steel Piles.....	216
Figure 7.4: Principle of sand raining device	217
Figure 7.5: Average sand relative density distribution along the depth of the sand sample	218
Figure 7.6: Sand and FRP preparation	219
Figure 7.7: Axial loading set-up.....	220
Figure 7.8: Lateral loading set-up	222
Figure 7.9: Surface roughness measurements	226
Figure 7.10: Influence of Surface roughness on FRP pile response	227
Figure 7.11: General pattern of test results	228
Figure 7.12: Pile surface and soil interface	229
Figure 7.13: Variations of pile load capacity against surface roughness	230
Figure 7.14: influence of loading rate on bearing capacity of the FRP Pile	231
Figure 7.15: Influence of vertical pressure on the bearing capacity of FRP pile.....	232
Figure 7.16: Influence of relative density on the bearing capacity of FRP pile.....	233
Figure 7.17: Influence of FRP Pile Configuration on the lateral capacity.....	234
Figure 7.18: Influence of FRP pile diameter on lateral load capacity	235
Figure 7.19: Lateral load behaviour for GFRP in long term at different condition.	238
Figure 7.20: Lateral load behaviour for CFRP in long term at different condition .	238
Figure 7.21: FRP piles after exposure to alkaline solutions.....	239
Figure 8.1: The interface friction surfaces	245
Figure 8.2: Three-dimensional FE mesh.....	246
Figure 8.3: Pile load versus settlement curves for testing piles	250
Figure 8.4: The FRP lube laminate structure.....	252
Figure 8.5: Effect of FRP material on axial load settlement response.....	253
Figure 8.6: Effect of sand pressure on FRP pile response	254
Figure 8.7: effect of sand dilation angle on the FRP pile response.....	255
Figure 8.8: Simulation of FRP pile/soil under lateral load	256

Figure 8.9: Comparison between experimental and FE results for both FRP piles .257

Figure 8.10: Contours showing the magnitude of both FRP piles and sand displacement.....257

Figure 8.11: Effect of FRP material on lateral load deflection response258

Figure 8.12: Effect of sand pressure on the lateral load deflection response.....259

Figure 8.13: The effect of Young's modulus on the FRP pile response under lateral load.....260

Figure 8.14: Different FRP tubes laminate configuration.....262

Figure 8.15: Effect of FRP tube laminate configuration.....263

Figure 8.16: Load deflection comparison between FRP and traditional piles264

LIST OF TABLES

Table 2.1: Comparison between FRP and steel (GangaRao and Vijay, 2010)	40
Table 2.2: Expression of different models of strength enhancement of FRP confined concrete	63
Table 2.3: Surface roughness parameters.....	76
Table 2.4: Advantages and disadvantages of interface testing apparatus	83
Table 3.1: Mechanical properties of FRP tubes	97
Table 3.2: Formulations for concretes and mortar batches	103
Table 3.3: Summary of test results.....	106
Table 3.4: Test Results FRP-confined concrete specimens	108
Table 4.1: Properties of the sands and glass beads used in this study	142
Table 4.2: Direct shear test results of sands and glass beads specimens	153
Table 4.3: Hardness Results	157
Table 4.4: Summary of interface shear test results on GFRP	160
Table 4.5: Summary of interface shear test results on CFRP	162
Table 4.6: Summary of interface shear test results on mild steel.....	164
Table 5.1: Interface shear for tested materials for GFRP at different aging conditions	188
Table 5.2: Interface shear for tested materials for CFRP at different aging conditions	188
Table 6.1: Hardness of testing continuum materials.....	200
Table 6.2: Average grain size diameter of the testing granular materials.....	200
Table 7.1: Axial loading program	224
Table 7.2: Lateral loading program.....	225
Table 7.3: Surface roughness parameters.....	227
Table 7.4: Surface roughness measurements (T=45°C).....	236
Table 8.1: Material properties used in the analysis	247
Table 8.2: Properties of CFRP and GFRP tubes	248
Table 8.3: FRP material stiffness matrix.....	249
Table 9.1: Research objectives and outlines	267

LIST OF ABBREVIATIONS

FRP	Fibre Reinforced Polymer
CFRP	Carbon Fibre Reinforced Polymer
GFRP	Glass Fibre Reinforced Polymer
AFRP	Aramid Fibre Reinforced Polymer
LA	Leighton Buzzard
M	Mersey
C	Congleton
D ₅₀	Mean Particle Size
GB	Glass Beads
HV	Vicker Hardness
SD	Standard Deviation
AE	Average Error
CISS	Constitutive Interface Shear Surface
LTIST	Long-Term Interface Shear Test
HV _{th}	Threshold Surface Hardness
HV _{cr}	Critical Surface Hardness
R _a	Arithmetic Mean Roughness
R _q	Maximum Profile Peak Height
R _t	Maximum Peak to Valley Height
R _n	Normal Relative Roughness
R _{sm}	Mean distance between Peaks
PR _a	Available Ploughing Resistance
PR _m	Mobilized Ploughing Resistance

NOMENCLATURE

A :	Cross sectional area of the shear box
D :	Pile diameter
d :	Confined concrete diameter
E_{11} :	Elastic modulus in the fibers direction (Longitudinal modulus)
E_{22} :	Elastic modulus in the perpendicular direction to fibers (Transverse in-plane modulus)
G_{12} :	In-plane shear modulus
G_{13} :	Out-of-plane shear modulus
f_c :	Compressive strength of the unconfined concrete
f'_c :	Compressive strength of the FRP tube confined concrete
f_l :	Hoop or lateral confining pressure
k_1 :	Confinement effective coefficient
I_d :	Relative density index
γ_{min} :	Minimum unit weight for sand
γ_{max} :	Maximum unit weight for sand
t :	FRP tube thickness
τ :	Shear stress
σ_n :	Normal stress
ΔR_t :	Relative roughness change
μ_p :	Peak Interface friction coefficient
μ_r :	Residual Interface friction coefficient
μ_i :	Internal shear Coefficient
V_f :	Fiber volume ratio
V_m :	Matrix volume ratio
δ :	Interface friction angle
φ :	Internal friction angle
ϵ_c :	Unconfined concrete strain corresponding to f_c
ϵ'_c :	FRP tube confined concrete strain corresponding to f'_c
ϵ_l :	Lateral or Hoop strain

ABSTRACT

Fibre reinforced polymer (FRP) composites represent an alternative construction material for deep foundations that have the potential to eliminate most of the durability concerns associated with traditional piling materials. Research studies and database related to the use FRP composite material as piling foundation is very limited. This research project was undertaken to investigate the structural and geotechnical behaviour of FRP composite piles. The originality of this study rests on the following pillars:

- Presenting a new understanding for the factors controlling the compressive strength of FRP tube confined concrete.
- Introducing the concept of constitutive interface surface which considers the effect of surface hardness and relative roughness on the interface shear coefficient.
- Studying the evolution of FRP pile surface roughness during the driving process.
- Investigating the effect of harsh environments on the shear behaviour of FRP-granular interface.
- Conducting an extensive experimental and numerical study to characterize the FRPs and soil parameters that control the behaviour of axially and laterally loaded FRP composite pile.

Experimental testing program was conducted in this study to examine the behaviour of two different FRPs tubes confined concrete under axial compression, and flexural load. Based on the experimental results of this study and test results available in the literature, a new design chart was proposed to predict the strength enhancement based on concrete strength and FRP lateral confinement.

An extensive laboratory study was conducted to evaluate the interface friction behaviour between granular materials and two different FRP materials. The interface test results obtained from experiment were used to examine a number of parameters known to have an effect on the interface friction coefficient. Furthermore, to

investigate the evolution of FRP pile surface roughness during the driving process laboratory tests were also conducted to quantify the interface shear induced surface roughness changes under increased normal stress levels. Moreover, interface tests were also conducted using three more counterface materials to define schematically the constitutive interface shear surface (CISS) in the three dimensional domain of surface roughness, surface hardness, and interface shear coefficient.

The long-term experimental program was also conducted in this study to assess the effect of different ageing environment conditions on FRP-granular interface shear coefficient. Acidic and alkaline aging environments were adopted in this study. The experimental program involved assessing the ageing effect on the testing FRP materials in terms of the changes in their hardness and surface roughness properties. Furthermore, the interface shear tests were conducted, using the unaged and aged FRP materials, to evaluate the effect of aging environments on FRP-granular interface shear coefficient.

A small-scale laboratory pile loading tests were carried out to assess the FRP pile behaviour under axial and lateral loads. The laboratory test results were used to verify/validate a numerical model developed by the commercial finite element package ABAQUS (6.11). Additional numerical analyses using the verified model were conducted to investigate the effect of different the FRPs and soil parameters on the engineering behaviour of FRP pile.

DECLARATION

No portion of the work referred to in the thesis has been submitted in support of an application for another degree or qualification of this or any other university or other institute of learning.

COPYRIGHT STATEMENT

The author of this thesis (including any appendices and/or schedules to this thesis) owns certain copyright or related rights in it (the “Copyright”) and s/he has given The University of Manchester certain rights to use such Copyright, including for administrative purposes.

Copies of this thesis, either in full or in extracts and whether in hard or electronic copy, may be made only in accordance with the Copyright, Designs and Patents Act 1988 (as amended) and regulations issued under it or, where appropriate, in accordance with licensing agreements which the University has from time to time. This page must form part of any such copies made.

The ownership of certain Copyright, patents, designs, trademarks and other intellectual property (the “Intellectual Property”) and any reproductions of copyright works in the thesis, for example graphs and tables (“Reproductions”), which may be described in this thesis, may not be owned by the author and may be owned by third parties. Such Intellectual Property and Reproductions cannot and must not be made available for use without the prior written permission of the owner(s) of the relevant Intellectual Property and/or Reproductions.

Further information on the conditions under which disclosure, publication and commercialisation of this thesis, the Copyright and any Intellectual Property and/or Reproductions described in it may take place is available in the University IP Policy (see <http://documents.manchester.ac.uk/DocuInfo.aspx?DocID=487>), in any relevant Thesis restriction declarations deposited in the University Library, The University Library’s regulations (see <http://www.manchester.ac.uk/library/aboutus/regulations>) and in The University’s policy on Presentation of Theses

ACKNOWLEDGEMENTS

I would like thank Allah (God) for giving me the patience, the knowledge and the strength to finish this work.

My deepest gratitude goes to my supervisor, Dr. Hossam Abuel-Naga for his continuous guidance during the study. He teaches me not only the professional knowledge but also the attitude towards life and work. His commitment to work and empathy to students make him a truly respectable teacher. I also thank my co-supervisor Dr. Wu. I would like to take this opportunity to thank to Dr. Craig for giving me encouraging and constructive advices. I wish him health and happiness after his retirement. Many thanks go to my friends and colleagues particularly to Mr. Mostafa and Mr. Haider for their kind encouragement.

Grateful thanks are extended to the staff of the Geotechnical, Structural and Laser Laboratories for their assistance rendered throughout the study. Mr. Martin Cruickshank had been extremely helpful during preparation experimental works. It was very difficult to assemble and modified the pile/soil chamber device. Also, special thanks to MACE school technician's staff specially Mr. David John, Mr. Phil Oakes, Mr. Bill Storey, and Mr. Dave Mortimer for their assistance during the experimental phase of this study.

Thanks should also be given to Carbon Composite Technology and Easy Composite Companies. Also, I wish to express my sincere appreciation to the Potters company staff specially Ms. Jane Manley. They made great effort to provide me the glass bead particles.

Last but definitely not least. I would like to thank, my father, and in loving memory of my mother, and my brothers. Special thanks to my wife, my sons Abdullah, Redhallah, Hasan and my beautiful daughter Fatima. This research won't be completed without their love and support from such a great family.

Hussein Shaia

PUBLICATIONS

Journal Papers

During the course of the research work, the candidate has submitted the following journal papers:

- 1- Shaia H and Abuel-Naga H., (2013) “Effect of surface roughness and hardness on interface shear strength of granular-continuum material” submitted to *Geotechnique Journal*.
- 2- Shaia H and Abuel-Naga H., (2013) “Effect of Ageing Environment on Fibre Reinforced Polymer/Granular Interface Shear Behaviour” submitted to *Canadian Geotechnical Journal*.
- 3- Shaia H and Abuel-Naga H., (2013) “Shaft Resistance Evolution of FRP-tube Confined Concrete Piles during the Driving Process” submitted to *Geotechnique Letters Journal*.

Published Conference Proceedings

The candidate also has participated in the following conference papers that have been published:

- 1- Shaia H., and Abuel-Naga H., (2012) “Experimental Study on Interface Shear Behaviour between Sand and Glass Fibre Reinforced Polymer” *International Symposium on Sustainable Geosynthetics and Green Technology for Climate Change (SGCC2011) 20 to 21 June 2012 Bangkok, Thailand*.
- 2- Shaia H., and Abuel-Naga H., (2012) “Behaviour of Sand Particles on FRP/Sand Interface Shear Strength” *Twelfth BGA Young Geotechnical Engineers Symposium (YGES12), University of Leeds., UK Tuesday 3rd-Wednesday 4th July 2012, Published in ICE virtual library <http://www.icevirtuallibrary.com/content/serial/gene> <http://www.britishgeotech.org.uk/>*

CHAPTER ONE: INTRODUCTION

1.1 Introduction

This introductory chapter is divided into three sections. The first section introduces the information of the statement of the problem for this study. The objectives and scope description are presented in section two. The last section of this chapter outlines the proposed organization of this study.

1.2 Statement of the Problem

Piles are usually made of different traditional materials such as timber, steel or concrete. Traditional piles have been used extensively for several decades. Problems coupled with use of these materials in harsh or organic soil and marine environments include deterioration of timber, corrosion of steel, degradation and marine borer attack of concrete. However, these traditional materials have limited service life and high maintenance costs when used in harsh environments. The Corporation of British Steel has assessed corrosion at rates up to 0.20 mm/year in industrial environments. In soil, the rate of the maximum corrosion reported is 0.03 mm/year in piles extracted after 25 years of service (Han et al., 2003). Attack on concrete occurs when there are high sulphate and chloride concentrations and low pH levels in the soils and ground water (Fleming et al., 2008). In the USA nearly 1.0 billion dollars annually is spent within the marine waterfront communities to replace or repair deteriorated (Lampo et al., 1998). Figure 1.1 shows examples of deteriorated and corroded traditional pile construction.



a) Degraded concrete pile

b) Corroded steel piles

Figure 1.1: Degradation of conventional piles

Recently, FRP composite materials are considered an attractive option for deep foundations due to their favourable intrinsic properties, such as: light weight, high specific strength, durability and speed of application. However, FRP composite technique provides an emerging and promising system for a variety of structural and geotechnical applications in which the FRP tube serve as a structural framework in piling foundation system. The use of FRP composite material in geotechnical engineering was started a few years ago and it is still somewhat limited compared to traditional materials. This is mainly because of their relatively higher initial cost, lack of database and absence of sufficient knowledge especially for these used in harsh marine environments. The study is also aimed to fill this gap in knowledge and to show how the developed geotechnical properties of FRP in term of shear mechanisms and interface resistance changes with aging environments.

A few studies and databases on FRP composites as piling materials showed some signs of encouragement that pushed researchers to proceed in the geotechnical field. The field programmes have been performed in several institutes and research centres in the United States (Pando et al., 2006). There is a very limited guideline available and the lack of information on the history of FRP composites as geotechnical issues

is one of the main obstacles that block their wide use in the United Kingdom industries. Therefore, this research is aimed at providing the structural and geotechnical engineering behaviour of two FRP composite materials (CFRP and GFRP) under different conditions.

1.3 Objectives and Scope

A number of research objectives are identified and systematically listed below in the two stated areas for the proposed experimental and numerical development.

1. Evaluate the structure performance behaviour of FRP tube confined concrete under pure compressive and flexural loads using two different FRP tubes (CFRP and GFRP).
2. Propose a topographic chart to assess the strength enhancement of FRP tube confined concrete using experimental and a large database results.
3. Investigate the geotechnical interface behaviour for FRP/granular materials within a geotribology framework. The study also investigates the change in surface roughness and interface shear coefficient of FRP materials under increased normal stress levels.
4. Provides a general conceptual understanding for the effect of hardness and roughness of a continuum surface on its interface shear behaviour against a granular material.
5. Develop the laboratory techniques for the accelerated FRP to investigate the ageing induced changes in FRP/Granular interface shear behaviour under different aging environments.
6. Explore the behaviour of different FRP piles subjected to axial and lateral loading tests.

7. Develop a 3-D axisymmetrical numerical model to simulate and validate the FRP pile/sand system based on experimental model tests using ABAQUS software package (6.11).

1.4 Thesis Organization

The current thesis consists of nine chapters including this introduction, with the content of each subsequent chapter summarized below:

Chapter 2: Presents background information on FRP composite materials in general and a literature review with specific focus on the FRP piling materials investigated in this research. This chapter also provides the background of the materials regarding the description of counterface FRP surfaces and methods by which the topography of geotechnical surfaces may be characterized.

Chapter 3: Describes the experimental program carried out on two types of FRP tubes confined concrete; Carbon Fiber Reinforced Polymer (CFRP) and Glass Fiber Reinforced Polymer (GFRP) tubes confined concrete. The details of the properties of materials, preparation of specimens, instrumentation, and the testing procedure were also presented in this chapter.

Chapter 4: Describes the extensive laboratory testing undertaken to assess the interface behaviour between FRP materials and granular materials. A comprehensive series of analyses use interface shear results to examine various important parameters. This chapter also presents the results of an additional experimental interface study that investigated the change in surface roughness and interface shear coefficient sheared against different types of sand under increased normal stress levels.

Chapter 5: Presents the long-term experimental testing of interface to assess the effect of different ageing environment conditions on FRP-granular interface shear

behaviour. Laboratory test procedure and specimens preparation details are also described in this chapter.

Chapter 6: Presents a general conceptual understanding for the effect of hardness and roughness of a continuum surface on its interface shear behaviour against a granular material.

Chapter 7: Describes the axial and lateral behaviour of both FRP piles installed in sand enclosed in a pressure chamber. The details of the tested materials, instrumentation FRP pile/soil scheme, pile load test set-up and test procedures are also described.

Chapter 8: Presents a three-dimensional numerical used to predict the FRP model tests in sand. The results obtained from numerical are then compared to the experimental model test. Additional investigations into the other unexplored parameters that effect on the FRP pile response are also presented using ABAQUS 6.11.

Chapter 9: Provides the summary and conclusions of this research. Recommendations and suggestions for future work are also given in this chapter.

CHAPTER TWO: BACKGROUND AND LITERATURE REVIEW

2.1 Introduction

Fibre reinforced polymer (FRP) refers to composite materials consisting of two phases; namely, the reinforcing phase and the matrix phase. The reinforcing phase is usually continuous fibre reinforcement, which is the load-carrying element of FRP and controls its stiffness and strength. The matrix phase in general provides protection and support for sensitive fibres as well as local stress transfer from one fibre to another. The matrix may have the form of polyester, vinylester, epoxy, phenolic, thermoplastic, etc. The reinforcement fibres are combined with the resin matrix material in a variety of forms to create the laminate. The reinforcement fibres can be made of carbon, glass, aramid, etc. Other terminology for composites include fibre reinforced polymer (FRP), glass fibre reinforced polymer (GFRP), carbon fibre reinforced polymer (CFRP), Aramid fibre reinforced polymer (AFRP), and others. The mechanical properties of FRP composites depend on several factors including the types of fibre and resin matrix, fibre orientation and volume of fibres. That is, mechanical properties such as strength are direction dependent and will differ in the fibre direction and the transverse direction.

FRP composite materials were originally developed to be used in defence and aerospace systems. They have been used in military and aerospace applications since 1940 to take advantage of their high strength, light weight, chemical resistance, good fatigue strength, and non-magnetic properties (Alampalli et al., 1999). The use of FRPs in civil engineering has recently started to gain more popularity around the world. Structural and geotechnical engineers are beginning to gain confidence and experience in applying this technology to civil structures. It has been used as internal reinforcement for beams, slabs and pavements and also as external reinforcement for rehabilitating and strengthening different structures such as columns, piles, and some bridge structures. One promising innovative structural system is FRP tubes confined concrete technique. These FRP tubes confined are constructed by simply filling

prefabricated FRP tubes with concrete which represent a formwork-free, steel-free, and corrosion-resistant alternative for construction of new infrastructures. Recently, the construction industry has introduced FRP tube confined concrete as an alternative construction material to current conventional piling materials.

This chapter gives background information related to the structure of FRP composite materials. The most important information on FRP composite and identification of its applicability in structure and geotechnical engineering are also described. FRP composite laminates which are used to fabricate FRP tubes which forms the backbone of the FRP tube member are also discussed including their manufacturing process and mechanics. This chapter also presents important information about the composite materials selected for this research as FRP piling foundation: glass and carbon fibre reinforced polymer (GFRP and CFRP). A comprehensive review of the published literature related to FRP confined concrete from the structure and geotechnical viewpoints are presented. The FRP structure, FRP surfaces topography and important equipments are also given in details.

2.2 FRP Composite Structure

A composite material can be defined as a combination of two or more phases that results in better properties than those of the individual components used alone. One constituent is called the reinforcing phase and the one in which it is embedded is called the matrix phase as shown in Figure 2.1. Reinforcement fibres can be all parallel (unidirectional continuous fibre composites), can be oriented at right angle to each other (cross ply or woven fabric continuous fibre composites), or can be oriented along several directions (multi-directional continuous fibre composites). Polymer matrix composites include polyester, vinylester, epoxy, phenolic, thermoplastic, etc. resins reinforced with glass (GFRP), carbon (CFRP), and aramid (AFRP) [(Daniel and Ishai, 1994) and (Kaw, 2006)]. Fibres and matrix components are combined together to form a composite unit (lamina). The properties of FRP composite material depend on the properties of the constituents, geometry, and distribution of the phases. One of the most important parameters is the volume (or weight) fraction of reinforcement, or fibre volume ratio.

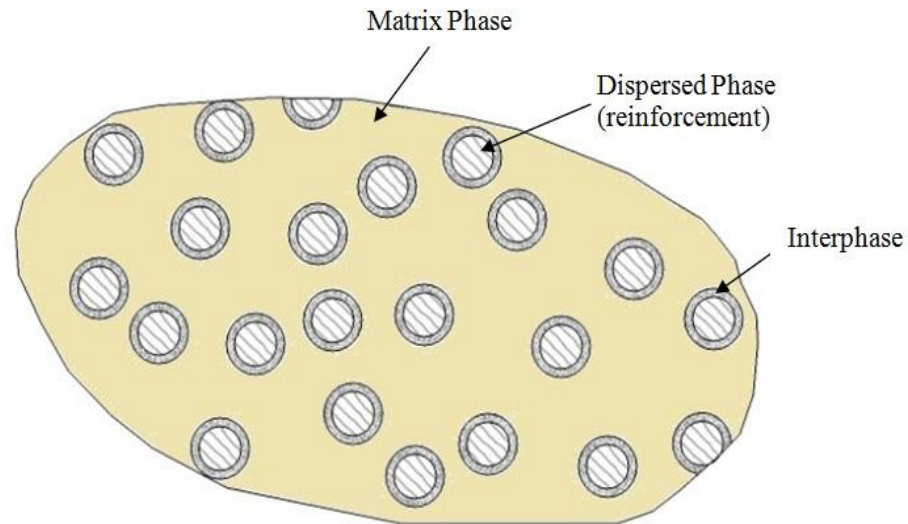
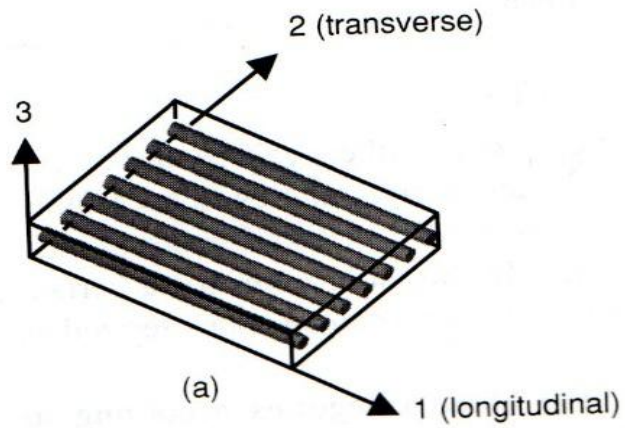


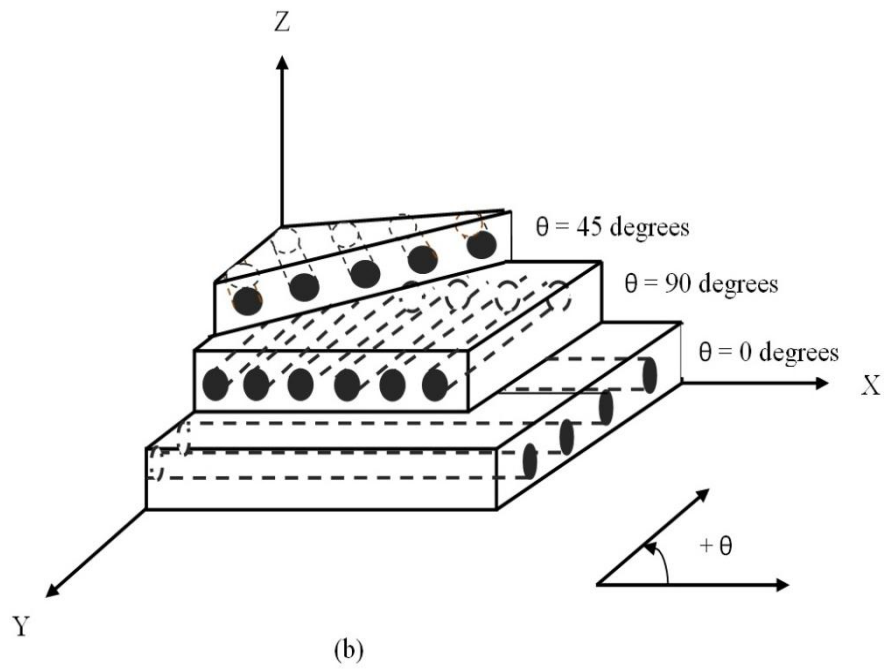
Figure 2.1: Phases of FRP Composite Materials (Daniel and Ishai, 1994)

2.3 FRP Composite Laminates

A lamina or a ply is a plane or curved layer of unidirectional fibres or woven fabric in a matrix. The lamina is considered an orthotropic material with principal material axes (1, 2, and 3) as shown in Figure 2.2a. A laminate is made up of two or more unidirectional laminates or plies stacked together at various orientations. Since the principal material axes differ from one ply to another, it is more convenient to analyze laminates using a common fixed system of coordinates (x , y , and z) as shown in Figure 2.2b. The orientation ply is given by the angle between the x -axis and principal axis-1 of the ply measured positive in a counter clockwise direction. The configuration of the laminate indicating its ply composition and exact location or sequence of various plies is called the layup. The configuration indicating, in addition to the ply composition, the exact location or sequence of the various plies is called the stacking sequence (Daniel and Ishai, 1994).



a) Unidirectional lamina



b) Multidirectional laminate

Figure 2.2: Lamina and principal coordinate axes

2.4 Types of Fibre Reinforcements

A reinforcement fibre is a material made into a long filament. Reinforcement fibres have some superiority over other materials because of their high stiffness, strength and light weight. Fibres do not necessarily need to be used in a continuous form. They can be used in a continuous or discontinuous form in the composite as desired. When used as continuous reinforcement, they have to be aligned in the matrix at the required percentage and direction. The main functions of fibres are to carry the load and provide stiffness, strength, thermal stability and other structural properties to the FRP (Tuakta, 2005). To perform these functions, the fibres in FRP composite must have high modulus of elasticity, high ultimate strength, low variation of strength among fibres, high stability of their strength during handling and high uniformity of diameter and surface dimension among fibres. The type of fibres used as the reinforcement is the basis for classification of FRP composites. There are three types of fibres dominating the civil engineering industry: carbon, glass and aramid fibres.

2.4.1 Carbon Fibre Reinforced Polymer (CFRP)

Carbon or “graphite” fibres are a type of high-performance fibre available for civil engineering application. This type of fibre is fabricated by controlled pyrolysis and crystallization of organic precursors at temperatures above 2000°C. In this process, carbon crystallites are produced and orientated along the fibre length. Carbon fibres are the most expensive, costing approximately 5 to 7 times the cost of glass fibres. They are lightweight and have a much higher stiffness and strength durability as compared with the other commonly used fibre types (Tuakta, 2005). They also have a very high resistance to dynamic loading, excellent fatigue and creep resistance, and low thermal expansion.

2.4.2 Glass Fibre Reinforced Polymer (GFRP)

Glass fibre reinforced polymer (GFRP) is the most commonly used fibre type for composite reinforcement. GFRP's are a processed form of glass, which is composed

of a number of oxides (mostly silica oxide), together with other raw materials (such as limestone, fluorspar, boric acid, clay). They are manufactured by drawing those melted oxides into filaments ranging from 3 μm to 24 μm . In fact, almost 90% of the fibres used in the low-cost composite industry are made of glass.

2.4.3 Aramid Fibre Reinforced Polymer (AFRP)

Aramid or aromatic polyamide fibre (AFRP) is one of the two high-performance fibres used in civil engineering application. AFRP's are synthetic organic fibres that offer higher strength and stiffness than glass fibres. The aramid fibres provide good damping properties resulting in higher resistance to abrasion and shock. They also have excellent fatigue and creep resistance, chemical resistance, and are very ductile. However, aramid fibres are not water resistance which can result in water absorption and growth in humid environments of up to 3% to 7%. They can also have some difficulty achieving strong bonds to the resin.

2.5 Resins

Resins are the polymer that bind the fibres together, hold them aligned and transfer the loads between the fibres in addition to protecting them from environmental factors and carrying shear loads. Resins provides the shape and rigidity of the material and binds the fibres together (Barney, 2004). They also protects the fibres from environmental degradation and protect the reinforcing from mechanical damage (eg. abrasion) (Harris, 1986). The resin provides resistance against ultra-violet light, chemicals, impact, and fire. Structurally, the resin provides lateral support against compression buckling and allows the transfer of stresses from the surface to the interior fibres. The most common types of resins used in civil infrastructure applications are epoxies, vinyl esters, and polyesters. A brief description of each type now follows.

2.5.1 Epoxy Resin

Epoxy resins have the best performance in the resins family because they contain a reactive functional group in their molecular structure. They are used in advanced composite materials for structural and aerospace applications more than all other resins. That is because of their several advantages over other resins such as their mechanical properties, resistance to chemicals, and excellent adhesion with most fibre types. The only obstacles that limit their wide use are the high cost and long curing times (Gindy et al., 2005).

2.5.2 Polyester Resin

Polyester resins are the most economical and widely used resins in composites manufacturing. It can be produced in mass quantities at lower cost and with a wide range of properties. Their rigidity can be controlled by the ratio of saturated to unsaturated acids (Gindy et al., 2005). These resins can be used with any type of glass or carbon fibres.

2.5.3 Vinly Ester Resin

Vinyl ester resins have moderate adhesive strengths compared to epoxy resins. They produced by the esterification of an epoxy resin with an unsaturated monocarboxylic acid. They have the performance advantages of epoxies and handling properties of polyesters. Vinyl ester resins have the performance advantages of epoxies and the handling properties of polyesters. The adhesive strengths are moderate compared to epoxy resins and they are more expensive than polyester (Fakirov and Bhattacharyya, 2007).

2.6 FRP/Matrix Mechanism

The basic mechanism and processes in the fibre/resin system are that the resin which surrounds and bonds every fibre in the unit transmits the load to the fibre through

shear stress τ , as shown in Figure 2.3. Because of the tension force P , a shear stress develops on the outer surface of the fibre, and its magnitude decreases from a high value at the end of the fibre to zero at a distance from the end. This stress will cause a tensile stress σ within the fibre cross section. The shear stress on the surface of the fibre is high near the ends of the fibre, and the tensile stress within the fibre is low. As the distance from the end increases, the shear stress decreases and the tensile stress increases. At a certain distance from the end, the shear stress becomes very small and the tensile stress reaches its maximum value (Reddy, 2004).

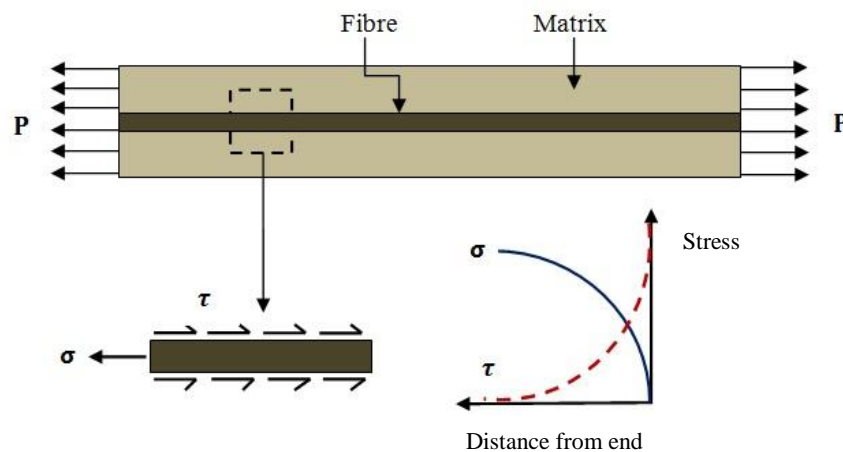


Figure 2.3: Load transfer between fibre and resin

2.7 FRP Composite Applications

The technology of composite materials has experienced a rapid development in the last two decades. Recently, the construction industry has begun using fibre reinforced polymers (FRP's) which have some advantages over traditional materials. FRP's have emerged as a potential solution to overcome some of the problems associated with structures built using traditional materials. Their specific strength and high resistance to corrosion and other electro-chemical reactions have made them attractive for some applications. During the two last decades, there has been a surge of activities in the civil engineering research community to test and demonstrate the viability of these new materials for the construction of more durable structures and for the repair and strengthening of existing structures.

The use of FRP's in pile foundation systems has started recently to gain more popularity in the United States. Europe and Japan have been using FRP's in geotechnical applications for many years. They have been used in a wide variety of new and old bridge projects (Alampalli et al., 1999). Applications include aerospace and civil engineering have been the largest. More details are discussed in the following sections.

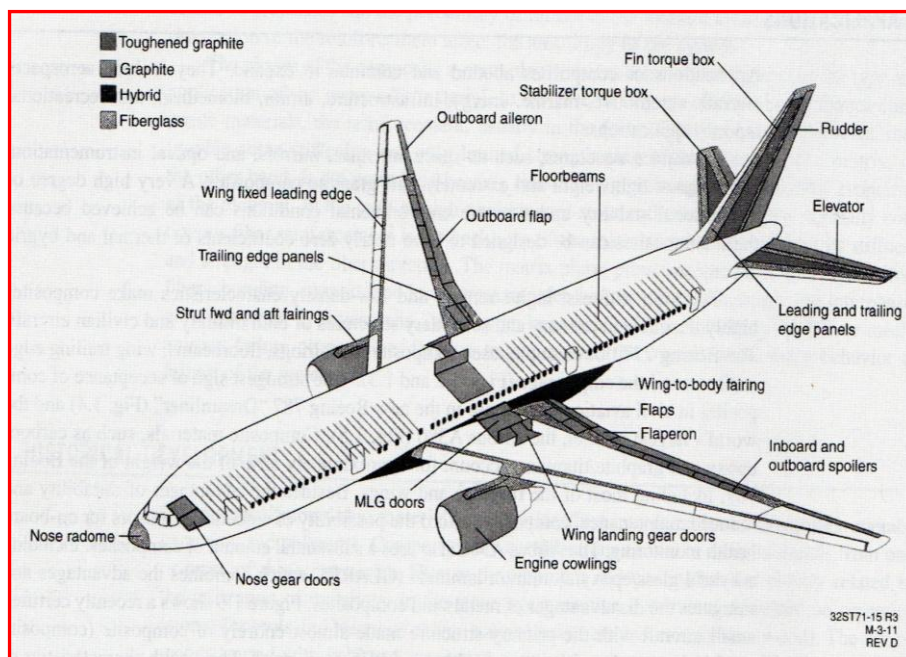
2.7.1 FRP in Aerospace Engineering

The aerospace industry has been utilizing fibre reinforced composite materials for its products for more than 50 years. FRP's also have very wide applications in spacecraft's. The weight reduction is the main reason for using such applications. Also their dimensional stability over a wide range of temperatures makes them favourable over other materials.

Military aircraft manufacturers were among the beginners who introduced FRP composite materials to be a replacement for traditional materials. The designers realized the tremendous potential of composite materials, especially their high specific strength, stiffness and light weight. This has lead to a rapid acceleration in the development of advanced composites in military and civilian aircraft applications. The Boeing 777, for example, uses composites in fairings, floor beams, wing tailing edge surfaces, and the empennage as shown in Figure 2.4. Composite materials, such as carbon/epoxy and graphite/titanium, account for approximately 50% of the weight of the Boeing 787, including most of the fuselage and wings.



a- Boeing 777 commercial aircraft



b- Diagram illustrating usage of composite materials in various components

Figure 2.4: Boeing 777 commercial aircraft

2.7.2 FRP in Civil Engineering

Every year a large number of construction members such as piles, columns, girders, and bridge piers are reaching their design service lives and need to be repaired. The major construction materials for these member structures are still concrete and steel. The rapid deterioration of concrete and corrosion of steel, especially in aggressive environments, such as marine areas, reduces the designed service life of the bridge structure. The use of the same materials to repair or rehabilitate the structure will not resolve the problem. A need for a long term, practical and economical solution is essential. New techniques in overcoming such problems have been utilized. The use of fibre reinforced polymer composites (FRP's) to replace the traditional materials in rehabilitating old and building new structures is becoming more common. FRP is the newest building material available in the market for large projects construction. The recent advancement in material technology and manufacturing techniques has made it easier to develop materials with the ability to satisfy conditions that could not be achieved by traditional materials. One promising innovative structural system is FRP tubes confined to concrete. This system consists of FRP round tube totally or partially filled with concrete as shown in Figure 2.5. The contained concrete is protected from severe environmental effects and deterioration resulting from freeze-thaw cycles.

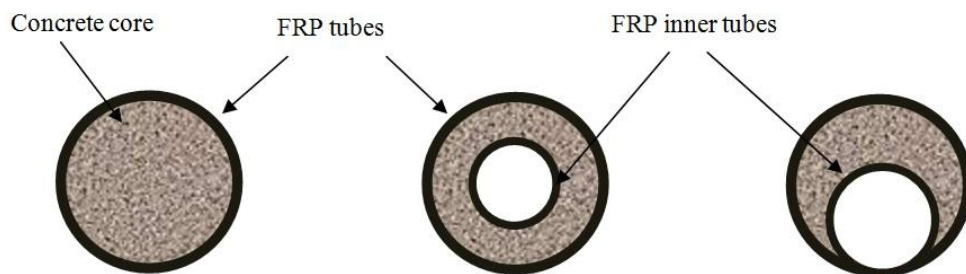


Figure 2.5: Different configuration of FRP tube confined with concrete
(Fam and Rizkalla, 2002)

Figure 2.6 shows also the different potential applications of FRP tubes confined concrete including marine piles, overhead sign structures, poles and posts bridge columns and piers, girders, large pipes and tunnels. The main focus of the present study is on FRP tube confined concrete used in piling foundation system.

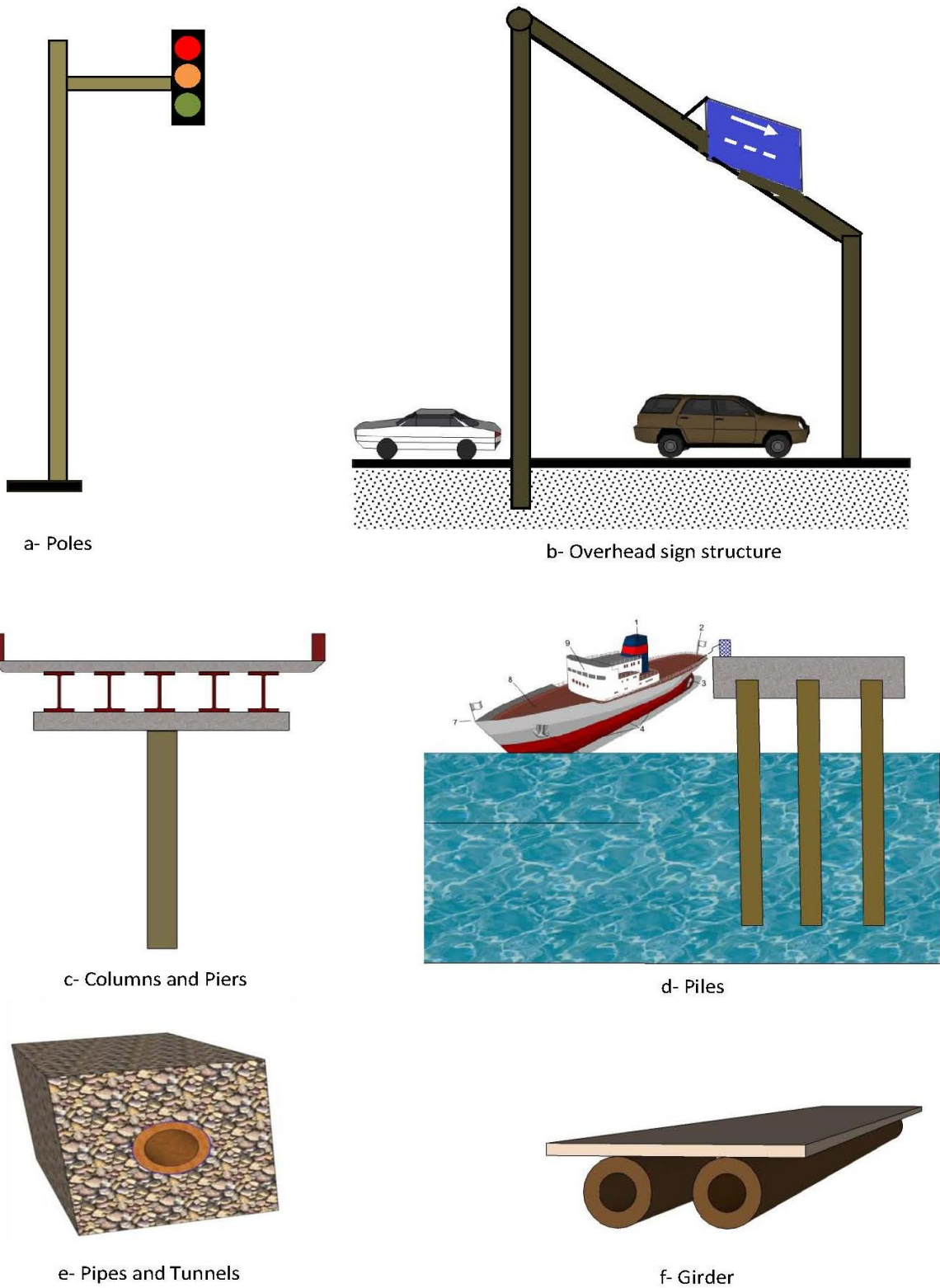


Figure 2.6: Different structural applications of concrete filled FRP tubes

2.8 Advantages of FRP

2.8.1 High Specific Strength and Stiffness

FRP show great enhancement in strength and stiffness properties (Keller, 2003). Table 2.1 describes an example of comparison of typical ranges of FRP composite characteristics with those of traditional steel material. These characteristics are gradually being used in the building construction industry for infrastructure applications.

Table 2.1: Comparison between FRP and steel (GangaRao and Vijay, 2010)

Property	Merit/Advantage (Rating)		Rating Scale
	FRP	Steel	
Strength/ Stiffness	4-5	4	1. Very low 2. Low 3. Medium 4. High 5. Very high
Weight	5	2	
Environment Durability	4-5	3	
Ease of Field Construction	5	3-4	
Ease of Field Repair	4-5	3-5	
Fire	3-5	4	
Transportation/Handling	5	3	
Toughness	4	4	
Acceptance	2-3	5	
Maintenance	5	3	

The combination of high specific mechanical characteristics such as strength and stiffness make the designers be able to develop the construction at lower weights and thicknesses. Furthermore, these characteristics enable civil engineers to consider new design concepts that would be limited by the specific properties of other construction materials. The second level bridge concept presents an example of FRP application which proposed by ApATeCh company to solve transport and traffic problems in the City of Sochi, as shown in Figure 2.7. The FRP composite material was used in this project for the erection of highway second level bridges, road interchanges and parking in the most congested zones of the city and of suburbs without traffic interruption on the main road, without interfering with the architectural area.



Figure 2.7: Second-level bridge in Moscow (<http://www.apatech.ru/>)

In civil applications, lightweight could result in various advantages such as better seismic resistance, ease of application of and a decrease in need for large foundation system. In addition, the drive to increase traffic ratings means that there is a huge potential to replace older and deteriorated bridge structures with FRP materials since lightweight from FRP materials can improve the live load capacity without the expense of new structures and approach works. The most common is replacing bridge decks made of traditional materials by those of FRP composites as shown in Figure 2.8.



Figure 2.8: FRP deck systems (<http://www.compositesworld.com/>)

2.8.2 Corrosion and Degradation Resistance

Problems coupled with these piles include deterioration of wood, corrosion of steel and degradation of reinforced concrete. The loss of section due to corrosion of steel and deterioration of concrete could cause a major problem because of the reduction in carrying capacity of the pile system. As mentioned earlier, FRP materials have the advantage over traditional materials in corrosion and degradation resistance. However, the main advantages of FRP composites among other traditional construction materials include lightweight, high strength-to-weight ratio, corrosion resistance, chemical and environmental resistance and low maintenance cost (Sakr et al., 2005). This advantages allows the FRP composites structures to have a long service life without additional rehabilitation costs [(Keller, 2003) and (Zobel et al., 2005)]. Every year a large number of structures are reaching their design service lives and need to be repaired or replaced. Figure 2.9 shows an example of composite drainage channels and standard reinforced concrete channels were done by ApATeCh Company. However, FRP can offer performance advantages when compared to the traditional materials. The use of composite FRP to replace the traditional materials in rehabilitating old and building new structures is becoming more common.



Figure 2.9: Comparison of the performance of FRP composite channel (left) and reinforced concrete channel (right) (Bernard Potyrala, 2011)

2.8.3 Quick and Easy Transport

The other advantage of use FRP composites in civil engineering applications includes their fast and easy installation. In civil engineering, the construction work is often characterized by long construction and installation periods, which can result not only in delays in the opening of facilities but also in considerable inconvenience to users (such as in the case of road diversions, lane blockages, and posting of speed). In addition, the construction process using traditional materials is often taking long time. The FRP can be handled and cut with little effort and easily conform to any structure shape or geometry. On the other hand, large FRP composite parts can be fabricated in the manufacture companies due to their light weight and can be transported to the construction site easily and installed using light equipment (rather than heavy and specialized), thereby reducing the costs of transportation and minimizing the amount of site work [(Lopez-Anido et al., 2000) and (Zobel et al., 2005)]. The quick and easy transport property might make the FRP composite an advance material for demountable constructions. An example is mobile assembly pedestrian walkways which have been installed in Russia with stair flights, all the elements of which are made of FRP materials as shown in Figure 2.10.



Figure 2.10: FRP composite pedestrian walkway in Russia

2.8.4 Aesthetics and Dimensional Stability

The aesthetics and dimensional stability of FRP construction is one of the most useful properties. FRP has proven to be a superior material through its dimensional stability and aesthetics. The high accuracy of dimensions measurements at the construction site compared to the traditional construction such as reinforced concrete often causes many difficult problems to contractors. The fabrication process such as pultrusion process method ensures dimensional accuracy. FRP offers advance and optimal aesthetics to the most elements of structure in the world today. It presents the possibility to obtain the required characteristics through the introduction of pigments, photosynthesis, required fine finish, surface texture, and colour (Zobel et al., 2005).

2.8.5 Electromagnetic Transparency

FRP composites structure has exhibited low/no electrical conductivity, thus they can be used for constructions located in areas of risk of electric shock, such as footbridges over the railway traction and bridges in factories. Figure 2.11 shows a popular example of Lleida Footbridge over railway. Lleida Footbridge, located about 2 km from the city of Lleida in Spain, crosses a roadway and a railway line between Madrid and Barcelona cities. The structure is consisted of a double-tied arch of 38 m span length with a rise of 6.2 m and 3 m wide. The total weight of the bridge is approximately 19 tons. The structure elements are made of fibre reinforced polymer using E-glass fibres combined with woven and complex mats with a minimum glass fibre content of 50%. The structure assembly was carried out by 8 people working over 3 months.



Figure 2.11: General view of the Lleida footbridge (Spain)
(Bernard Potyrala, 2011)

2.9 Disadvantages of FRP Material

2.9.1 Higher Costs

The application FRP composites costs are categorized as short-term and long-term costs. The short-term cost includes the FRP material cost, the fabrication process cost, and construction cost. The long-term cost of FRP composites is more difficult to evaluate because it involves various unpredictable costs, such as maintenance, deconstruction, and disposal costs.

However, FRP composites material has been successfully established, construction industry is very cost-sensitive. It is also difficult to evaluate the FRP construction life-cycle costs because a limited number of relevant projects have been constructed using FRP materials (Lopez-Anido et al., 2000).

2.9.2 Lack of Durability

Although FRP composites have been used extensively in d marine applications there is still a lack of design rules. This lack of in-depth knowledge of the durability of FRP composite in real service condition restricts its extensive use in structural rehabilitation works. A lack of durability can cause serious safety and serviceability problems for structures. Therefore, the assessment of FRP materials at long-term condition in term of structural and geotechnical properties is considered as the main part of this research.

2.9.3 Low Fire Resistance

In civil engineering construction, fire resistance is important above all for structural elements exposed to a fire. FRP materials are in principle combustible and have low fire resistance, sometimes producing unhealthy gases. There are some types available that are fire-retardant, self-extinguishing and do not exhibit a development of toxic fumes, but there is little knowledge on their loss of strength in fire. The loss of strength begins much earlier compared with steel.

2.9.4 Lack of Design Standards

Civil design is generally dominated by the use standards and guidelines predicated on the use of well-documented and standardized material types. Civil engineers are trained to utilize appropriate materials in appropriate manners, according to these standards and guidelines. They do not need expertise in material science to design, construct, and maintain structure elements of conventional material like traditional materials. However, application of FRP composites at the current stage requires more database and knowledge of material behaviour and manufacturing processes for more than for the traditional materials. Therefore, extensive studies and database are needed to evaluate the behaviour of using FRP materials especially for structural and geotechnical applications.

2.10 Traditional and FRP Piling Foundations

A pile is a long, columnar element made of timber, steel, concrete, or a combination of these materials. Piles can be found in different types of cross sections as shown below in Figure 2.12. The most common shapes are the H-section for steel piles, circular sections for concrete piles and polygonal sections for prestressed piles.

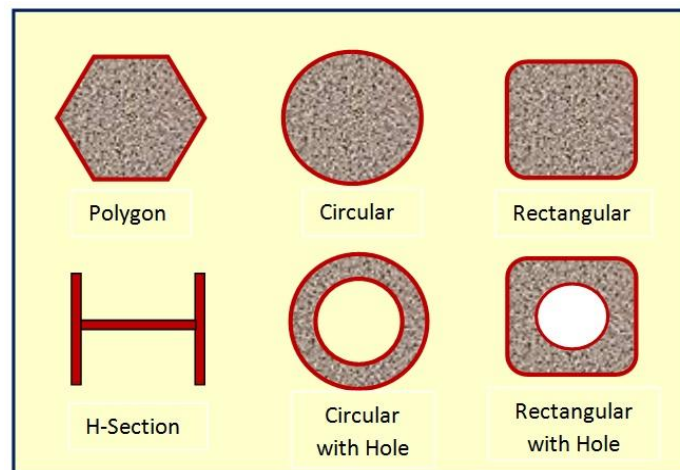


Figure 2.12: Common piles shapes

Most common composite piling products are made of timber and concrete or steel, and more recently plastic and steel or FRP tubes confined concrete. A brief description of the available pile materials is given below.

2.10.1 Timber piles

Timber piles are the oldest type of the pile foundations that have been used to support structural loads. In many ways, timber is an ideal material for piling, as it has a high strength to weight ratio. Several types of timber such as softwoods and hardwoods are used in piling. The advantages of using this type of piles includes: their availability, ease of handling and ease of cutting to desired lengths. Timber piles have been used extensively in fendering applications because of their energy-absorbing qualities. Timber piles (round or square) have cross sections from 250 mm

to 500 mm (Aysen, 2005). Working loads of timber piles are usually less than 500 kN because of their relatively small-cross section and difficulties in driving them in soil conditions that allow greater working loads (Fleming and Elson, 2008). Timber piles in marine structures are liable to be severely damaged by the mollusc type borers which infest the sea water in many parts of the world, particularly in tropical seas. Timber piles are driven with pointed ends, which may be protected, by steel or a cast-iron shoe. Similarly a driving cap may be installed on the driving end to protect the butt from hammering effects.

2.10.2 Concrete Piles

Concrete is the most common traditional construction material used today. It can be classified in general into three broad categories; namely, precast concrete piles, cast-in-place concrete piles and composite concrete piles (Tomlinson, 1994). The advantages of concrete piles include: pile length can be adjusted to suit field requirements and that they are suitable for a wide range of loads. Their main disadvantages include chemical deterioration due to contaminated groundwater from manufacturing plant wastes and leaky sewers or seawater, damage due to freezing and thawing, damage due to handling and driving stresses and damage due to concrete material defects such as cavities and soil pockets. The most destructive agents for reinforced concrete piles are sodium and calcium chlorides. These salts penetrate through the concrete cracks to the reinforcing and create an electrical current, which causes the reinforcement to corrode. This corrosion process is accompanied by expansion, which tends to induce high tensile stresses in the surrounding concrete causing cracking and spalling. In marine environments, the variation of temperature and freezing and thawing cycles lead to further concrete degradation. Also concrete piles in seawater are susceptible to sulphate attack. Magnesium sulphate and sodium sulphate attack the tricalcium aluminate. The resulting ettringite ($\text{CaO} \cdot \text{Al}_2\text{O}_3 \cdot 3 \text{CaSO}_4 \cdot 32\text{H}_2\text{O}$) is a swelling material, which leads to an increase in the size of concrete cracks and deterioration of the concrete (Siddique, 2008).

2.10.3 Steel piles

Steel piles are gaining popularity because of their many advantages. They are strong, light to handle, can be extended to any length and are capable of carrying heavy loads to deep strata. Various types of steel piles are used in practice such as pipe piles, H-section piles, square section piles and tapered and fluted tubes (Monotubes). Steel pipe piles can either be driven open ended or closed open ended. Despite the widespread use of steel piles, they are susceptible to deterioration during their service life due to corrosion, especially in industrial and marine environments. Corrosion of steel piles can be reduced by coatings containing heavy metals but these metals are harmful to the environment.

2.10.4 FRP Composite Piles

There are several types of composite piles available on the market. Review of the available literature shows that currently there are five common types of composite piles which are considered as potential substitutes [(Pando et al., 2006) and (Iskander et al., 2001)]. These include plastic encased steel pipe core piles, reinforced plastic piles, FRP confined concrete piles, fibreglass pultruded pipe piles and plastic lumber piles as shown in Figure 2.13. The FRP tube confined concrete pile is investigated in this work. The study involves using two FRP composite piles; Carbon Fiber Reinforced Polymer (CFRP) and Glass Fiber Reinforced Polymer (GFRP) tubes confined concrete.

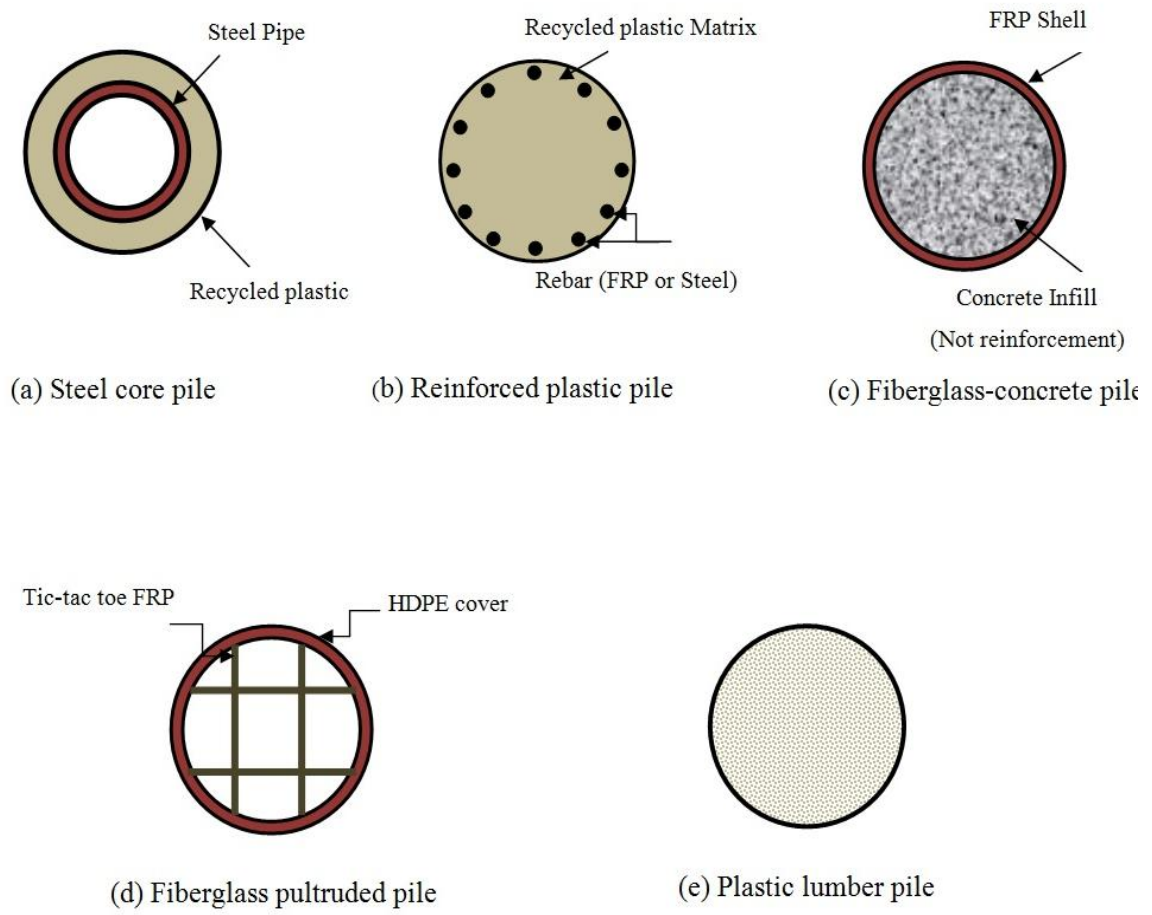


Figure 2.13: Common types of composite piles (Iskander and Hassan, 1998)

2.10.4.1 Steel Core Piles

Steel core piles type consists of two parts, a recycled plastic shell encasing a steel pipe core as shown in Figure 2.13a. The steel pipe core provides the structural strength and the plastic shell provides the necessary environmental protection. Piles are available in 200-600 mm outer diameter and up to 23 m long. The structural pipe cores range from 100-400 mm outer diameter with the wall thickness ranging between 6 and 40 mm. These piles are usually produced in 6 m segments and pipes are connected together with threaded coupling [(Horeczko, 1995) and (Guades et al., 2011)]. The most common uses for this pile type are as fender piles and pier piles in regions with marine influence. These types of piles were first installed at Berth 120 in the Port of Los Angeles.

2.10.4.2 Reinforced Plastic Piles (RPP)

Reinforced plastic piles are composed of extruded recycled plastic matrix reinforced with fibreglass rebars or steel rods, as shown in Figure 2.13b. The plastic matrix is chemically treated with antioxidants and ultraviolet inhibitors to retard the effect of UV light on the plastic (Taylor, 1995). RPP piles are available in 250-400 mm diameters and are reinforced with 6 to 16 fibre glass reinforcing bars ranging in diameter between 25 and 30 mm [(Hanna, 2002) and (Guades et al., 2011)]. Depending on the structural requirements for the specific piling application, the type, size, and numbers of reinforcing elements are selected.

2.10.4.3 FRP-Confined Concrete Piles

FRP piles usually consist of an acrylic-coated FRP tubular section filled with concrete Figure 2.13c. The main role of FRP the tube is to provide a stay-in-place structural framework for the concrete infill, act as noncorrosive reinforcement, gives confinement to concrete in compression and protect the concrete from severe environmental effects (Mirmiran and Shahawy, 1996). The fibres have very high strength and modulus but they are very fine (about 7-15 μm in diameter) and they are very brittle. On the other hand, the concrete infill offers internal resistance in the

compression zone and increases the stiffness of the member and prevents local buckling of the FRP tube (Fam and Rizkalla, 2001). FRP tube acted as reinforcement in the axial and hoop directions, in addition to its function as a permanent formwork for the concrete. FRP tube may be ductile or brittle and they have a high resistance to chemical attack. By combining fibres and resin, a material is produced with strength close to that of the fibres and with the chemical resistance of the plastics. This type of pile was selected as testing materials in this study using two FRP tubes (CFRP and GFRP).

2.10.4.4 Fibreglass Pultruded Piles

Fibreglass pultruded pipe piles are composed of outer fibreglass sheet fitted with a fibreglass grid to provide structural strength. The grid consists of two sets of orthogonal plates joined at four intersecting points and forms a tic-tac-toe pattern as shown in Figure 2.13d. The grid inserts are sometimes filled with HDPE, plastic lumber, or polyethylene foam fills. In fender piling applications, the shell and inserts are used to help absorb the vessel impact and connect fendering fittings (Guades et al., 2011).

2.10.4.5 Plastic Lumber Piles

Plastic lumber piles consist of a recycled plastic matrix with randomly distributed fibreglass reinforcement in the matrix as illustrated in Figure 2.13e. Trimax produces a variety of structural members made of plastic lumber. The dense solid outer tube is bonded to the peripheral surface of the inner plastic core which is foam-filled to reduce total weight. Various additives can be mixed with the plastic materials to enhance the performance of the structural member (Iskander and Hassan, 1998).

2.11 Rules of FRP Composites

The mechanical properties of a composite are strongly influenced by the proportions and properties of the matrix and the fibres. The commonly used method in expressing constituents' proportions is by volume fraction. The fibre reinforced polymers consist of the fibre and the matrix, thus the fibre volume fraction is defined as the ratio of the volume of fibre to the total volume,

$$V_f = \frac{\text{fibre volume}}{\text{composit volume}} \quad 2.1$$

Also, the matrix volume ratio,

$$V_m = \frac{\text{matrix volume}}{\text{composit volume}} \quad 2.2$$

and,

$$V_f + V_m = 1 \quad 2.3$$

For a composite element of initial length L loaded in 1- direction, as show in Figure 2.14, an elongation of ΔL in the direction of loading has occurred.

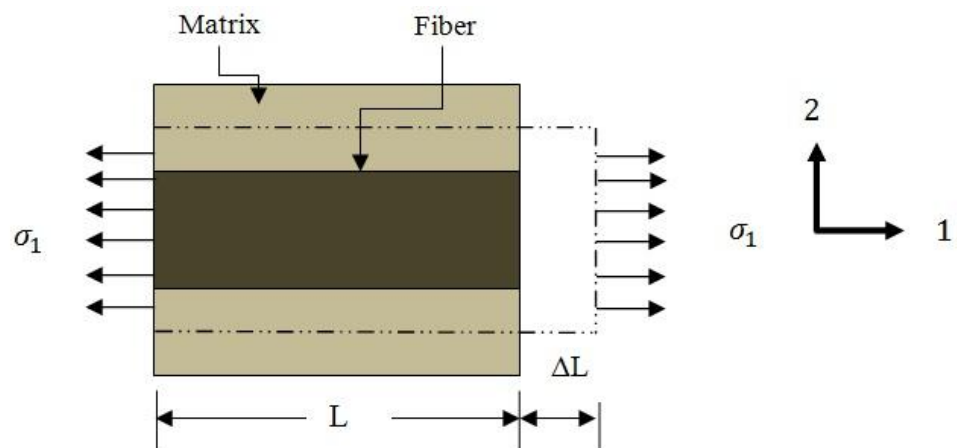


Figure 2.14: Deformation of a composite element under axial tensile stress

The strain in the composite can be given as:

$$\varepsilon_1 = \frac{\Delta l}{l} \quad 2.4$$

where ε_1 applies to both the fibre and the matrix. Since both materials are elastic then the stress-strain relation in the direction of the fibre can be given as:

$$\sigma_f = E_f \varepsilon_1 \quad 2.5$$

$$\sigma_m = E_m \varepsilon_1 \quad 2.6$$

The total area on which stress is applied is the summation of the fibre area and matrix area,

$$A = A_f + A_m \quad 2.7$$

Then the total force on the composite element can be given as:

$$P = \sigma_1 A = \sigma_f A_f + \sigma_m A_m$$

Then,

$$\sigma_1 = \varepsilon_1 (E_f V_f + E_m V_m)$$

where:

$$V_f = \frac{A_f}{A} \quad \text{and} \quad V_m = \frac{A_m}{A}$$

and,

$$\sigma_1 = E_1 \varepsilon_1$$

From that it can be found that:

$$E_1 = E_f V_f + E_m V_m \quad 2.8$$

This equation is known as the rule of mixtures for the apparent Young's modulus of the composite material in the fibres direction (Jones 1999).

The apparent modulus in the transverse direction can be calculated in a similar manner:

$$E_2 = \frac{E_f E_m}{V_m E_f + V_f E_m} \quad 2.9$$

2.12 Stress-Strain Relation for Orthotropic Materials

The stress strain relations for a composite material can be expressed using Hooke's law

$$\sigma_i = C_{ij} \varepsilon_j \quad i, j=1 \quad 2.10$$

where, σ_i , and ε_j are the stress and strain vectors respectively and C_{ij} is the material elastic stiffness matrix.

In orthotropic materials where there are two orthogonal planes of material symmetry, the stress-strain relations can be expressed with nine independent constants in the stiffness matrix in the form:

$$\begin{bmatrix} \sigma_1 \\ \sigma_2 \\ \sigma_3 \\ \tau_{23} \\ \tau_{31} \\ \tau_{12} \end{bmatrix} = \begin{bmatrix} C_{11} & C_{12} & C_{13} & 0 & 0 & 0 \\ C_{12} & C_{22} & C_{23} & 0 & 0 & 0 \\ C_{13} & C_{23} & C_{33} & 0 & 0 & 0 \\ 0 & 0 & 0 & C_{44} & 0 & 0 \\ 0 & 0 & 0 & 0 & C_{55} & 0 \\ 0 & 0 & 0 & 0 & 0 & C_{66} \end{bmatrix} \begin{bmatrix} \varepsilon_1 \\ \varepsilon_2 \\ \varepsilon_3 \\ \gamma_{23} \\ \gamma_{31} \\ \gamma_{12} \end{bmatrix} \quad 2.11$$

The strain-stress relation can also be expressed in a similar manner according to Hooke's law:

$$\varepsilon_i = S_{ij} \sigma_j \quad i, j = 1 \quad 2.12$$

where: S is the compliance matrix which is the inverse of the stiffness matrix C . In expanded form, the equation (2.12) can be written in the following form,

$$\begin{bmatrix} \varepsilon_1 \\ \varepsilon_2 \\ \varepsilon_3 \\ \gamma_{23} \\ \gamma_{31} \\ \gamma_{12} \end{bmatrix} = \begin{bmatrix} S_{11} & S_{12} & S_{13} & 0 & 0 & 0 \\ S_{12} & S_{22} & S_{23} & 0 & 0 & 0 \\ S_{13} & S_{23} & S_{33} & 0 & 0 & 0 \\ 0 & 0 & 0 & S_{44} & 0 & 0 \\ 0 & 0 & 0 & 0 & S_{55} & 0 \\ 0 & 0 & 0 & 0 & 0 & S_{66} \end{bmatrix} \begin{bmatrix} \sigma_1 \\ \sigma_2 \\ \sigma_3 \\ \tau_{23} \\ \tau_{31} \\ \tau_{12} \end{bmatrix} \quad 2.13$$

where S_{ij} are the compliance coefficients ($[C]=[S]^{-1}$)

$$\begin{aligned} C_{11} &= \frac{S_{22}S_{33} - S_{23}^2}{S}, & C_{12} &= \frac{S_{13}S_{23} - S_{12}S_{33}}{S}, \\ C_{22} &= \frac{S_{33}S_{11} - S_{13}^2}{S}, & C_{13} &= \frac{S_{12}S_{23} - S_{13}S_{22}}{S}, \\ C_{33} &= \frac{S_{11}S_{22} - S_{12}^2}{S}, & C_{23} &= \frac{S_{12}S_{13} - S_{23}S_{11}}{S}, \\ C_{44} &= \frac{1}{S_{44}}, & C_{55} &= \frac{1}{S_{55}}, & C_{66} &= \frac{1}{S_{66}} \end{aligned}$$

where: $S = S_{11}S_{22}S_{33} - S_{11}S_{23}^2 - S_{22}S_{13}^2 - S_{33}S_{12}^2 + 2S_{12}S_{23}S_{13}$

The compliance coefficients for an orthotropic material in terms of engineering constants can be given as:

$$\begin{aligned} C_{11} &= \frac{E_1(1 - \nu_{23}\nu_{32})}{Q}, & C_{12} &= \frac{E_1(\nu_{21} + \nu_{31}\nu_{23})}{Q}, \\ C_{22} &= \frac{E_2(1 - \nu_{13}\nu_{31})}{Q}, & C_{13} &= \frac{E_1(\nu_{31} + \nu_{21}\nu_{32})}{Q}, \\ C_{33} &= \frac{E_3(1 - \nu_{12}\nu_{21})}{Q}, & C_{23} &= \frac{E_2(\nu_{32} + \nu_{12}\nu_{31})}{Q} \end{aligned} \quad 2.14$$

$$C_{44} = G_{23}; \quad C_{55} = G_{13}; \quad C_{66} = G_{12}$$

And,

$$Q = 1 - \nu_{12}\nu_{21} - \nu_{23}\nu_{32} - \nu_{31}\nu_{13} - 2\nu_{12}\nu_{23}\nu_{31} \quad 2.15$$

Where:

- E_1, E_2 and E_3 = Young's moduli in the 1, 2, and 3 directions respectively.
- $\nu_{12}, \nu_{23}, \nu_{13}$ = Poisson's ratios, (the first subscript denotes the loading direction, and the second subscript denotes the strain direction).
- G_{12}, G_{23} and G_{31} = Shear moduli in the 1-2, 2-3, and 3-1 planes respectively.

2.13 Structural Behaviour of FRP Piles

2.13.1 Behaviour under Axial Load

Fibre reinforced polymer (FRP) composites have been increasingly used in concrete construction. The application of FRP-tube confined concrete technique, has mostly been used in civil engineering field such as precast piles, girders, and pier columns [(Fam et al., 2003, Mirmiran and Shahawy, 2003)]. FRP technique provides an emerging and promising system for a variety of structural applications in which the tubes serve as a structural formwork. It is also shown to enhance both strength and ductility of concrete columns by providing confinement to the concrete core (Nanni and Bradford, 1995). The FRP tube can be used for confined of column element (Saadatmanesh et al., 1994), or as a pour form for new construction of cast-in-situ or precast columns (Mirmiran and Shahawy, 1996).

Several experimental studies have been conducted for evaluate the structural behaviour of FRP-tubes confined with concrete under axial compression. In the early 1980s, the concept of FRP-tube confined concrete was proposed by (Fardis and Khalili, 1981), who analyzed the behaviour of circular and rectangular FRP tube-confined concrete columns. These structures have shown several advantages over the traditional reinforced concrete columns. They have demonstrated an increase in the compressive strength and a reduction in structural weight. They have also shown that an FRP tube directly serves as a formwork and hence reduces the cost, increases the speed of construction, and improves the durability. A circular FRP tube system was proposed by (Mirmiran and Shahawy, 1996). In their works, the tube was a multilayer composite shell that consisted of at least two plies: an inner ply of axial fibres, and an outer ply of hoop fibres. It possessed the same advantages as that of the FRP tube proposed by (Fardis and Khalili, 1981).

Most researchers [(Mirmiran et al., 1998), (Purba and Mufti, 1999, Watanabe et al., 1997) and (Toutanji and Deng, 2002)] indicated a bilinear response for FRP-confined concrete specimens under axial loading. The bilinear response consists of two distinct regions as shown in Figure 2.15. In the first region, the behaviour is

similar to that unconfined concrete, since lateral expansion of the confined concrete is insignificant. The second region is recognized as that in which the FRP is fully activated, the stiffness is generally stabilized around a constant rate. The response of the region is mainly dependent on the stiffness of the FRP tube show a simplified stress-strain response of a concrete specimen confined with an FRP tube. The branches OA and O \bar{A} denote the first linear zone in axial and lateral direction, respectively. The branches AB and A \bar{B} denote the second linear zone in the axial and lateral direction, respectively. In the second zone of the stress-strain curve, the compressive stress and the confining pressure are variables and reach their maximum values when the FRP system fails.

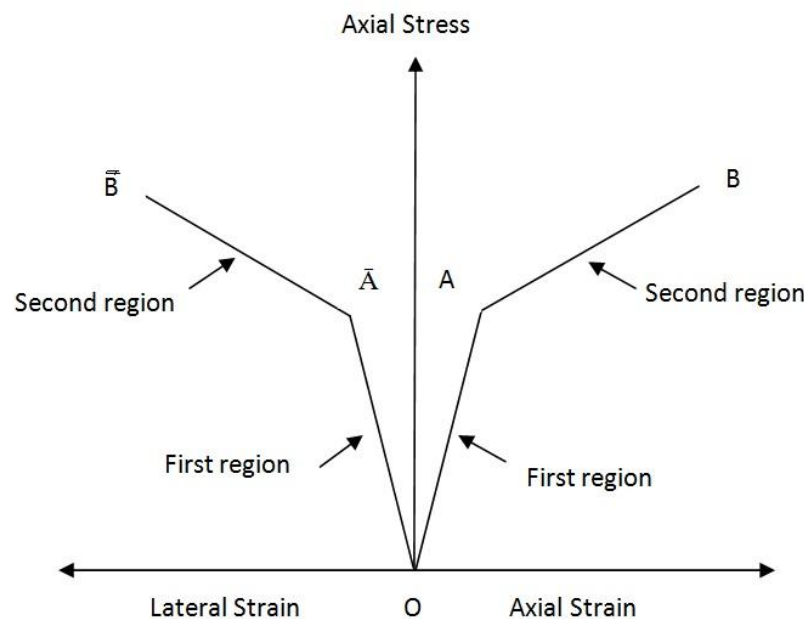


Figure 2.15: Simplified stress-strain curves of FRP tube confined concrete
(Saafi et al., 1999)

2.13.2 Mechanics of FRP Confinement

In most applications, the mechanism of lateral confinement provided by an FRP tube to concrete is passive in nature. When the concrete is subject to axial compression, it expands laterally. This expansion is confined by the FRP tube, which is loaded in tension in the hoop direction. As the FRP is subjected to tension in the hoop direction eventual failure occurs when its hoop tensile strength is reached. This failure mechanism dictates that the fibres, or the main fibres in cases when fibres in more than one direction are present, are oriented in the hoop direction. The confining action in FRP-tube confined concrete is schematically illustrated in Figure 2.16.

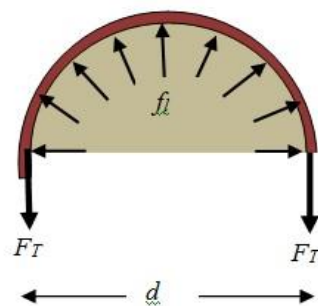
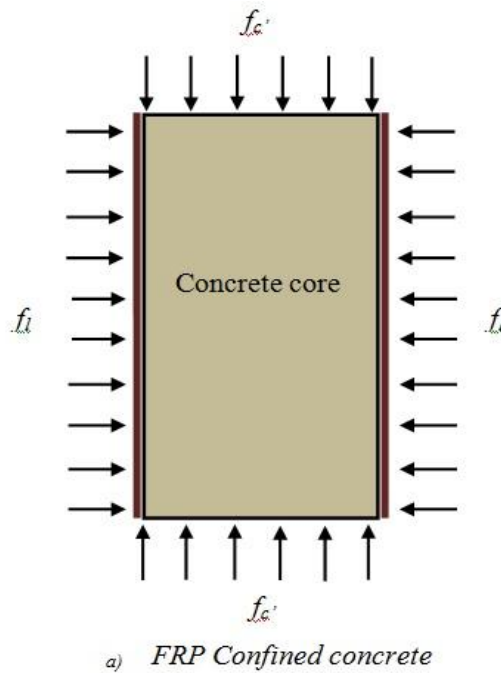


Figure 2.16: Confining action of fibre-reinforced polymer

However, it is expected that the structural behaviour of a FRP-tubes confined concrete will depend on the properties of the FRP tube and the core concrete. Several studies have concentrated on assessing the strength enhancement of different two FRP-tubes confined concrete in the literature. Some of the most important models in this field have been listed in Table 2.2 and most of these existing models for FRP-confined concrete adopted the concept of (Richart et al., 1929), in which the strength at failure for concrete confined by hydrostatic fluid pressure takes the following form:

$$f'_c = f_c \left[1 + k_1 \frac{f_l}{f_c} \right] \quad 2.16$$

where:

f'_c : Is the compressive strength of the FRP-tube confined concrete.

f_c : Is the compressive strength of the unconfined concrete.

f_l : Is the Hoop or (Lateral) confining pressure, and

k_1 : Is the confinement effective coefficient.

The maximum confining pressure exerted by the FRP tube is determined by assuming that the concrete fails when the wrap reaches its failure stress:

$$f_l = \frac{2t \times f_{FRP}}{d} \quad 2.17$$

Where:

f_{FRP} : Is the tensile strength of FRP material in the hoop direction.

d : Is the diameter of the confined concrete, and

t : Is the total thickness of the FRP tube,

Numbers of studies have been carried out on FRP confined concrete specimens, leading to a variety of models and equations for predicting the strength enhancement of FRP confined concrete. Most of these models are empirical in nature and have

been calibrated against their own sets of experimental data. However, for FRP assessment purposes, a new topographic chart for predicting the strength enhancement is an urgently needed step towards rational design guidelines. Therefore, an experimental data and large test database assembled from an extensive survey of existing studies is presented and employed to assess the strength enhancement of FRP confined concrete. The experimental and database results encompass a wide range of values of the significant variables and can therefore be used for a systematic assessment of FRP confined concrete based on the unconfined concrete and confinement lateral pressure.

Table 2.2: Expression of different models of strength enhancement of FRP confined concrete

Model No.	Author	Fibre Type	Ultimate Strength Expression (f'_c)	Ultimate axial strain (ϵ'_c)
1	Fardis and Khalili, (1981)	GFRP	$f_c + 4.1f_l$	$\epsilon_c + 0.001 \left(\frac{E_{FRP}}{df_c} \right)$
2	Saadatmanesh et al. (1994)	GFRP & GFRP	$f_c \left[-1.254 + 2.254 \sqrt{1 + \frac{7.94 f_l}{f_c}} - 2 \left(\frac{f_l}{f_c} \right) \right]$	$\epsilon_c \left[1 + 5 \left(\frac{f'_c}{f_c} - 1 \right) \right]$
3	Karbhari and Gao,(1997)	GFRP & GFRP	$f_c \left[1 + 2.1 \left(\frac{f_l}{f_c} \right)^{0.87} \right]$	$\epsilon_c + 0.01 \left(\frac{f_l}{f_c} \right)$
4	Mirmiran, (1997)	GFRP	$f_c + 4.269 \cdot f_l^{0.587}$	-----
5	Samaan and Shahawy (1998)	GFRP	$f_c + 6.0f_l^{0.7}$	-----
7	Saafi et al. (1999)	GFRP	$f_c \left[1 + 2.2 \left(\frac{f_l}{f_c} \right)^{0.84} \right]$	$\epsilon_c \left[1 + (537 \epsilon_l + 2.6) \left(\frac{f'_c}{f_c} - 1 \right) \right]$
8	Toutanji (1999)	CFRP & GFRP	$f_c \left[1 + 3.5 \left(\frac{f_l}{f_c} \right)^{0.85} \right]$	$\epsilon_c \left[1 + (310.57 \epsilon_l + 1.9) \left(\frac{f'_c}{f_c} - 1 \right) \right]$
9	Lam and Teng (2003)	CFRP & GFRP	$f_c \left[1 + 3.3 \left(\frac{f_l}{f_c} \right) \right]$	$\epsilon_c \left[1.75 + 5.53 \left(\frac{f_l}{f_c} \right) \left(\frac{\epsilon_l}{\epsilon_c} \right)^{0.45} \right]$
10	Teng et al. (2007)	CFRP & GFRP	$f_c \left[1 + 3.5 \left(\frac{f_l}{f_c} \right) \right]$	$\epsilon_c \left[1 + 17.5 \left(\frac{f_l}{f_c} \right) \right]$

Notes: f_c = compressive strength of unconfined concrete, f'_c =The compressive strength of the confined concrete. ϵ_c = ultimate strain of unconfined concrete. ϵ'_c = ultimate strain of confined concrete. ϵ_l = Hoop or lateral strain of GFRP or CFRP confined concrete, f_l = Hoop or Lateral confining pressure, E_{FRP} = Elastic modulus of FRP

2.13.3 Behaviour under Flexural Load

Pile foundations are structural members that give support and transfer loads from one structure to another. In the field applications, pile can be considered as a special type of column that carries axial and flexural loads but with different cases of boundary conditions. The application of the FRP tubes confined concrete technique is new and rapidly increasing in the field of civil engineering structures. Although the beneficial effects of confinement of concrete are less in flexural as compared to axially loaded members, other advantages such as utilization of the FRP tubes as stay-in-place framework, ease of fabrication and speed of erection still makes this system attractive. The FRP tubes system can be utilized successfully for different flexural structural members such as: piles, overhead sign structures, poles, bridge girders, pipes and tunnels. One of the earliest attempts to produce FRP/concrete beam elements was done by Fardis and Khalili, (1981). They simply proposed pouring concrete into FRP boxes. They also pointed out the mechanical role of FRP and concrete as follows:

1. FRP carries the tensile forces in the tension zone.
2. It provides partial confinement of concrete in the compression zone, enhancing strength and ductility.
3. The concrete core provides compressive strength and rigidity and prevents local buckling of the FRP casing.

In fact, extensive research programs have been conducted to investigate the behaviour of FRP tubes and FRP tubes confined concrete under pure compression load. Unfortunately, relatively few studies have focused on static flexural strength of FRP tubes confined concrete. Experimental investigation has been conducted on large-scale FRP tubes and control hollow GFRP and steel tubes tested in bending by (Fam and Rizkalla, 2002). The diameter of the beams ranged from 89 to 942 mm and the spans ranged from 1.07 to 10.4 m. The study investigated the effects of concrete filling, cross-sectional configurations including tubes with a central hole, tube-in-tube with concrete filling in between, and different laminate structures of the GFRP tubes. The study demonstrated the benefits of concrete filling, and showed that a

higher strength-to-weight ratio can be achieved by providing a central hole. It was concluded that the flexural behaviour was highly dependent on the stiffness and diameter-to-thickness ratio of the tube, and, to a much lesser extent, on the concrete strength. Test results suggested that the contribution of concrete confinement to the flexural strength was insignificant; however, the ductility of the member was improved.

Fam and Rizkalla, (2003) also investigated experimentally the flexural behaviour of concrete confined GFRP tubes ranging in diameter from 90 to 942 mm, using test results of eight beams. Figure 2.17 shows a typical test set-up for beams tested in bending using stroke control and four-point load configuration. It was found that in bending, concrete filling is more efficient for thin-walled tubes or tubes with low stiffness in the axial direction than it is for stiff or thick-walled tubes. It prevents local buckling and increases the flexural strength and stiffness. Fam and Rizkalla, (2003) reported that the flexural strength can be increased by increasing the wall thickness. However, the failure mode could change to compression. The balanced reinforcement ratio is dependent on the laminate structure of the tube and generally is smaller for tubes with higher stiffness in the axial direction.



Figure 2.17: Tests set up for bending tests on FR pile
(Fam and Rizkalla, 2003)

Mohamed and Masmoudi, (2012) carried out the experimental flexural program for a total of seven FRP tube confined concrete beams of 213 mm diameter and 2000 mm long. Five FRP tube confined concrete beams and two control specimens without tubes were tested under four-point bending as shown in Figure 2.18. One control specimen was reinforced with spiral steel while the other had no transverse reinforcement. The test parameters used in this investigation include the type of internal reinforcement (steel or glass fibre reinforced polymer bars), the type of transverse reinforcement (spiral-steel or fibre reinforced polymer tubes), fibre reinforced polymer tube thickness and the concrete compressive strength. Their test results indicate that the FRP tube enhances the crack and ultimate moment capacities of the test specimens, whereas it provides a longitudinal reinforcement on the tension side. In addition, improvement to the crack moment equation is suggested to account for the effect of confinement.

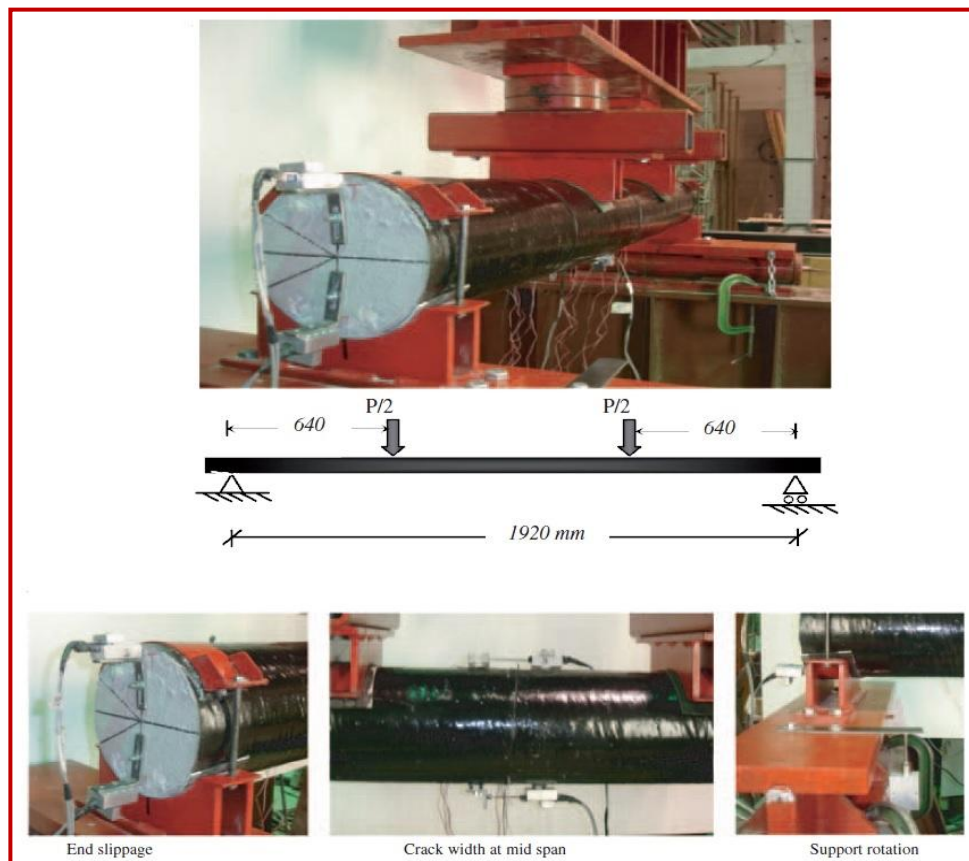


Figure 2.18: Test setup (Mohamed and Masmoudi, 2012)

To date, several studies on FRP tube confined to concrete have focused on the effect of flexural loads in short term condition (control condition). Accordingly, degradation of FRP materials in geotechnical engineering field such as buried in soils or waterfront environment is an important concern due to their lack of a long-term track record. Therefore, is an urgent need to assess the durability and behaviour of composite piling made of FRP in aggressive environment for long term usage in term of flexural strength.

2.14 Geotechnical Behaviour of FRP Piles

2.14.1 FRP Pile Response to Axial Loads

Few studies are available in the literature on FRP piles, probably due to their novelty. Han and Frost, (1999) examined buckling loads of FRP piles during installation and service life. Their study showed that critical buckling loads of FRP piles depend on the shear effect coefficient, the lateral soil resistance, the overall boundary condition, the embedment ratio, and the critical length. Pando et al., (2000) performed a full-scale pile load test using FRP tubes confined concrete and prestressed concrete piles. Their experimental test consisted of static axial load and lateral load tests. They found that the axial geotechnical capacities of the test piles decreased in order from the prestressed concrete pile to the FRP pile to the FRP pile. Mirmiran and Shahawy, (2003) conducted field tests using FRP tube filled concrete and prestressed concrete piles to evaluate their drivability. Their results showed that neither pile head damage nor separation between FRP tube and concrete core were observed when driving FRP-tube confined concrete. Fam et al., (2003) carried out a full-scale field test for two pile types (concrete filled FRP composite and prestressed concrete piles). At each level, two strain gages were placed near the two opposite faces of the pile, as shown in Figure 2.19 .

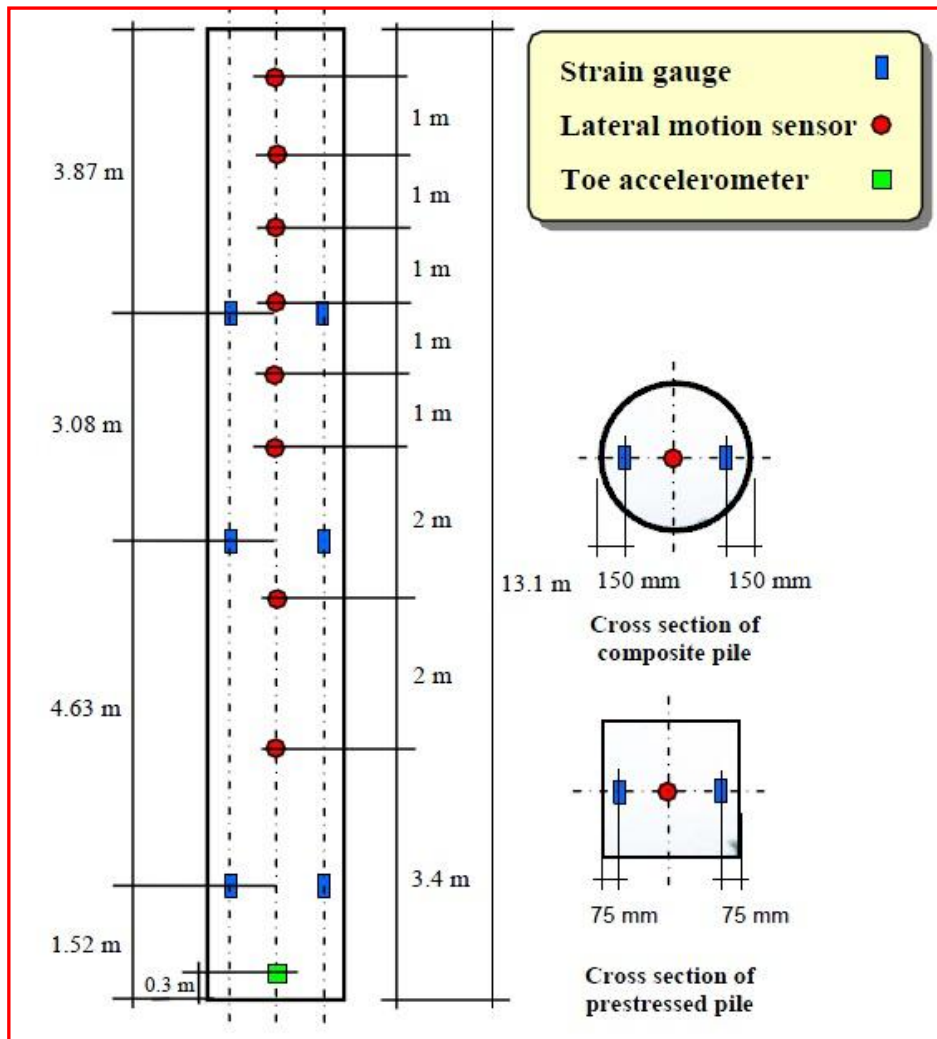


Figure 2.19: Test pile instrumentation (Fam et al., 2003)

Axial load tests were performed on both test piles seven days after pile driving. The equivalent static load versus pile head axial displacement for the prestressed concrete and FRP-concrete piles for the three cycles are shown in Figure 2.20.

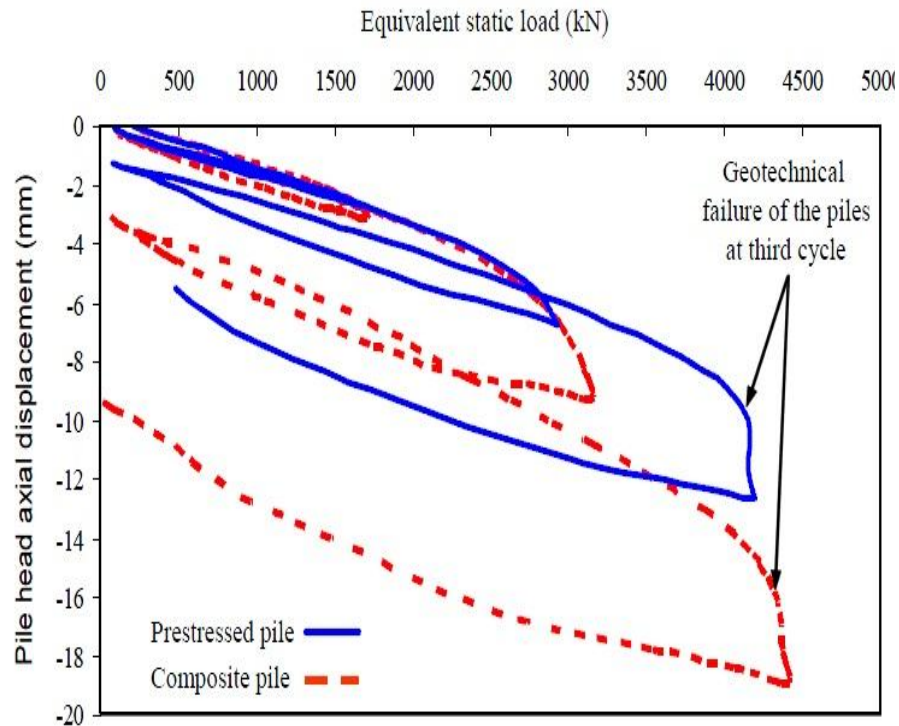


Figure 2.20: Pile displacement-axial static load (Fam et al., 2003)

2.14.2 FRP Pile Response to Lateral Loads

Pile foundations are commonly used to transfer vertical loads, arising primarily from gravity (e.g., the weight of a superstructure). Examples of structures where piles are commonly used as foundations are tall buildings, bridges, offshore platforms, defence structures, dams and lock structures, transmission towers, earth retaining structures, wharfs and jetties. However, in all these structures, it is not only the vertical loads that the piles carry; often the piles are subjected to lateral loads and moments. In fact, there are some structures (e.g., oil production platforms, earth retaining structures, wharfs and jetties) where the primary function of piles is to transfer lateral loads to the ground (Basu et al., 2008).

The lateral loads and moments may act on piles in addition to axial loads. The collapse of a pile due to lateral loads may occur in two modes. For short piles, the pile can rotate as a rigid body and failure can occur within the soil mass. Above the centre of rotation, passive soil pressure will develop in front of the pile, while below the centre of rotation, passive soil pressure will develop behind the pile, as shown in Figure 2.21a. For longer piles, a plastic hinge will develop at some depth down the pile shaft, and only the upper part of the pile will undergo significant displacement as shown in Figure 2.21b (Fleming et al., 2008). Therefore, the calculation of the failure load will be only based on the limiting pressure acting over the upper part of the pile above the plastic hinge.

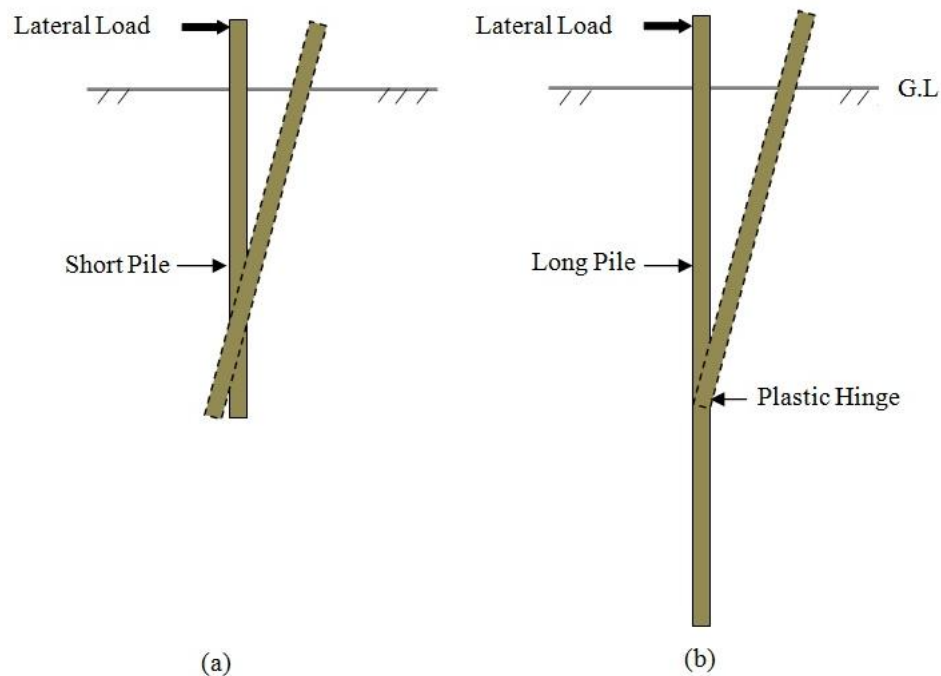


Figure 2.21: Definition of (a) short and (b) long piles in terms of lateral loading

Broms, (1964) provided solutions for the ultimate lateral resistance of a pile assuming a distribution of the lateral pile-soil pressure and considering the static of problem. Meyerhof, (1995) accounted for the effect of load eccentricity and inclination on the ultimate load capacity.

Several experimental studies have been conducted to examine the performance of traditional piles under lateral loads. Meyerhof, et al., (1988) conducted lateral load tests on single model piles and small group using different pile materials including steel, timber and nylon installed in loose sand and soft clay. They found that the relative stiffness of the pile (the ratio of stiffness of pile to soil stiffness) has a major impact on the lateral performance of tested piles. For the same conditions, higher lateral resistance is mobilized for the stiffer pile material than in the case of a flexible pile material. Mahmoud and Burley, (1994) carried out lateral load tests on circular and square short model piles installed in sand. They highlighted the important effect of the cross-sectional shape of the pile. EI-Naggar and Wei. (1999) conducted an experimental study on tapered and straight-sided steel piles in loose sand. Their test results showed an increase of the lateral capacity of tapered piles up to 77% compared to the equivalent cylindrical piles.

For composite piles, very little field information is available on lateral loading behaviour. Han and Frost, (1999) pointed out that in order to reasonably predict the load deflection response of a laterally loaded composite pile, the shear deformation effects should be taken into account. Fam et al., (2003) conducted lateral load test on both the concrete filled FRP composite and prestressed concrete piles. These two piles had the same width, but one with a circular cross-section and another with had a square cross section as shown in Figure 2.22. Their test system is similar to that used for the axial load test; however, the setup was placed horizontally in order to produce a lateral load. The equivalent lateral static load versus the lateral deflection behaviour of the two piles at the loading points is shown in Figure 2.23.

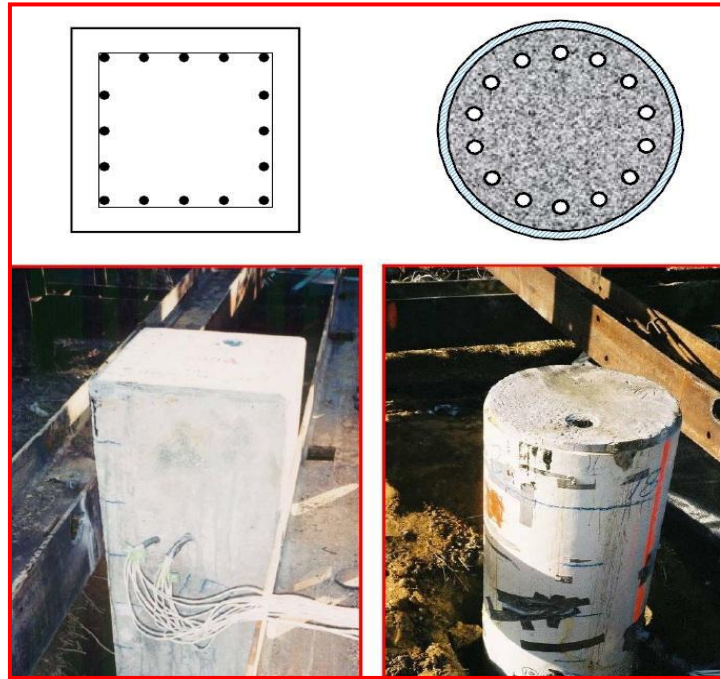


Figure 2.22: FRP composite and prestressed piles (Fam et al., 2003)

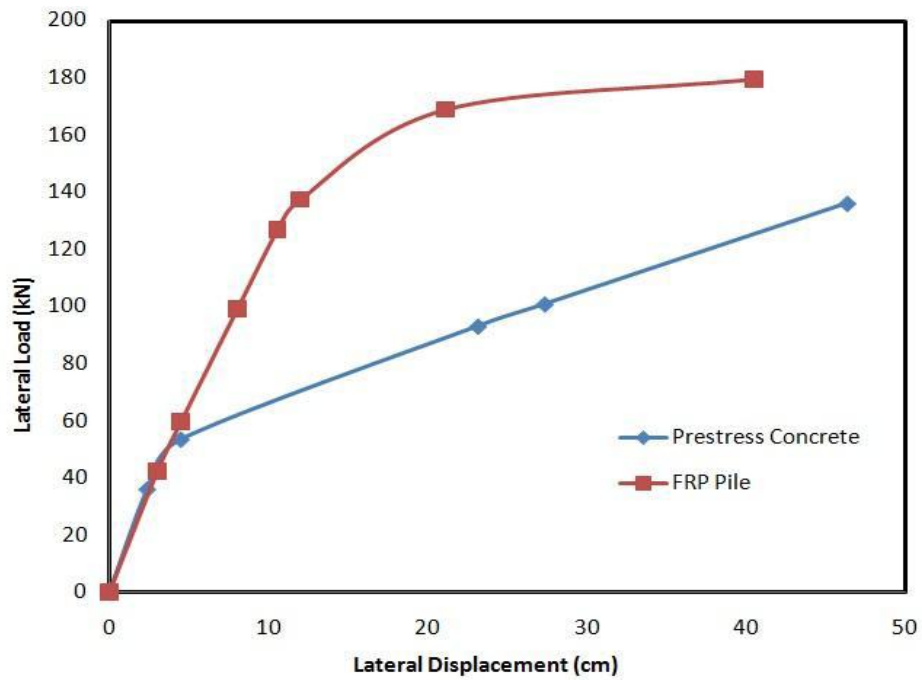


Figure 2.23: Lateral load-displacement response of pile (Fam et al., 2003)

Regrettably, few field and experimental tests available have studied the behaviour of FRP composite pile subjected to lateral loads and therefore, there is a dearth of experimental data. In fact, there is needed to improve and to gain a great understanding of the behaviour of FRP composite piles under lateral loading. Also, a further investigation must be assessed studies in this research. These parameters include; the type of FRP pile tube, the fibre tube configuration and sand properties.

2.15 FRP Surface Characterization

The primary reason for evaluating the FRP surface was because it is most directly relatable to the interface shear tests conducted as part of geotechnical study in this research. The most important characterization of FRP composite materials is mechanical surface properties. The mechanical surface properties include surface hardness and roughness. Hardness is the property of a material that enables it to resist plastic deformation, usually by penetration. However, the term hardness may also refer to resistance to bending, scratching, abrasion or cutting. Surface roughness is a quantitative measure of surface texture topography which describes the profile of the surface. Relatively, a little work has been performed into developing surface characterization methods applicable to geotechnical interfaces or to incorporate the results of these analyses into design procedures. However, this section is divided in two parts. The first part describes the roughness surface parameters which used to describe and quantify surface topography in this research. The second part describes in more details of the hardness testing methods.

2.15.1 Description of FRP Surface Roughness

The topography of most real surfaces is made up of superimposed waves of various wavelengths. The term “waviness” is used to describe long wavelength, high amplitude undulations on which a series of short wavelength, lower amplitude irregularities are superimposed. These short wavelength irregularities constitute surface roughness however, the length at which waviness becomes roughness is not

fixed but depends on the application and the length scales of interest (Dove et al., 1996).

Microtopography refers to one of these superimposed profiles at a localized region of the surface. This region could be on a peak of an asperity, side-slope or valley of a surface profile but does not include the overall surface topography. In geotechnical applications roughness of a surface must be defined in terms of the predominant length scales of soil grains at the interface. The surface roughness may be better defined in terms of the predominant length scales of sand soil grains at the interface. For example, study of microtopography may prove to be important in describing the surface roughness topography when fine-particles are placed in contact with FRP composite materials.

Quantification of surface texture typically involves asperity height and distribution, and computation of the index of surface roughness. Figure 2.24 presents a summary of a general terminology used to describe surfaces. Topography of surface refers to the “peaks”, “valleys” and “side slopes” and vertical relief between peaks and valleys that constitute a certain texture.

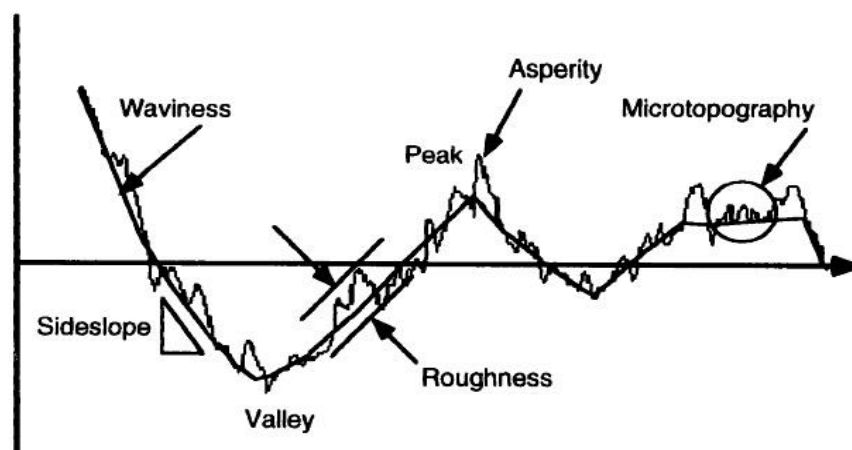


Figure 2.24: Terminology used to describe topography used by (Dove et al., 1996)

2.15.2 Surface Roughness Parameters

Various researchers have shown that the surface topography characterization has a predominant effect on the interface shear characteristics [(Potyondy, 1961), (Brumund and Leonards, 1973), and (Frost et al., 2002)]. Various roughness parameters have been developed to characterize the surface topography, which is of vital importance for interface shear behaviour.

In general, surface roughness is characterized by the asperity height and the spatial distribution of them across the surface. These parameters include average roughness (R_a), arithmetic mean roughness (R_q), Maximum Profile Peak Height (R_p), maximum peak to valley height (R_t), and the mean distance between peaks (R_{sm}). Figure 2.25 and Table 2.3 present the surface roughness parameters and definitions that are widely used to characterize the surface topography. Moore, (1972) stated that the distribution of asperity R_t and R_q are adequate to completely characterize the surfaces statistically. Kishida and Uesugi, (1987) and Paikowsky, (1995) used a “modified” (normalized) roughness parameter (R_n) in which the parameter (R_t) was scaled to the mean grain size of the soil particles (D_{50}).

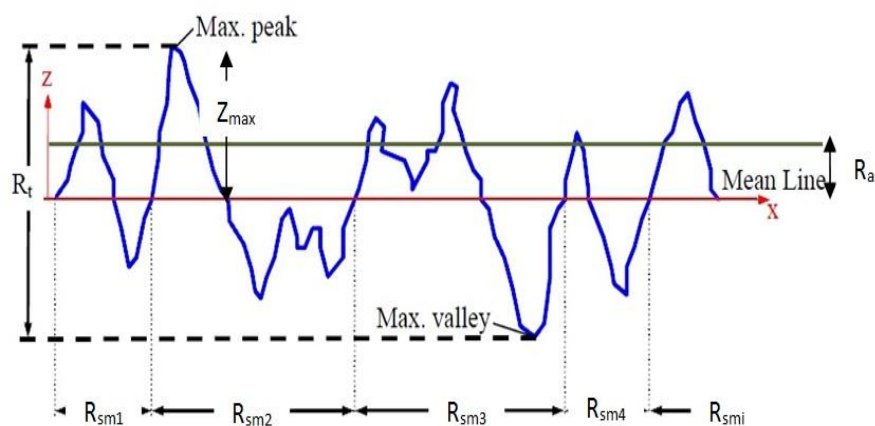


Figure 2.25: Surface roughness parameters

Table 2.3: Surface roughness parameters

Parameter	Source	Formula
R_a	(ISO-Standards, 1997) and (Whitehouse, 2010)	$R_a = \frac{1}{L} \int_0^L z(x) dx$
R_q	(Stachowiak and Batchelor, 1993) and (Whitehouse, 2010)	$R_q = \sqrt{\frac{1}{L} \int_0^L z^2 dx}$
R_p	(Whitehouse, 2010)	$R_p = \frac{1}{L} \int_0^L (z_{max} - z) dx$
R_n	(Kishida and Uesugi, 1987)	$R_n = \frac{R_t}{D_{50}}$
R_{sm}	(Whitehouse, 2010)	$R_{sm} = \frac{1}{N} \sum_{i=1}^N R_{smi}$

Early studies on interface behaviour in geotechnical engineering have been evaluated roughness surface by using qualitative terms such as “smooth” and “rough” or “textured” (Potyondy, 1961). Although this approach still has been adopted in several recent publications, more researches are interested in using quantitative methods to describe interface roughness (Dove and Frost, 1996), and (Uesugi and Kishida, 1986). Use of modified roughness parameter (R_n) is advancement over the use of (R_t) alone since the profile length considered is based on the size of the soil particle as shown in Figure 2.26. A modified roughness, R_n was defined by in Table 2.3 is clearly illustrated in Figure 2.26 (Kishida and Uesugi, 1987).

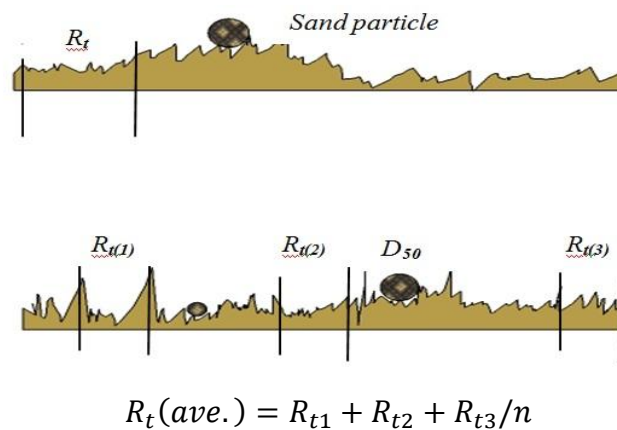


Figure 2.26: Definition of R_t and R_n (Kishida and Uesugi, 1987)

According to these most studies, the behaviour of an interface friction depends not only on the roughness of the material surface but also on the grain size of the soil in contact with it. However, use the modified roughness surface ($R_n=R_f/D_{50}$) is advancement over the use of (R_a) or (R_p) alone the profile length considered is based on the size of the soil particle. Also, the (R_{sm}) will be computed during the material surface profile measurements.

2.15.3 Profile Roughness Device

The classical stylus profilometer is the most popular method of making profile roughness measurements. It operates in a manner analogous to a phonograph and consists of a finely ground stylus, typically in the order of (5 μm) in diameter at the tip which in traversed over the surface at a controlled rate thereby making a recording of the profile, as shown in Figure 2.27.

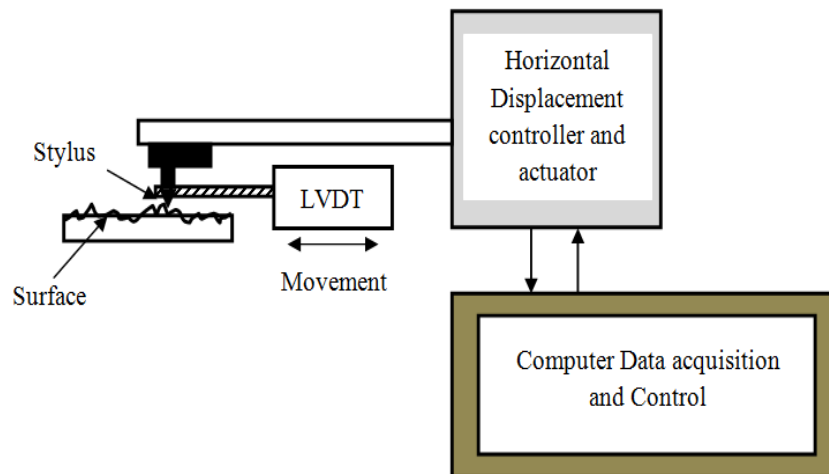


Figure 2.27: Schematic Diagram of Stylus Instrument

In this study, an available stylus profile instrument was used to measure the profile roughness parameters of tested materials as shown in Figure 2.28. This technique is described in more detail in chapter four.

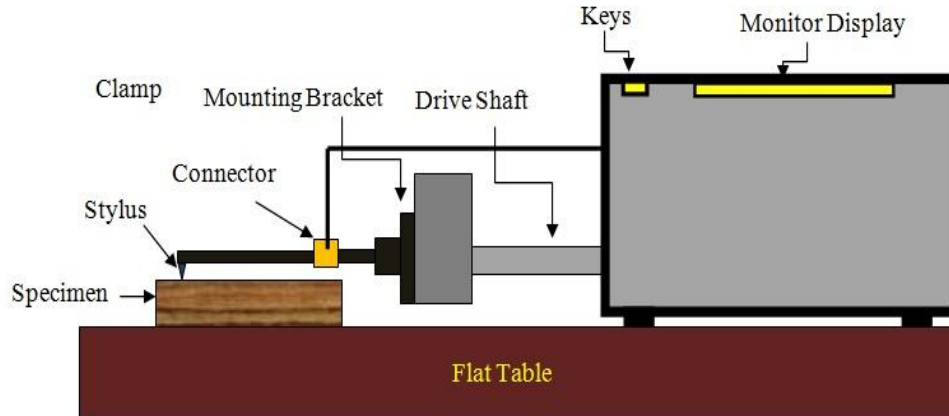


Figure 2.28: Schematic Diagram of Stylus instrument used in present study

2.15.4 Hardness Tests

Hardness is the property of a material that enables it to resist plastic deformation, usually by penetration. However, the term hardness may also refer to resistance to bending, scratching, abrasion or cutting (Alavdeen et al., 2006). Hardness which depends on stiffness and viscoelastic properties of the material is defined as the resistance of a plastic material to indentation (ASTM D2240-05, 2005). Presently, several testing methods are available, including the Brinell, Rockwell, and Vickers hardness testing methods. These methods are commonly used in material science and mechanical engineering. In general, they can determine indentation hardness of substances ranging from very soft materials, such as rubber, to very hard materials, such as steel, by using different scales. In this study, the Vickers hardness (HV) test method is used to determine the hardness number of tested materials. More details about this test are given in chapter four.

2.16 FRP/Soil Interface Mechanism

The design of structure systems where soil is in contact with construction materials such as concrete, steel or composites is widespread. Knowledge of the shear resistance at interfaces between soils and other materials is thus a key design consideration and is of interest in soil structure interaction problems. The geotechnical design situations shown in Figure 2.29 are examples of typical applications which occur in everyday practice and require knowledge of the interface behaviour of soil/material system. For example, the projects involving deep foundation systems as in Figure 2.29a which use driven piles, and drilled shafts. A deep foundation is loaded by the superstructure; the resisting force is initially generated by the mobilization of shaft friction. As the load increases, a portion of the resistance is provided by end bearing. The distribution of the resistance between side friction and end bearing is strongly influenced by the soil conditions and local construction practice. Knowledge of interface friction behaviour is also important in-situ soil characterization methods for other examples in Figure 2.29. In geotechnical engineering, the strength of an interface is described through the coefficient of interface friction, $\tan \delta$. Throughout this research, this is defined as:

$$\tan \delta = \frac{\tau}{\sigma} \quad 2.18$$

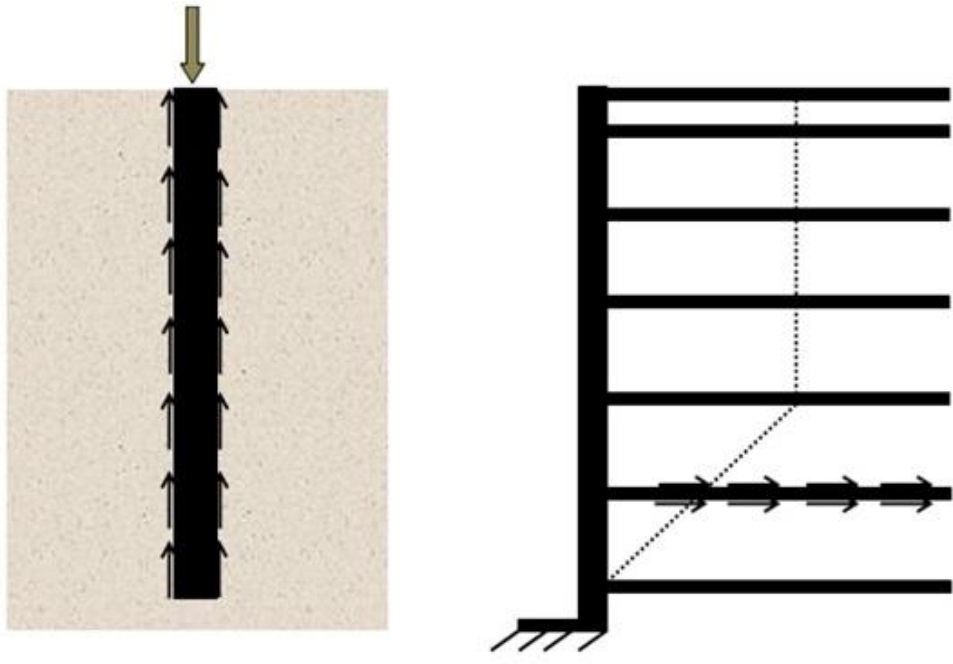
where:

τ : Shear strength,

σ : Applied normal stress, and

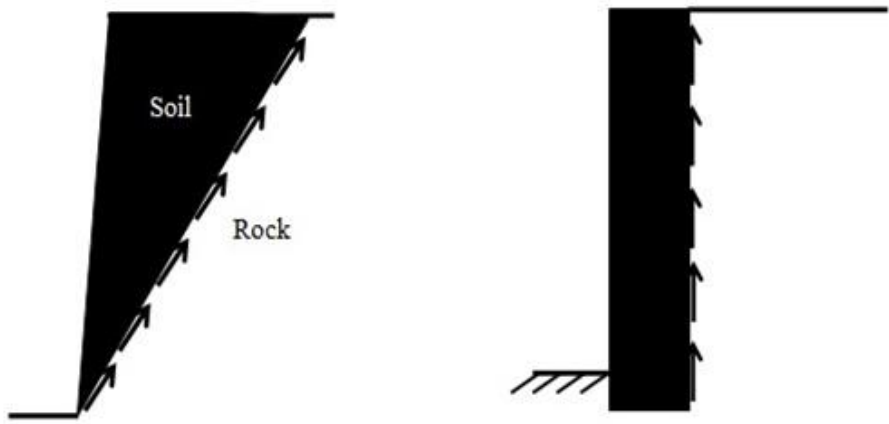
δ : Interface friction angle between construction material and soil.

The information related to interface shear strength of FRP and granular soil mechanism is evaluated in this study. A review of factors controlling the interface shear behaviour of FRP/granular soil interfaces will be provided. Those factors are generally considered in evaluating the interface shear strength of these interfaces and must quantitatively be estimated to fully understand the mechanism of interface shear response and development of shear stress-displacement curves.



a) Pile Foundation

b) Reinforced Structure



c) Slope Stability

d) Retaining Wall

Figure 2.29: Examples of Geotechnical Interfaces

2.17 Interface Test Apparatus

Reliable laboratory test needs appropriate apparatus. Table 2.4 reviews the various types of interface apparatus. Each type of apparatus has advantages as well as disadvantages. These characteristics are summarized as follows:

Among these apparatus, an annular shear apparatus does not suit for the element tests of interface friction. It is indeed geometrically similar to the interface friction of pile. The normal stress on the interface, however, is higher than the confining pressure (Kishida and Uesugi, 1987).

For the other three types of apparatus, the ring torsion type is theoretically most idealistic: it has the endless interface. The endless interface enables it to avoid the non-uniformity of normal and shear stresses at the ends of the interfaces. A ring torsion apparatus, however, involves many technical difficulties. The operator must be highly skilled and extremely careful in preparing uniform sand with a uniform shaped surface. The surface of the metal ring must be finished evenly. The metal ring must be seated on the sand surface evenly and in the correct position.

The direct shear box is a more commonly available piece of apparatus and much easier to use. It can produce consistent results for its simplicity. It is also, an automated apparatus that uses feedback from vertical and horizontal load cells and displacement transducers to provide real-time control of vertical and horizontal loading. The principle of the direct shear box is very simple. A normal load F_N is applied to the top box to produce a vertical normal stress $\sigma = F_N / A$, where A is the cross-sectional area of the direct shear box. A steadily increasing displacement, which causes an increasing shear force F_N , is applied to one half of the direct shear box, while the other half is restrained and equipped with a load measuring apparatus.

Similar to in direct shear testing, if a mass of soil is made to slide on the surface of FRP, steel and concrete materials while a normal load is applied normal to the sliding surface, a test similar to that described above can be carried out to determine

the frictional characteristics of a construction/soil interface. This forms the basis of the interface shear test which can be used to measure the angle of interface shearing resistance. The horizontal displacement of soil in the bottom half of the box relative to that in the top half takes place gradually while the force F_N is increasing. Eventually a maximum shear stress (point B in Figure 2.30) is reached, which is termed the peak shear stress. After the peak, the shear resistance falls off as shown by region BC, at this stage it is considered that the failure of the interface has occurred. However, an available direct shear apparatus was modified to enable the testing of sands and FRP interfaces. More details on character sets are given in Chapter four.

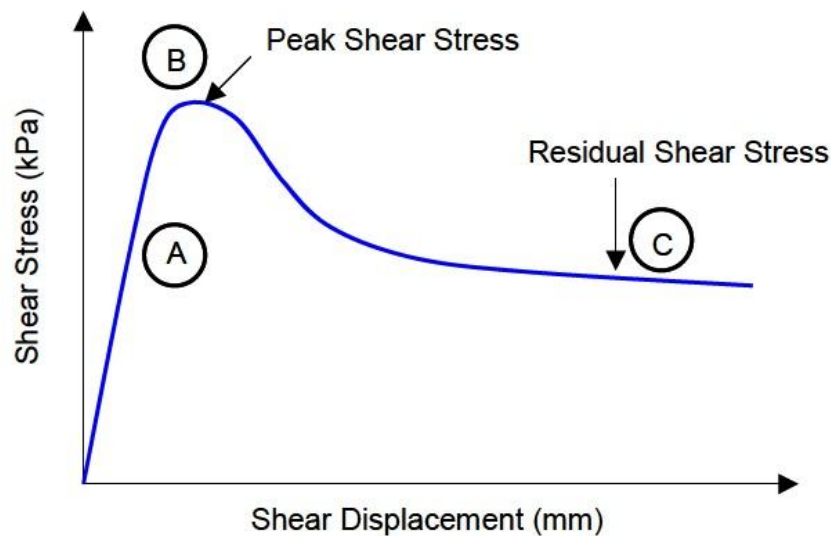
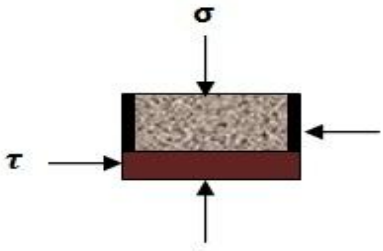
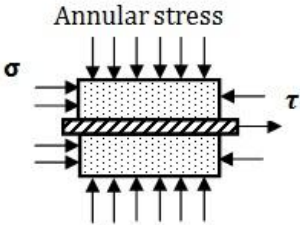
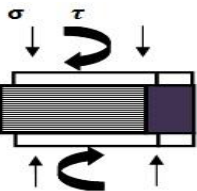
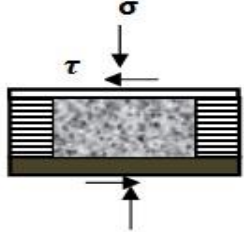
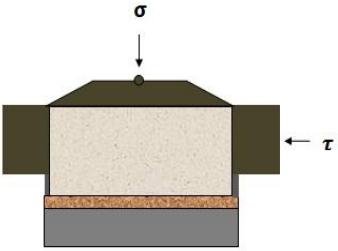


Figure 2.30: Typical plot of shear stress-displacement

Table 2.4: Advantages and disadvantages of interface testing apparatus

Testing Apparatus	Apparatus Name	Reference	Advantages	Disadvantages
	Direct shear	<ul style="list-style-type: none"> • Potyondy, (1961) • Desai et al., (1985) • Uesugi and Kishida, (1986) 	<ul style="list-style-type: none"> • Commonly available device • Simple preparation and operation. • Simple procedure • Solid surface can be either above or below soil sample 	<ul style="list-style-type: none"> • Displacement factors not separated. • Interface area may change shear.
	Annular shear	<ul style="list-style-type: none"> • Brumund and Leonards, (1973) 	<ul style="list-style-type: none"> • Geometrically similar to pile shaft 	<ul style="list-style-type: none"> • Normal stress unknown. • Stress concentration at the ends
	Ring torsion	<ul style="list-style-type: none"> • Yoshimi and Kishida, (1981). • Lemos, (1986) 	<ul style="list-style-type: none"> • No end effect "endless" • Constant interface area. • Displacement factors can be observed by x-ray photo 	<ul style="list-style-type: none"> • Complicated system and procedure. • Difficult to prepare uniform sand mass in a ring shape. • Solid overlying the soil.

Continued

Testing Apparatus		Reference	Advantages	Disadvantages
	<p>Simple shear</p>	<ul style="list-style-type: none"> • Uesugi and Kishida, (1986) • Uesugi et al., (1990) 	<ul style="list-style-type: none"> • Constant interface area, • Displacement factors can be measured separately • Simple preparation 	<ul style="list-style-type: none"> • Stress concentration at ends
	<p>SB 1 Shear box</p>	<ul style="list-style-type: none"> • Present Work 	<ul style="list-style-type: none"> • Constant interface area, • Test operation is relatively easy • Simple procedure. • Tests can be performed relatively quickly. • Suit for traditional and composite construction materials • Displacement factors can be measured separately 	<ul style="list-style-type: none"> • Soil sample cannot be tested under that more closely approximate those in the field • Soil deformation cannot be observed

The interface friction between pile construction materials and soil is by no means a trivial problem in geotechnical engineering. Many studies have shown the importance of the interface friction between construction materials and soils. Potyondy, (1961) has probably been one of the chief sources of design interface friction values for steel counter faces for the last five decades. Potyond's work involved determination of "interface friction" between different soils and construction materials. He performed stress and strain controlled interface shear tests using sand, clay, silt and mixture of sand and clay. The construction materials consisted of "smooth" and "rough" steel, wood (parallel and perpendicular to the grain and "smooth" and "rough" concrete. The qualitative descriptors "smooth" and "rough" were used since no interface characterization was performed. Potyondy found, that the friction coefficient for dense dry silt and sand decreased when the normal stress was increased from 48 to 144 kPa. The magnitude of this decrease was approximately 1 degree for steel, 2 degrees for wood, and 1 to 2 degrees for concrete. For saturated dense sand, the friction coefficient decreases only slightly for these surfaces. Potyondy concluded that interface friction was dependent on moisture content, surface roughness and soil type and gradation.

Yoshimi and Kishida, (1981) evaluated the friction of granular materials against machined low carbon structural steel specimens using a ring shear apparatus. The unique aspect of this work is that the authors quantified the surface roughness of steel specimens specially machined to varying roughness in a highly non-symmetric ruled surface texture pattern. They evaluated the roughness of the specimens using the parameter R_t , as measured using a stylus profilometer. The soils used in the tests were Toyoura, Tonegawa, and Nigata sands which had relatively small mean grain sizes (D_{50}) of about 0.2 mm, 0.27 mm, and 0.57 mm respectively. Tests were performed at normal stresses of 105 kPa and at relative densities of 40% to 90%. They found that the coefficient of friction increased with the increasing surface roughness. It was also observed that the relative density had little effect on the measured friction coefficient.

Kishida and Uesugi, (1987) used a simple shear apparatus to measure the interface friction coefficient between sand and steel, as shown in Figure 2.31. They used a

modified roughness parameter R_n . The steel counterface were machined to varying roughness and sieved Toyoura sand with D_{50} of 0.19 mm was used for the tests which were performed at normal stresses of 78 kPa. The results showed that as roughness increased, the interface friction also increases with an approximately linear relationship up to a roughness value where shear failure occurred in the soil and not at the interfaces.

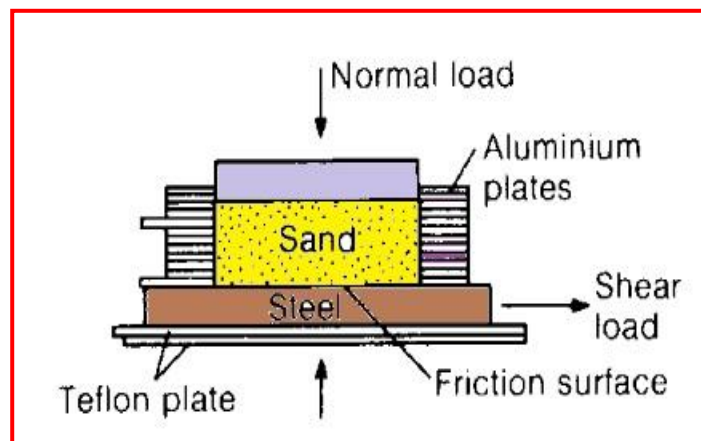


Figure 2.31: Simple shear apparatus used by (Kishida and Uesugi, 1987)

O'Rourke et al., (1990) made a detailed study of the behaviour of Ottawa sand in contact with smooth HDPE and polyvinyl chloride (PVC) geomembranes and PVC pipe. It was found that the hardness of the counterface relative to the soil influenced the shear mechanisms on smooth HDPE/Ottawa sand interfaces. They proposed that the primary shear mechanisms were sliding and rolling based on observations of the scars in the geomembrane after shear.

Paikowsky, (1995) examined the distribution of friction forces between granular materials and aluminium using a specially developed dual interface apparatus. The granular materials examined include four sizes of glass beads and Ottawa sand. Counter surfaces were prepared by either machining, sand blasting or grinding the aluminium. The normalized roughness parameter, R_n , as proposed (Kishida and Uesugi, 1987) was used to describe the relative roughness. The results of this investigations showed that interface friction angle of Ottawa sand on aluminium and steel increased from 14° (smooth) to 47° (rough).

2.18 Soil Particle Shape

The soil particle shape (i.e. rounded versus angular) in contact with construction materials is one of the other important factors in defining of interface shearing mechanism (i.e. sliding, rolling, ploughing) developed at the interface during shearing. The behaviour of particulate materials with different surface was studied by (Frost et al., 1999). They evaluated different sand/structures adjacent to the interface during shearing with a typical direct shear box. They reported that the shear mechanisms for sub-rounded and angular uniform sands adjacent to geomembranes were directly influenced by the surface roughness of the geomembranes material as follows:

- The mechanism of failure for smooth surfaces was sliding of the particles along the interface with minor changes in density up to a distance of two particle diameters ($2 \times D_{50}$).
- The size of the affected zone within the soil sample increased to a distance of six particle diameters ($6 \times D_{50}$) from the interface as the geomembrane surface becomes rougher.

In addition, (Dove and Frost, 1999) have shown that the main component of the interface friction force was ploughing at all normal stress levels for interface shear tests conducted with angular blasting sand as opposed to sub-rounded to rounded Ottawa 20-30 sand. They pointed out that the increased amount of wear/scar on geomembrane surface after shearing directly corresponds to increased force due to ploughing, and consequently, increased shear stress at the interface. They concluded that the interface shear strength for granular soil-geomembrane interfaces are controlled by the mechanisms of friction acting during shearing such as slippage, rolling, or ploughing which depends on sand particle angularity in addition to normal stress level at the interface and relative hardness of counterface materials.

Figure 2.32 presents the typical strength envelopes from direct interface shear tests reported by Dove and Frost (1999) where the friction angles were determined from

traditional linear fit-line regression of their data. They mentioned that the blasting sand (angular shape) has exhibited higher friction coefficient and the spherical glass micro-beads gave the lowest interface friction angle. Ottawa 20-30 sand had a friction coefficient intermediate between the blasting sand and the glass micro-beads. All the particulate materials used in their study had similar mean grain size (D_{50}). The only difference was the shape/angularity of the particulate materials selected to be sheared against smooth geomembranes.

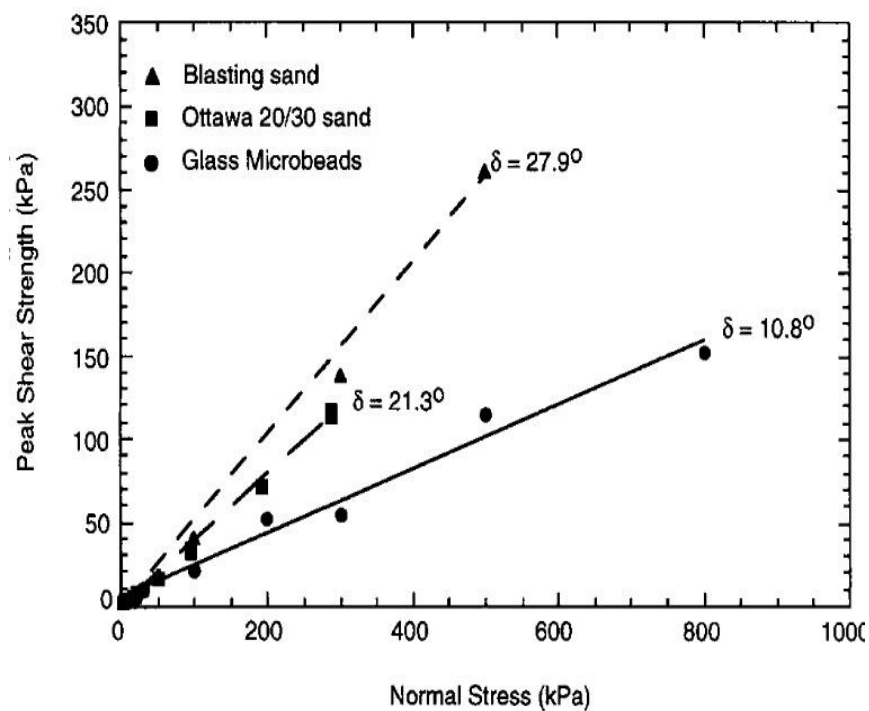


Figure 2.32: Strength Envelopes from interface shear tests on peak interface shear response between particulate materials and smooth geomembranes (Dove and Frost, 1999)

2.19 Mean Grain Size (D_{50})

The mean grain size of the granular soil particles (D_{50}) in contact with the FRP composite surface could be effect on the coefficient of interface friction (μ_p). An experimental study of FRP/sand interface was studied by (Frost and Han, 1999) using a typical direct shear apparatus. They showed that the peak interface friction coefficient between (FRP) composite and sand decreases as the mean grain size (D_{50}) increases as shown in Figure 2.33 . It was mentioned that this finding concurs with that of (Rowe, 1961) that large particles have a lower friction angle than small particles with the same mineralogy when a mass of the particles slides on identical rough surfaces. This conclusion of this study was supported by the results of Frost and Han (1999) such that two data points of Ottawa 20-30 sand (OTW) falls within the range of the data for glass beads which is due to both Ottawa 20-30 and glass beads (GB) having the same mineralogy and round particle shape. Furthermore, it was point out that Valdosta Blasting Sand (VBS) reasonably had a higher interface friction coefficient than that of Ottawa 20-30 and glass beads as it is an angular material.

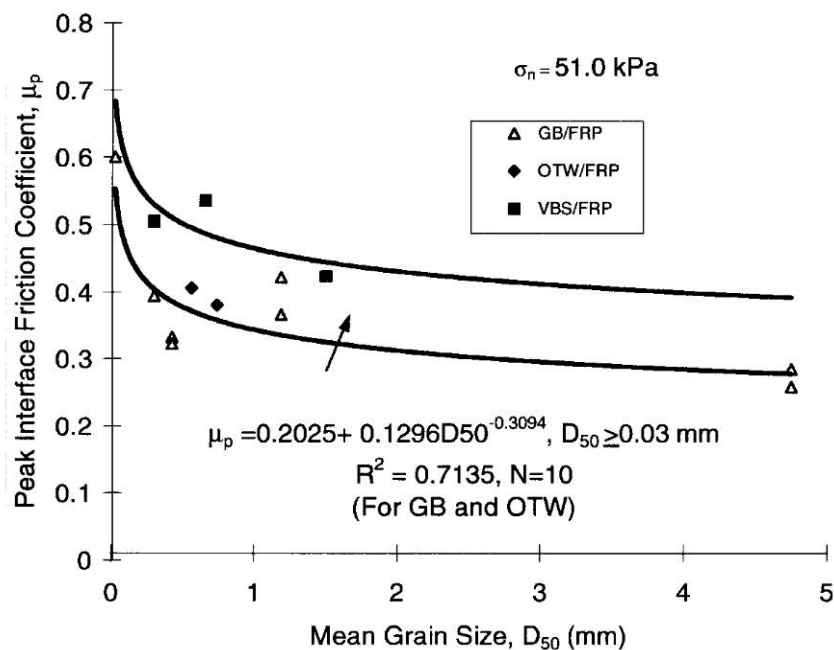


Figure 2.33: Influence of (D_{50}) on μ_p (Frost and Han, 1999)

2.20 Soil Density

The initial density or state of granular materials influences the shear strength developing at the interfaces in addition to its significant effect on the “internal” friction angle (ϕ) of the particulate material itself. Frost and Han, (1999) explained that the peak internal friction angle for specimens in a loose state is close to the friction angle at steady state, although the difference increases with an increase in relative density based on the experimental results and observations obtained from interface shear tests of FRP composite sands having different particle angularity. This statement is also consistent with the steady-state theory revealed by (Vaid et al., 1990) The typical relationship between peak interface friction angle and relative density at a fixed normal stress with tests on angular Valdosta Blasting Sand (VBS) is shown in Figure 2.34. The interface friction angle increases with relative density while the friction angle at steady state remains constant.

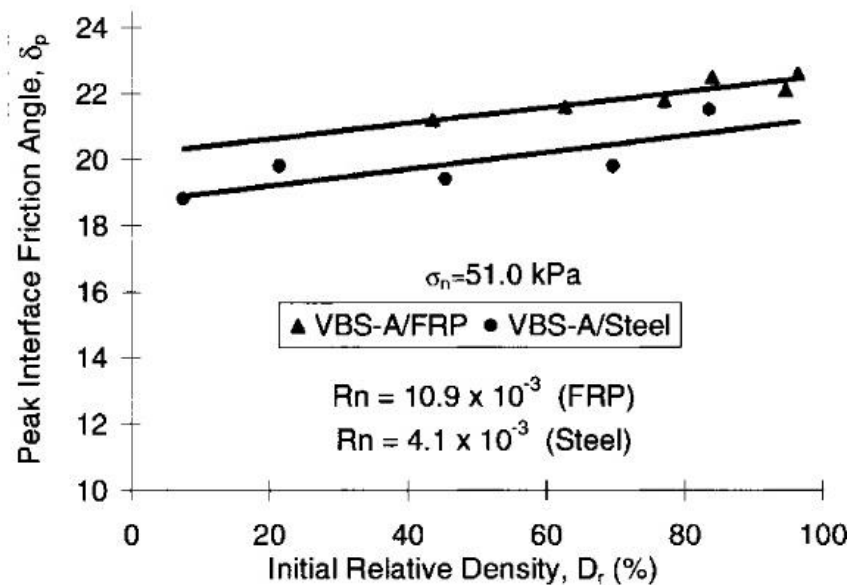


Figure 2.34: Relationship between interface friction angle and relative density (Frost and Han, 1999)

2.21 Long-Term Study

As mentioned before, FRP composite materials have recently been used in civil engineering construction with apparent success. Due to its application in an environment that can contain significant amounts of chemicals, strength degradation may pose a risk to its durability. The degradation of polymers upon exposure to adverse conditions depends on the macromolecular structure, the presence of additives, and the presence of contaminants commonly present in FRP materials. The principal result of this degradative mechanics is the loss of mechanical strength that may lead to unfavourable engineering performance and a shorter life cycle. Pando et al., (2002) conducted a study on the durability of FRP tube confined concrete piles. They stressed that the primary mechanisms of strength and stiffness loss considered are related to moisture absorption, fibre/matrix interface damage, and stress crack corrosion of the fibre and matrix degradation through chain scission. Moisture content of submerged FRP composites increases through diffusion. The absorbed moisture can act as a plasticizer of the composite resin, and can cause matrix cracking, fibre-matrix debonding, and corrosion of glass fibres. For instance in the study of Pando et al. (2002) , the recorded strength and stiffness reductions was on the order of 20% and 5%, respectively, for E-glass/vinyl ester composites submerged in 25 degrees Celsius water for a period of 200 days. The implications of such strength and stiffness reduction on the design of composite piles can be significant, especially in deflection critical designs.

However, the ageing environment on FRP has a significant effect on the physical and mechanical engineering properties of polymers such as compressive and tensile strength. While, the effect of ageing environment on the interaction of these materials in contact as occurs at interfaces between FRP and granular materials have not yet covered in the existing literature of FRP-geotechnology. Therefore, the current study attempts to investigate the influence long-term aging environment on the interface friction behaviour of FRP composite materials. The major contribution to the interface friction is particles behaviour at the damage touching topography. The study is concentrated on the details of the FRP surfaces, sand particles

behaviour, and acceleration conditions. Accordingly, degradation of FRP materials immersed in aggressive environment is an important concern due to their lack of a long-term interface track record.

2.22 Numerical Studies

The Finite Element Method (FEM) is a numerical method which can approximate and solve complex geotechnical problems to within acceptable boundaries. The FEM analysis can be achieved through the use of many sophisticated many software packages such as (ADINA, ABAQUS, CRISP, FLAC, and PLAXIS). Many FEM studies have been performed by various researchers to investigate the vertical and lateral responses using traditional piles [(Trochanis et al., (1991) Khodair and Hassiotis, (2005), and Zhan et al., (2012)]. Unfortunately, there is a lack in the numerical studies related to use FRP composite materials as piling foundation. Therefore, a Finite Element (FE) model using ABAQUS is developed to validate the experimental results. This study is also provided more detailed understanding of the important parameters governing the FRP pile response under axial and lateral loads.

2.23 Summary

This chapter has reviewed records and information related to the FRP used in this research. Significance is given to history, material types and properties, structural behaviour, geotechnical performance, and durability of FRP composite piles. Results of the literature review shows that there has only been a limited study on the geotechnical performance of the composite piles. There is a necessity for more experimental tests to carefully assess and verify the geotechnical performance of the composite piles to be used in developing reliable design procedures. Additionally, the geotechnical properties of the FRP materials at the interface defining the shear behaviour and the state of the interface as well as the interface friction and contact behaviour between FRP materials have not been described extensively. The literature review indicates that the following knowledge gaps exist:

- The existing FRP models for confined concrete, mainly FRP-confined concrete need further study to propose a unified and specific expression to predict the peak stress and corresponding strain.
- The interface friction behaviour between FRP and sand particles involves many aspects which include equipment, factors affecting interface shear behaviour, analysis of the data and the interpretation of the results. Each one of these topics has many aspects. The presence of FRP in contact with soil makes the study even more complicated and it demands study of the interfaces from the point of view of tribology science.
- To date, the long-term interface friction behaviour for FRP materials has not yet studied and needs a further attention to understand the effect of long-term condition on FRP composite materials.
- The use of FRP composite material in civil engineering was started a few years ago and is still very limited due to the shortage in knowledge of the structural and geotechnical behaviour of these materials. Research studies

and database related to the use FRP composite material as piling foundation is very limited (Han, 1997) and (Pando et al., 2006). Therefore, further research is needed in this area to provide better understand of the behaviour of FRP composite piles under different conditions.

- Further numerical studies are needed to investigate the FRP materials for pile foundation. The previous FE studies relatively did not address the FRP tube as piling foundation.

CHAPTER THREE: STRUCTURE BEHAVIOUR OF FRP TUBES CONFINED CONCRETE

3.1 Introduction

Over the last few years, the application FRP tube confined concrete for different structural applications (piles, column, girder, bridge piers) has been started. The FRP tubes benefits are in confinement, protective purposes, and providing strength enhancement. Despite a large research effort, a proper model to predict the behaviour of FRP confined concrete has not yet been established. Most of the available models are empirical in nature and have been calibrated against their own sets of experimental data. This chapter presents the results of an experimental investigation concerning the compressive behaviour of FRP tubes confined concrete. The experimental work can be divided into two phases. The first phase involves the experimental results describe axial compression test results of 24 concrete cylinders confined FRP tubes. Three batches of concrete representing lower, medium and higher and one mortar batch were used. Two types of FRP materials (CFRP and GFRP) were utilized to in different configuration. In addition, a large database was assembled from an extensive survey of existing studies and employed to assess the experimental results for FRP-confined concrete. Finally, a new topographic chart was proposed to predict the strength enhancement of FRP confined concrete based on the unconfined concrete strength and FRP lateral confinement.

FRP composites represent an alternative construction material without many of the performance disadvantages of traditional materials. The use of FRP as a pile material can eliminate deterioration problems of conventional piling materials in waterfront environments and aggressive soils. This research also presents the preliminary results of an experimental study conducted to assess the durability of piling made of FRP in aggressive soils for long-term usage in foundation engineering applications. An accelerated testing protocol permitting prediction of the behavior of plastic piles was developed. Specimens were exposed to solutions with fixed acidic ($\text{pH}=2$), and

basic (pH=12) at elevated temperatures (Juran, 2001). An aging testing protocol permitting prediction of the flexural behaviour of FRP was developed. Both CFRP and GFRP specimens were exposed to different aggressive environments (acidic and alkaline) at 45°C elevated temperature (3 years aging time estimation). The long-term time of the FRP confined concrete specimen was estimated based on the time shift factor suggest by (Riebel and Keller, 2007). They explained that the acceleration of the chemical reactions using higher temperatures thereby enables long-term strength predictions.

A comparison between the flexural control results and those predicted in the long-term is presented. The lack of long-term performance and durability data of FRP composites is an important concern that must be addressed to permit confidence in the use of these materials for long-term load-bearing applications. The specimens were instrumented to measure the behaviour in terms of the load-deflection and load-strain responses.

3.2 Experimental Program

3.2.1 Tested Materials

3.2.1.1 FRP Tubes

Two types of FRP tubes, carbon and glass fibre reinforced polymer tubes (CFRP and GFRP), were used in this program. Table 3.1 presents detailed descriptions of the FRP tubes including their diameter, wall thickness, fibre laminate configuration and the Young's modulus (E_{11} and E_{22}) which were provided by the manufactures. The laminate configuration of CFRP tube is consists of 85% unidirectional layers Toray T700 which is the carbon fibre layers oriented at 0° and 15% E-glass fibres oriented at 90°. The E-glass (80/20) refers to the fact that the unidirectional material is actually only 80% unidirectional (UD) with 20% of the fibre which is oriented at 90°. Whereas, the GFRP laminate configuration tube is composed of core layers 90% unidirectional layers oriented at 0°, middle layers 6% oriented at 90° and 4% oriented at direction $\pm 45^\circ$.

Table 3.1: Mechanical properties of FRP tubes

Tube type	Unit	CFRP*	GFRP
Outer diameter	mm	63.0	60.0
Wall Thickness	mm	2.0	2.2
Fibre orientation	----	[0°/90°/0°/90°/0°]	[0°/90°/±45°]
Longitudinal Modulus, E_{11}	MPa	135000	50000
Transverse in-plane Modulus, E_{22}	MPa	10000	40000

*0° layers are Toray T700;
90° layers are E-Glass(80/20).

3.2.1.2 FRP Hoop Testing

Tensile properties in the hoop direction were evaluated using the split disk test method. The split disk tests were performed in accordance to ASTM D-2290-08 (ASTM 2008a). The hoop tensile properties of both CFRP and GFRP tubes were determined by testing three specimens cut from each tube in the longitudinal direction. Then, the surfaces of tube specimens were cleaned and instrumented by two strain gauges. Figure 3.1 shows the details of the test tube coupon and location of strain gauges on the specimen surface.

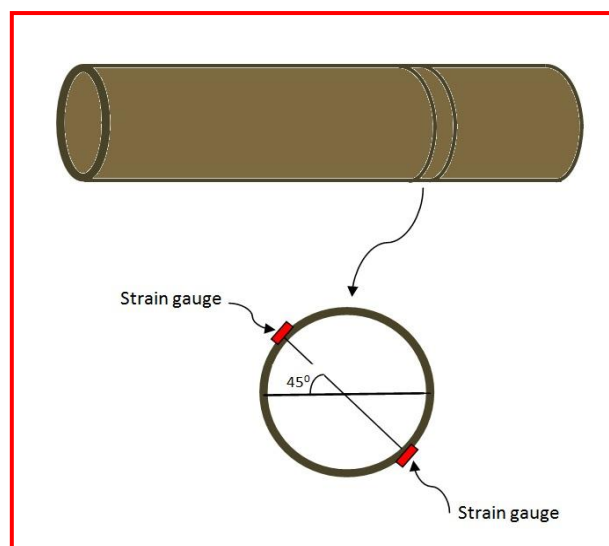
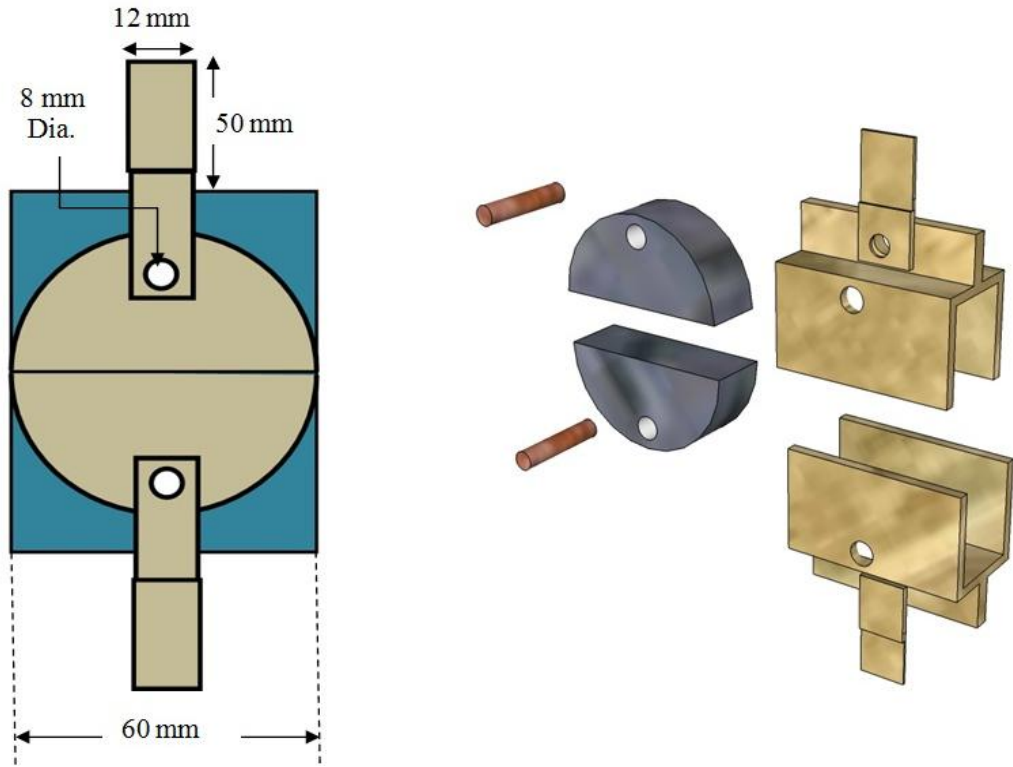


Figure 3.1: Details of tube specimen and strain gauges locations

The split disk specimens were precision made and assembled from the high carbon steel in the workshop at the University of Manchester to fit the FRP tube. Two semi-circular stiff steel solid of a similar circularity to that of the CFRP and GFRP rings were used to apply the tension force as shown in Figure 3.2. As expected, the highest hoop tensile force values were obtained for the specimens of tube type GFRP which has a greater thickness and high transverse modulus compared to CFRP according to the information of mechanical properties provided by the manufacturing companies.



a) Schematic of split-disk tension fixture



b) Split-disk instruments

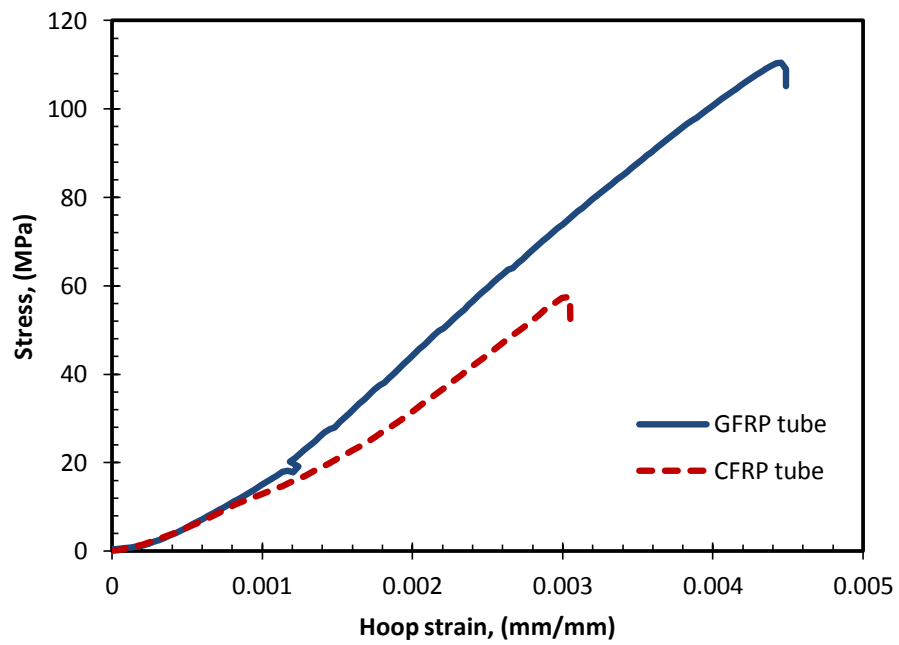
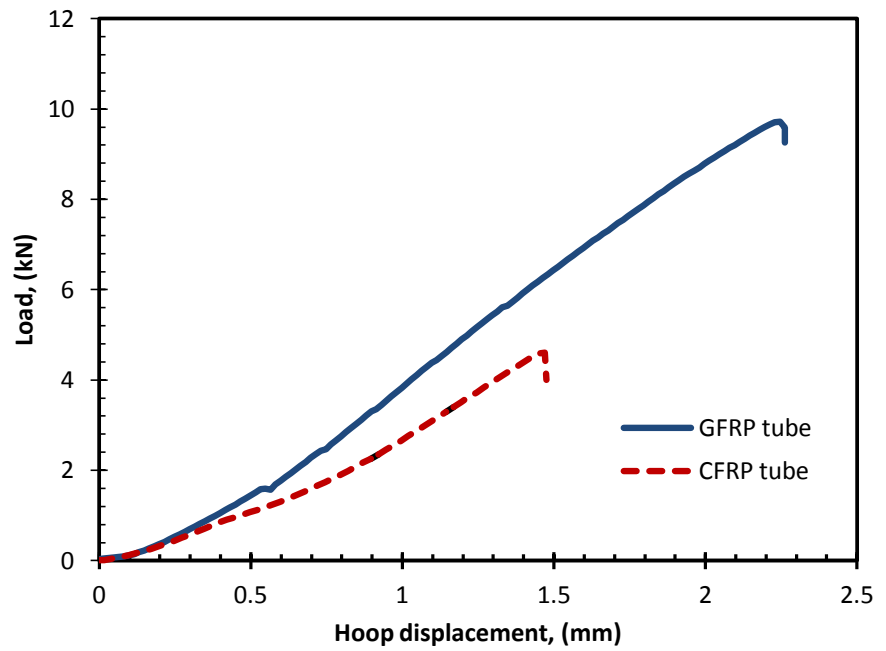
Figure 3.2: Split-ring fixture

The tests were carried out using a 200 kN Instron test frame machine operated at a constant rate of displacement of 2.5 mm/min. The typical split disk test setup is shown in Figure 3.3.



Figure 3.3: Hoop tensile test

Figure 3.4 shows the load-displacement and the typical stress-strain relationships for each type of the tubes for the split-disk test. The results refer that the highest hoop tensile force values which were obtained for the specimens of GFRP tube. It can be seen that GFRP tubes show a much better performance compared to CFRP specimen. This is an expected result considering that glass fibres are much stronger and stiffer than the carbon fibres in the hoop direction which has the largest thickness and high hoop moduli. However, the mechanical properties of each fibre reinforced polymer (FRP) type are dependent on the type of fibre laminate properties and configuration. Figure 3.5 shows a picture of the failed tube rings specimens for both CFRP and GFRP specimens.



Stress-strain relationship for spilt-disk test

Figure 3.4: Load-displacement and stress-strain relationships for spilt-disk test



a) CFRP Rings



b) GFRP Rings

Figure 3.5: FRP failure modes

3.2.2 Concrete Mixtures

Three concrete batches (A, B and C) in term of normal, medium and higher strength of concrete and one mortar batch (M) batch were prepared to take into consideration the effect of strength on the compressive behaviour of the FRP tubes confined concrete. Type I Portland cement, gravel, natural sand, water, silica fume and superplasticiser were used to prepare these concrete types. In previous studied there is a lack of work for using FRP tubes confined mortar. Therefore, it is important to understand its behaviour under compression loading. Superplasticiser and silica fume were added to improve the strength of the concrete. Details of the concrete and mortar mixtures designs are shown in Table 3.2. The mortar batch will be used also to fill FRP piling tube elements as will be described later in this chapter for flexural behaviour

Table 3.2: Formulations for concretes and mortar batches

Batch Type	A	B	C	M
Cement-Sand-Aggregate ratio	1:1.5:3	1: 1.5: 2.5	1: 2: 3	1: 2: 0
Water-cement ratio	0.45	0.36	0.36	0.40
Silica fume %	----	----	10 to cement	10 to cement
Superplasticiser %	----	2.5 to cement	2.5 to cement	1.5 to cement

3.2.2.1 Preparation of Specimens

The CFRP and GFRP tubes were cut with a water-cooled saw to make the length to diameter ratio of the tubes $(L/D) = 2$. Before casting the FRP tube specimens, eight steel cylinders moulds were prepared as (control) unconfined specimens. Steel moulds should be clean and lubricated with release oil in order to make it easier to demould after concrete or mortar hardening. The procedures for mixing the material and casting specimen are described in the following steps:

- Weighing or measuring the material by weight-scale and measuring cup.
- All materials were mixed in blender, stirred sufficiently, and then poured in the tubes and cylinder moulds as shown in Figure 3.6.
- Vibrating table was used to guarantee expulsion of air voids.

After casting, the specimens were left at the room temperature (20°C) for 24 hours, and then the specimens were remould and marked. Finally, the specimens were kept under the water and at 20°C . FRP tubes confined concrete and control cylinders are taken out of the water-tank on the same day for curing process. Capping sulphur specimens need to place at the top and bottom of the compressive cylinder at least one day before testing, to make sure there was a uniform loading on the surface of the compressive cylinder when they were tested.

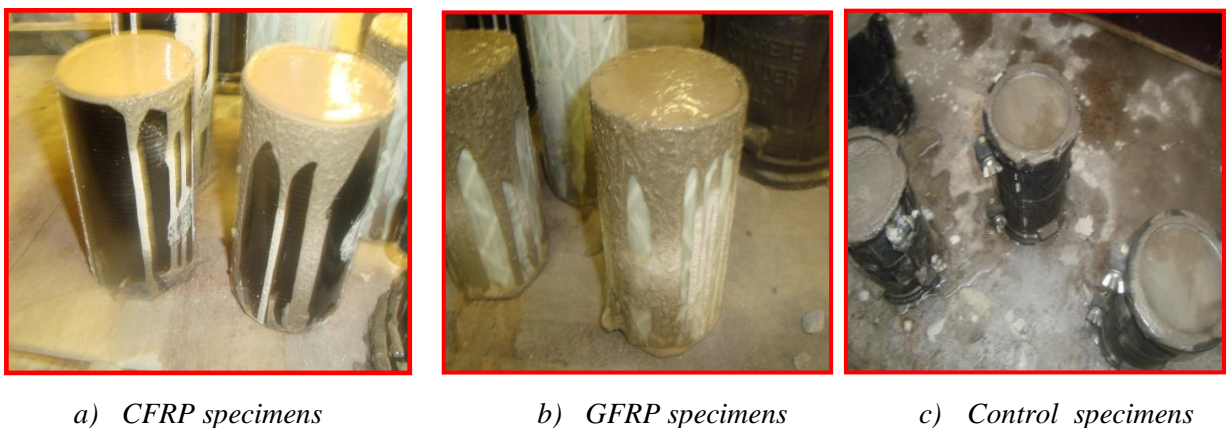


Figure 3.6: FRP's tubes confined concrete and control specimens

3.2.2.2 Instrumentation

Two pairs of electrical resistances strain gauges provided by Tokyo Sokki Kenkyujo Co. Ltd. Japan of type FLA-6-II-SL and a resistance of 120 ohms were used for each specimen. Each specimen was instrumented with four 10 mm strain gauges located at its mid-height and attached to its exterior surface. Two gauges were attached in the axial direction at 180° apart to measure the average axial strain and the other two gauges were attached in the lateral (hoop) direction at 180° apart and 90° from the axial strain gauges to measure the average radial strain. Finally, the wires of the strain gauges were soldered to a terminal and a 2 m long wire was soldered to the strain terminal for connection to the data acquisition system. The data acquisition system recorded the load and strains simultaneously during testing. Figure 3.7 shows the instrumentation layout of test specimens.

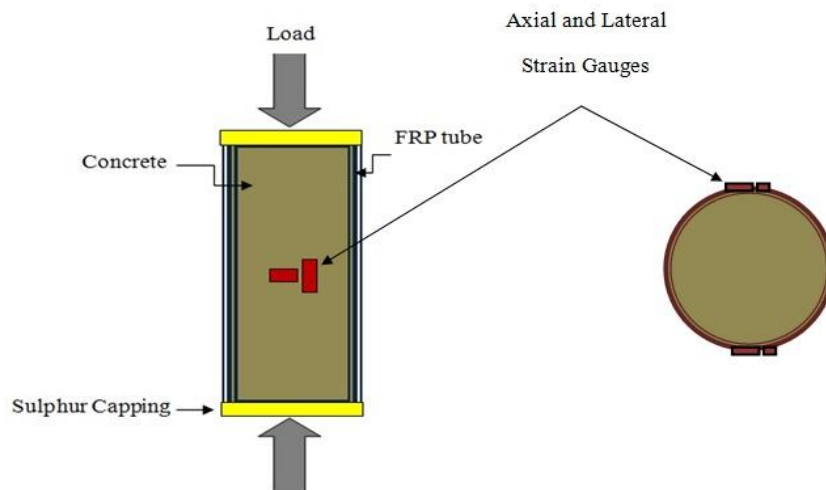


Figure 3.7: Layout of instrumentation of FRP tubes confined concrete and unconfined cylinders

3.2.2.3 Testing of Control Specimens

As mentioned earlier, control specimens were prepared from three different concrete and one mortar batches used in this program. For each batch, two specimens were prepared at the time of casting of FRP-tube confined specimens. The unconfined compressive strength (f_c) and strain (ϵ_c) at 28-day obtained from various concrete and mortar control specimens are listed in Table 3.3.

Table 3.3: Summary of test results

Concrete Batch Type	Specimens No.	f_c (MPa)	ϵ_c (mm/mm)
A	A-1	34.0	0.00182
	A-2	35.3	0.00210
B	B-1	48.8	0.00242
	B-2	47.3	0.00234
C	C-1	59.3	0.00249
	C-2	58.8	0.00235
M	M-1	60.0	0.00281
	M-2	55.5	0.00264

3.2.3 Experimental Results and Discussion

A total of 24 FRP tubes confined concrete were prepared for the three of concrete and one mortar batches (3 specimens for each batch). A total of 12 specimens for each CFRP and GFRP tubes confined concrete were tested under axial compression load. Figure 3.8 shows the experimental test set-up for all specimens used in this study. All specimens were loaded axially using hydraulic testing machine. The assembled computer data acquisition system can directly record the load with displacement data.



Figure 3.8: FRP-Tube Confined Concrete testing set-up

Table 3.4 presents a summary of the average experimental results for each batch in terms of the confined concrete compressive strength f'_c , the ratio of FRP-tube confined concrete strength to unconfined concrete strength f'_c/f_c , the tensile strength of the FRP in the hoop direction f_l , the ultimate axial strain ϵ'_c , and hoop strain ϵ_l of the both the CFRP and GFRP confined concrete specimens. A series of parameters calculated from stress strain curves were utilized to evaluate the effects of the failure mode, unconfined concrete strength, and stress-strain response. These parameters are discussed in the following sub-sections.

Table 3.4: Test Results FRP-confined concrete specimens

Batch Type	FRP Tube ID	f_c Average	f'_c	f_l	f_l/f_c	f'_c/f_c	ε'_c	ε_l
A	CFRP	34.8	43.6	4.25	0.122	1.252	0.0038	0.0034
			41.6	4.25		1.195	0.0039	0.0038
			43.3	4.25		1.250	0.0036	-----
	GFRP		53.7	8.30	0.24	1.540	0.0050	0.0062
			55.2	8.30		1.580	0.0049	-----
			52.7	8.30		1.514	0.0048	0.0070
B	CFRP	48.0	54.8	4.25	0.090	1.141	0.0040	0.0033
			56.9	4.25		1.185	-----	-----
			55.2	4.25		1.150	0.0043	0.0031
	GFRP		63.1	8.30	0.173	1.300	-----	0.0073
			62.2	8.30		1.290	0.0058	0.0071
			60.9	8.30		1.268	0.0055	0.0068

-----: Strain gauge damaged before specimen failure

Continued

Batch Type	FRP Tube ID	f_c Average	f'_c	f_l	f_l/f_c	f'_c/f_c	ϵ_c'	ϵ_l
C	CFRP	59.0	66.1	4.25	0.072	1.121	0.0041	0.0030
			64.3	4.25		1.100	0.0040	0.0031
			63.5	4.25		1.100	0.0043	0.0032
	GFRP		71.5	8.30	0.141	1.121	0.0068	0.0081
			73.1	8.30		1.245	0.0055	0.0072
			72.2	8.30		1.223	0.0053	0.0071
M	CFRP	57.8	64.8	4.25	0.074	1.120	0.0046	0.0034
			65.1	4.25		1.127	-----	-----
			63.8	4.25		1.104	0.0041	0.0030
	GFRP		70.1	8.30	0.144	1.212	0.0061	0.0078
			68.5	8.30		1.185	0.0058	0.0072
			66.8	8.30		1.156	0.0055	0.0067

-----: Strain gauge damaged before specimen failure

3.2.4 Behaviour of FRP-Tube Confined Concrete Specimens

3.2.4.1 Failure Mode

The failure mode for the both FRP tubes confined specimens was due to the failure of the FRP composite tubes. The fracture of the FRP tubes occurred along the total height of the cylinders started from top or bottom. Cracking noise was heard during the early to middle stage of loading, revealing the fracture of the concrete core. At higher levels of confining pressure; sounds were heard clearly due to fracture of the fibres in FRP tubes. After the failure of confinement, the concrete was observed to disintegrate, the concrete core fail immediately. Figure 3.9 shows the failure modes for two types of the FRP tube confined concrete specimens. The ultimate failure was in a very explosive manner without any warning for specimens of tubes CFRP tube confined specimens. For the GFRP specimens, the tube fibres were torn according to a broken line but always in their longitudinal direction. This failure mode indicates that the both FRP tubes add significant contribution to the strength, stiffness and ductility. However, the fibre laminate configuration influences the failure mode of the FRP tube (Li, 2006) .

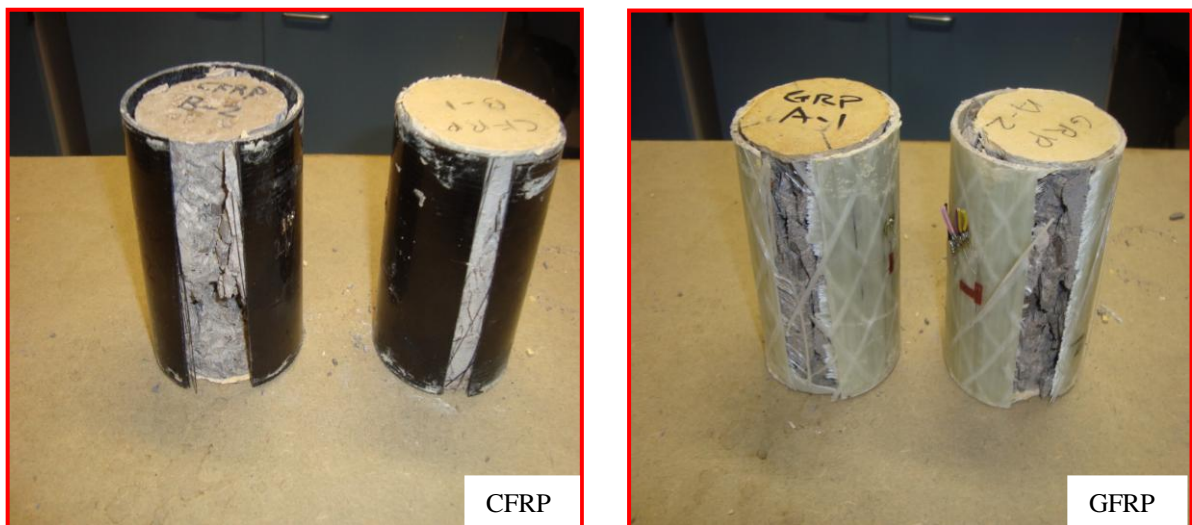


Figure 3.9: Failure mode of FRP-tube confined concrete

In general, the failure mode of the FRP concrete specimens confined with carbon or glass occurs by tensile fibres failure. All specimens failed due to the rupture of the fibre in the hoop direction at the ultimate hoop stress. This indicates that the concrete expands and this expansion is resisted by the FRP when an FRP tube confined concrete specimen is subject to axial compression. The concrete confined with GFRP tube showed higher strength compared to those confined with CFRP tube due to different properties and configuration. The GFRP tube has high moduli in the hoop direction and this mainly attributed to the high stress and strain.

3.2.4.2 Compressive Strength

The concrete strength plays an important role on the FRP confined concrete behaviour as shown in Figure 3.10. It can be seen that FRP tube confinement greatly increases the compressive strength of unconfined concrete. Figure 3.10 also showed that the lower the concrete strength is, the higher the strengthening ratio (f'_c/f_c) of the specimens. For instance, for GFRP tubes confined concrete A, the compressive strength of the confined concrete is 1.60 times respectively that of the unconfined concrete. This number becomes 1.30 and 1.22 for Batch B and C respectively and 1.18 for mortar. This is because, before concrete cracks, the confinement comes from the Poisson's effect and the contribution by the FRP tube to the load carrying capacity is insignificant; once the concrete is cracked, the FRP will be activated gradually due to the lateral expansion or dilation of the core concrete caused by the gradual crushing of the concrete, and the FRP tube will become the main load carrying body. If the core concrete has a lower strength, the concrete will be damaged by a smaller load and the FRP tube will be activated at an early stage. Similar findings can be observed from specimens having different concrete strength confined with CFRP tubes.

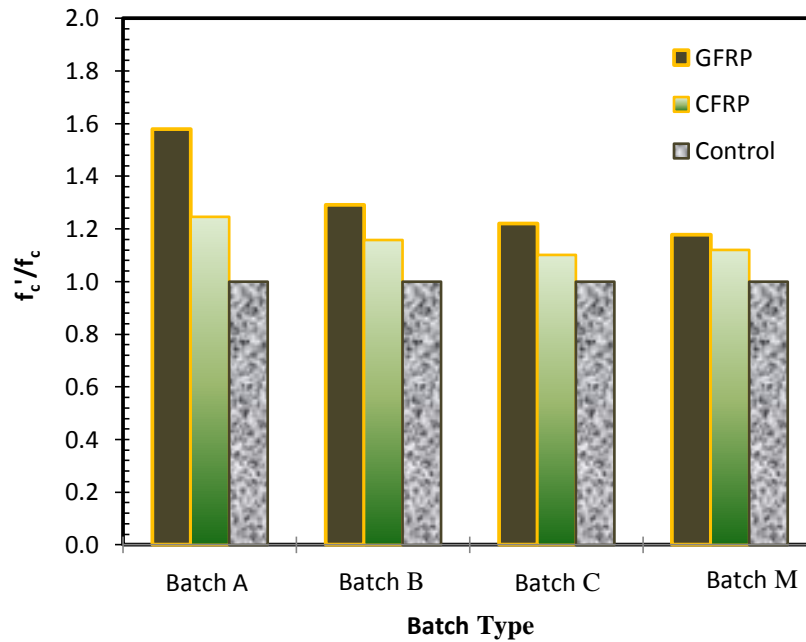


Figure 3.10: Effect of batch strength on FRP-tube confined concrete

The influence of the unconfined concrete strength on the FRP tube confined concrete has been plotted in Figure 3.11 for the tested CFRP and GFRP tubes confined concrete. The horizontal axis represents the confinement ratio as measured by the hoop confinement pressure of FRP divided by the unconfined strength (f_t/f_c). Indeed, the strength gain at failure linearly increases with the confinement ratio. The linear regression results show that the strength increases were more significant with confinement ratio and is more pronounced for lower strength concretes.

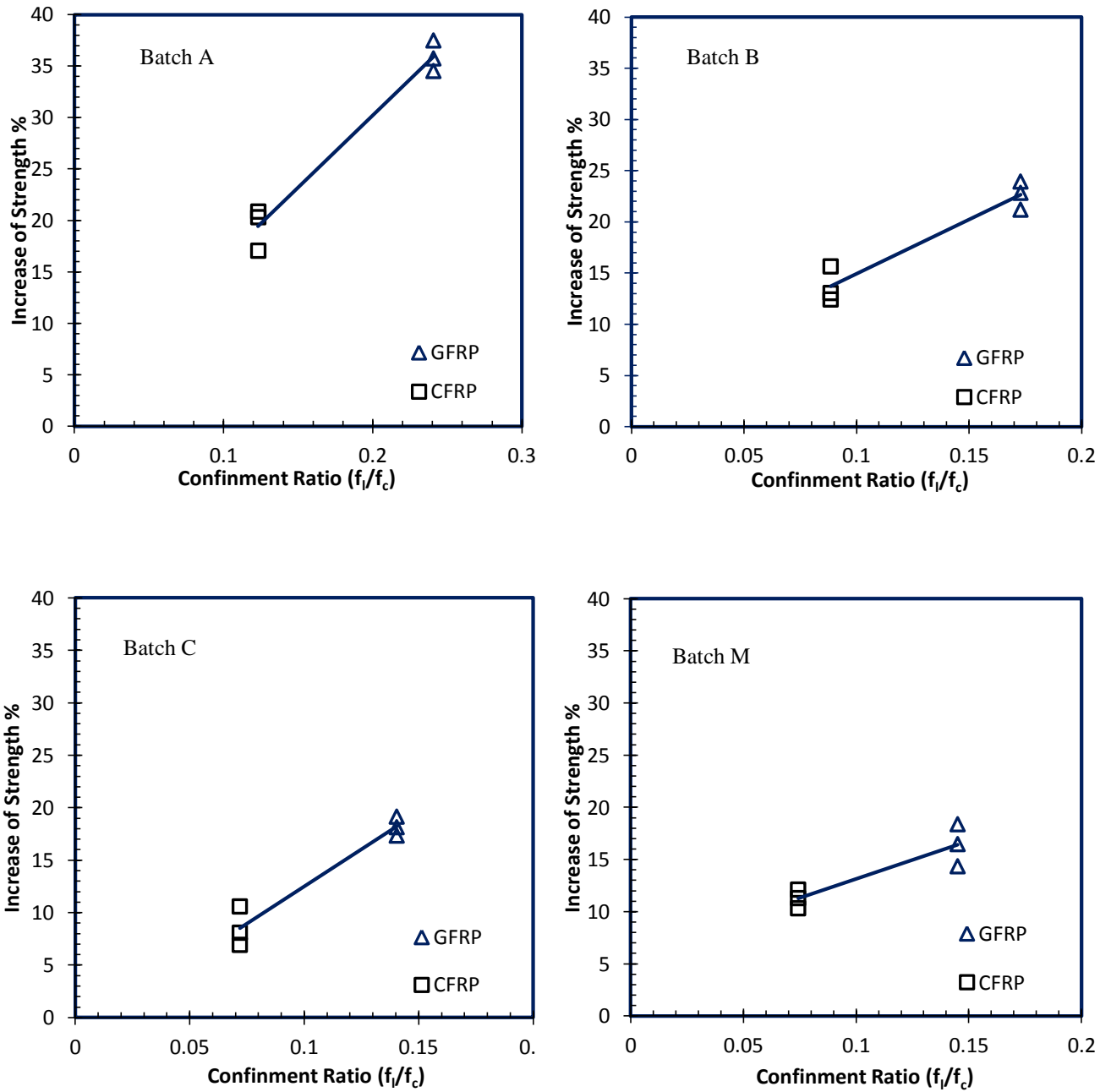


Figure 3.11: Relationship between strength gain and confinement ratio

3.2.4.3 Stress-Strain Response

The test results described in Table 3.4 show that FRP tube confinement can significantly enhance the ultimate strengths and strains of the specimens. The typical stress strain behaviour of FRP tube confined concrete is largely dependent on the level and mechanical properties of FRP confinement. Figure 3.12 displays the axial stress plotted as a function of axial strain (drawn on the right side) and the axial stress expressed as a function of lateral strain (drawn on the left side) for CFRP and GFRP tubes confined concrete based on the concrete batch type.

In general, the stress-strain response of the FRP tube confined concrete specimens can be divided into two regions as illustrated previously in Figure 2.15 in Chapter two. In the first region, the curve ascends rapidly slightly above the ultimate unconfined concrete strength, which is similar to the behavior of unconfined concrete. In this region, the stress and strain produced over the concrete, due to confinement, are very small. The first region is essentially a linear response governed by the stiffness of unconfined concrete, which indicate virtually no confinement is activated in the FRP tubes since the lateral strain in the concrete is very small. In the second region, the concrete is cracked and the FRP tube is fully activated, improving the compressive strength, and ductility of the specimens. The response in this region seems mainly dependent on the stiffness of the FRP tube.

The stress-strain curves show that the axial stress behaviour for the concrete specimens confined with GFRP was always higher than these confined with CFRP. This is due to the confinement action provided by fibre reinforcement in GFRP tube in the hoop direction at fibre orientation 90° . However, a greater enhancement in strength was observed for the GFRP specimens as they have much greater thickness and high moduli, thus leading to a greater confinement pressure. This also could be attributed the stiffness of confinement action provided by fibre reinforcement of the GFRP in the hoop direction.

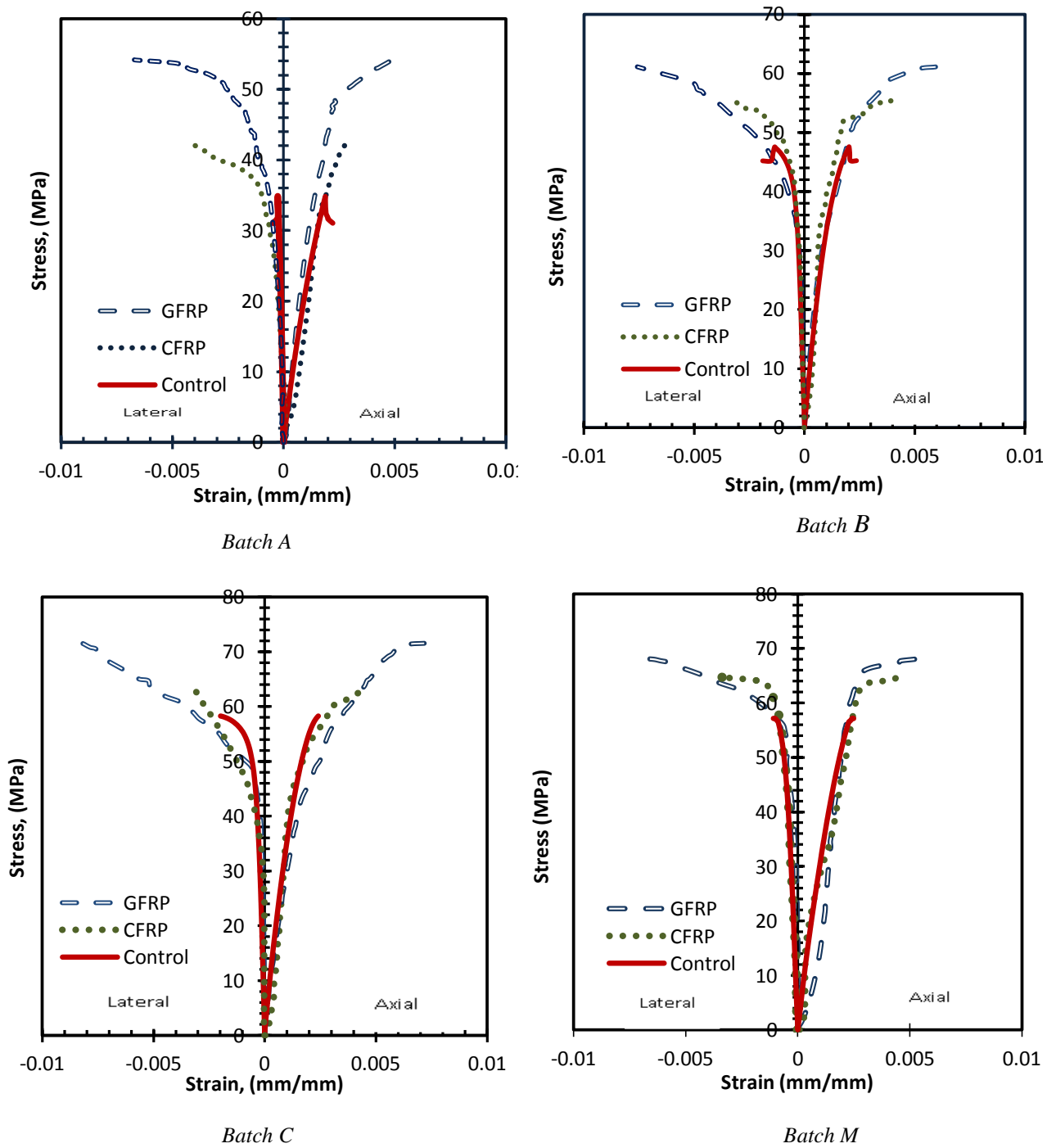


Figure 3.12: Stress-strain behaviour of FRP specimens.

3.2.5 Confinement Modelling

As mentioned earlier in section 2.13.2 in Chapter Two, different models and equations has been reported in the literature by many researchers to predict the strength of FRP confined concrete by modify Richart et al. Equation (2.16). Richart et al.,(1929) subsequently showed that the model is also suitable for steel-confined concrete. Fardis and Khalili, (1981) suggested that Richart et al.'s 1928 model could be directly used for FRP confined concrete, but the effectiveness coefficient should be adjusted according to the characteristics of FRP confined concrete. However, a number of strength models have subsequently been proposed specifically for FRP confined concrete, which employ Equation (2.16) with modified expressions and proposed k_1 to 2.1, 3.3, and 3.5 [(Karbhari and Gao, 1997), (Lam and Teng, 2003), and (Teng et al., 2007)] respectively.

In the following sections, it can be seen that new equations were proposed to estimate the ultimate stress and strain of FRP confined concrete tubes according to the current experimental results. These equations were used as the basis to develop a new model which incorporates the new expressions for peak confined stress f'_c and strain ϵ'_c .

3.2.5.1 Ultimate Compressive Strength

In this study, a new empirical equation is proposed, based on the experimental data. The lateral confinement ratio (f_l/f_c) of these specimens varies from 0.072 to 0.24 and the resulting strengthening ratio varied from 1.10 to 1.58. However, all experimental data were put together in Figure 3.13 and show a clear overall linear relationship between the strengthening ratio (f'_c/f_c) and the lateral confining ratio (f_l/f_c). It was found that the best fit line equation was the given $k_1=2.44$. However, the following equation for the axial compressive strength of the FRP-tube confined concrete is therefore proposed for design use:

$$f'_c = f_c + 2.24 f_l \tag{3.1}$$

f_l : is the lateral confining pressure which is given by Eq. (2.17) in Chapter Two. The ultimate compressive strength of FRP-confined concrete can be calculated as:

$$f'_c = f_c \left[1 + 2.44 \left(2 \frac{t f_{FRP}}{d f_c} \right) \right] \tag{3.2}$$

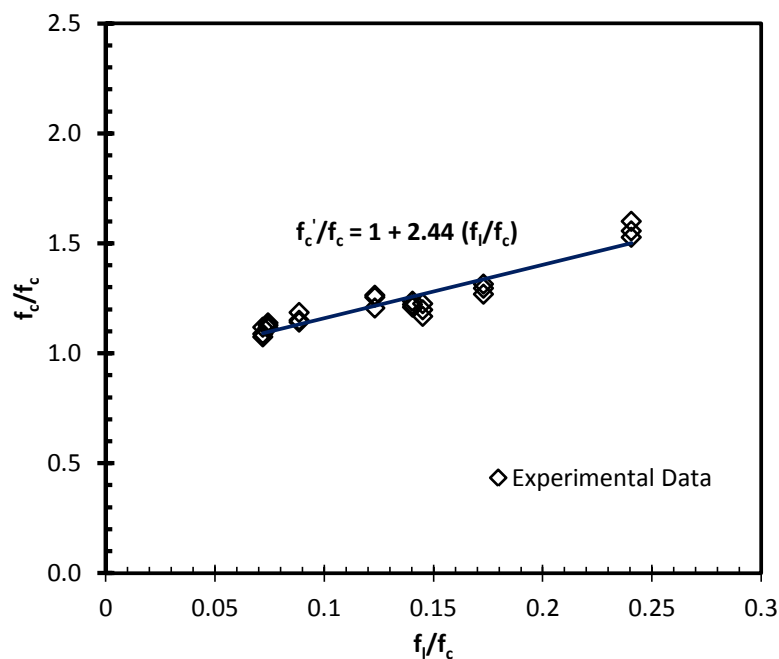


Figure 3.13: Relationship between strength gain and confinement ratio

3.2.5.2 Ultimate Compressive Strain

Tests by other researchers [e.g (Fardis and Khalili, 1981) and (Karbhari and Gao, 1997)] predicting the ultimate strain of FRP confined concrete based on confinement ratio f_l/f_c . Based on this concept, the expression below was proposed to predict the ultimate strain using the regression analysis of the experimental work with a correlation factor of 78% as shown in Figure 3.14.

$$\varepsilon'_c = \varepsilon_c \left[1.37 + 5.5 \left(2 \frac{t f_{FRP}}{d f_c} \right) \right] \quad 3.3$$

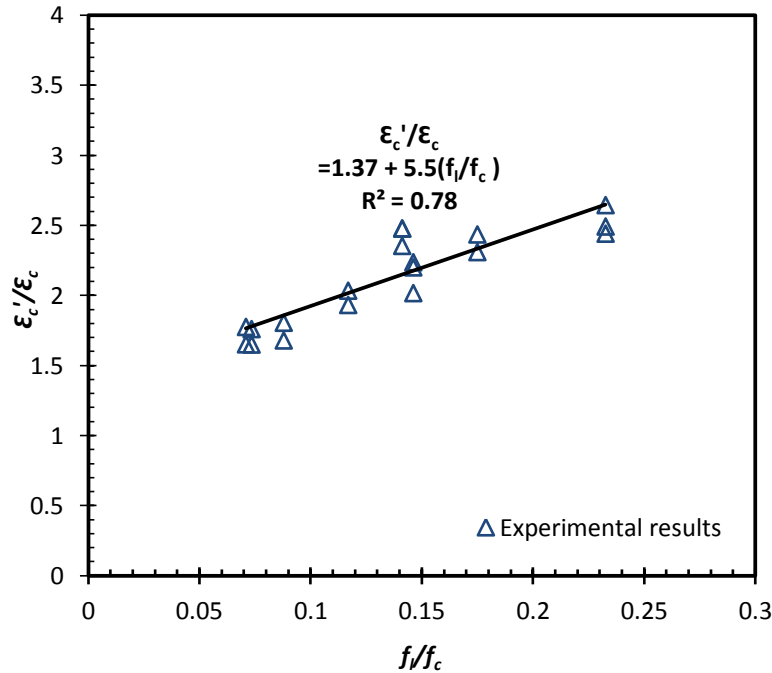


Figure 3.14: Relationship between strain gain and confinement ratio

3.3 Results in Relation to Previous Tests

As mentioned in section 2.15 in Chapter two, there are different models showed different strength enhancement due to different confinement ratio f_t/f_c and different concrete grades. Therefore, a comparison between the present experimental results and the proposed equations given in Table 2.2 is required to evaluate the accuracy of these equations considering a wide range of confining pressure and concrete grades. The comparison between the experimental results and the proposed equations are shown in Figure 3.15 and Figure 3.16. Also, the accuracy of each model is quantitatively is evaluated by computing the average error (AE) and standard deviation (SD) of the errors. The errors in the evaluation of f'_c are calculated as follows:

$$Error = \left(\frac{f'_{c(pred.)} - f'_{c(exp.)}}{f'_{c(exp.)}} \right) \times 100 \quad 3.4$$

The average error for N specimens is computed as:

$$AE = \frac{1}{N} \sum_{i=1}^N Error_i \quad 3.5$$

Table A-1 (see appendix A) summarizes the results by showing AE and SD for the models in predicting for all the current FRP confined concrete specimens. Figure 3.17 compares AE and SD values for f'_c for various models. However, the following comments are made for the predictions of the current FRP confined concrete results using these models.

- The two models proposed by and (Mirmiran, 1997) and (Samaan and Shahawy, 1998) are given similar behaviour to the present experimental results. The results of (Samaan and Shahawy, 1998) are shifted up, i.e., overestimated values compared to the experimental results.
- The error is larger for specimens with high confinement for those with the highest values of the ratio f_l/f_c . This may be due to the use of formulas that overestimate the effectiveness of high lateral pressures (Fardis and Khalili, 1981), (Saadatmanesh et al., 1994) (Toutanji, 1999).
- Mirimiran model presents relative agreement in the first part but as the values of f_l/f_c increase the two curves are dispersed and if can be made an extrapolation, a great difference will be resulted.

However, from all the previous results it can be concluded that these model equations cannot be generalized for a wide range of lateral confinement and unconfined concrete. Therefore, a new topographic chart which can incorporate a wide range of concrete confined with different FRP materials is finally suggested

step towards rational design guidelines. Details of this proposing chart can be discussed in the following section.

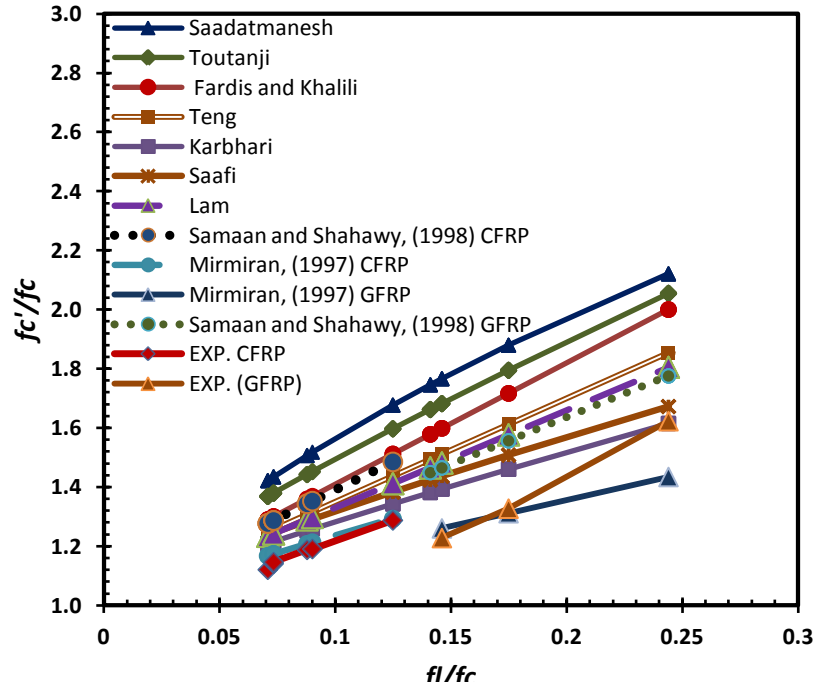


Figure 3.15: Comparison between the experimental model and nine previous models

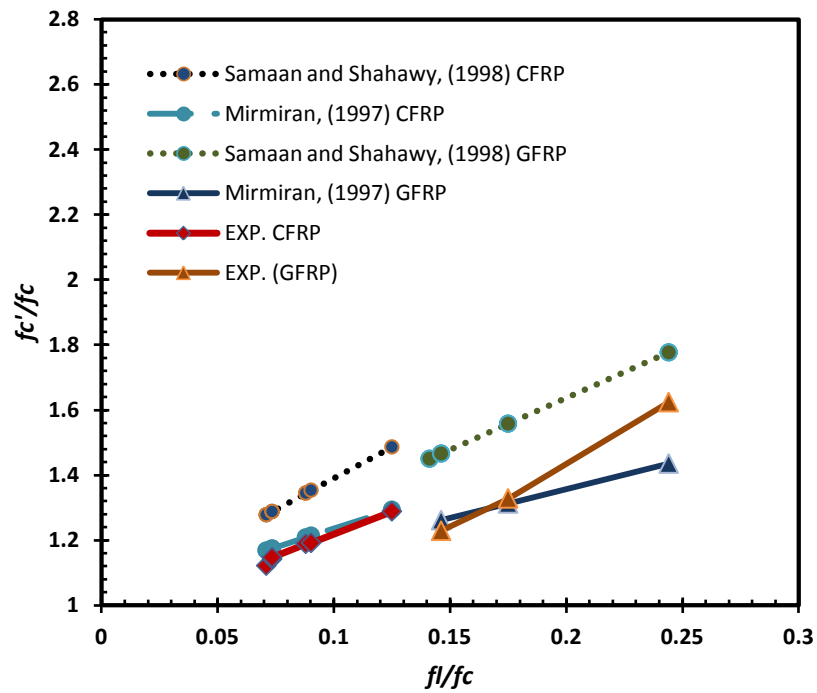


Figure 3.16: Comparison between the experimental results with the nearest two models

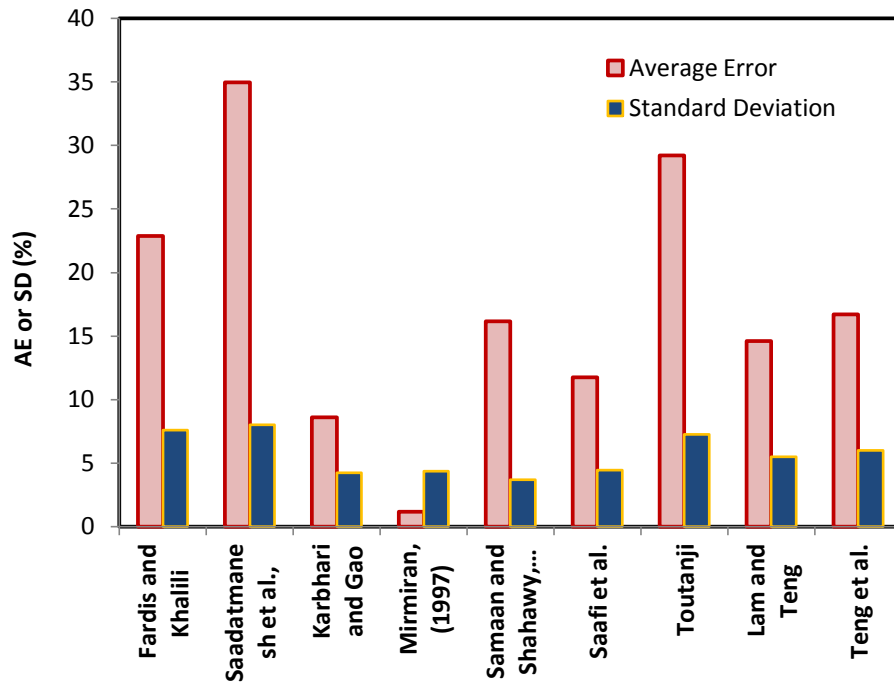


Figure 3.17: Comparison of f_c' predictions by various models

3.4 FRP-confined Concrete Strength Enhancement

As mentioned earlier, different models showed different strength enhancement due to confinement ratio f_l/f_c and unconfined concrete strength. Therefore, a new topographic chart which can incorporate a wide range of concretes confined with different FRP materials is an urgently needed step towards rational design guidelines.

In the current study, a large test database assembled from an extensive survey of existing studies with the limited number of tested specimens is presented and employed to assess the strength enhancement for FRP confined concrete. Therefore, the test results from 162 (138 specimens conducted by 17 different researchers and 24 specimens from the current study) are collected to predict the strength enhancement for FRP confined concrete in relation to unconfined concrete strength.

Thus, the test data can be divided based on the concrete strength into two sets: Data Set 1 for those tests with FRP filled concrete with strength between 20-39MPa and Data Set 2 for those tests with FRP confined filled concrete with strength between 40-60 MPa. Figure 3.18 displays the plots of strength ratio versus measured confinement ratio for the current tests and tests by others (see Table A-2 in Appendix A). This figure shows that strength enhancement due to confinement tends to be lower for high strength concrete and is more obvious for a higher confinement ratio.

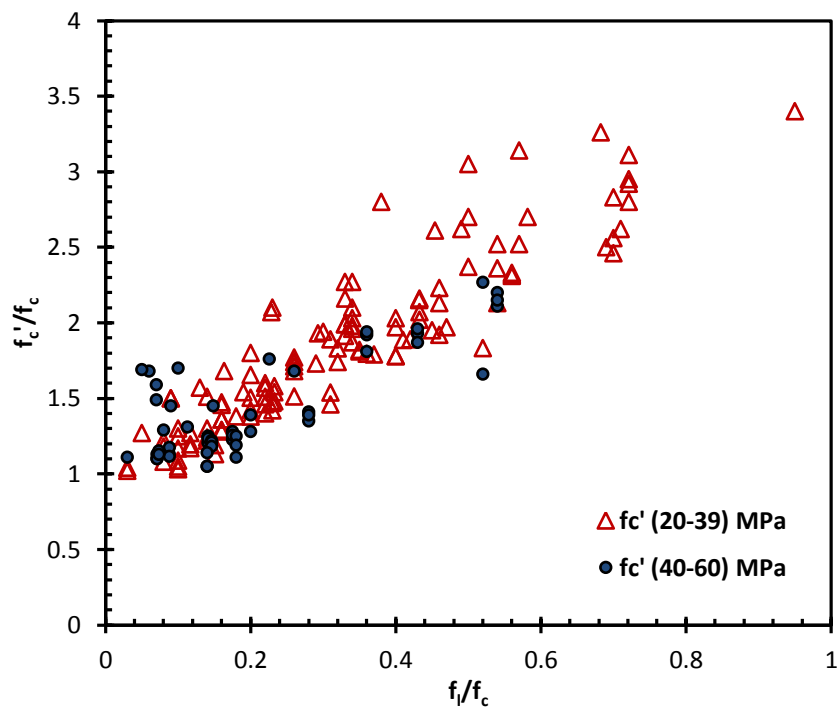
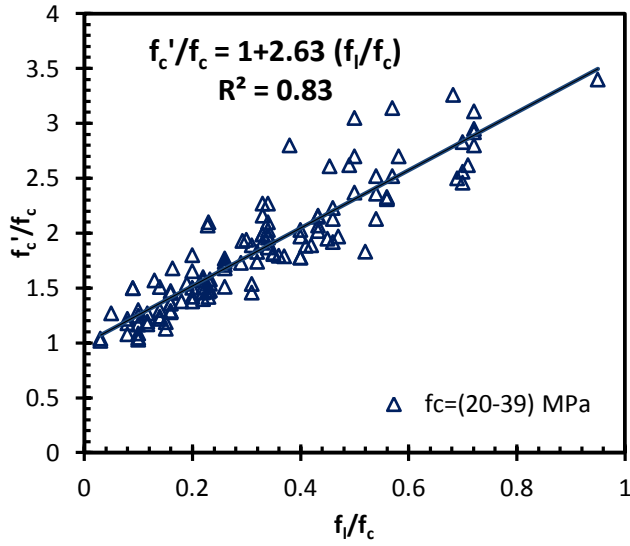


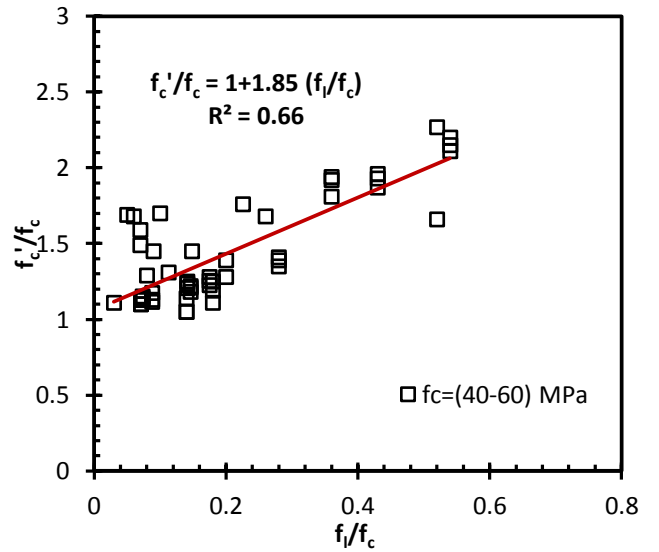
Figure 3.18: FRP confined concrete strength based on f_c range

The two data sets are plotted separately in Figure 3.19 to compare the relationships between compressive strength gains and confinement ratio. A slightly higher strength enhancement factor k_l is observed for the data set1 results of FRP confined specimens. It can be seen more clearly that the strength enhancement is influenced by the unconfined concrete strength from the relationship between the three parameters in (Figure 3.19 a and b). This observation had already been confirmed by the experimental observations of this study as discussed earlier in section 3.2.4.2.



Data set 1

Trend line for f_c (20-39)



Data set 2

Trend line for f_c (40-60)

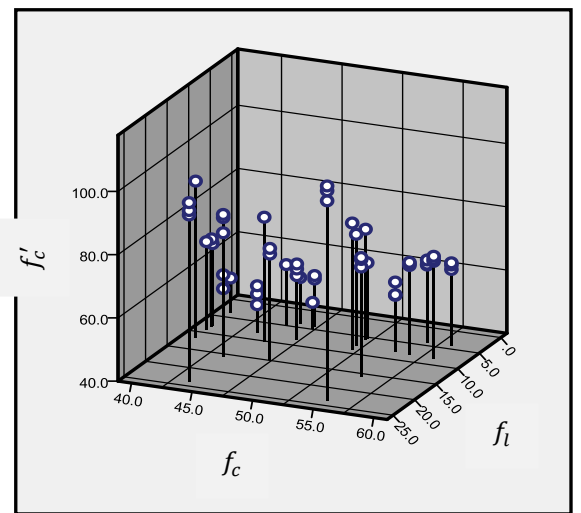
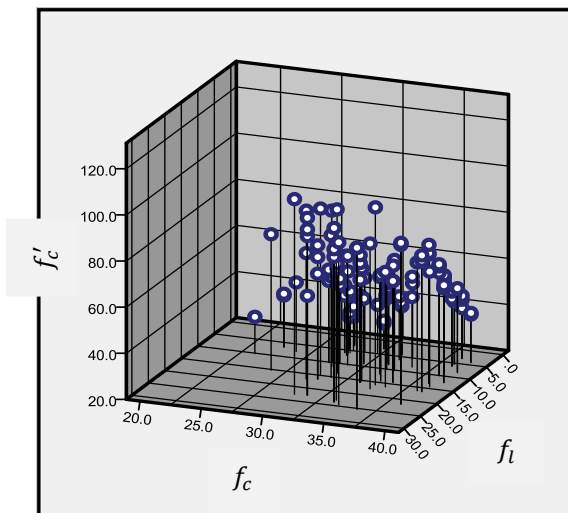


Figure 3.19: Effect of unconfined concrete strength on FRP strength enhancement

However, it can be concluded from this study and previous works that the FRP confined concrete performance is mainly depends on two significant variables. The main variables in this model are the unconfined concrete strength f_c and lateral confinement pressure f_l . The enhancement strength prediction of FRP confined concrete for the current and previous studies leading to a variety models. Therefore, the suggestions chart was proposed using the topographic approach to determine the strength enhancement based on f_c and f_l values as shown in Figure 3.20. The entire database has been represented in a graph in the form of XYZ contour using Origin Pro 8.1. Where X-axis represents the f_c , Y-axis represents f_l and Z-axis represents the ranges which (f'_c/f_c) lies in. These contours had been treated using the characteristics of the Origin Pro 8.1 program to enhance the final look of the graph using the curve fitting approach for each curve separately.

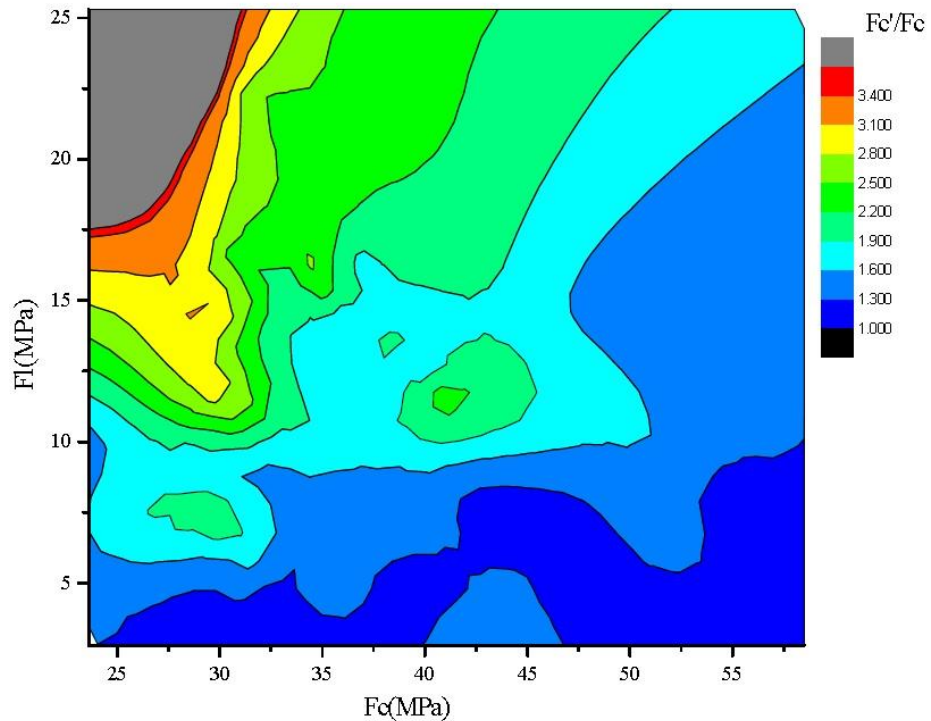


Figure 3.20: Representation of the entire data base in the form of contours

By neglecting up and down estimated values it can be get the modified smooth contours lines as shown in Figure 3.21. The main aim of this representation is to predict the range of the confined compressive strength of concrete for different values of concrete compressive strength and different levels of the confining pressure. A comparison between the experimental results and the proposed equations can be done easily by considering the previous contour lines in Figure 3.21. For a constant ratio of the confining pressure to the concrete compressive strength f_l/f_c , the equations will give the same enhancement to the confined concrete. Nevertheless, the values of f_l or f_c which form Figure 3.21 the degree of enhancement will be changed. On the other hand, for the same level of confining pressure i.e. f_l is constant, as the concrete grade increases, the level of enhancement will be reduced by using the equations while from Figure 3.21, the level of enhancement sometimes increases and sometimes not depending on the concrete grade and the value of f_l . From the previous figure it can be concluded that, the equations can not predict accurately the value of concrete confining compressive strength f_c especially in concrete grades f_c range from 25 to 35 MPa and confining pressure f_l ranging from 11 to 18 MPa.

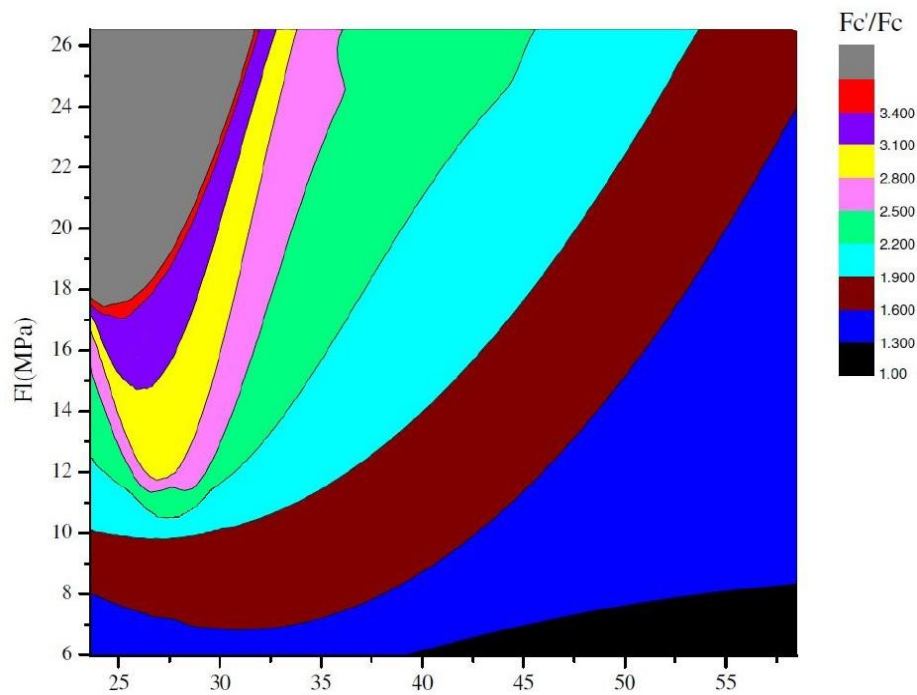


Figure 3.21: Contour lines of the data base after curve fitting

3.5 Flexural Behaviour

3.5.1 Control Specimen Behaviour

Two FRP composite tubes are used in this study; (GFRP) and (CFRP). Both tube specimens have an average outer diameter of 20 mm and a wall thickness of 1.25 mm. The CFRP and GFRP tubes used in this test have similar laminate configuration to those used in the axial loading tests. The dimensions of FRP piles used in this study were chosen to represent a pile shaft segment with total length of 300 which are used as piling foundation test in as described later in Chapter Six. Both tubes were filled with the same mortar batch which is used in the axial testing program.

However, this section describes the second phase of the experimental program undertaken to evaluate the flexural behaviour of the FRP tubes confined concrete. Both FRP composite tubes were prepared and subjected under four-point bending test. The Electrical strain gauges produced by Tokyo Sokki Kenkyujo Co. Ltd. Japan of type FLA-6-II-SL and a resistance of 120 ohms were used to measure strains in axial directions of the tubes. Deflection at mid-span was monitored using a Linear Variable Displacement Transducer (LVDT). Displacement and strain readings as well as the load were recorded during the tests using a data acquisition system. Figure 3.22 shows the schematic of the instrumentation of flexural test. The loads were applied using loading shaft machine which transfers the loads to the round surface of the FRP pile through a steel frame connected to the machine shaft, as illustrated in Figure 3.23.

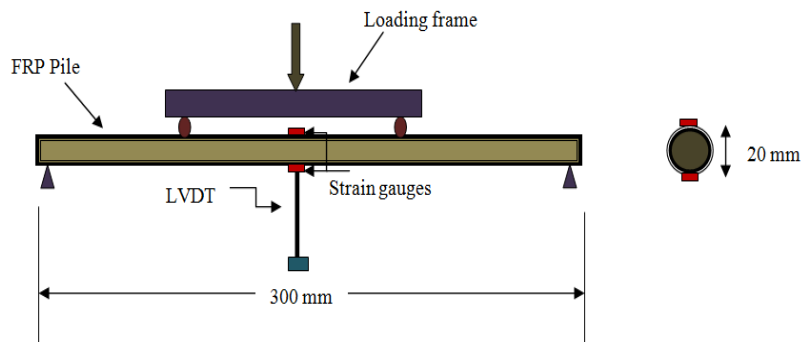


Figure 3.22: Schematic of test setup for FRP piles



a) CFRP Specimen



b) GFRP Specimen

Figure 3.23: CFRP and GFRP confined mortar tubes under loading system

The behaviours of the CFRP and GFRP tubes are compared in Figure 3.24. Both specimens utilize mortar-filled tubes of identical dimensions and wall thickness. The elastic moduli in the axial directions were 135 and 50 GPa for CFRP and GFRP tubes respectively. The post-cracking up to failure in the second part (Figure 3.24) represents the cracked FRP tubes confined concrete specimen with reduced moment of inertia. In this part, after cracking is almost proportional to the effective axial elastic moduli of the laminates. Both specimens response depict the progressive failure of the FRP layers, which was initiated by splitting of the transverse (90°) FRP layers due to matrix cracking. This splitting was followed by rupture or crushing of the longitudinal FRP layers (0°).

It can also be seen that the CFRP tube achieved higher strength than the GFRP tube due to the high tensile strength and modulus in the axial direction. The CFRP achieved a 25% higher strength. Figure 3.25 show the load-axial strain behaviour of the CFRP and GFRP tubes respectively. This figure is attributed to the difference in tensile strength of the tubes as indicated by the ultimate tensile strains measured.

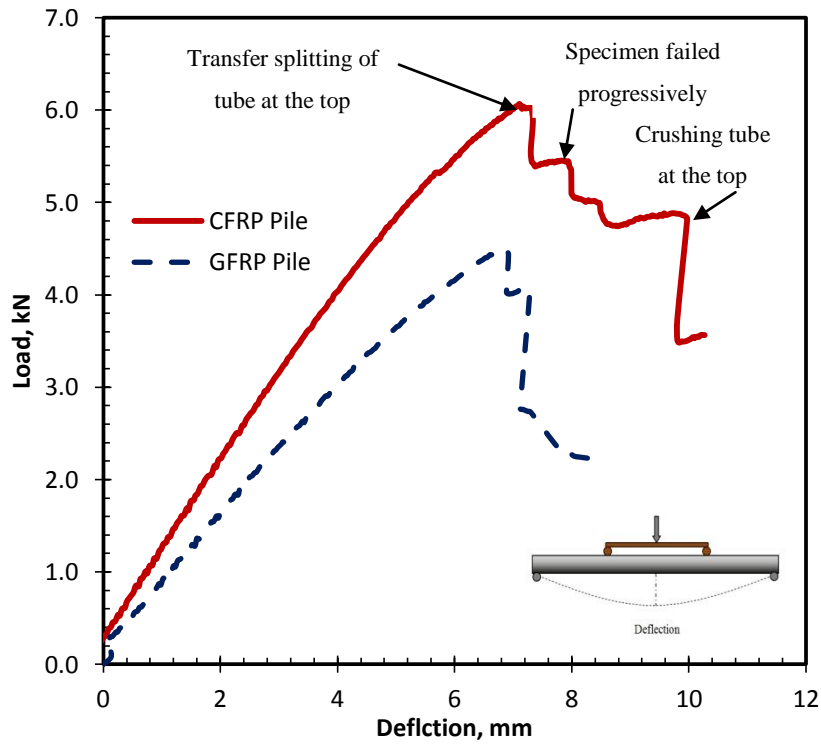


Figure 3.24: Load-deflection behaviour of CFRP and GFRP piles

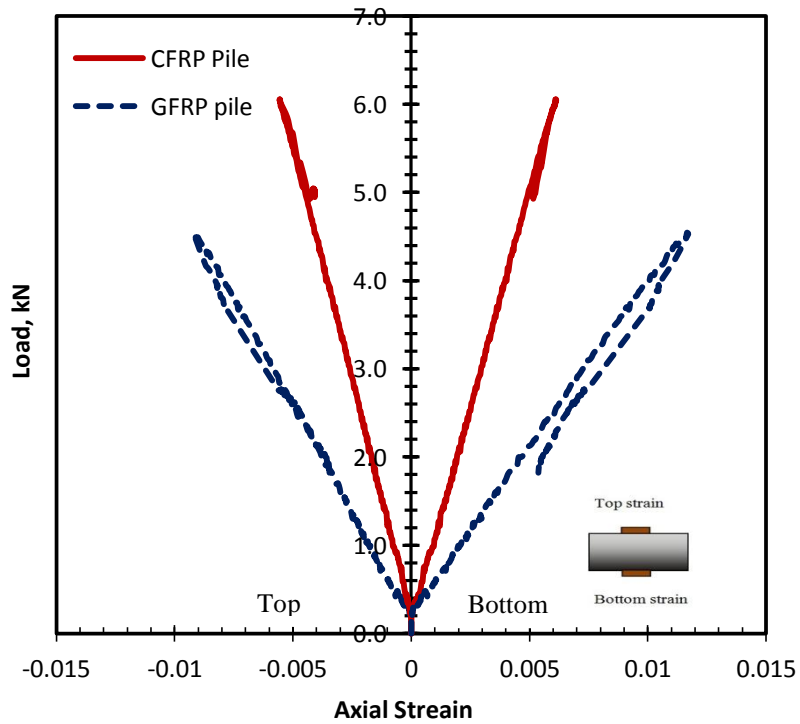


Figure 3.25: Load-axial strain behaviour of CFRP and GFRP piles

3.5.2 Long-Term Specimen Behaviour

Although composites FRP materials such as piles, piers and bridge components have been used in marine and waterfront applications, they are still fairly new compared to the traditional materials. Due to the increased use of FRP in civil engineering, the durability performance of FRP materials in term of flexural behaviour has been an important research topic in recent years. One of most important features in this research project is to evaluate the long-term flexural behaviour of FRP composite material. A long term program is needed with specific aggressive environmental to evaluate the FRP product during service life. Therefore, it is imperative to carry out an independent study to examine the long-term performance of the FRP composites materials in aggressive environments in terms of flexural strength.

The testing program involves immersing the GFRP and CFRP testing tubes confined mortar in two different aqueous solutions; NaOH (pH=12), and HCl (pH=2) which represent acidic and alkaline environments, respectively, for 24 weeks. Furthermore, as the chemical reaction can be accelerated as the temperature increases (Arrhenius 1912), FRP tube specimens exposed to each pH level were aged under elevated temperature (45°C) to obtain specimen ages within the duration of the experiment 24 weeks (3 years aging time). The specimens were accelerated using an automatic oven as shown in Figure 3.26.



Figure 3.26: Oven used for acceleration process

After 180 days exposure to the aqueous solutions, CFRP and GFRP were left 24 hours in the lab for the instrumentation process. Then, both specimens were taken out and tested in bending using four-point loads to evaluate the flexural strength at different aggressive solutions. Figure 3.27 shows the results of typical load-deflection behaviour of CFRP and GFRP confined mortar in terms of pH value. It can be seen that specimens immersed at both aggressive conditions exhibited reduction in flexural strength compared to control specimens. It was proposed that these reductions were due to a separation between the fibre and the matrix resin that occurred in the aggressive environments at the 45°C condition. Acid and alkaline solutions may degrade and damage the fibre matrix interface and leading to a reduction in the structure performance of FRP tube [(Bisby, 2006) and (Riebel and Keller, 2007)]. In the other word, both solutions may cause degradation of the resin and cause the adhesion between the fibre and the resin to weaken.

The effect of the aggressive solution on flexural strength was much more pronounced in pH=12 than that pH=2 as shown in Figure 3.28. For instance, for CFRP tubes exposed at pH=2, the flexural strength decreased by 20% while the CFRP tube strength decreased by 40% for those exposed in pH=12. In contrast, the GFRP tube strength reduction in flexural was about 30% and 50% at pH=2 and pH=12 respectively. It can be concluded that the alkali solution appears to be a slightly more aggressive environment than the acid solution. Small white blisters were observed on the external surface of both specimens after exposure, especially those exposed to alkaline solution (pH=12). This due to the fact that the alkaline solution can be penetrate the FRP and affect the fibres typically causing embrittlement of the individual fibres resulting in a reduction of both longitudinal and transfer properties. This is likely due to be combination of mechanism involving chemical attack by alkalis on the fibres themselves, and subsequent growth of hydration products on the surface of the fibres (Murphy et al., 1999). This observation was also explained by (Katsuki, 1995) investigation. They clarified that alkali penetration was found on the GFRP rod. They presented results showing the penetration of Sodium (Na) in sections of GFRP rods with immersed time 7, 30 and 120 days as shown in Figure 3.29. Sodium covers the black area within the FRP rods

due to penetration. On the other hand, tiny and dark brown coloured spots were also found in the specimen after exposure to immersion along the CFRP and GFRP tubes surfaces which were exposed in pH=2. This finding indicates that these brown spots may be caused by some kind of chemical reaction between HCL and tube matrix.

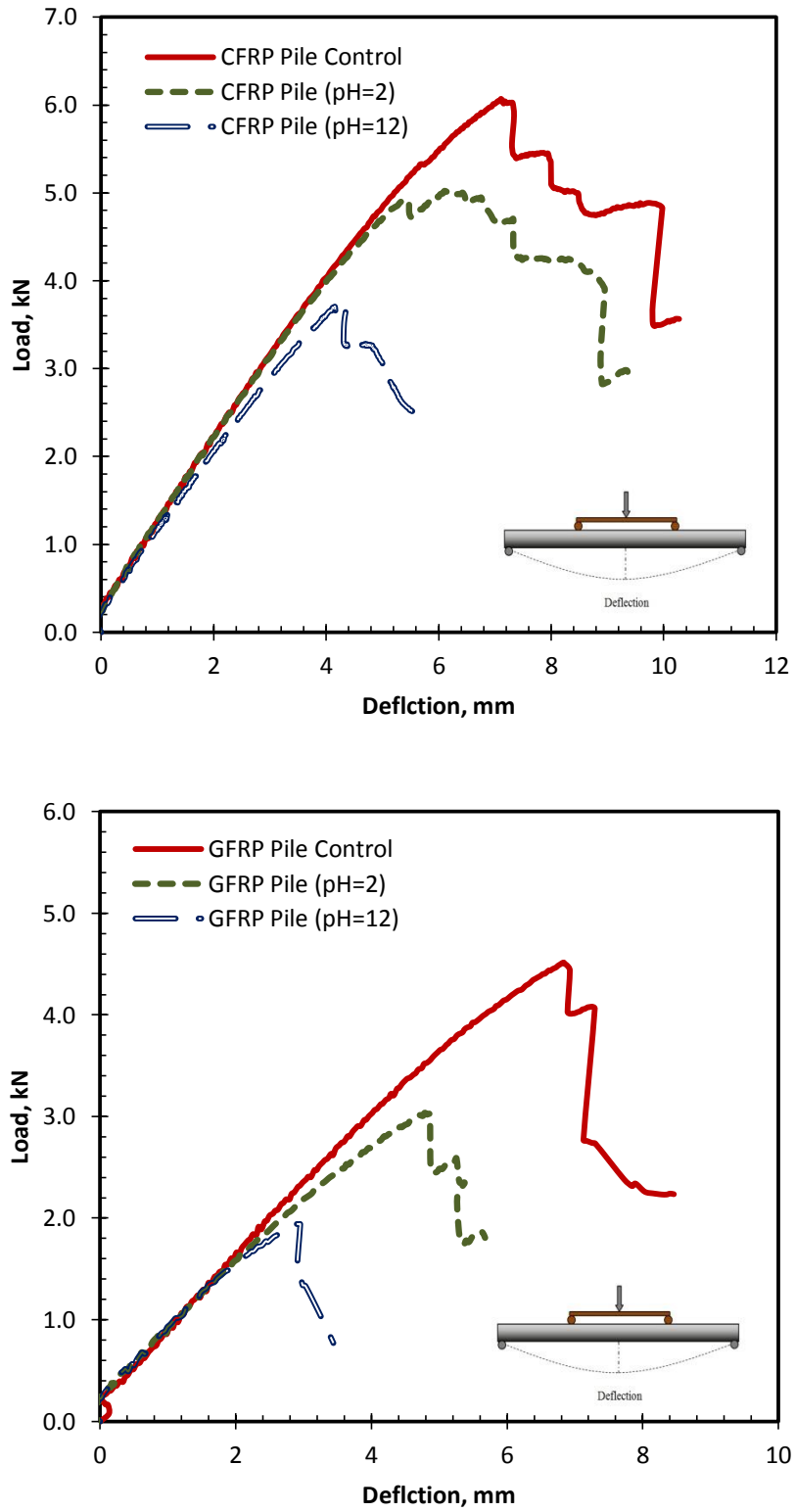


Figure 3.27: Load-deflection behaviour of GFRP piles at long-term

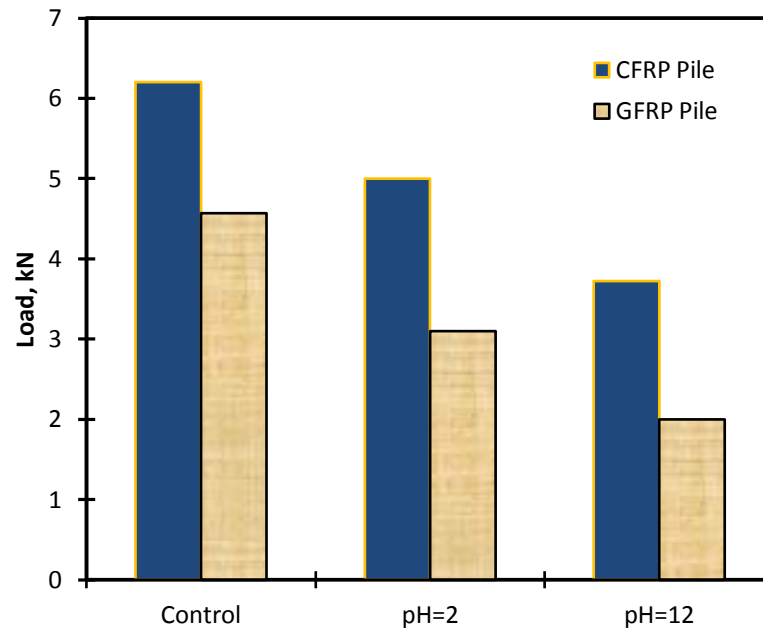


Figure 3.28: Long-term effect on flexural behaviour at different pH level

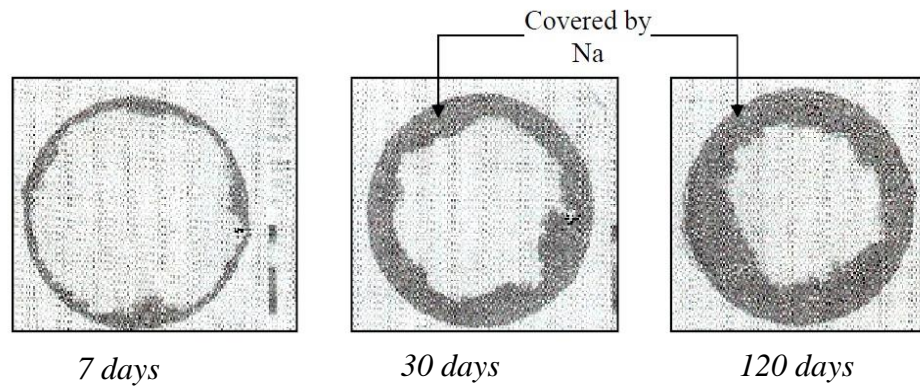


Figure 3.29: GFRP rod section immersed on alkaline solution at different time (Katsuki, 1995)

3.6 Summary

The behaviour of small FRP tubes filled with three different concrete strengths and mortar under concentric axial loading have been presented. The experimental results for 8 unconfined cylinders, 24 FRP tubes, 12 CFRP tubes and 12 GFRP tubes were tested under axial load. Existing strength models for FRP confined concrete have been reviewed and compared with available experimental data collected from an extensive literature survey. This chapter has also presented the long-term (aging) experimental programs conducted to examine the flexural behaviour of FRP tubes confined mortar tested under four point bending load. Two aggressive environments (acid and alkaline) were used to degrade the FRP specimens at elevated temperature 45⁰C. The findings presented in this chapter can be summarized as follows:

- The experimental results clearly demonstrate that composite wrapping can enhance the structural performance of FRP confined concrete in terms of both strength and strain.
- As the results of existing tests show a clear overall linear relationship between the strength of confined concrete and lateral confining pressure provided by FRP, the additional complexity in representing this relationship in many of the existing models appears to be unnecessary. A suggested topographic chart has therefore been proposed for the prediction of the strength of FRP-confined concrete based on the analysis of existing test and other results.
- For the flexural behaviour, CFRP tubes achieved higher strength than GFRP tubes due to the high tensile strength and modulus in the axial direction.
- The effect of the aggressive solution on flexural strength was much more pronounced in pH=12 than that pH=2.

CHAPTER FOUR: INTERFERENCE CHARACTERISTICS OF FRP/SAND

4.1 Introduction

FRP composite material properties used in pile foundation can differ significantly from those of traditional materials in anisotropy, stiffness, surface hardness, and surface roughness. These differences may produce differences in the behaviour of interfaces between the piles and the surrounding soil. The interface behaviour between the pile material and surrounding soil constitutes a considerable component of the pile capacity and load transfer characteristics as shown schematically in Figure 4.1. To date, most interface testing has been performed on traditional pile materials. Relatively few studies have been made on interface shear behaviour between FRP composite materials and soils [(Han, 1997) and (Pando et al., 2002)]. There is a lack of information regarding the behaviour of pile/soil system which includes these materials. However, determination of interface friction characteristics between FRP materials and granular is an important to facilitate their design and evaluate their behaviour under loading.

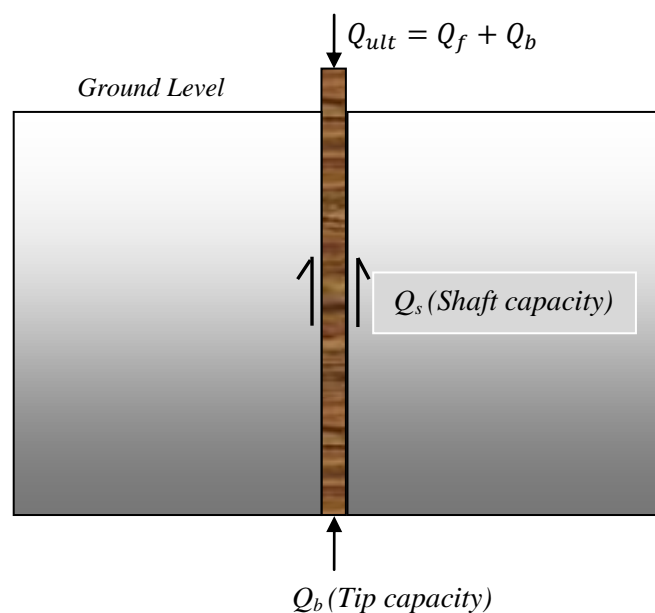


Figure 4.1: Pile's side friction (skin friction) and end bearing

This study presents the results of interface shear testing conducted on FRP/granular materials as main part of this study. To relate surface roughness, particle angularity, relative density, and normal stress with the interface shear behaviour. Various series were performed and discussed.

The surface roughness of FRP piles may be significantly altered during the driving installation process. This change could affect the interface pile design parameters. Therefore, an accurate quantification of this change is required to precisely determine the pile shaft resistance. Therefore, this study is investigated the change in surface roughness and interface shear coefficient of two different FRP counterface surfaces that sheared against different types of sand under increased normal stress levels. However, a conceptual explanation is provided in this study to interpret the observed behaviour.

4.2 Tested materials

4.2.1 Granular Materials

Four British types of sands (Leighton Buzzard type A, Leighton Buzzard type B, Mersey and Congleton) sands were used in this investigation. Leighton Buzzard sand is available in a commercially graded form for laboratory use. The main mineral composition is quartz sand with sub-angular particles. Mersey sand has been used by Bolton, (1986) to clarify the concepts of friction and dilatancy in relation to the selection of strength parameters for design. It consists predominantly of medium grained sand with sub-angular to angular particles. Congleton sand consists of silicate sand with a uniform grading of angular grains. To investigate the effects of particle size and shape (rounded versus angular) on FRP interface shear response, three different glass beads (GB) having different mean grain sizes (D_{50}) were used. The glass beads samples were provided by Potters Europe Company in the UK. The microscopic views of the sands and glass beads are shown in Figure 4.2 and 4.3 respectively. The grain size distribution of the tested sands is shown in Figure 4.4 . The physical properties of each sand soil are given Table 4.1.



Leighton Buzzard sand A



Leighton Buzzard sand B

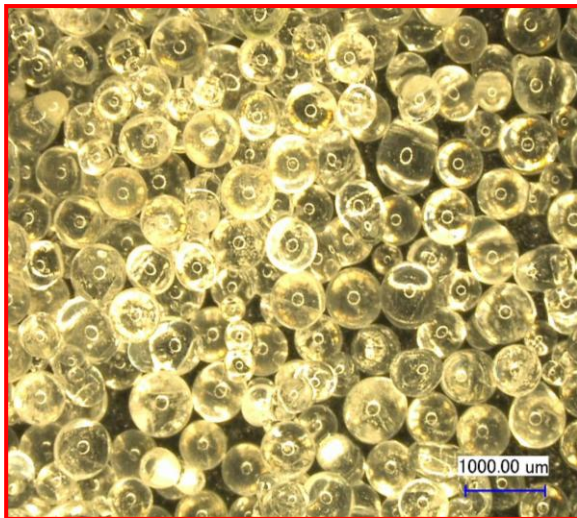


Mersey sand

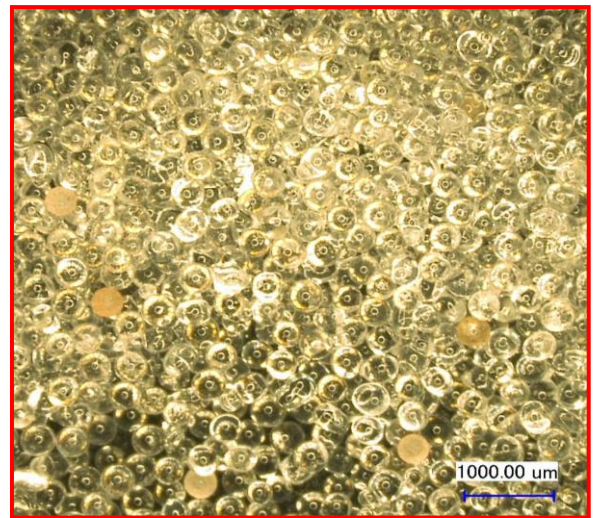


Congleton sand

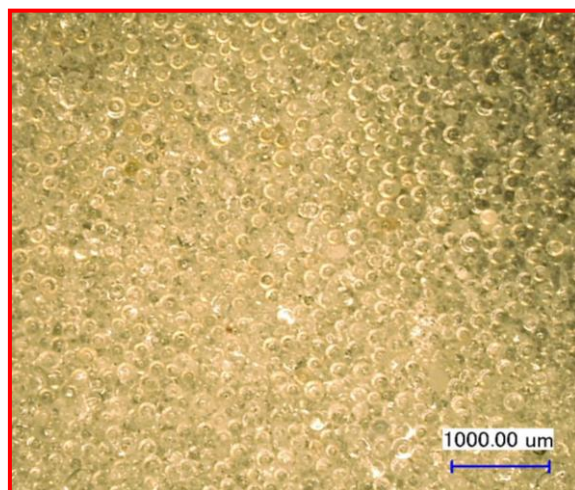
Figure 4.2: Microscopic photos showing the tested sands



Glass Beads A



Glass Beads B



Glass Beads C

Figure 4.3: Microscopic photos showing the glass beads sands

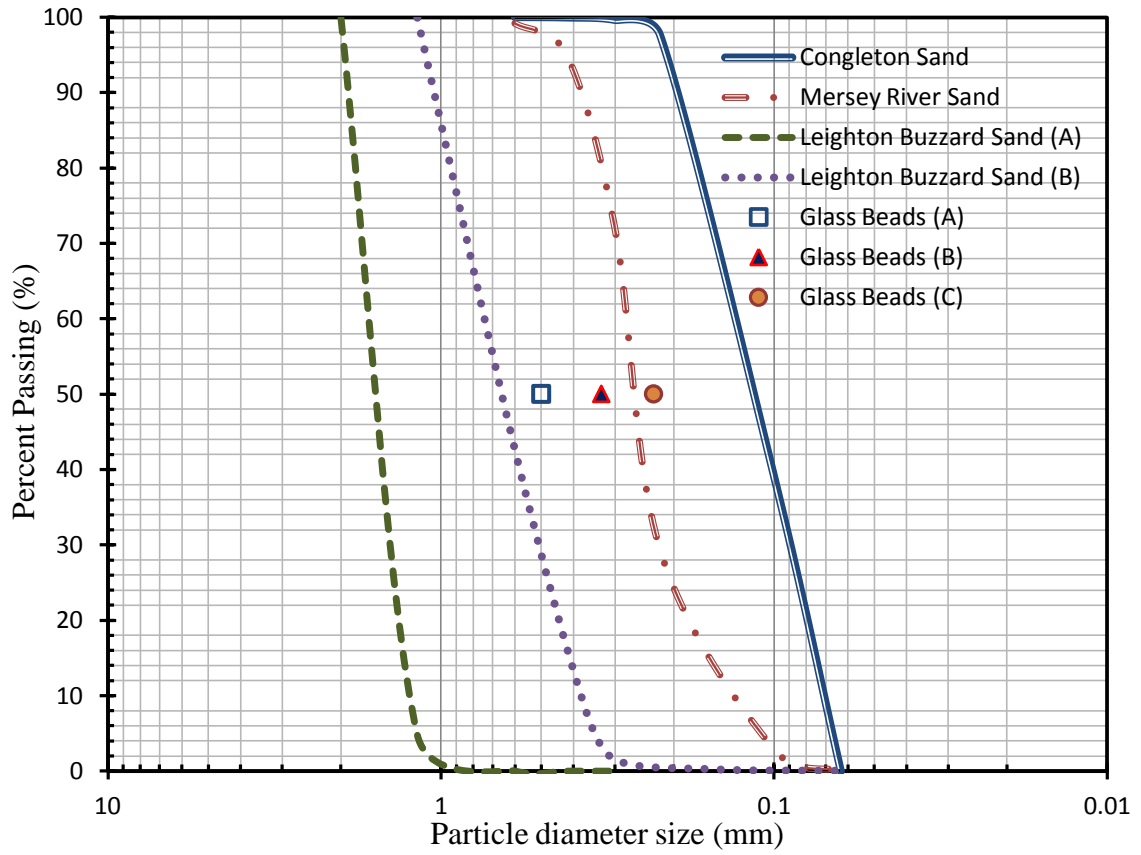


Figure 4.4: Grain size curves of tested sands and glass beads

Table 4.1: Properties of the sands and glass beads used in this study

Parameter	Symbol and unit	Leighton Buzzard A	Leighton Buzzard B	Mersey	Congleton	Beads A	Beads B	Beads C
Maximum dry Density	γ_{\max} (kN/mm ³)	17.36	17.61	17.36	17.11	16.11	16.26	16.50
Minimum dry Density	γ_{\min} (kN/mm ³)	15.21	16.01	15.20	14.91	14.76	14.90	14.94
Index Properties	D ₁₀ (mm)	1.3	0.39	0.14	0.06	0.5	0.31	0.2
	D ₃₀ (mm)	1.4	0.5	0.22	0.09	0.5	0.31	0.2
	D ₅₀ (mm)	1.65	0.65	0.26	0.12	0.5	0.31	0.2
Coefficient of Uniformity	C_u^*	1.30	1.92	2.07	2.33	1	1	1
Coefficient of Curvature	C_c^*	0.87	0.85	1.19	0.96	1	1	1

*Note: $C_u = D_{60}/D_{10}$;
 $C_c = D_{30}^2/(D_{10} \times D_{60})$.

4.2.2 Direct Shear Tests

The direct shear tests were conducted to determine the internal friction angles of the tested sand and glass beads. All tests were carried out at shearing rate of 0.52 mm/min. The direct shear tests were performed in accordance with British Standard (BSI 1377: Part 7: 1990). All sand specimens were prepared by means of air raining technique and tamping as shown in Figure 4.5. A predetermined quantity of sand was allowed to carefully put freely fall into the shear box mould at a constant height and then the soil surface carefully levelled with the top surface of the upper shear box. Any required dense specimen in the shear box was achieved by tamping after the process of raining. Sand raining technique makes it possible to obtain good-quality specimens of sand that are very homogeneous (Amini and Chakravrtty, 2004). The relative density (density index) of the sand specimens can be calculated as follows.

$$I_d = \left(\frac{\gamma_d - \gamma_{min}}{\gamma_{max} - \gamma_{min}} \right) \left(\frac{\gamma_{max}}{\gamma_d} \right) \quad 4.1$$

Where:

I_d : Density index,

γ_d : Soil dry density,

γ_{min} and γ_{max} are the minimum and maximum dry unit weights for sand.

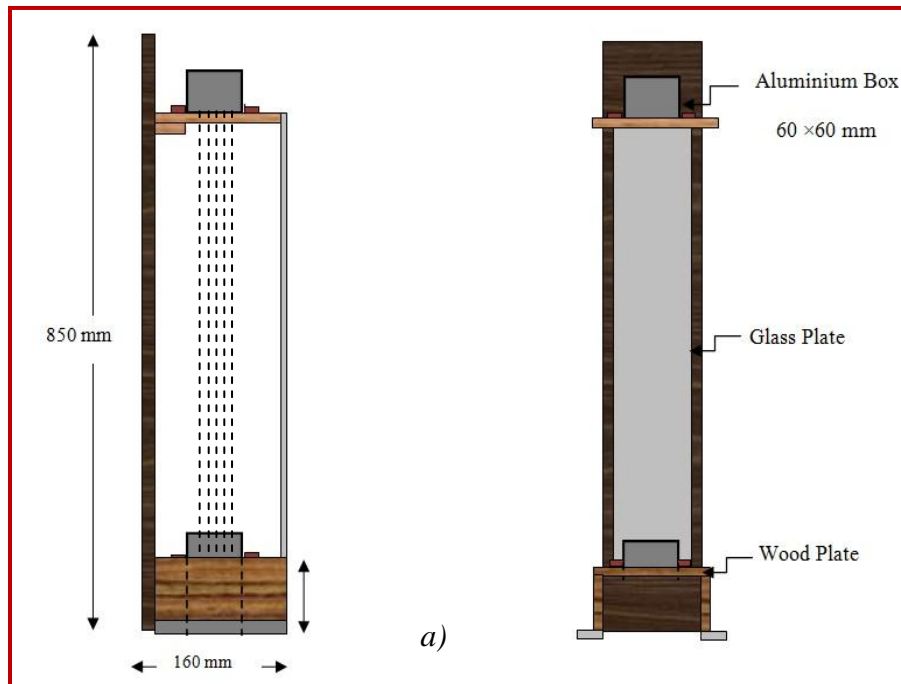


Figure 4.5: Schematic view of the: a) Sand Raining Frame. b) Sand preparation

However, good consistency was achieved by raining sand from a fixed height to achieve certain desired densities.

Figure 4.6 shows the relationship of drop height versus density index of Congleton sand achieved for this particular sand over a total of 31 measurements made between drop heights of 10 to 90 cm.

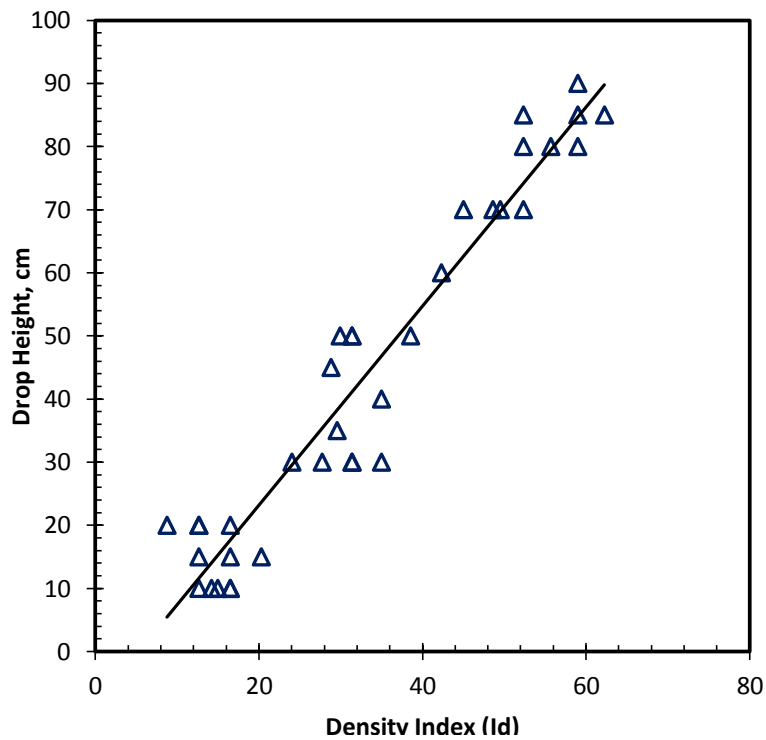


Figure 4.6: Density Index of viruses drop height

Direct shear test results, in terms of shear stress versus horizontal displacement curves are presented in Figure 4.7 through Figure 4.13 for the tested sand and glass bead specimens. For all of the stress-displacement curves, a peak shears stress followed by a stress reduction towards a residual shear stress with a nearly constant volume state. The peak and residual friction angles obtained from the direct shear tests are summarized in Table 4.2.

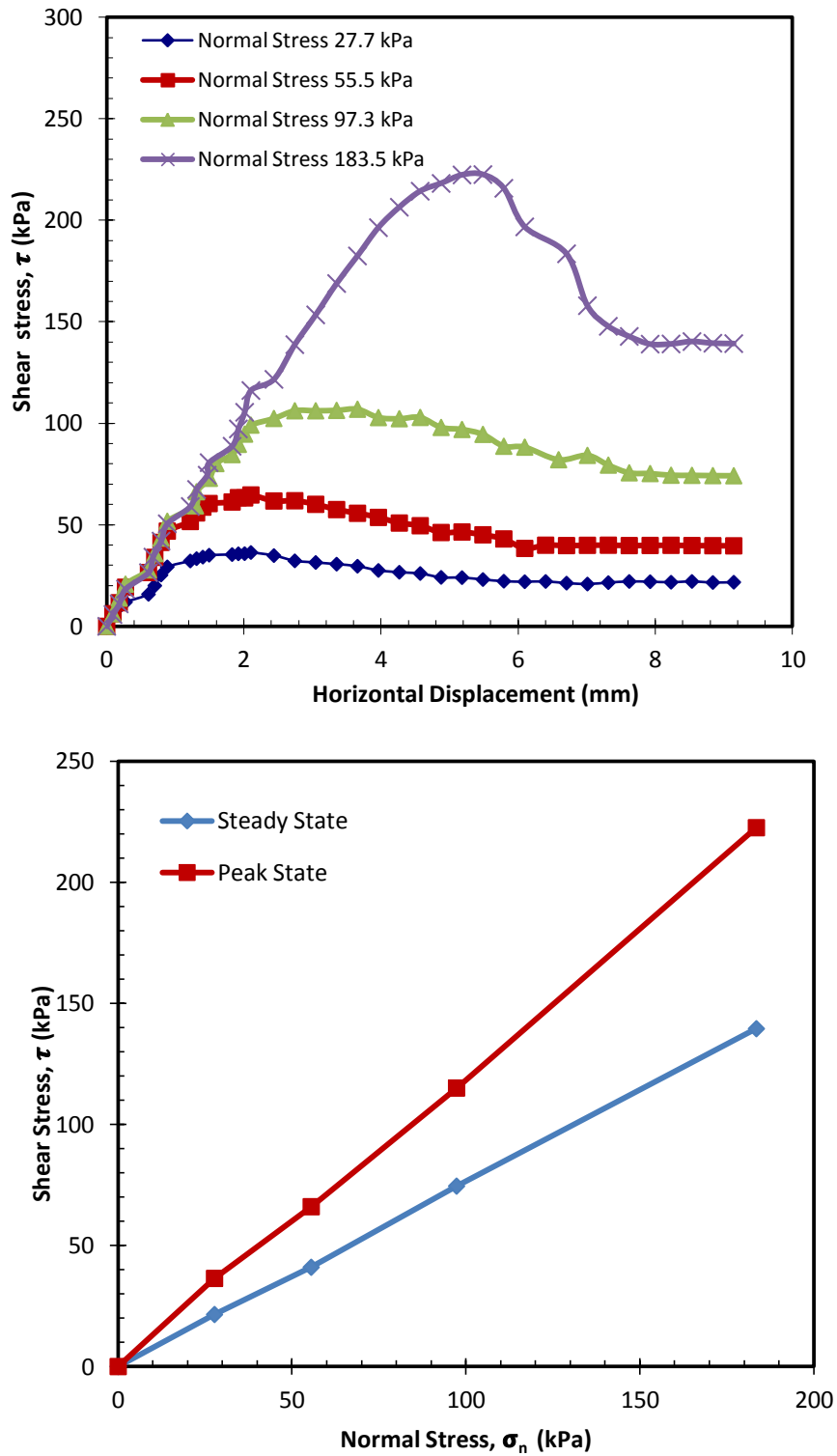


Figure 4.7: Direct shear test results for Leighton Sand A (Average Id = 87 %)

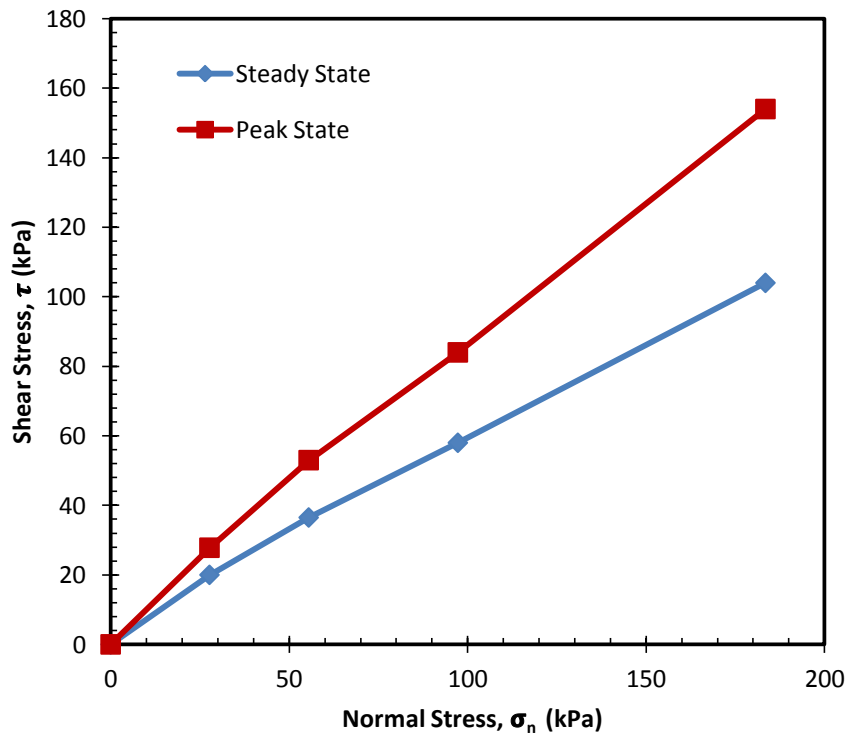
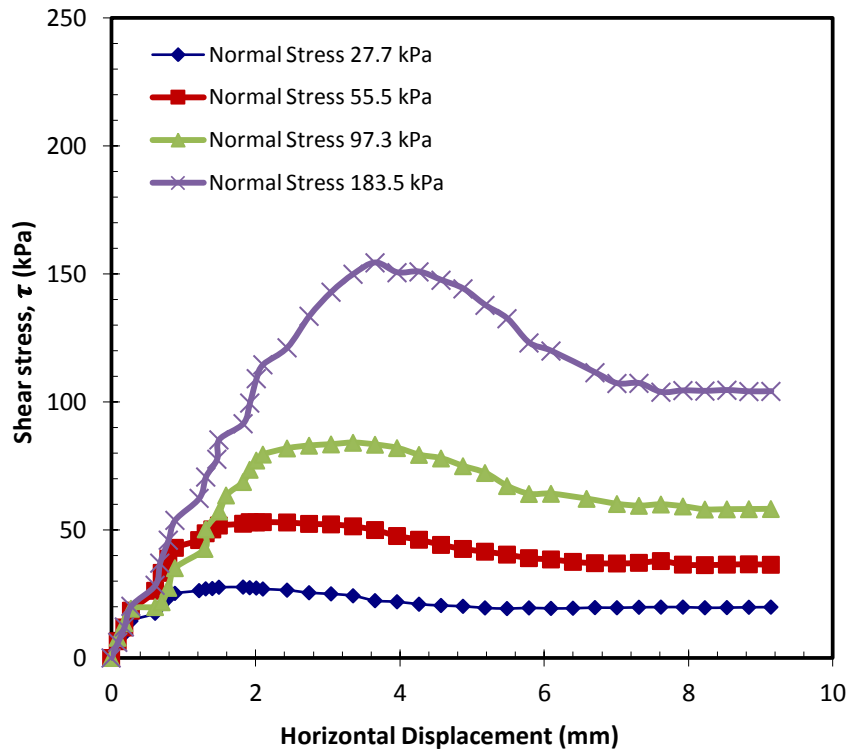


Figure 4.8: Direct shear test results for Leighton Sand B (Average $I_d = 90\%$)

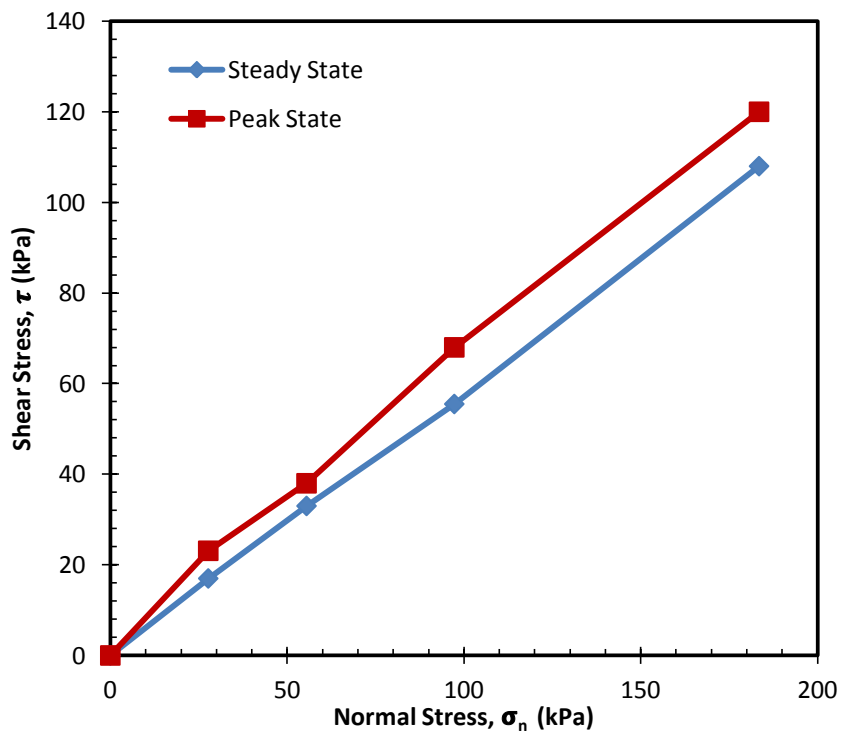
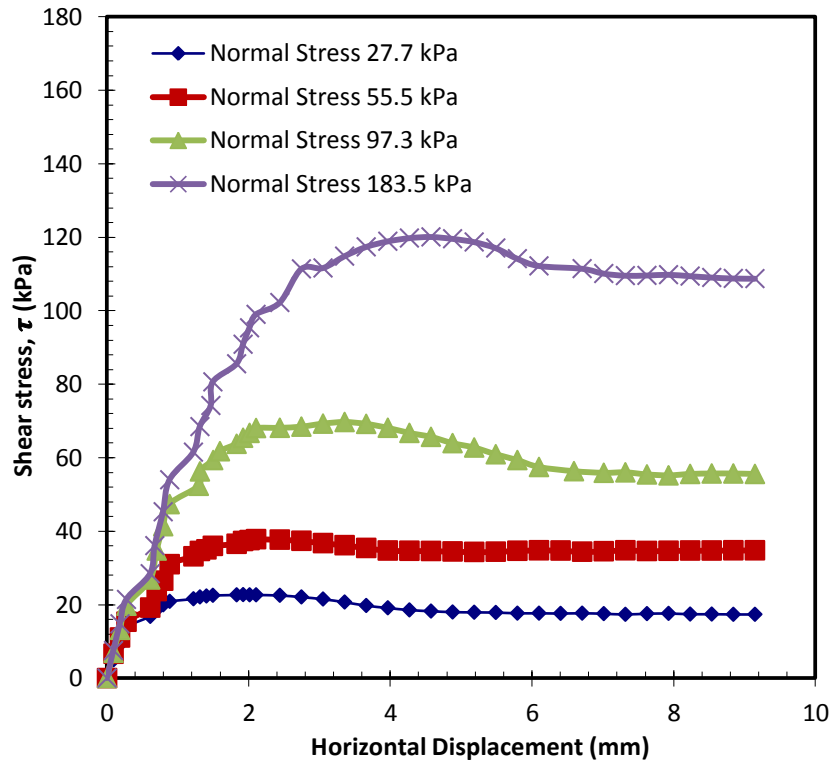


Figure 4.9: Direct shear test results for Mersey Sand (Average $I_d = 90\%$)

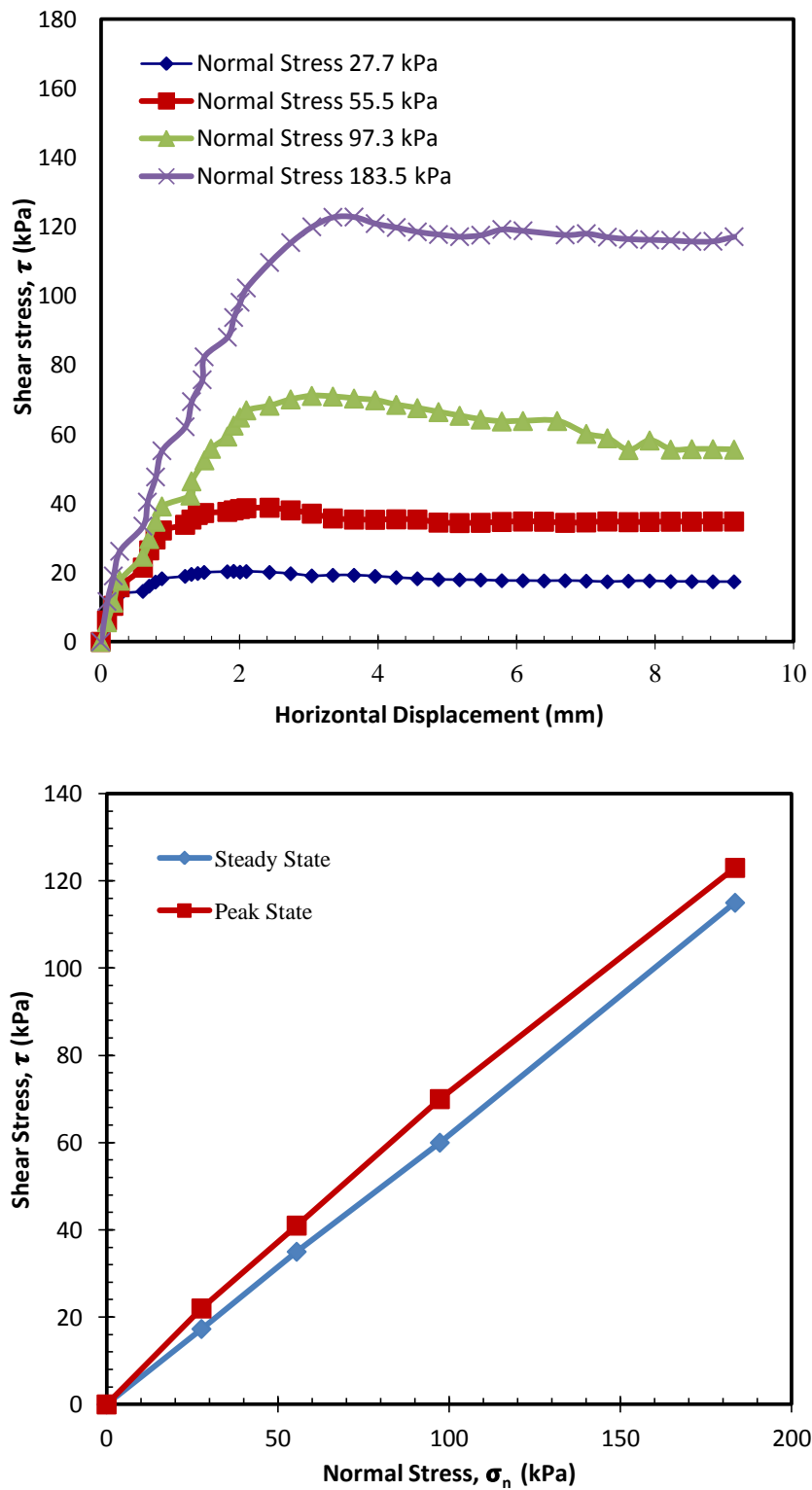


Figure 4.10: Direct shear test results for Congleton sand (Average Id = 91 %)

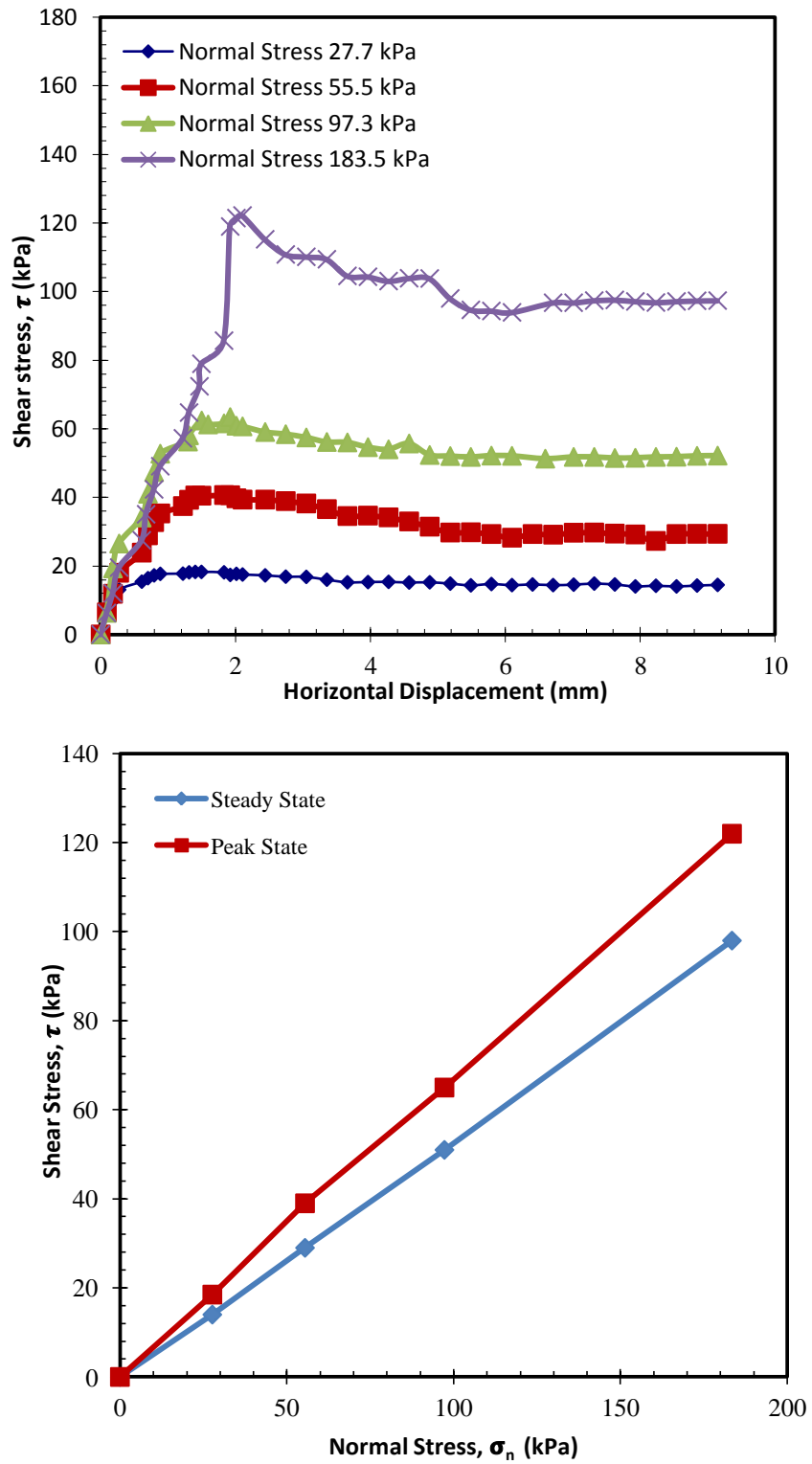


Figure 4.11: Direct shear test results for Glass Beads A (Average $I_d = 87\%$)

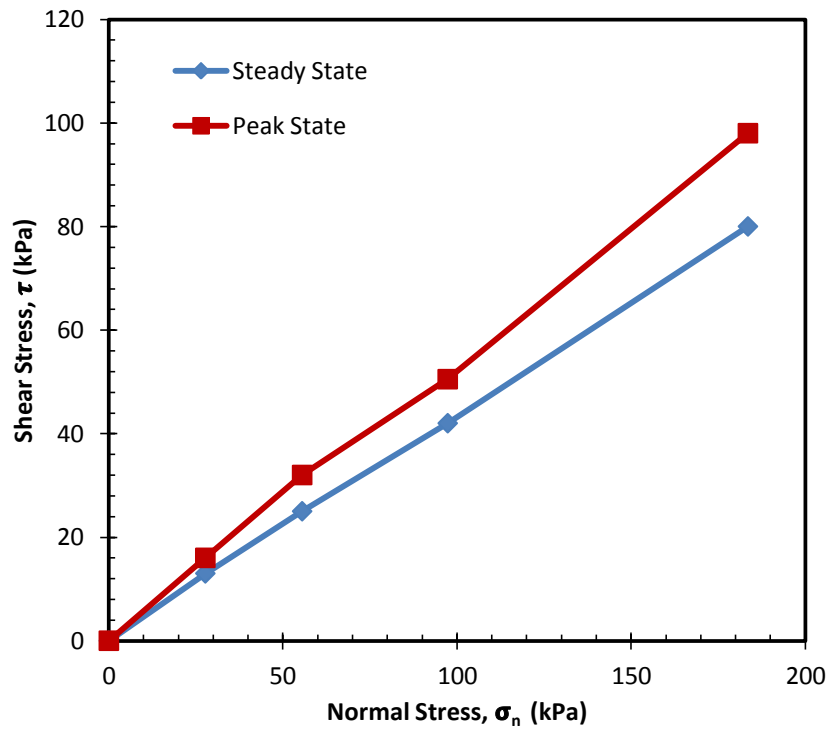
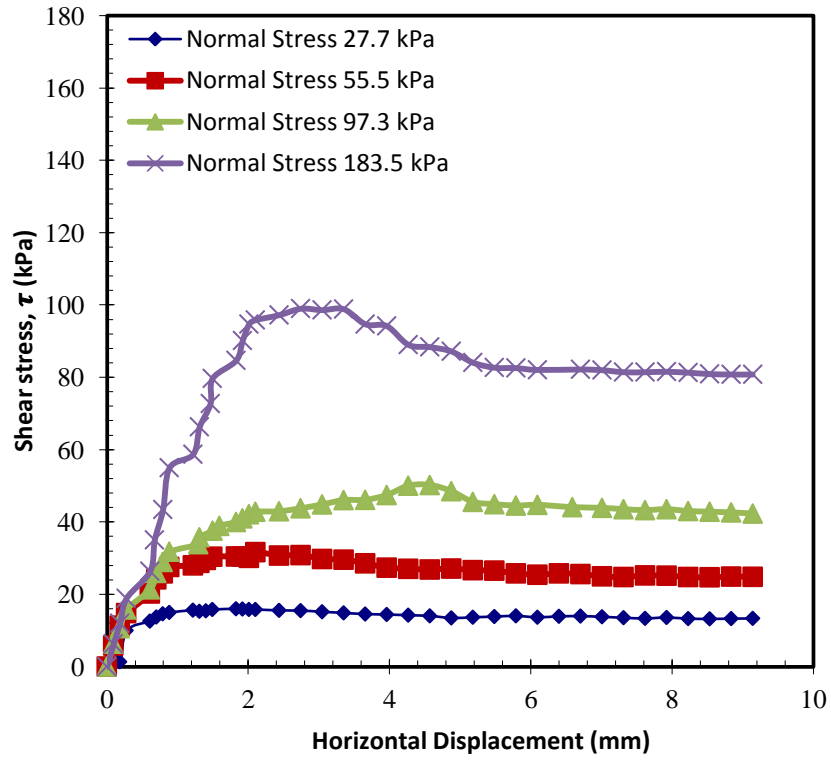


Figure 4.12: Direct shear test results for Glass beads B (Average Id = 88 %)

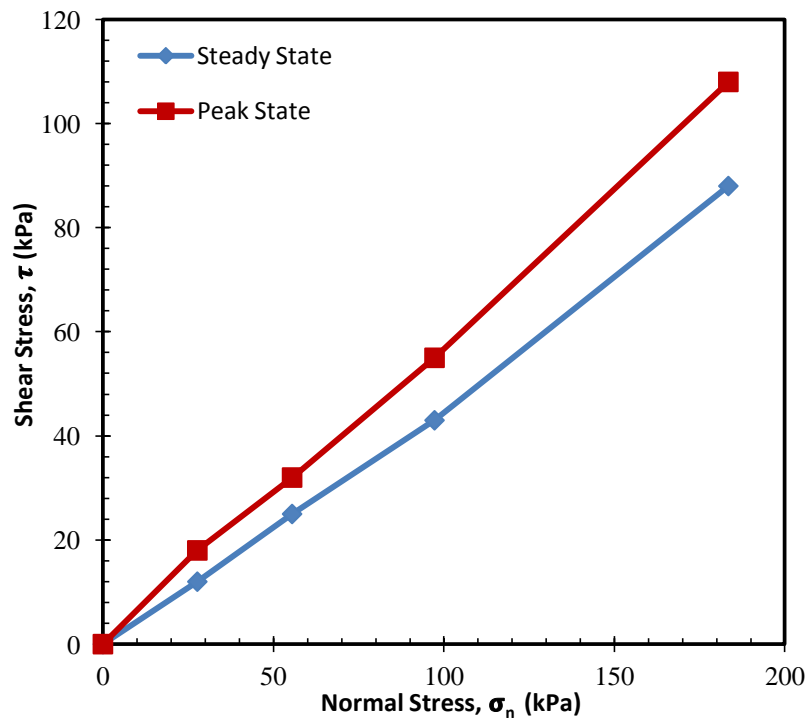
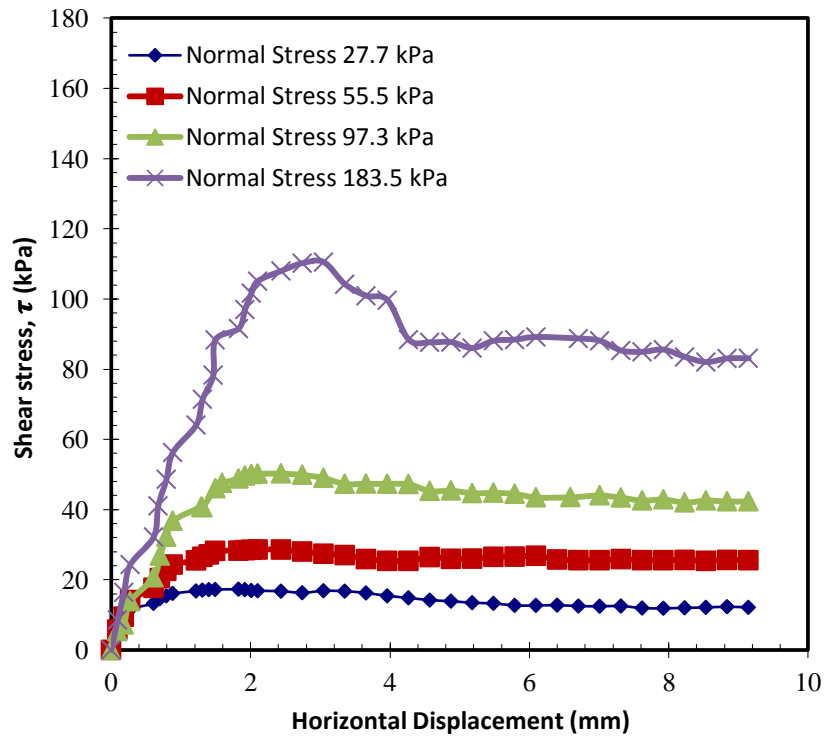


Figure 4.13: Direct shear test results for Glass beads C (Average Id = 91 %)

Table 4.2: Direct shear test results of sands and glass beads specimens

Soil type	D ₅₀	Normal stress (σ_n) kPa	ϕ_{po}	ϕ_{ro}	Density Index (I _d) %
Leighton Buzzard Sand (A)	1.65	27.7	50	37	90.0
		55.5	49	36	90.5
		97.3	49	37	89.5
		183.5	50	37	90.0
Leighton Buzzard Sand (B)	0.65	27.7	44	35	93.0
		55.5	43	33	92.7
		97.3	40	30	90.0
		183.5	40	30	90.0
Mersey Sand	0.26	27.7	35	31	89.8
		55.5	33	30	88.0
		97.3	35	31	90.0
		183.5	35	32	90.0
Congleton Sand	0.12	27.7	36	31	92.5
		55.5	34	32	91.5
		97.3	32	31	90.0
		183.5	34	32	90.5
Glass Beads (A)	0.50	27.7	32	26	85.5
		55.5	33	28	92.0
		97.3	29	27	84.5
		183.5	30	27	84.5
Glass Beads (B)	0.31	27.7	30	25.0	80.5
		55.5	30	24.5	82.0
		97.3	28	23.5	82.0
		183.5	29	23.5	83.5
Glass Beads (C)	0.20	27.7	33	24	90.5
		55.5	31	23	89.5
		97.3	30	22	88.0
		183.5	31	24	90.0

4.3 Counterface Materials

4.3.1 FRP Materials

Two different FRP composite materials namely; Glass Fiber Reinforced Polymer (GFRP) and Carbon Fiber Reinforced Polymer (CFRP) plates are used as testing materials in this study. Both materials have similar thickness (2.5 mm). CFRP is manufactured from 100% carbon filaments and suitable for use in a wide range in general engineering whereas, GFRP is manufactured from E-glass fibre filaments. The epoxy resin material is used as a matrix part in the manufacturing process for both materials.

4.3.2 Mild Steel

The low-carbon mild steel specimen 2.5 mm thickness was used in this study for comparison purposes. The plate was machined to make a specimen in appropriate size to fit into the modified shear interface apparatus.

4.4 Measurement of Surface Roughness

The surface roughness of each CFRP, GFRP and mild steel materials in this study was conducted using Taylor-Hobson stylus profilometer. As mentioned in section 2.15.2, the material surface roughness is characterized herein in terms of maximum roughness value of the profile R_t and the average mean line spacing R_{sm} . The R_t parameter was measured as it adequately evaluates the normal relative roughness ($R_n = R_t/D_{50}$) based on sand mean particle diameter (D_{50}). Kishida and Uesugi, (1987) proposed that the reference gauge length should be close to the mean particle size diameter of tested sand as shown in Figure 4.14.

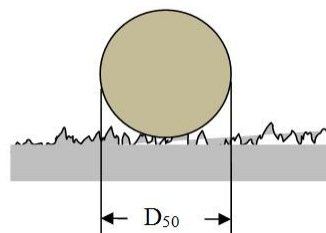


Figure 4.14: Gage length ($L=D_{50}$)

Accordingly, the surface roughness measurements of GFRP, CFRP, and mild steel specimens were performed based on this concept. The average value of surface roughness parameter R_t for each tested material which determined from above test are plotted in Figure 4.15. The roughness parameter R_t increase with gauge length. Therefore, it is noted that the GFRP specimen has higher value of R_t than CFRP and steel specimens.

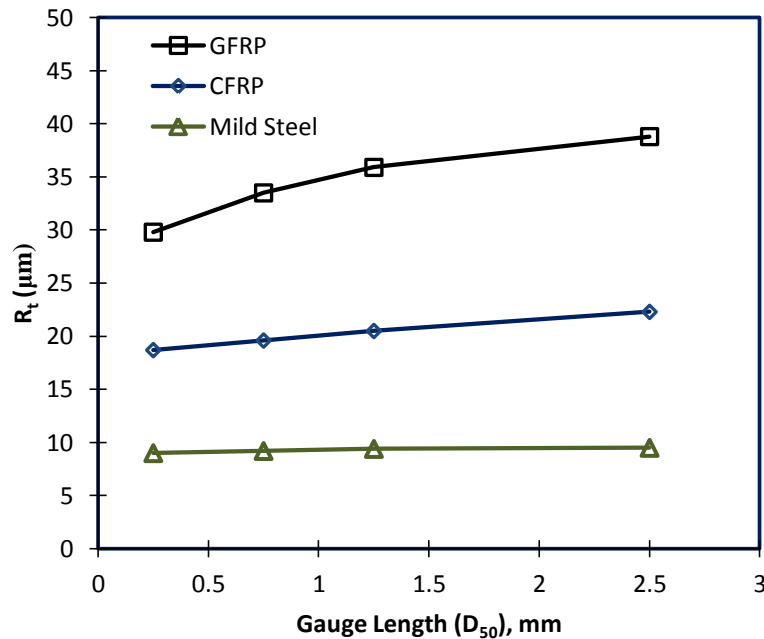


Figure 4.15: Surface roughness parameter R_t with gauge length $L=D_{50}$ for counterface material

4.5 Hardness Tests

Hardness is the property of a material that enables it to resist plastic deformation, usually by penetration. However, the term hardness may also refer to resistance to bending, scratching, abrasion or cutting. The hardness of the interface material is another important parameter for consideration when studying interface behaviour (O'rouke et al., 1990). The surface hardness of the tested materials was investigated by means of the Vickers hardness test. The Vickers hardness test method consists of indenting the test material with a diamond indenter, in the form of a pyramid with a

square base and an angle of 136 degrees between opposite faces subjected to a test force ranging between 1gf to 100 Kgf as illustrated in Figure 4.16. The full load is normally applied for 10 to 15 seconds. The two diagonals of the indentation left in the surface of the material after removal of the load are measured using a microscope and their average calculated. The Vickers hardness value was calculated as the load divided by the surface area as:

$$HV = \frac{2F \sin \frac{136}{2}}{d^2} \quad 4.2$$

Where:

HV: is the Vicker hardness

F: is the applied load in Kg.

d: is the average length of the two diagonal, *d*₁ and *d*₂ in mm.

The results of the hardness tests are summarized in Table 4.3

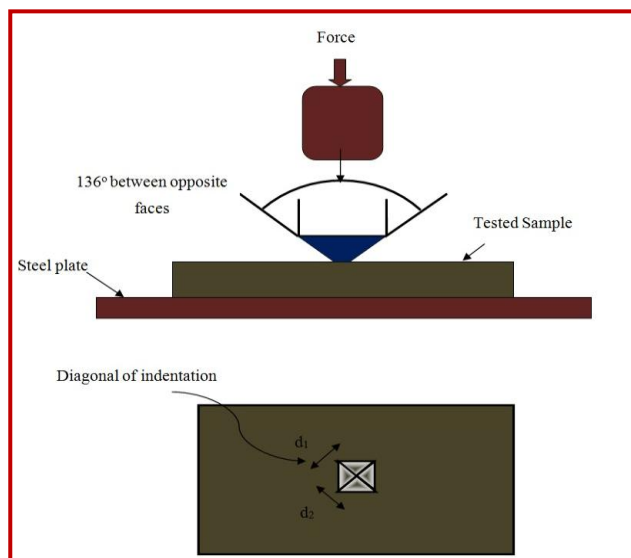


Figure 4.16: Vicker hardness scheme

Table 4.3: Hardness Results

Tested Material	Vickers Hardness(HV)		
	Test No.	Mean	Standard Deviation
GFRP	5	65	2.14
CFRP	5	49	1.58
Mild Steel	5	105	4.48

4.6 Interface Shear Tests

4.6.1 Specimen preparation

The GFRP, CFRP and mild steel plates were cut to dimensions (110×80 mm) that fit into the bottom half of the interface shear box. Each plate was cleaned and glued to timber block using two components from cohesive material (epoxy resin and epoxy hardener) as shown in Figure 4.17. The specimens were left al laboratory temperature for at least 48 hours for the plate to harden adequately before tested.



Figure 4.17: GFRP plate glued to the timber block

4.6.2 Testing Procedure

In this study, the interface shear tests were carried out using a modified direct shear box. The upper half of shear box was modified by reducing its contact area with the tested surface as shown in Figure 4.18a. The bottom half of a direct shear box was replaced by a timber block to which a GFRP, CFRP or mild steel plate was attached to the upper half and the sand is placed only in the upper half so that shearing takes place between the sand and tested material plate as illustrated in Figure 4.18b. The interface area sand and plate remains constant during a test even if sliding occurs. Similar to direct shear testing, if a mass of sand is made to slide on the surface of a tested material plate while a load is applied normal to the sliding surface, normal load F_N is applied to the top box on the cap to produce normal stress $\sigma = F_N / A$, where A is the interface cross-sectional area. A steadily increasing displacement, which causes an increasing shear force F_s , is applied to one half of the direct shear box, while the other whole box is restrained and equipped with a load measuring device. This forms the basis of interface shear test which can be used to measure the angle of interface shearing friction.

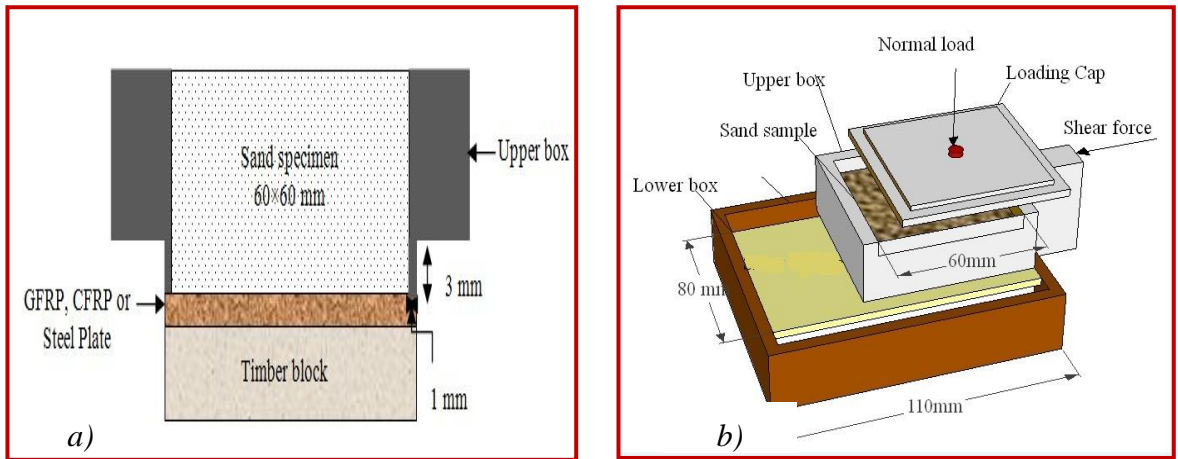


Figure 4.18: Details of modified Interface shear apparatus

4.6.3 Interface Shear Tests

The results of the interface shear resistance tests are analyzed in this section in terms of peak and residual shear interface friction for tested materials. Eighty four tests are carried out on the different FRP/sand and mild steel/sand interface combination by varying the normal load and repeating the test at shearing rate 0.52 mm/min. For each normal load, the maximum shear stress can be read off and plotted against the corresponding value. The interface friction tests performed in this study are summarized in Tables 4.4, 4.5 and 4.6.

Table 4.4: Summary of interface shear test results on GFRP

<i>Sand type</i>	D_{50}	σ_n (kPa)	(I_d) %	R_t (μm), $L=D_{50}$	R_{Sm} (μm)	R_n	μ_r	μ_p
LB-A	1.60	27.7	80.5	39.8	194.4	0.025	0.33	0.43
		55.5	81.5				0.30	0.44
		97.3	80.0				0.28	0.42
		183.5	81.0				0.26	0.40
LB-B	0.65	27.7	89.0	32.6	179.0	0.050	0.46	0.51
		55.5	87.0				0.45	0.50
		97.3	84.5				0.42	0.47
		183.5	89.0				0.40	0.47
M	0.26	27.7	88.0	30.1	127.8	0.116	0.44	0.53
		55.5	85.0				0.43	0.52
		97.3	85.5				0.43	0.50
		183.5	89.0				0.41	0.49
C	0.12	27.7	93.0	30.1	112.6	0.255	0.52	0.62
		55.5	92.0				0.48	0.59
		97.3	87.0				0.48	0.58
		183.5	88.0				0.47	0.56

Continued

<i>Sand type</i>	D_{50}	σ_n (kPa)	(I_d) %	R_t (μm), $L=D_{50}$	R_{Sm} (μm)	R_n	μ_r	μ_p
GB-A	0.5	27.7	81.5	34.1	173.4	0.068	0.35	0.37
		55.5	80.0				0.31	0.34
		97.3	83.0				0.30	0.32
		183.5	80.0				0.26	0.29
GB-B	0.31	27.7	79.0	30.1	137.0	0.097	0.30	0.37
		55.5	81.0				0.29	0.35
		97.3	81.5				0.30	0.36
		183.5	80.0				0.31	0.33
GB-C	0.20	27.7	88.0	29.6	117.0	0.148	0.29	0.36
		55.5	85.0				0.26	0.37
		97.3	85.5				0.25	0.36
		183.5	89.0				0.25	0.33

Notes: LB-A: (Leighton Buzzard Sand Type A., LB-B: Leighton Buzzard Sand Type B), M: (Mersey Sand), C: (Congleton Sand), GB-A: (Glass Beads Type A), GB-B: (Glass Beads Type B), GB-C: (Glass Beads Type C.) σ_n =Normal stress, I_d = Relative density index, R_t = maximum roughness value, R_n =Relative normal roughness, μ_r =Residual interface coefficient, μ_p =Peak interface coefficient

Table 4.5: Summary of interface shear test results on CFRP

<i>Sand type</i>	D_{50}	σ_n (kPa)	(I_d) %	R_t (μm), $L=D_{50}$	R_{Sm} (μm)	R_n	μ_r	μ_p
LB-A	1.60	27.7	80.5	21.8	118.4	0.014	0.21	0.37
		55.5	81.5				0.21	0.33
		97.3	83.0				0.20	0.31
		183.5	81.0				0.18	0.29
LB-B	0.65	27.7	89.0	19.6	105.5	0.030	0.22	0.39
		55.5	87.0				0.21	0.36
		97.3	84.5				0.20	0.34
		183.5	89.0				0.21	0.32
M	0.26	27.7	88.0	19.8	103.5	0.076	0.39	0.45
		55.5	85.0				0.38	0.42
		97.3	85.5				0.36	0.41
		183.5	89.0				0.34	0.37
C	0.12	27.7	93.0	19.7	105.6	0.160	0.37	0.50
		55.5	92.0				0.39	0.51
		97.3	87.0				0.41	0.49
		183.5	94.0				0.40	0.47

<i>Sand type</i>	D_{50}	σ_n (kPa)	(I_d) %	R_t (μm), $L=D_{50}$	R_{Sm} (μm)	R_n	μ_r	μ_p
GB-A	0.5	27.7	80.5	20.1	107.5	0.040	0.19	0.28
		55.5	81.5				0.17	0.24
		97.3	83.0				0.15	0.22
		183.5	81.0				0.14	0.17
GB-B	0.31	27.7	78.0	18.8	114.8	0.060	0.20	0.27
		55.5	81.0				0.21	0.27
		97.3	80.0				0.18	0.26
		183.5	81.0				0.18	0.25
GB-C	0.20	27.7	88.0	17.4	107.2	0.087	0.25	0.30
		55.5	85.0				0.24	0.30
		97.3	85.5				0.23	0.27
		183.5	89.0				0.21	0.26

Notes: LB-A: (Leighton Buzzard Sand Type A), LB-B: (Leighton Buzzard Sand Type B), M: (Mersey Sand), C: (Congleton Sand), GB-A: (Glass Beads Type A), GB-B: (Glass Beads Type B), GB-C: (Glass Beads Type C). σ_n =Normal stress, I_d = Relative density index, R_t = maximum roughness value, R_n =Relative normal roughness, μ_r =Residual interface coefficient, μ_p =Peak interface coefficient

Table 4.6: Summary of interface shear test results on mild steel

<i>Sand type</i>	D_{50}	σ_n (kPa)	(I_d) %	R_t (μm), $L=D_{50}$	R_{Sm} (μm)	R_n	μ_r	μ_p
LB-A	1.60	27.7	80.0	9.5	128.0	0.006	0.17	0.25
		55.5	80.0				0.18	0.24
		97.3	79.0				0.16	0.21
		183.5	80.0				0.15	0.19
LB-B	0.65	27.7	82.0	9.1	102.1	0.013	0.18	0.29
		55.5	81.0				0.19	0.26
		97.3	84.5				0.20	0.25
		183.5	88.0				0.21	0.25
M	0.26	27.7	86.0	8.9	91.7	0.03	0.30	0.32
		55.5	85.0				0.25	0.29
		97.3	85.5				0.24	0.27
		183.5	89.0				0.23	0.24
C	0.12	27.7	86.0	8.7	91.1	0.07	0.25	0.34
		55.5	84.0				0.23	0.31
		97.3	85.0				0.24	0.30
		183.5	86.0				0.24	0.27

Continued

<i>Sand type</i>	D_{50}	σ_n (kPa)	(I_d) %	R_t (μm), $L=D_{50}$	R_{Sm} (μm)	R_n	μ_r	μ_p
GB-A	0.5	27.7	77.0	9.3	116.8	0.018	0.18	0.25
		55.5	74.0				0.16	0.19
		97.3	76.0				0.15	0.18
		183.5	74.0				0.12	0.15
GB-B	0.31	27.7	77.0	8.1	104.8	0.026	0.16	0.23
		55.5	79.0				0.18	0.21
		97.3	81.5				0.18	0.19
		183.5	80.0				0.18	0.20
GB-C	0.23	27.7	82.0	7.8	74.4	0.034	0.18	0.22
		55.5	79.0				0.17	0.22
		97.3	79.0				0.18	0.20
		183.5	81.0				0.19	0.19

Notes: LB-A: (Leighton Buzzard Sand Type A), LB-B: (Leighton Buzzard Sand Type B), M: (Mersey Sand), C: (Congleton Sand), GB-A: (Glass Beads Type A), GB-B: (Glass Beads Type B), GB-C: (Glass Beads Type C). σ_n =Normal stress, I_d = Relative density index, R_t = maximum roughness value, R_n =Relative normal roughness, μ_r =Residual interface coefficient, μ_p =Peak interface coefficient

4.6.4 Discussion of Results

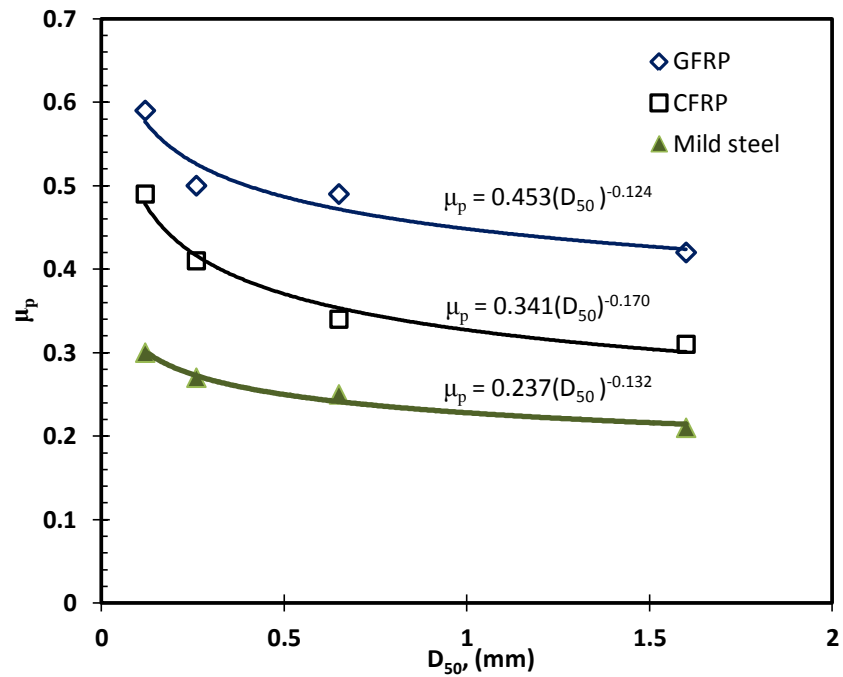
Previous works on the interface friction behaviour was mostly studied using traditional construction materials. It has been reported that the interface friction behaviour between sand and construction materials is influenced by three main parameters. They are the surface roughness of construction material, the mean particle size, and the shape of sand particles. As mentioned in chapter two, there is limited numbers of studies were performed on the interface between FRP composite materials and soils [(Frost and Han, 1999), and (Pando et al., 2002)]. These studies have not investigated the important parameters that influencing the interface friction resistance at different FRP composite surfaces. This study is more specifically aimed at ascertaining the manner in which surface manufactured in different technique affect the frictional interaction at the sand/FRP interface. The other advantage of this program is that the interface shear apparatus is conducted using the modified shear type which has less disadvantages characterize. Clearly, there is a need to examine and evaluate the important following parameters that influenced on FRP/granular.

- Mean particle size (D_{50}),
- Surface roughness (R_t),
- Sand relative density,

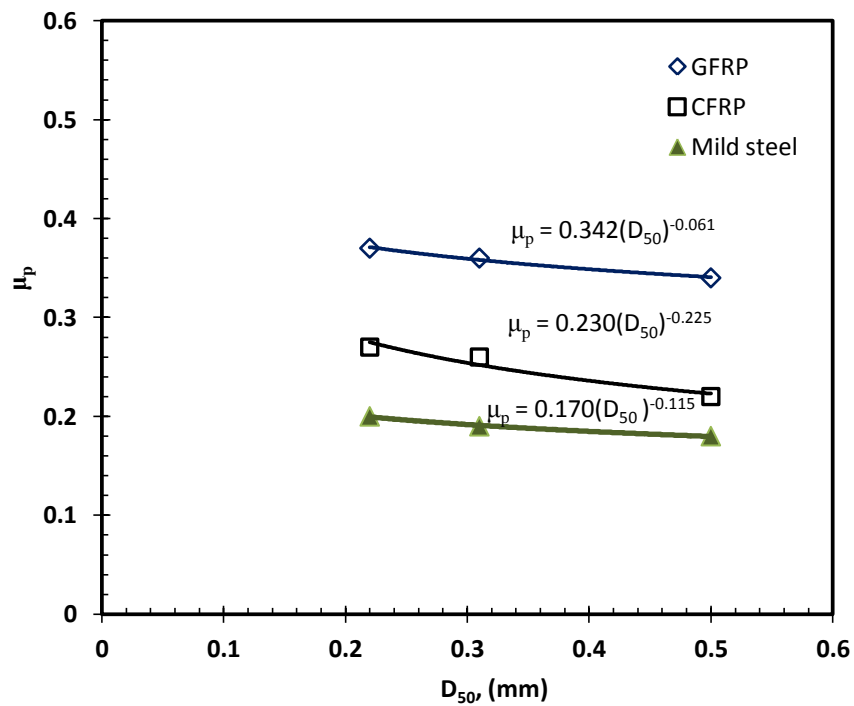
The influence of above parameters is studied relative to sand and glass beads properties with tested material surface characteristics during interface behaviour.

4.6.4.1 Mean particle size (D_{50})

In fact, the mean particle size is one of most important parameters that influenced by the interface friction. The relationship between the peak interface friction coefficient (μ_p) and mean grain size of tested sand and glass beads based on above table data is shown in Figure 4.19.



a) Sand/tested materials interface



b) Glass beads/ tested materials interface

Figure 4.19: Influenced of D_{50} coefficient interface friction at $\sigma_n=97.3$ kPa

The coefficient of interface friction decreases with an increase in the mean grain size. At the same surface, the coefficient of interface friction parameter is smaller for larger D_{50} . This relation is more consistent with the test by (Rowe, 1962) on the interface friction between quartz particles and quartz block. The results also show other important information that the influence of D_{50} of glass beads is less significant compared to sand D_{50} during interface shear friction. Since all tested sands are sub-angular to angular materials, it is quite reasonable that these types of sands have a higher interface friction coefficient than glass beads.

4.6.4.2 Surface Roughness (R_t)

As mentioned earlier, the roughness parameter ' R_t ' (unit microns) was used to report the surface roughness of tested materials. Figure 4.20 shows the results obtained for tested sands in interface shear tests performed at 97.3 kPa. As it can be seen, the coefficient interface friction increases with increasing R_t and with the decrease of mean particle diameter D_{50} . According to these results, the behaviour of an interface shear friction depends not only on the surface roughness of the material surface but also on the grain size of the soil in contact with it. For this reason a more correct way to define the roughness of the interface is to refer to a normalized roughness parameter ($R_n = R_t/D_{50}$). Figure 4.21 shows the variation in peak interface coefficient friction with R_n for various tested material with sand and glass beads respectively. It can be seen that interface coefficient friction tends to increase significantly with increase in magnitude of normalized surface roughness. When the surface type is smoother and the R_n value equal to zero, the coefficient of interface friction for sand or glass beads with tested material can be considered as the "true interface friction". It is more reasonable for tested sands have higher interface friction coefficient than GB. Since the particle of sand are angular but those GB are round. As the relative roughness increases, the interface friction coefficient approaches the internal friction coefficient of sand, which means the shear failure occurs within the sand mass. The difference of the interface friction coefficients for glass beads and other sands materials becomes smaller with an increase with relative roughness. This indicates that sand angularity of small particles plays less important role in interface behaviour than large particles.

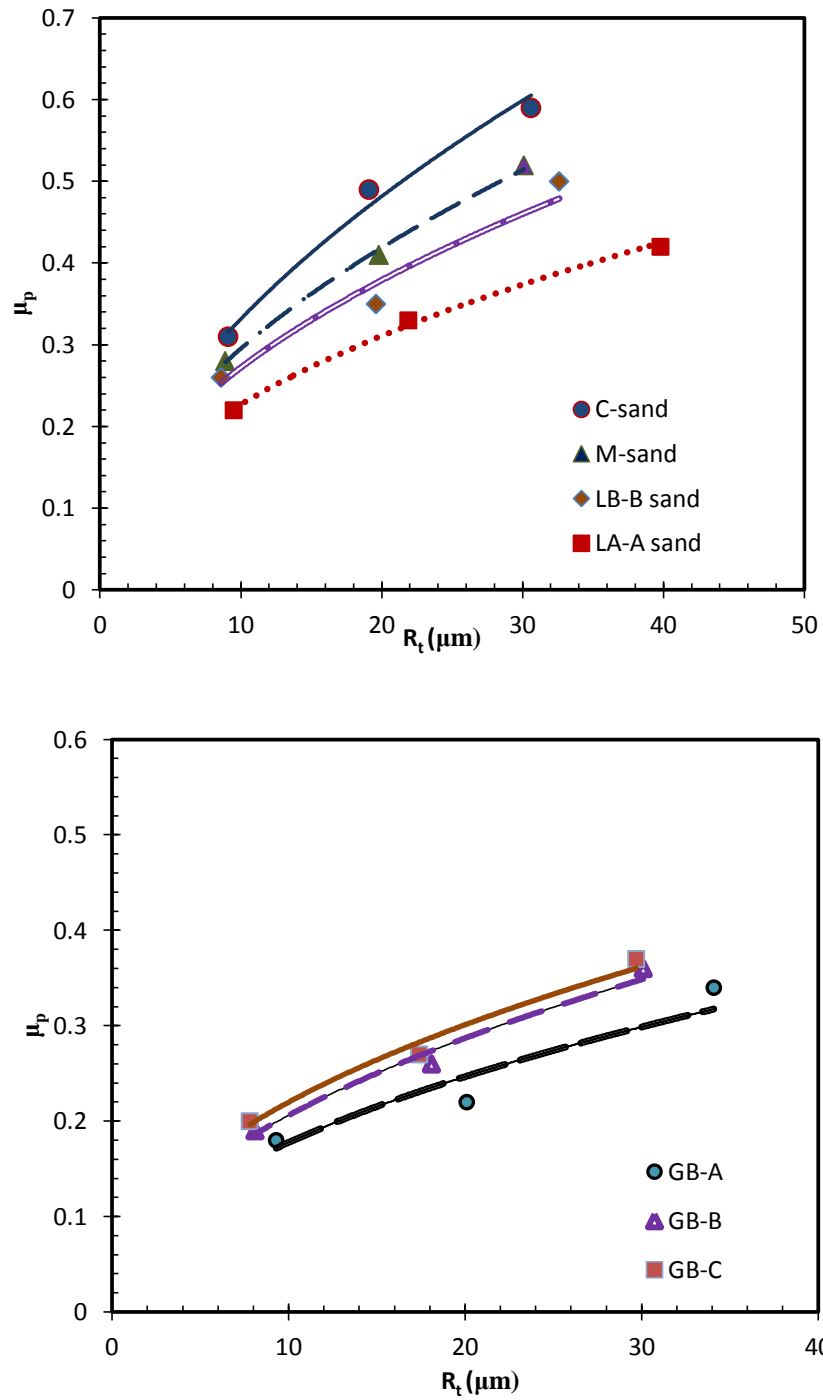
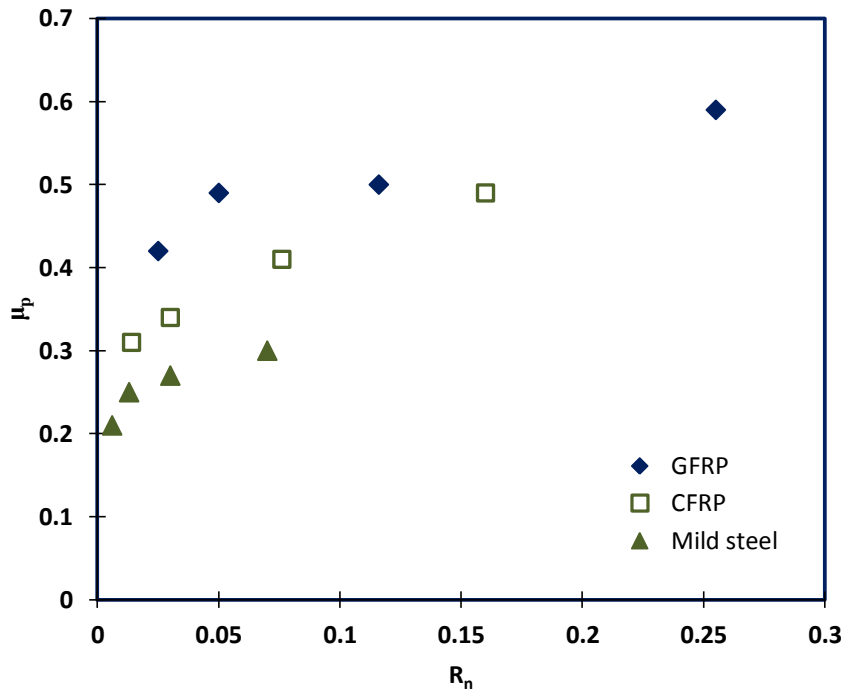
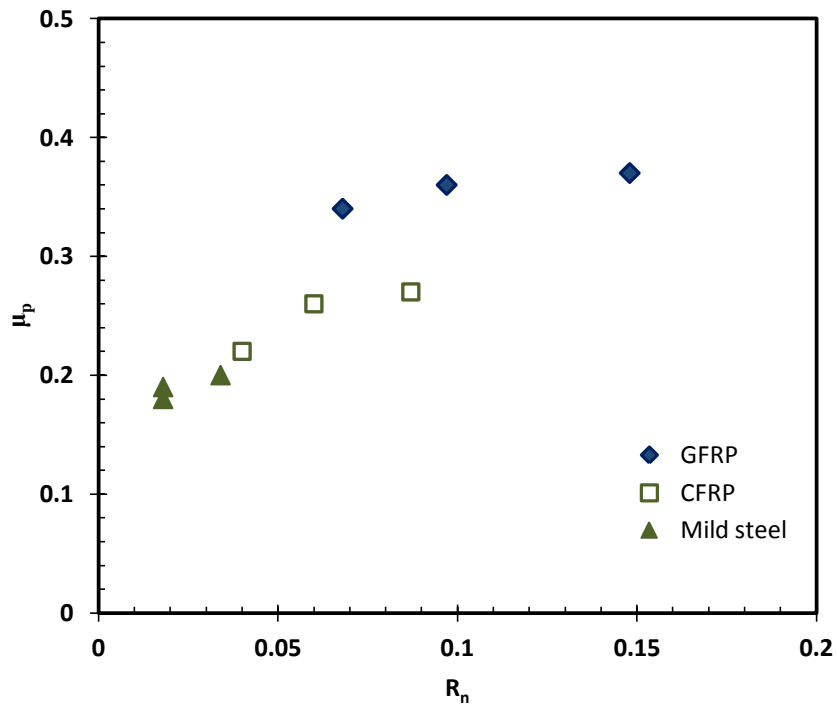


Figure 4.20: Influence of R_t on coefficient interface friction at $\sigma_n=97.3$ kPa



a) Sand/tested materials interface



b) Glass beads/ tested materials interface

Figure 4.21: Influenced of R_n on coefficient interface friction at $\sigma_n=97.3$ kPa

4.6.4.3 Sand relative density

The relative density of soil can play an important role in interface friction behaviour of sand/FRP and mild steel. Figure 4.22 shows the variation of coefficient interface friction with relative density index I_d of the Congleton sand/FRP and Congleton sand/mild.

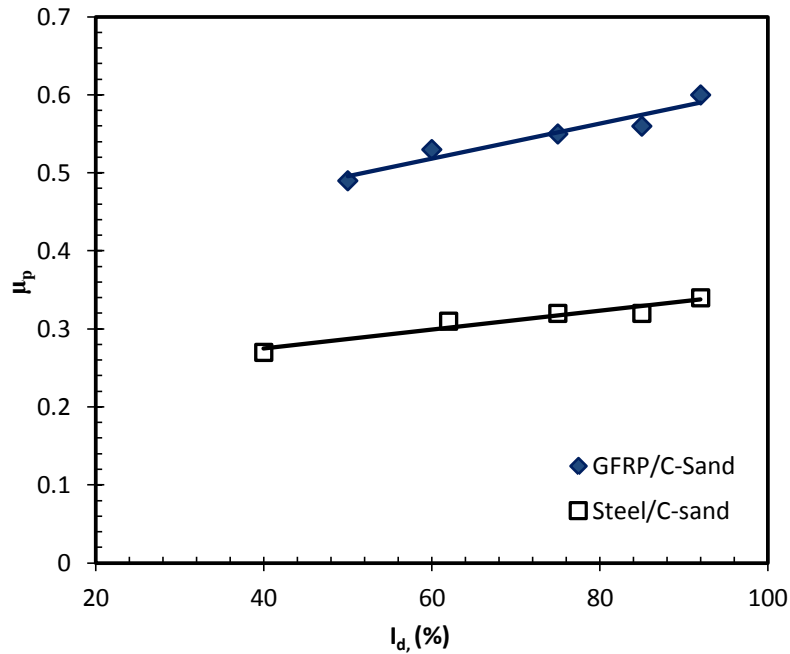


Figure 4.22: Relationship (I_d) and peak coefficient of interface friction

The experimental data was conducted at normal stress 97.3 kPa and the roughness surface parameter for GFRP and mild steel surfaces R_t are 29.2 and 8.6 μm respectively. The difference in the peak interface friction coefficient for GFRP/Congleton sand from the loose state and dense state is about 0.1. Based on this value, the difference in the interface friction angle for these interfaces states is less than 6° . This is finding concurs with observation obtained by Lehane, (1993) and (Frost and Han, 1999).

4.7 Effect of Driving Process on the FRP surface

FRP composite piles are usually installed by driving method (Sakr et al., 2005). Therefore, during the installation process, FRP pile's shaft will be subjected to interface shear process under different normal stress levels which is function of the driving depth as shown in Figure 4.23.

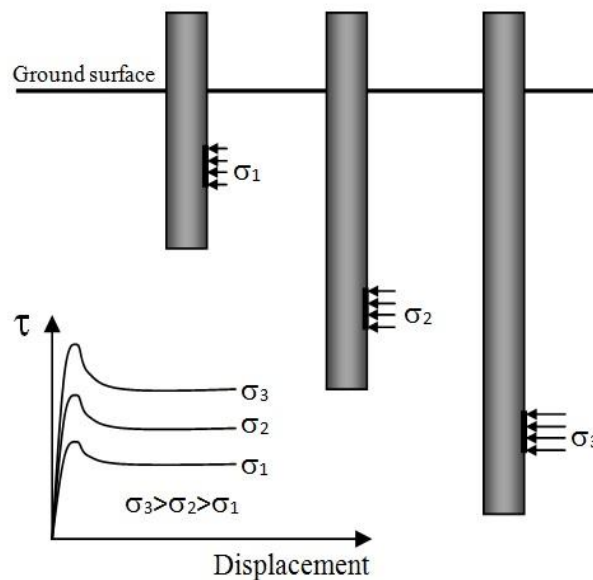


Figure 4.23: Evolution of normal and shear stress at a specific area element on the pile shaft during the driving process

The coefficient of the interface friction is dependent on the sliding and ploughing resistances where their contributions are mainly function of the normal stress and the hardness of the counterface surface. Sliding will tend to dominate for a hard counterface material whereas ploughing gets activated beyond a critical normal stress for a softer counterface (Dove and Frost, 1999). As the FRP material has a moderate surface hardness compared to steel, it is expected that ploughing mechanism could take place during FRP composite pile driving process. Ploughing includes severe plastic deformation that damages the counterface surface asperities as the granular particles remove and displace material from the surface during translation. Furthermore, ploughing is often accompanied with development of

microcracks in the counterface. Therefore, the surface roughness of FRP materials may be significantly altered during installation process. Evaluation of this change in the surface roughness is required to achieving an accurate interface pile design.

Few studies have been directed to quantify the interface shear induced surface roughness change and its effect on the interface shear coefficient. (Zettler et al., 2000) have observed that the surface roughness of geomembranes is increased when sheared against granular medium. They attributed the observed change in geomembrane surface roughness to particles ploughing effects under shearing process. Fuggle et al., (2006) investigated the change in the surface roughness of different types of infrastructure pipe as a result of an interface shearing process against granular materials. In general they concluded that the surface roughness of FRP pipe materials did not change under the shearing process. This result could be attributed to the low normal stress (50 kPa) that has been used by (Fuggle et al., 2006) which could be less than the critical normal stress value that is required to activate the ploughing process (Dove and Frost, 1999).

Based on the above discussion, there is still need to investigate the behaviour of the interface shear induced FRP surface roughness and interface shear coefficient changes under increased normal stress levels. However, the following subsections present the results of an experimental study that investigated the change in surface roughness and interface shear coefficient of FRP counterface surfaces that sheared against of sand under increased normal stress levels.

4.7.1 Shear Induced Surface Roughness Changes

A cumulative relative roughness change, ΔR_t , is used to quantify the surface roughness change. It is defined as follows:

$$\Delta R_t = \left[\frac{(R_t)^f - (R_t)^i}{(R_t)^i} \right] \times 100 \quad 4.3$$

where $(R_t)^i$ and $(R_t)^f$ are the initial after the completion of the interface shear test under each normal stress level, respectively. The test results in Figure 4.24 suggest that $\partial\Delta R_t/\partial\sigma_n$ can be considered as normal stress level independent. Furthermore, $\partial\Delta R_t/\partial\sigma_n$ is function of surface hardness, HV, and the normalized roughness parameter $R_n=R_t/D_{50}$. It increases as HV increases and decreases as R_n increases.

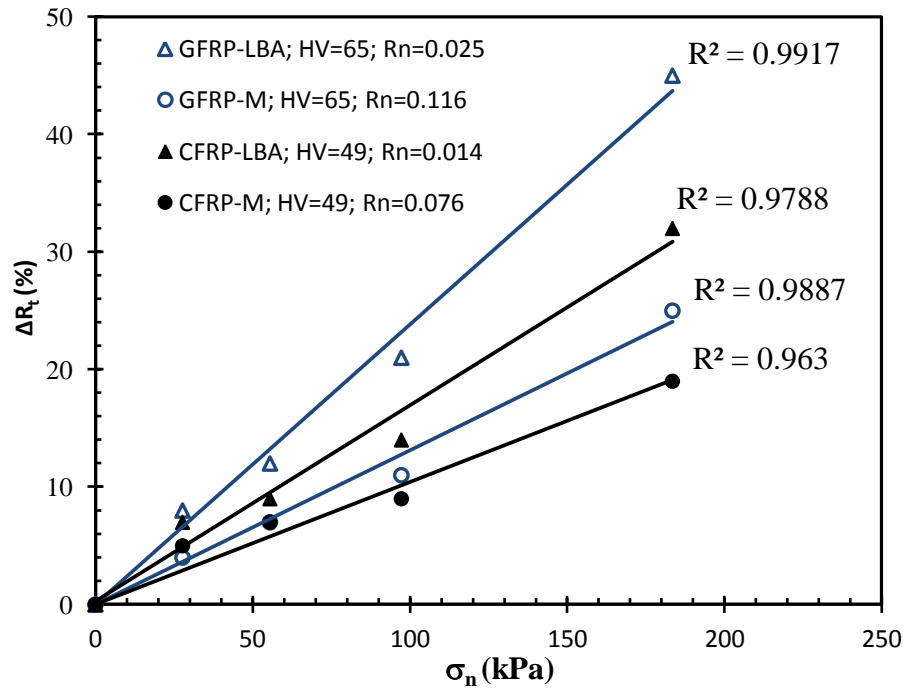


Figure 4.24: Evolution of surface roughness as the normal stress increases

The test results in Figure 4.24 shows that GFRP (HV=65) shows a low abrasion resistance (higher $\partial\Delta R_t/\partial\sigma_n$) compared to CFRP (HV=49). According to (Caceres, 2002), the wear behaviour of the materials is related to competitive processes of delamination, micro-ploughing and micro-cracking. The former is present in highly ductile material and it is accompanied by fatigue striations. Micro-cracking and micro-ploughing, which could increase the surface roughness, are present in harder material. As GFRP is harder than CFRP in terms of HV value, GFRP is expected to have a higher $\partial\Delta R_t/\partial\sigma_n$.

The effect of R_n on $\partial\Delta R_t/\partial\sigma_n$ can be explained in terms of D_{50} of the granular material. As D_{50} increases R_n decreases, the number and area of particles contacting the counterface surface decreases causing the actual contact stress per particle to increase. In fact, the possibility of damaging the counterface surface by micro-cracking and ploughing processes increases as contact stress per particle increases (Dove and Frost, 1999). Therefore, LB-A sand ($D_{50}=1.60$ mm) is expected to induce more surface roughness changes than M sand ($D_{50}=0.26$ mm).

4.7.2 Evolution of the Interface Shear Coefficient

The results in Figure 4.25 illustrate that the peak interface shear coefficient, μ_p , decreases as the normal stress increases, and $\partial\mu_p/\partial\sigma_n$ can be considered as R_n independent. This behaviour could be explained in terms of the following three mechanisms: (1) interface shear induced surface roughness increase as shown in Figure 4.24; (2) change of the contact area per particle as the normal stress increases (Dove and Frost, 1999); (3) interface shear induced striations in the counterface continuum surface (Renard et al., 2012).

According to Uesugi and Kishida, (1986), μ_p increases as the surface roughness increases. As the surface roughness increases under the interface shearing process, as shown in Figure 4.24, μ_p is expected to increase as the normal stress increases. However, as the results in Figure 4.25 show an opposite behaviour, it can be concluded that the interface shear induced surface roughness increase cannot be invoked on its own to explain the observed $\partial\mu_p/\partial\sigma_n$ in Figure 4.25.

For elastic polymer surfaces, Dove and Frost (1999) explained the observed decrease of μ_p as the normal stress increases in terms of the contact area per particle that increases as normal force increases but at a rate lower than the applied normal stress causing reduction of both of the contact stress per particle and μ_p . According to the experimental results in Figure 4.25, it can be expected that the second mechanism should have a predominant role over the first mechanism.

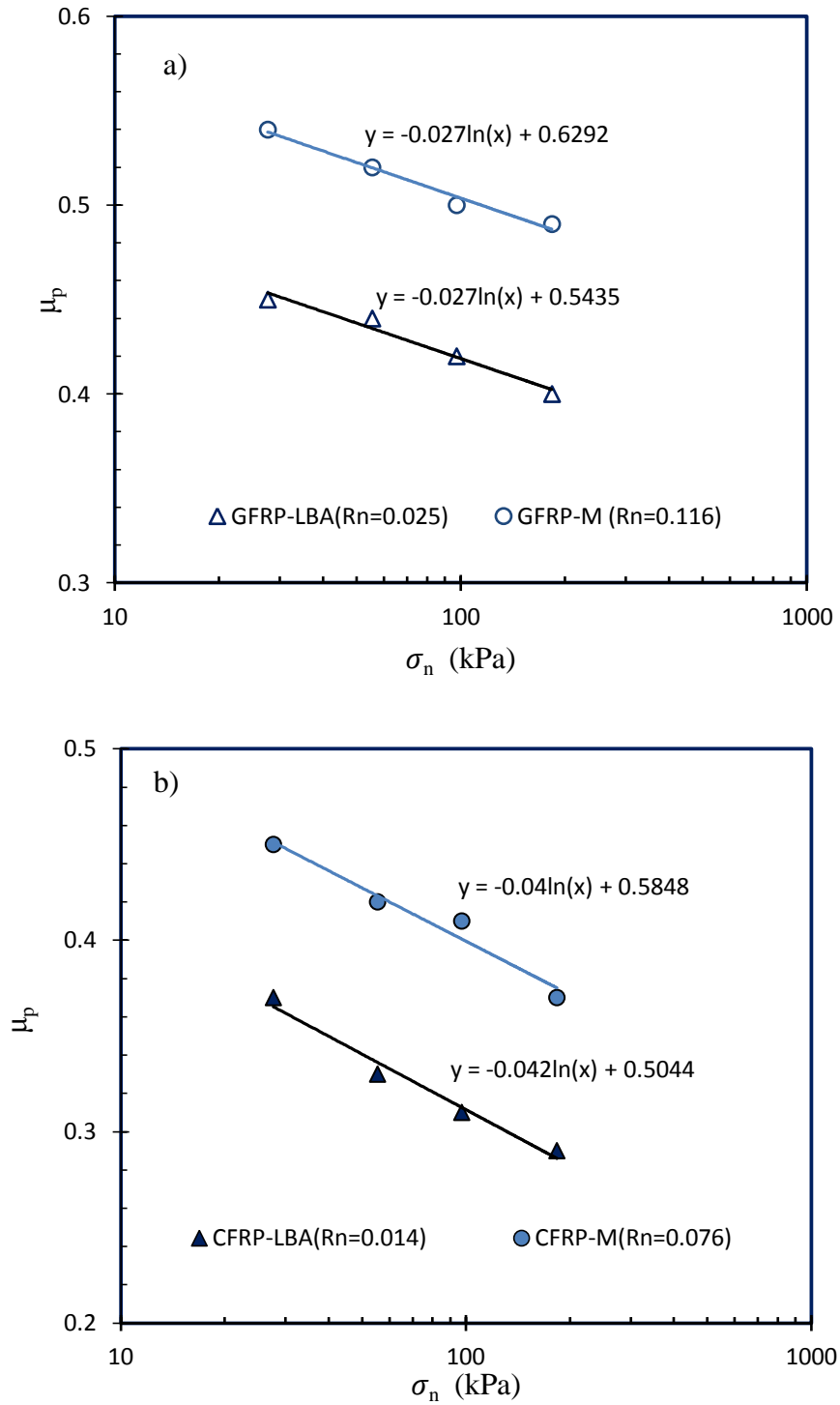


Figure 4.25: Evolution of the peak interface shear coefficient as the normal stress increases

As the second mechanism has an elastic nature and the first mechanism should increase μ_p , it was expected that μ_p values obtained from unloading normal stress path should be greater than the obtained μ_p values under the loading normal stress path. The interface shear friction coefficient measurements under loading/unloading cycle in terms of the applied normal stress are shown in Figure 4.26 for GFRP-LBA and GFRP-M. The results in Figure 4.26 show that μ_p values under the unloading path are lower than the irreversible trend. This result indicates that the above two mechanisms are not enough to explain the observed behaviour in Figure 4.26.

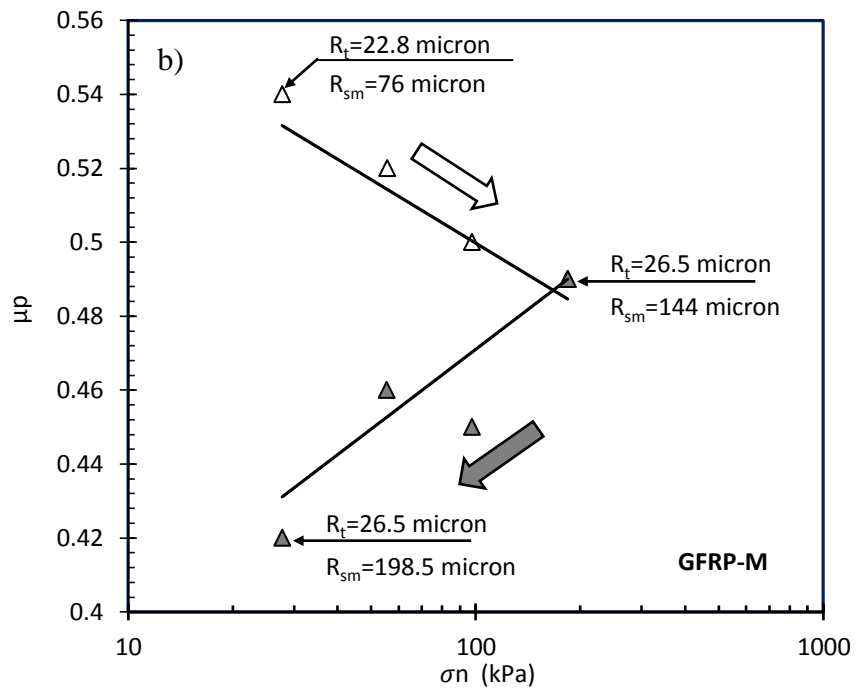
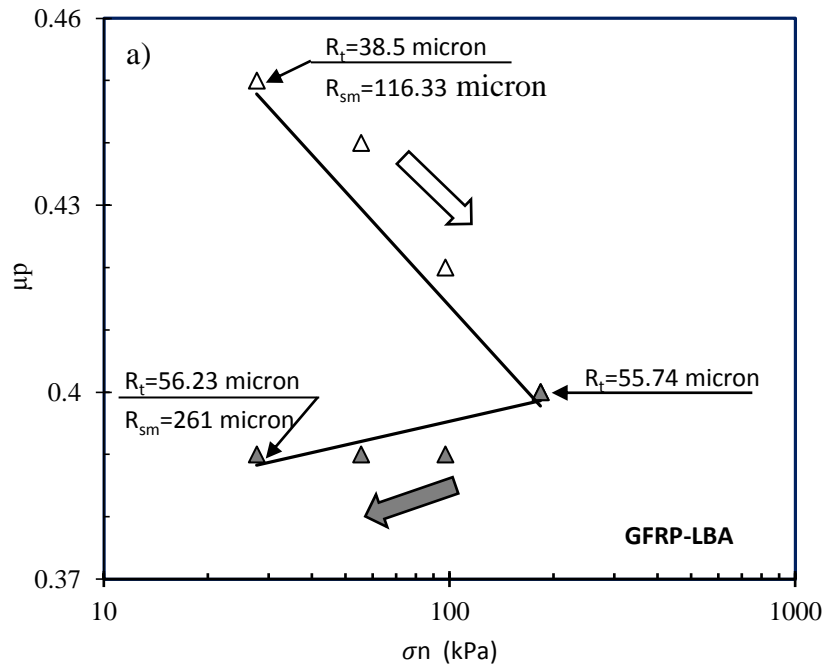


Figure 4.26: Evolution of the peak interface shear coefficient under loading/unloading normal stress path

The concept of interface shear induced striations is similar to the mechanism of scratching a surface with an indenter [(Bowden and Tabor, 1966), (Gee, 2001), and (Flores et al., 2008)]. As the interface shear process between continuum surface and granular material involves movement of particles along the counterface surface, irreversible micro-cracks and ploughing in form of striations (long thin groove) parallel to the shearing direction can be created in the counterface surface as shown in Figure 4.27, (Renard et al., 2012). Therefore, the counterface surface is expected to have irreversible longitudinal passes after completing the interface shear test under a lower normal stress. So, when the same counterface surface is sheared under the next higher normal stress, these passes will be used by the granular particles as preferential translating passes along the counterface surface. Consequently less particle translating resistance is expected. Therefore, the interface shear coefficient will decrease.

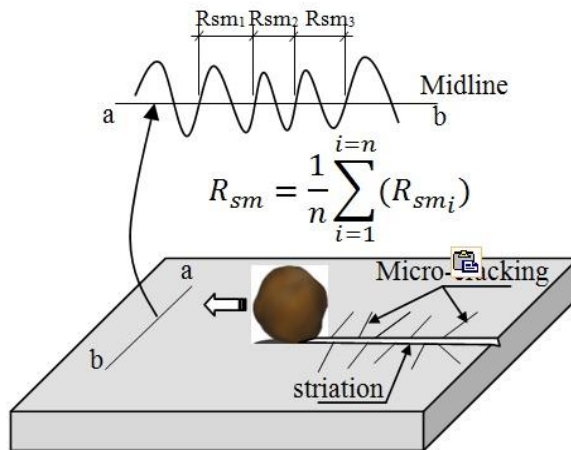


Figure 4.27: Interface shear induced striation

The spacing surface profile parameter, R_{sm} , measured in a direction perpendicular to the shearing direction can be used to quantify the interface shear induced striations as shown in Figure 4.27. The parameter R_{sm} expresses the average spacing between two crossing points on the midline that includes high and low peaks as shown in Figure 4.27 (Gadelmawla et al., 2002). The development of striations can be noticed by monitoring the change in R_{sm} value. The results in Figure 4.26 show the R_{sm} value

increases significantly (more than double) after subjecting the GFRP to loading/unloading interface shear path. Furthermore, the results in Figure 4.26 also show that R_t does not change under the unloading path.

Based on the above discussion, the change of interface shear coefficient, $\Delta\mu_p$, under increased normal stress levels can be schematically conceptualized as shown in Figure 4.28 where the first and the third mechanism are irreversible whereas the second mechanism is reversible. However, the third mechanism should have a predominant role over the first and the second mechanisms in order to get a net $\Delta\mu$ change similar to the observed behaviour in Figure 4.26.

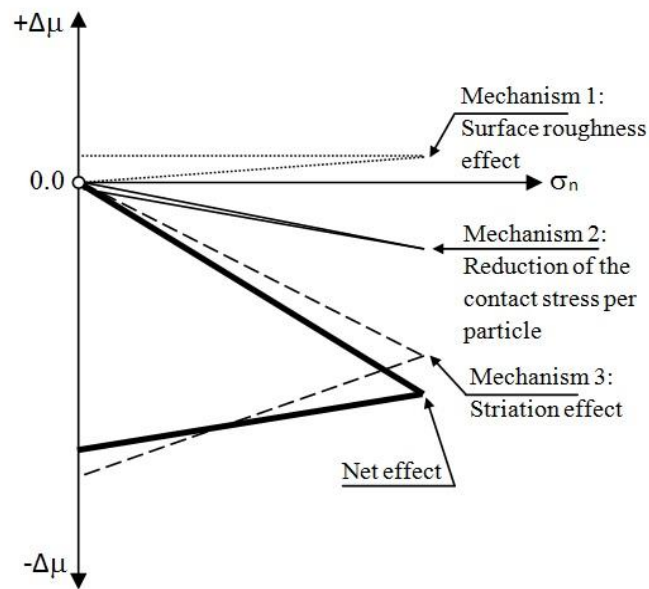


Figure 4.28: Schematic conceptual explanation for the effect of the different proposed mechanisms on the change of the interface shear coefficient as the normal stress increases

Therefore, the above schematic conceptual explanation (Figure 4.28) is practical importance in the design of many geotechnical systems. Shaft resistance of deep foundations, soil/FRP interface strength and the stability of mechanically stabilized structures depend on shear of earth materials against manufactured surfaces. The outcomes of this study could help the practitioners in considering the pile driving installation effects on the interface design parameters.

4.8 Summary

In this chapter, the details of the entire interface experimental program, including the tested materials and their properties, the methods of sample and equipment preparation, surface roughness, characterization of surface hardness of tested materials were described. The interface shear tests involving the particulate material (i.e. sand and glass beads) with two FRP composite materials (i.e. GFRP and CFRP) and one traditional material (mild steel) were performed by utilizing a modified shear apparatus. The results and analyses presented herein demonstrate that the shear mechanisms and resulting friction coefficients of particulate/FRP interface systems are dependent on a combination of several factors including polymeric material physical/mechanical properties (e.g. Surface roughness and hardness), granular soil particle shape (i.e. angularity /roundness), density, and normal stress levels. An additional experimental investigation was conducted to investigate the change in surface roughness and interface shear coefficient of two different FRP counterface surfaces that sheared against two different types of sand under increased normal stress levels. However, the following points and observations can be made regarding the experimental results:

- Surface roughness (R_t), mean particle size (D_{50}), and granular type were found to have significant effect on the peak interface friction coefficient (μ_p).
- In general, the angular particles give slightly higher interface friction coefficient than the rounded particles.

- The interface friction coefficients, both peak and residual, were found to increase with increasing normalized roughness parameter, $R_n=R_t/D_{50}$.
- The test results also indicate that the peak interface shear coefficient decreases as the normal stress increases. This behaviour could be explained in terms of the interface shear induced surface roughness increase, the change of the contact area per particle as the normal stress increases, and the interface shear induced striations in the counterface continuum surface.

CHAPTER FIVE: LONG-TERM INTERFACE BETWEEN FRP/SAND

5.1 Introduction

Traditional piling materials such as concrete, steel and timber suffered strength degradation and their repair cost is significant especially if installed in aggressive/harsh marine environment. Problems associated to these traditional pile materials include deterioration of wood, corrosion of steel and degradation of reinforced concrete making its service life reduced. A relatively new trend in deep foundation industry is to use composites as a substitute for traditional materials in piling system. FRP composites pile presents an alternative solution to avoid most of the traditional piles' performance shortcomings. It used to overcome the low durability of conventional concrete piles in waterfront and aggressive environments. In fact, FRP tube plays two roles; strengthening the concrete by the confinement effect, and protecting the concrete from the aggressive environment (Iskander and Hassan, 2001). Few studies have investigated the geotechnical behaviour of FRP piles [(Frost and Han, 1999), (Pando et al., 2002), and (Sakr et al., 2005)]. Furthermore, as the service life of this new composite pile should be about 100 years, the possible degradation of FRP under different aging environments was also assessed in terms of FRP mechanical properties (Iskander and Hassan, 2001).

FRP/soil interface shear behaviour controls pile's shaft resistance, an attention should also be paid to the possible effect of FRP degradation on FRP-soil interface shear behaviour. To the authors' knowledge this subject is not yet covered in the existing literature of FRP-geotechnology. This chapter presents the experimental program to investigate the influence of ageing environment on FRP/granular interface shear behaviour under different aging environments. The testing materials in this study include two different FRP materials; Glass Fibre Reinforced Polymer (GFRP) and Carbon fibre Reinforced Polymer (CFRP), and two different granular materials in terms of particle shape and D_{50} . Acidic and alkaline aging environments were adopted in this study. The experimental program involves assessing the ageing

effect on the testing FRP materials in terms of the changes in their hardness and surface roughness properties. Furthermore interface shear tests were conducted, using the un-aged and aged FRP materials, to evaluate the effect of aging environments on FRP-granular interface shear coefficient.

1. Tested materials.
2. Test Procedures.
3. Long-term Interface Shear Tests
4. Discussion of Results.

5.2 Tested Materials

FRP specimens: A total of 24 FRP specimens, comprising of 12 CFRP and 12 GFRP specimens, were mainly used for the long-term interface program.

Chemical Solutions: Two different aggressive solutions were used acidic (HCL), and alkaline (NaOH) representing aggressive environments which were supplied by Fisher Scientific Company. The following environments have been selected in this study:

- Acidic environment of aqueous solution of HCL at pH=2.
- Alkaline environment of aqueous solution of NaOH at pH=12

5.3 Test Procedures

The testing program involves immersing the GFRP, CFRP in two different aqueous solutions; NaOH (pH=12), and HCl (pH=2) which represent acidic and alkaline soil environments, respectively, for 24 weeks. Furthermore, as the chemical reaction can be accelerated as the temperature increases (Arrhenius 1912), FRP specimens exposed to each pH level were aged under two different elevated temperatures (45 °C and 80°C) to obtain different specimen ages within the duration of the experiment

(24 weeks). The procedure steps for ageing the tested specimens in long-term as follows:

1. The FRP specimen's surfaces were wiped and cleaned before testing.
2. The hardness and surface roughness were measured before and after aging time.
3. The specimens were divided to four groups for the acceleration. Each group is consisted 12 specimens (3 specimens for each material).
4. Four plastic boxes (40×35×22 cm) were prepared. Each two boxes filled with aqueous solutions (one acidic and one alkaline) stored in two an electrical automatic ovens.
5. The specimens was deteriorated to solution type were fully immersed and aged 24 weeks using two ovens at different elevated temperatures (45° and 80°C).
6. The solutions were replaced every month with fresh ones and the pH was maintained at 2 and 12 in acidic and alkaline solutions respectively during acceleration period.

An Accumet PH meter and temperature device was used to measure of the degree of acidity or alkalinity and temperature as shown in Figure 5.1. The pH values for both acid and alkaline containers were measured and checked weekly several times to maintain acidic and alkaline conditions during the period of acceleration process as shown in Figure 5.2 .



Figure 5.1: pH and temperature measurements

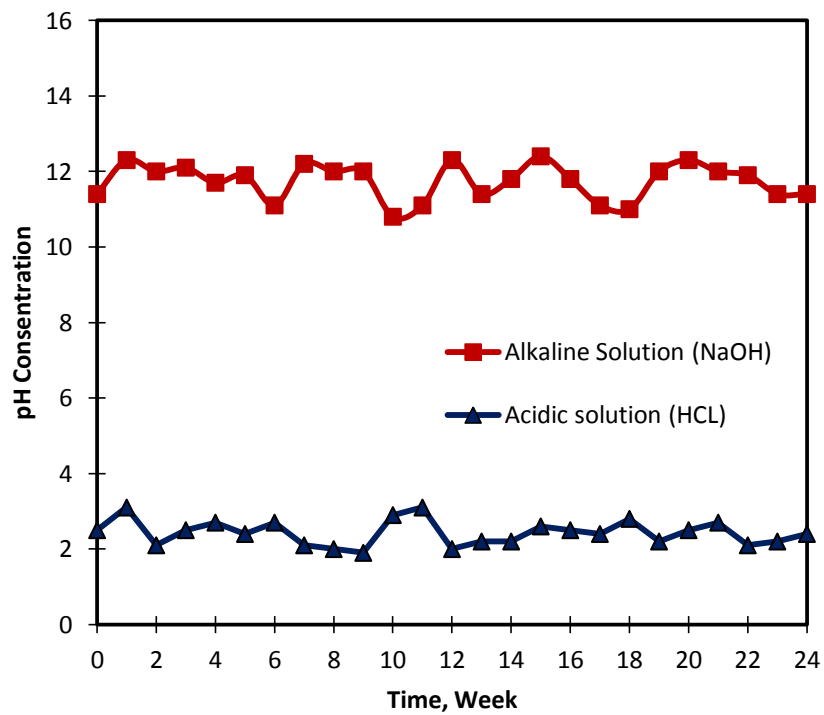


Figure 5.2: Variation in pH with time of the acidified and alkaline solution during acceleration period

5.4 Long-Term Interface Shear Tests (LTIST)

An experimental research study including series of laboratory interface tests at two aggressive environments and temperatures between different (CFRP and GFRP) with different particulate materials (rounded, angular granular materials) was performed. The experimental program involves assessing the ageing effect on the testing FRP materials in terms of the changes in their surface roughness and hardness properties. Furthermore interface shear tests were conducted, using the unaged and aged FRP materials, to evaluate the effect of aging environments on FRP-granular interface shear coefficient.

5.5 Behaviour of GFRP and CFRP in LTIST

The interface shear strength tests were carried out using aged FRP material. Table 5.1 and 5.2 provide the details of the various interface tests conducted in this study using Congleton (CG) and glass beads (GB-B). It can be seen that the interface coefficient friction was increase after subjected to the adopted aging environment. Both aqueous solutions were caused degradation of composite resins surface lead to increase the surface roughness.

The typical interface friction coefficient between GFRP and Congleton sand was presented in Figure 5.3. It can be seen from this figure that the interface friction strength was increased with acceleration temperature at the same aggressive solution. However, both GFRP and CFRP composite become relatively rougher after aging and acceleration and show high surface resistance at high acceleration temperature especially in acid solution. The results after aging show that the increase in R_t value for each testing FRP material (GFRP and CFRP) is almost similar under the acidic (pH=2), and alkaline (pH=12) aging environments. However, the alkaline aging environment induces a greater increase in HV than the acidic aging environment. In general, the obtained results in suggest that the applied aging environments in this study have more effects on GFRP than on CFRP. This point will be discussed in details at the end of this chapter.

Table 5.1: Interface shear for tested materials for GFRP at different aging conditions

GFRP at pH=2						
Temp. °C	HV	R _t	Glass Beads (GB)		Congleton (CG)	
			R _n	μ _p	R _n	μ _p
45	71.5	36.2	0.17	0.47	0.30	0.58
80	79.0	40.3	0.13	0.54	0.33	0.60
GFRP at pH=12						
Temp °C	HV	R _t	Glass Beads (GB)		Congleton (CG)	
			R _n	μ _p	R _n	μ _p
45	121.7	34.0	0.10	0.45	0.28	0.57
80	132	39.3	0.12	0.46	0.32	0.60

Table 5.2: Interface shear for tested materials for CFRP at different aging conditions

CFRP at pH=2						
Temp °C	HV	R _t	Glass Beads (GB)		Congleton (CG)	
			R _n	μ _p	R _n	μ _p
45	68	17.1	0.05	0.43	0.14	0.50
80	74	23.1	0.07	0.47	0.19	0.52
CFRP at pH=12						
Temp °C	HV	R _t	Glass Beads (GB)		Congleton (CG)	
			R _n	μ _p	R _n	μ _p
45	94.4	19.4	0.06	0.43	0.16	0.50
80	98	19.3	0.06	0.46	0.16	0.50

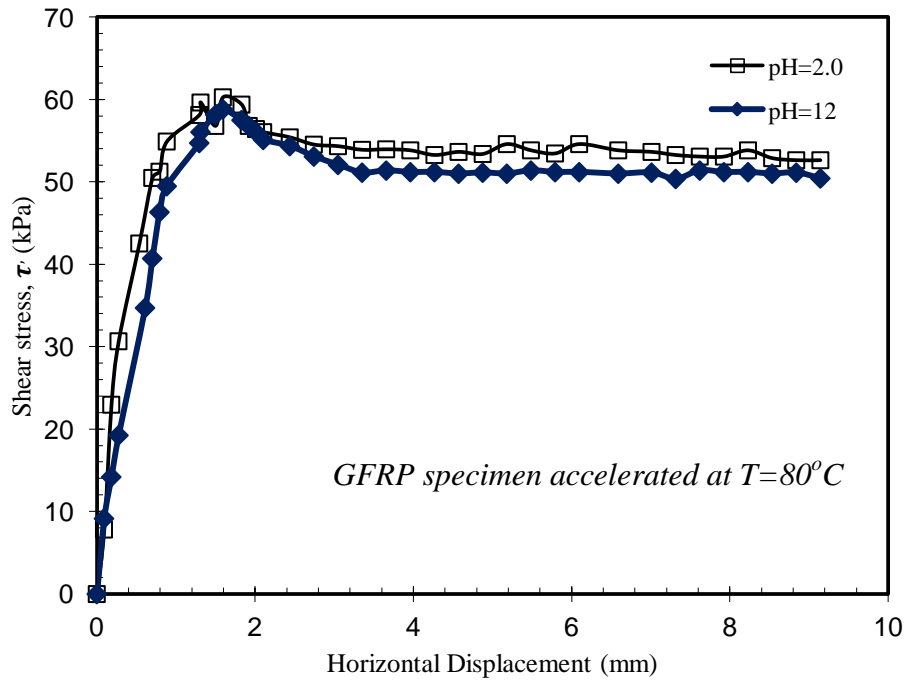
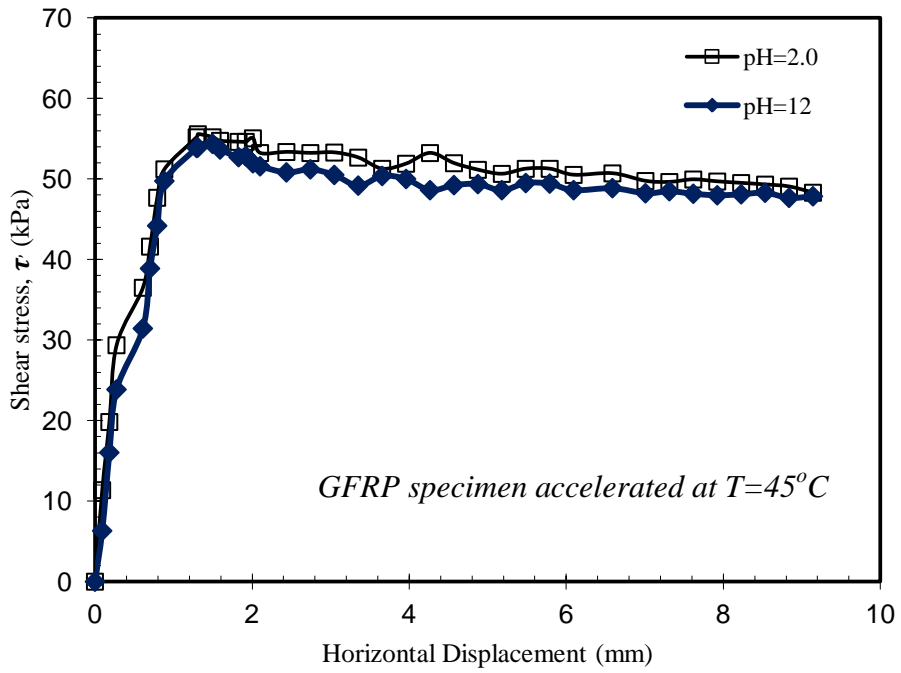


Figure 5.3: Shear Stress–displacement curves at different pH values at various temperatures

5.6 Discussion of Results

5.6.1 Aging Effects on R_t and HV

In order to assess the surface roughness R_t and hardness HV of unaged and aged FRP testing specimens, the control and aged interface results were used for this purpose. Figure 5.4 shows the aging induced changes in HV and R_t of the FRP testing specimens under different aging environment conditions. The values between the brackets represent the temperature of the aging environment. The control specimen points at temperature of 20°C represent HV and R_t of the testing FRP materials as received from the manufacturer. The results in Figure 5.4 illustrate that for both FRP materials (GFRP and CFRP), HV and R_t have been increased after subjected to the adopted aging environments in this study. The results in Figure 5.4 also show that the increase in R_t value for each testing FRP material (GFRP and CFRP) is almost similar under the acidic (pH=2), and alkaline (pH=12) aging environments. However, the alkaline aging environment induces a greater increase in HV than the acidic aging environment. In general, the results in Figure 5.4, suggest that the applied aging environments in this study have more effects on GFRP than on CFRP.

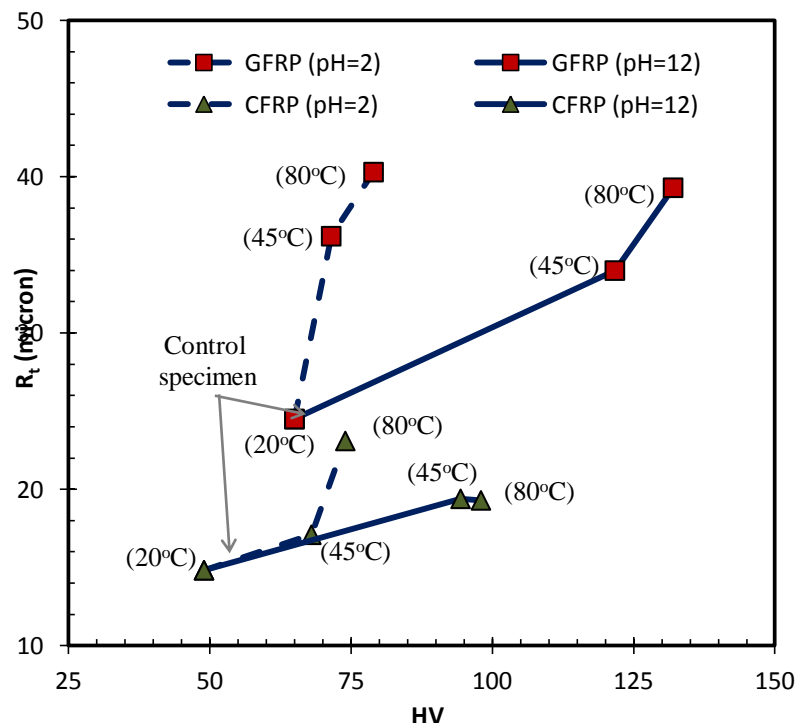


Figure 5.4: Ageing induced changes in HV and R_t of FRP testing materials

In fact, it should be mentioned that the observed difference in the ageing effects on GFRP and CFRP has no relation with the type of reinforced fibre (glass and carbon) as the tested engineering properties in this study (HV and R_t) are mainly matrix-dominated properties. Therefore, the observed difference in ageing effects should be explained in terms of the possible difference in matrix properties of GFRP and CFRP testing materials. However, as epoxy was the matrix material for both of them, the observed difference in aging effects could be attributed to the possible difference in GFRP and CFRP epoxy curing process which controls the properties of cross-linked polymer network. In fact, it is known that the extent and distribution of cross-links dictate the physical, mechanical, and thermal properties of the epoxy material (Bandyopadhyay and Odegard, 2012). Therefore, any change in the curing method could affect the engineering properties of the matrix materials (Xu et al., 2009).

The observed increase in the hardness of GFRP and CFRP after subjected to the applied ageing environments could be attributed to the expected additional epoxy curing process that could take place during the ageing process. In fact it is a common practice in FRP manufacturing process to under-cure the epoxy in order to avoid the inherently brittleness of the fully cured epoxy (Perrin et al., 2009). This deliberately under-curing process of epoxy resin produces low cross-linked polymer network density. In fact, as the adopted ageing process involves immersing the testing specimens in aqueous solutions at elevated temperatures, plasticization of the epoxy resin is expected (De'Nève and Shanahan, 1993). This behaviour allows the polymer chains to become mobile, and promotes cross-linking process. Consequently, this allows the curing reaction to tend to completion (Kajorncheappunngam et al., 2002). Gupta et al., (1985) have shown that the mechanical properties of epoxy improve as its cross-link density increases. Therefore, the epoxy mechanical properties such as surface hardness are expected to improve under wet ageing condition.

In addition to that, (Lee and Peppas, 1993) indicate that immersing the epoxy in aqueous solutions could also generate micro-cracking due to polymer chain scission that can be caused either by water-induced hydrolysis or by swelling. Therefore, the generation of micro-cracking during the ageing process could explain the increase in

the surface roughness of the testing FRP specimens after subjected to the different aging environments as shown in Figure 5.4.

Based on the above discussion, the results in Figure 5.4 suggest that the alkaline aging environment (pH=12) promotes better curing reaction and better cross-linking properties than the acidic aging environment. In fact, this difference can be attributed to the difference in the amount of liquid that could diffuse into GFRP and CFRP specimens which is function of the chemical properties of the aqueous solution and the affinity of the diffusing molecule to specific groups present in the epoxy (Diamant et al., 1981).

The observed greater ageing effect at temperature of 80°C than at 45°C could be attributed to the fact that both moisture diffusion and chemical reaction are faster when the aqueous temperature increases (Iskander and Hassan, 2001). Consequently, for a certain aging time, better FRP curing rate can be achieved as the aqueous temperature increases.

Finally, it should be mentioned that the reported ageing deterioration of the structural mechanical properties of FRP materials such as compressive and tensile strength [(Iskander and Hassan, 2001) and (Pando et al., 2002)] did not contradict with the observed ageing induced improvement in the FRP hardness property. As the surface hardness property of FRP is a matrix-dominated property whereas the compressive and tensile strength depend on matrix and fibre properties, and more importantly the fibre-matrix interfacial bond condition. Under the wet ageing environment, the matrix properties could improve due to aging induced curing process, however, the interfacial bond could be significantly deteriorated due to wicking of the diffused moisture along the fibre matrix interface which resulting in loss of micro structural integrity (Thomason, 1995).

5.6.2 Aging Effects on FRP-granular Interface Shear Coefficient

As FRP-granular interface shear behaviour is mainly controlled by the engineering properties of the granular and FRP-matrix materials, the observed aging effects on

hardness and surface roughness of FRP material, as show in Figure 5.4, would control the aging evolution of FRP-granular peak interface shear coefficient, μ_p , under the different adopted aging environments. Several previous studies in the literature have discussed the effect of the surface hardness (HV), and the surface roughness in terms of the relative surface roughness coefficient, $R_n=R_t/D_{50}$, on continuum-granular interface shear coefficient. Although these studies have concluded that μ increases as R_n increases, there is no agreement about the effect of HV on μ_p . Dove et al., (2006) have shown that μ_p increases as HV increases whereas the (O'Rourke et al., 1990) and (Frost et al., 2002) have shown an opposite behaviour.

The peak interface shear coefficient, μ_p , of each unaged (control) and aged FRP testing materials was presented between brackets, as shown in Figure 5.5, for Glass beads and Congleton sand. The presentation of μ_p results in HV- R_n plan, where the ageing paths could be recognized, was adopted to link the ageing induced changes in surface roughness and hardness with the interface shear property. In general, the results in Figure 5.5 show that subjecting GFRP and CFRP to the different adopted aging environments in this study increases its interface shear coefficient. However, the results in Figure 5.5b imply that the aging evolution of μ_p for Congleton sand is insignificant compared to the results of Glass beads (Figure 5.5a). In fact, this behaviour can be explained in terms of the differences between μ_p of the control specimens and the internal shear coefficient of the granular material, μ_i . For Glass beads and Congleton sand, μ_i is equal to 0.52 and 0.62, respectively. Uesugi and Kishida, (1986) have shown that μ_p increases as R_n increases. However, when μ_p approaches μ_i at a critical R_n value, the value of μ_p will be R_n independent and almost equal to μ_i . Therefore, as the values of μ_p of the control specimens of Congleton sand are very close to the μ_i value of Congleton sand, the room for μ_p improvement as R_n increases due to aging effect is very limited compared to the tests where Glass beads is used.

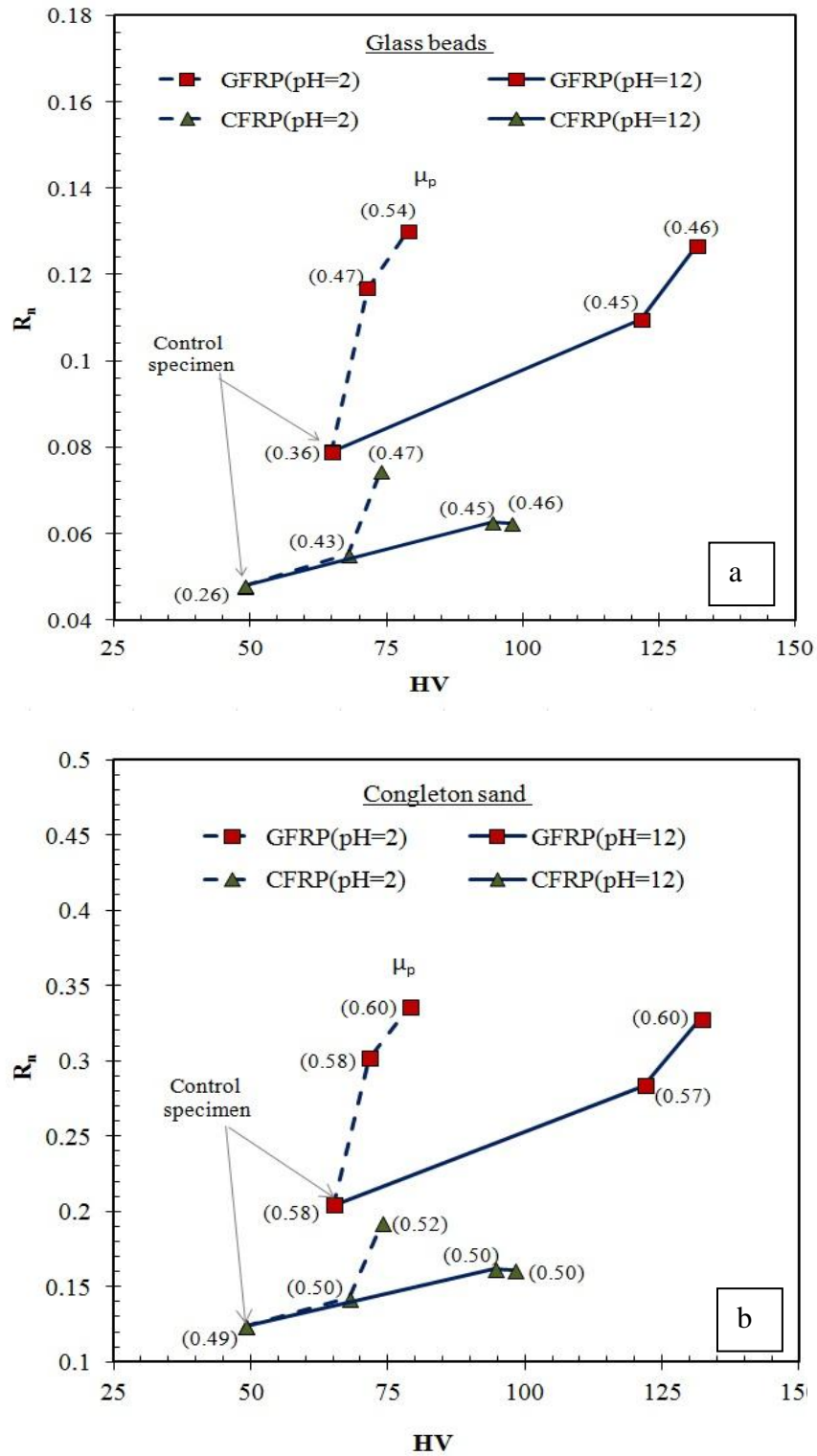


Figure 5.5: The effect of ageing induced changes in HV and R_t of FRP testing materials on peak interface shear coefficient, (μ_p)

In order to understand the effect of HV and R_n changes on μ_p , the interface test results were presented in R_n - μ_p and HV- μ_p plots as shown Figure 5.6. The test results suggest a reasonable bilinear relation between R_n and μ_p where μ_p increases as R_n increases as shown in Figure 5.6a. In fact this finding is in line with the outputs of the previous studies in literature [(Frost and Han, 1999, Kishida and Uesugi, 1987) and (Frost and Han, 1999)]. On the other hand, the results in Figure 5.6b indicate that the surface hardness changes have a minor effect on μ_p at least for the testing FRP materials in this study.

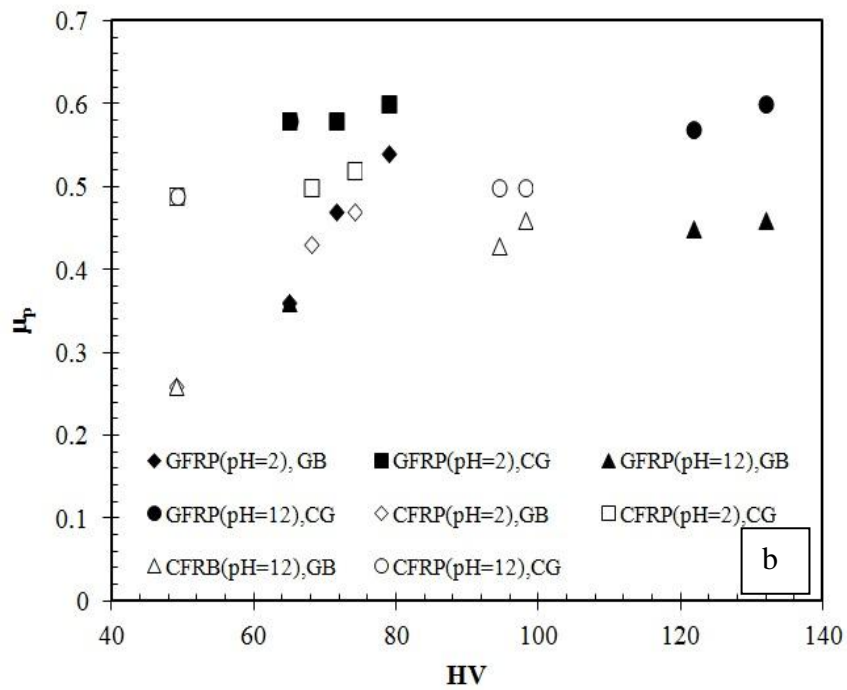
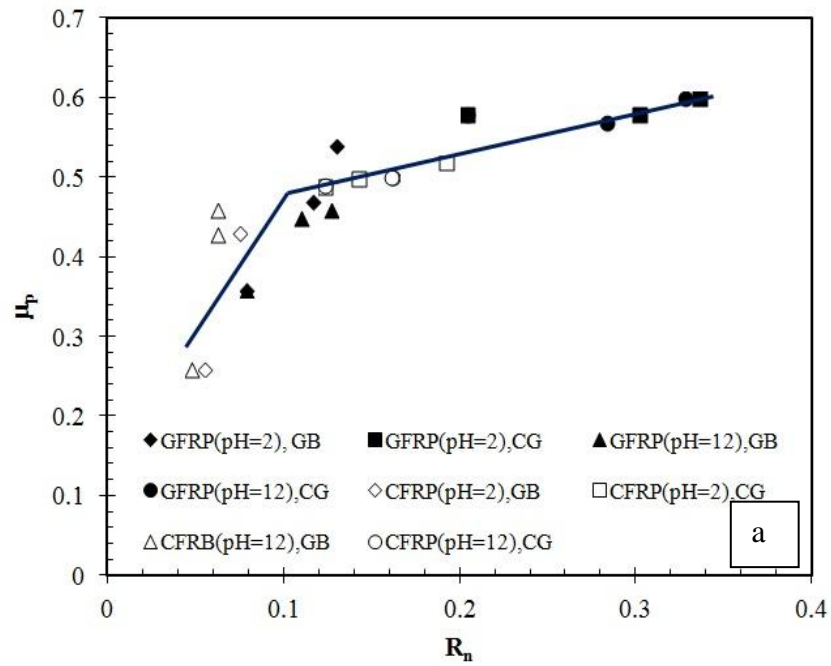


Figure 5.6: Effect of R_n and HV on μ_p

5.7 Summary

The experimental program involves assessing the ageing effect on the testing FRP materials in terms of the changes in their hardness and surface roughness properties. Furthermore interface shear tests were conducted, using the unaged and aged FRP materials, to evaluate the effect of aging environments on FRP-granular interface shear coefficient. From the results of this study, the following conclusions and observations were made:

- The interface coefficient friction was increase after subjected to the adopted aging environment. Both aqueous solutions were caused degradation of composite resins surface lead to increase the surface roughness.
- The results of this study indicated that although aging under the adopted environments in this study could have detrimental effects on the structural mechanical properties of FRP, it improves the FRP interface shear property as it is a matrix-dominated property.
- The improvement in the FRP interface shear behaviour could be mainly attributed to the observed increase in surface roughness under aging process.

CHAPTER SIX: EFFECT OF SURFACE ROUGHNESS AND HARDNESS ON THE INTERFACE SHEAR STRENGTH

6.1 Introduction

The aim of this chapter is to provide a general conceptual understanding for the effect of hardness and roughness of a continuum surface on its interface shear behaviour against a granular material. Although a wide consensus is available in the literature about the effect of roughness of continuum surface on the interface shear behaviour, there is no such agreement about the effect of hardness of the continuum surface. A carefully designed experimental program was conducted in this study to investigate this point. The results of this study were exploited to define schematically the constitutive interface shear surface (CISS) in the three-dimensional domain of surface roughness, surface hardness, and interface shear coefficient. The proposed CISS in this study provides a robust mean to: (i) understand the coupling effect of continuum surface roughness and hardness on the interface shear behaviour, (ii) interpret the observed different results in the literature.

6.2 Constitutive interface shear surface (CISS)

In fact, most of interface shear behaviour is controlled by the engineering properties of granular and the applied normal stress level [(Uesugi and Kishida, 1986), (Frost and Han, 1999), and (DeJong and Westgate, 2009)]. In fact, these studies have concluded that μ_p increase as R_n increases. However, there is no agreement about the influence of HV on μ_p . Dove et al., (2006) have shown that μ increases as HV increases whereas the (O'Rourke et al., 1990) and (Frost et al., 2002) have shown an opposite behaviour. Therefore, further research is still required in this topic to clarify this point. Therefore, an additional experimental investigation was conducted in this study to provide a better understanding for the effect of R_n and HV on interface shear behaviour. In the following sections, the testing materials and the conducted experimental program will be presented. The obtained results of this study were

exploited to define schematically the constitutive interface shear surface (CISS) in the three dimensional domain of surface roughness, surface hardness, and interface shear coefficient. The proposed CISS in this study provides a robust mean to: (i) understand the coupling effect of continuum surface roughness and hardness on the interface shear behaviour, (ii) interpret the observed different results in the literature. Then, the obtained results will be discussed and interpreted, and finally the conclusions of this study will be drawn.

6.2.1 Experimental Results

In order to achieve the objective of this study, the testing program was designed to characterize the geometric features of the constitutive interface shear surface (CISS) within HV- R_n - μ_p domain. For this purpose, the testing granular and counterface continuum materials in this study were selected to measure the evolution of μ_p as R_n changes at different six HV values. Therefore, the obtained results will represent six lines on CISS at different vertical cross-section within HV- R_n - μ_p domain as shown in Figure 6.1. The developed CISS by this approach can be used to understand the coupling effects of R_n and HV on μ_p . The developed CISS by this approach can be used to understand the coupling effects of R_n and HV on μ_p .

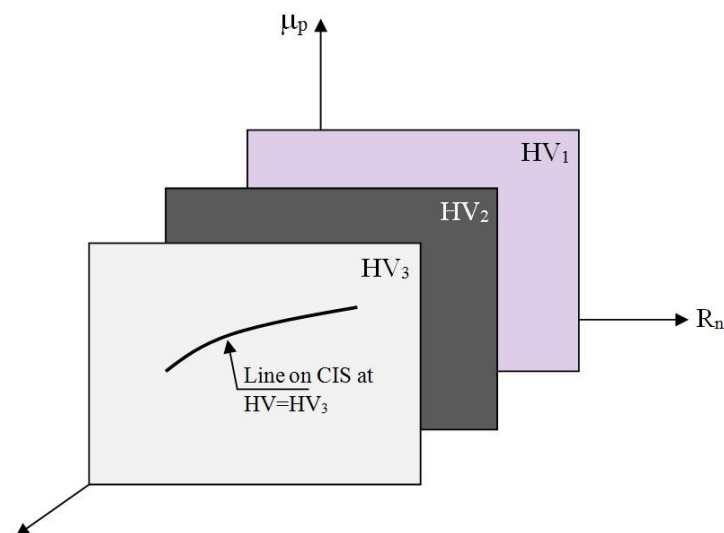


Figure 6.1: Schematic representation for the design methodology of the experimental program

Six different counterface continuum materials, in terms of HV values, were used in this study as listed in Table 6.1. To change R_n at constant HV, each counterface continuum material was sheared against four or five different rounded glass beads materials in terms of their D_{50} values as listed in Table 6.2. Therefore, at constant HV, each developed line on CISS will be determined using four or five different R_n values. However, for GFRP to get some interface shear results at low R_n values, the surface of GFRP was polished to reduce its roughness. Therefore more points were used to develop GFRP line on CISS. The rounded glass beads material was selected to exclude the effect of particle shape on μ_p that will be hard to control if natural granular materials had been used. However, the interface friction tests were conducted in this study in term of tested material to define schematically the constitutive interface shear surface (CISS) in the three dimensional domain of surface roughness, surface hardness, and interface shear coefficient.

Table 6.1: Hardness of testing continuum materials

Tested Material	Hardness (HV)
GFRP	65
CFRP	49
Copper	80
Aluminium	38
Mild Steel	109
High Carbon Steel	225

Table 6.2: Average grain size diameter of the testing granular

Glass Beads Material	D_{50} (mm)
GB1	1.0
GB2	0.5
GB3	0.31
GB4	0.20
GB5	0.075

6.2.2 Test Results and Discussion

The interface shear test results of the conducted experimental program in this study are plotted in R_n - μ_p plane, as shown in Figure 6.2. In general, the obtained results emphasise the importance of considering the coupling effect of HV and R_n on μ_p as it suggested that the R_n - μ_p relation is HV dependent. At constant R_n values, the test results in Figure 6.2a show that μ_p values for GFRP (HV=65) are higher than μ_p values for CFRB (HV=49). However, μ_p values for the high carbon steel (HV=225) drop even below CFRB (HV=49) values.

Using the test results in Figure 6.2, the evolution of μ_p as HV changes, at constant $R_n=0.1$ (path ab), can be obtained as shown in Figure 6.3. The results in Figure 6.3 display the existence of three different zones, in terms of μ_p -HV behaviour, and two special HV values in μ_p -HV plot at a constant R_n . In zone 1, μ_p increases as HV increases whereas an opposite behaviour occurs in zone 2. However, μ_p becomes almost HV independent in zone 3. The HV value at the maximum value of μ_p in μ_p -HV curve can be defined as the threshold surface hardness value, HV_{th} whereas the HV value where μ_p starts to be HV independent can be called as the critical surface hardness value, HV_{cr} .

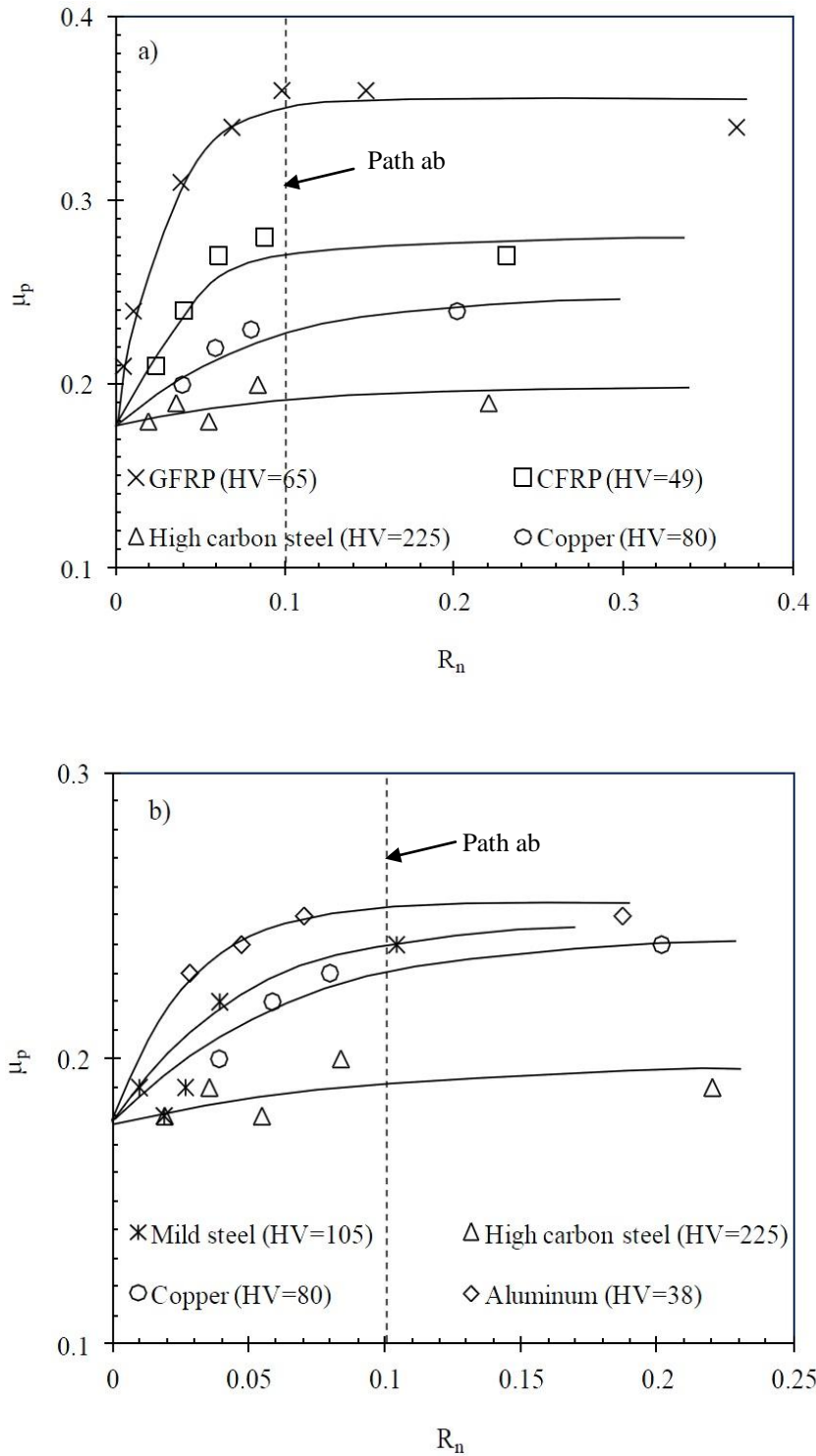


Figure 6.2: Interface shear test results

According to μ_p -HV curve in Figure 6.3, $HV_{th} = 70$ and $HV_{cr} = 99$. It should also be mentioned that the concept of the critical surface hardness value has been introduced and discussed earlier by [(Tabor, 1954), (Bowden and Tabor, 1954), (Scholz and Engelder, 1976)].

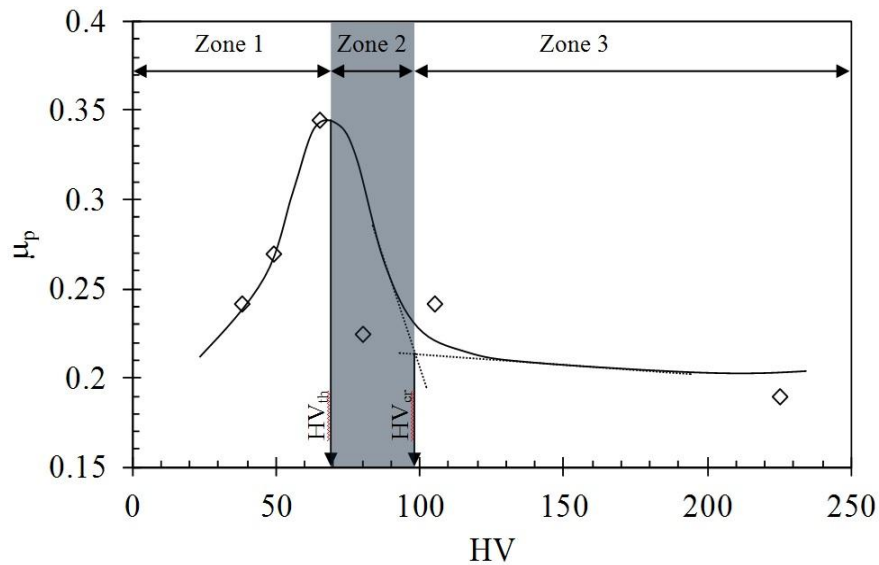


Figure 6.3: Relation between HV and μ_p at $R_n=0.1$

The observed behaviour in Figure 6.2 and Figure 6.3 can be exploited to schematically envisage the evolution of the HV- μ_p relation as R_n changes as shown in Figure 6.4 where the following simplification assumption was proposed. For the perfect smooth surfaces ($R_n= 0.0$), and the very soft surfaces (very low HV) where ploughing resistance is insignificant the value of μ_p^s is only controlled by the adhesion sliding resistance, μ_{ps} which could be considered equal for these two special cases. Considering the results in Figure 6.2 and Figure 6.3 and the conceptual understanding for the effect of R_n on HV- μ_p in Figure 6.4, the geometric configuration of CISS in zones 1 and 2 can also be envisaged as shown in Figure 6.5. However, it should be mentioned that μ_{ps} , HV_{th} , HV_{cr} , and μ_p - R_n relation at constant HV are function of the engineering properties of granular materials (particle shape) and the applied normal stress level. Further studies are required to assess the effect of these factors on the geometric characteristics of CISS.

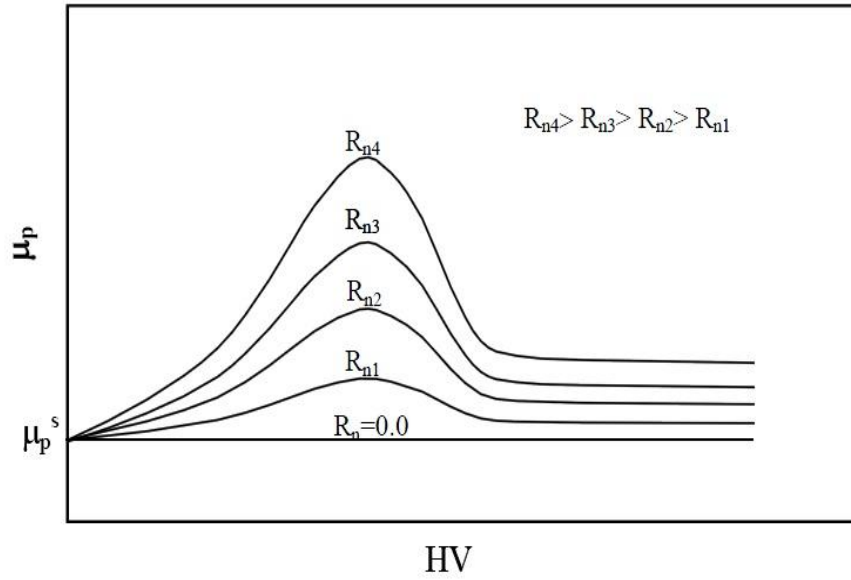


Figure 6.4: Schematic idealization for the effect of R_n on $HV-\mu_p$ relation

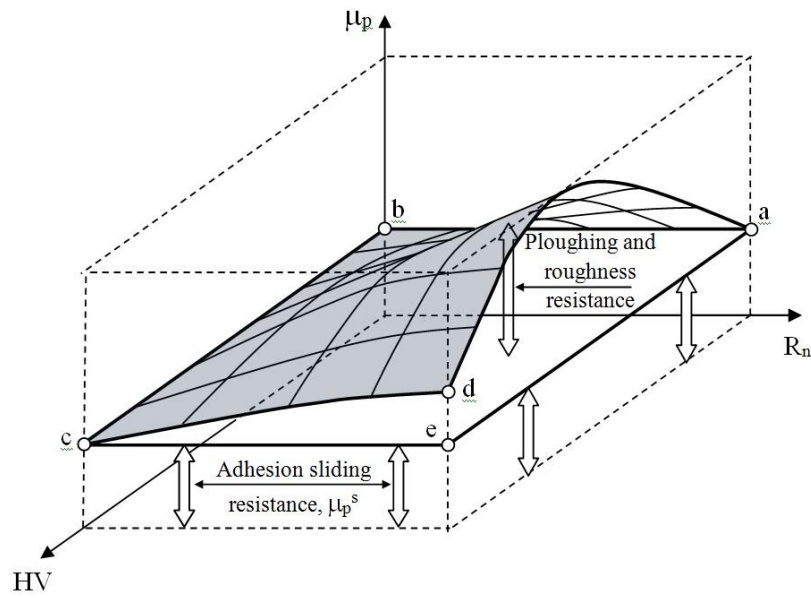


Figure 6.5: Schematic representation of the proposed CISS in zones 1&2

6.2.3 Conceptual explanation of the proposed CISS

As mentioned above, for the special cases (lines ab, and bc in Figure 6.5) low μ_p is expected as sliding can occur with essentially no particle rearrangement and therefore no volume dilation or contraction will occur. However, if R_n is increased for the surfaces with very high HV (line cd in Figure 6.5), sliding at the interface results in a higher μ_p as particles must be displaced towards the granular structure through rolling and sliding processes to pass over the asperities of the continuum surface. At a constant R_n value (line ad in Figure 6.5), as HV changes the μ_p value is controlled by rolling, sliding, and ploughing process. Ploughing occurs when the shearing induced local contact stress at an asperity exceeds the level required to damage it, forcing particles to remove or displace material from the surface during translation. When ploughing occurs in addition to sliding, μ_p increases.

The effect of HV on μ_p at constant R_n can be interpreted considering the concept of the available and the mobilized ploughing resistance of the surface asperities. The available ploughing resistance, PR_a , is a material property which is expected to have a direct proportion with the surface roughness Figure 6.6a, whereas the mobilized ploughing resistance, PR_m , depends on the shearing induced local stresses at the surface asperities and its relative ability to damage the surface. Therefore, $PR_a \geq PR_m$. However, the interface shear resistance is only affected by the mobilized ploughing resistance.

The path ab in R_n -HV plane, where HV is changing at constant R_n , as shown in Figure 6.6b, will be used to explain the observed HV- μ_p relation in Figure 6.3 . In zone 1 (soft HV surfaces), the shearing induced local stresses at the surface asperities are expected to be equal to or greater than PR_a . Therefore, the mobilized ploughing resistance, PR_m , during the shearing process is anticipated to be equal to the PR_a and μ_p will increase as HV increases as shown in Figure 6.6. However, beyond a certain HV value, HV_{th} , the ability of the particle to plough the counterface surface will decrease as the shearing induced local stresses at the surface asperities could be less

than PR_a . Consequently, PR_m will be less than PR_a and it could be almost nil at certain high HV value, HV_{cr} , as shown in Figure 6.6a. Therefore, μ_p will decrease as HV increases within the medium HV zone (zone 2), as shown in Figure 6.6b. Furthermore, μ_p will be HV independent for the hard HV surfaces with $HV > HV_{cr}$ (zone 3) as shown in Figure 6.3. Finally, at constant R_n , the proposed CISS also suggested that $d(\mu_p)/d(HV)$ is function of R_n within zones 1 and 2 as shown in Figure 6.4. It increases as R_n increases. This behaviour is in agreement with (Childs, 1992) who linked the mobilized ploughing resistance with the surface roughness.

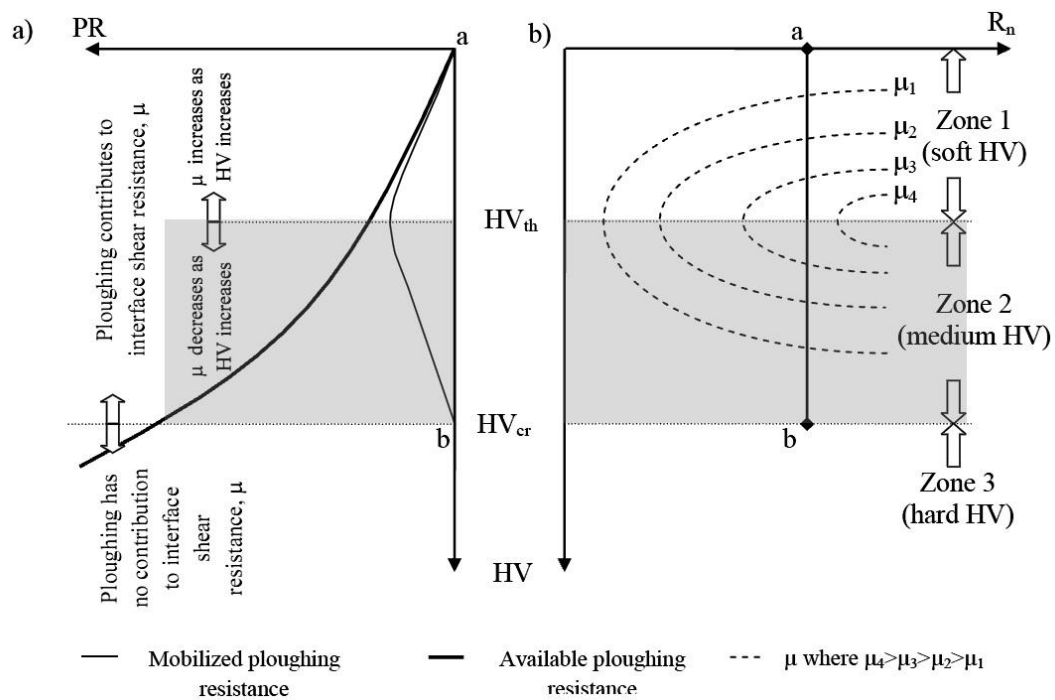


Figure 6.6: Interpretation of HV- μ_p relation, at constant R_n , using the concept of the available and the mobilized ploughing resistances

6.2.4 Qualitative Interpretation for the different Results in the Literature

The proposed CISS in this study could almost explain the observed different μ -HV behaviours in the literature [(Dove et al., 2006), (Frost et al., 2002), and (O'Rourke et al., 1990)]. The particle-scale experimental results by (Dove et al., 2006) that show that μ -HV is function of surface roughness and μ increases as HV increases could be represented schematically by paths ab, and cd in HV- R_n plane as shown in Figure 6.7a. Path ab represents schematically the three interface shear tests conducted by (Dove et al., 2006) using three different counterface surfaces having roughly similar R_n and different HV values whereas path cd represents schematically another two tests conducted using two different counterface surfaces having also different HV values and roughly similar R_n but higher than R_n of the first three surfaces.

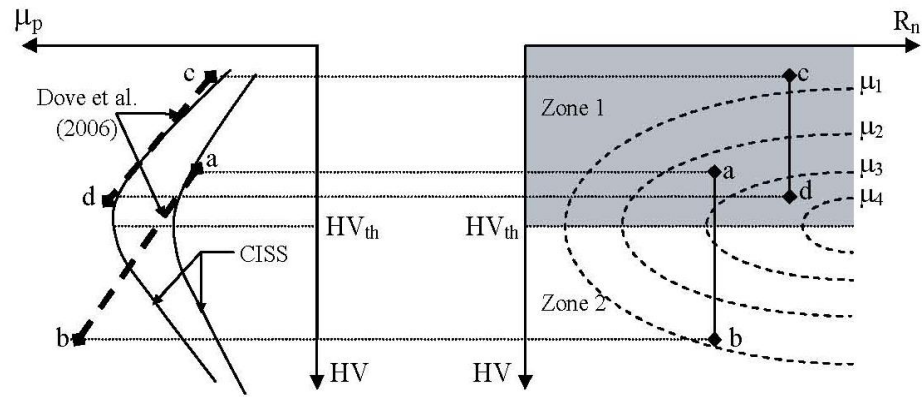
The granular material used by (Dove et al., 2006) for both paths was one size of glass beads. The schematic μ -HV relations for both paths according to the test results by (Dove et al., 2006) and the conceptual prediction using the proposed CISS are shown in Figure 6.7a.. Reasonable agreement could be observed in terms of μ -HV relation and the effect of R_n on it within zone 1. However, the concept of HV_{th} was not observed by (Dove et al., 2006) due to the particle-scale test conditions by (Dove et al., 2006) that did not allow the particle to roll during shear which is one of the major microscopic particle movement mechanisms (Oda et al., 1982). Such movement restriction could increase PR_m at higher HV values.

The geometric characteristics of CISS developed by (Frost et al., 2002) using DEM numerical experimental program also agrees well with the proposed CISS in this study for the paths in zone 2 (paths ab and cd in Figure 6.7b) In fact, the disagreement in zone 1 between CISS by (Frost et al., 2002) and the one proposed in this study could be attributed to the DEM numerical limitations in representing the effect of surface hardness on ploughing resistance especially for soft HV surfaces. In fact, Frost et al. (2002) used an indirect approach for this purpose which involves

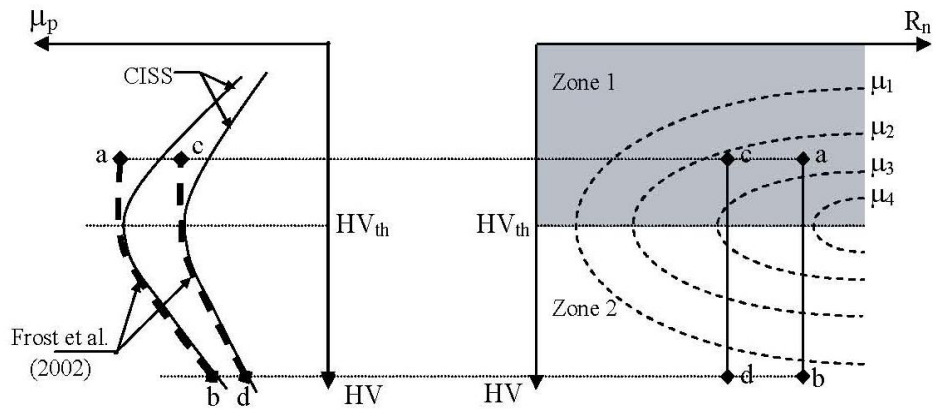
increasing the particulate-continuum surface friction coefficient to include the ploughing effect on μ_p .

The observed μ -HV relation by O'Rourke et al. (1990), which shows a decrease in μ_p as HV increases, could also be explained by the proposed CISS in this study. In fact, as O'Rourke et al. (1990) did not report the roughness of the continuum surfaces used in their study, the interface test path of O'Rourke et al. (1990) could not be described in HV- R_n plane. However, the observed behaviour by O'Rourke et al. (1990) can be obtained from the proposed CISS in this study either in zone 1 or 2 using path ab or bc, respectively, as shown in Figure 6.7c.

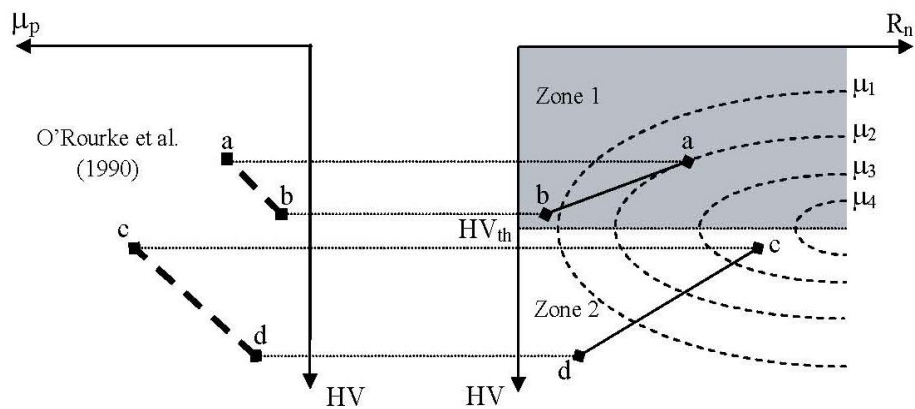
Finally, based on the above discussion it can be concluded that the difference between the reported HV- R_n relation by Dove et al. (2006) and those by Frost et al. (2002), and O'Rourke et al., (1990) does not imply the incorrectness of either of them, as the reported disagreement could be attributed to the fact that these previous studies were able to only disclose a part of the CISS surface due to some experimental or computation limitations. However, as the developed CISS in this study is based on a carefully designed experimental program that covers a wide range in R_n -HV domain, the two conflicting behaviours could be observed and interpreted in terms of the effect of HV on the mobilized ploughing resistance.



a) Dove et al. (2006)



b) Frost et al. (2002)



c) O'Rourke et al. (1990)

Figure 6.7: Schematic explanation for the different test results in the literature using the proposed

6.3 Summary

The testing program was designed to characterize the geometric features of the constitutive interface shear surface (CISS) within HV- R_n - μ domain. For this purpose, the testing granular and counterface continuum materials in this study were selected to measure the evolution of μ as R_n changes at different six HV values. The following conclusions can be drawn from this test program:

- The results of this study were exploited to define schematically the constitutive interface shear surface (CISS) in the three dimensional domain of surface roughness, surface hardness, and interface shear coefficient.
- Based on the conducted experimental program in this study a CISS was proposed which introduces a new understanding for the effect of HV and R_n on interface friction coefficient. The proposed CISS in this study shows that μ_p increases as HV increases.
- The proposed CISS in this study could successfully interpret the different observed behaviour in the literature.

CHAPTER SEVEN: FRP PILEING BEHAVIOUR UNDER LOADING

7.1 Introduction

FRP Composite piles are being considered as alternatives to conventional piles because these piles may have lower maintenance costs and longer service lives, especially for marine applications and in other harsh environments. From the available literature, it is clear that the amount of the experimental work on FRP-pile confined concrete specimens is very limited compared to the conventional pile. However, it is obvious that further experimental research is required on pile confined with FRP tube. In this study, two types of FRP were fabricated in different laminate configurations. The test FRP pile program described herein involved CFRP and GFRP piles tested to the axial and lateral load. The focus of this chapter is on the test experimental program including descriptions of the testing materials, preparation procedure and loading tests.

A lack of in-depth knowledge of the long-term durability of (FRP) composite in real service condition restricts its extensive use in geotechnical works. Therefore, it is important to evaluate the engineering behaviour of these materials under aging environment condition to permit more confidence in use it as piling system. Consequently, a long-term study was undertaken to assess the effect of FRP degradation on the pile capacity in term of lateral load. The study focused on both FRP piles specimens were exposed to different aqueous solutions; NaOH (pH=12), and HCl (pH=2) which represent acidic and alkaline soil environments, respectively, for 180 days at elevated temperatures 45°C. The FRP pile specimens were aged using the similar mechanism that provided in Chapter five. At the end of ageing process, the pile lateral capacity of the aged FRP piles were determined to observe and compare their results in term of aggressive environment type.

The behaviour of FRP pile during different static loading tests can be accurately modeled using a small pressure chamber to simulate field confinement pressure. A

series of laboratory tests have been conducted using chamber facility technique to better understand the performance of piles subjected to these loading conditions. However, the main object of this chapter is to investigate the engineering performance of FRP composite piles subjected to different loading modes through. This chapter is divided into three sections:

- Experimental Arrangements: Describes the test setup, and tested materials, and material preparation.
- Experimental Program: Describes the FRP pile/sand and loading system procedures.
- Discussion of results.

7.1.1 Test Setup

A small-scale modelling facility was assembled and developed at the workshop in The University of Manchester. The test setup herein was used to examine the FRP model pile (300 mm in length and 20 mm diameter) embedded in sand. The benefits of using small-scale pile modelling and smaller scale chamber testing is the ability to evaluate different parameters. Many researchers have been widely used the pressure chamber to simulate the pile-soil model [(Wei and El Naggar, 1998) and (El Naggar and Sakr, 2000)].

FRP-pile model installation setup consists of a pressure chamber, GDS pump, LVDT, load cell and data acquisition system. Figure 7.1a shows a schematic view of the experimental testing setup while a photograph of the FRP pile/soil chamber testing arrangements used in this program is also taken as shown in Figure 7.1b. Below is a detailed description of the test setup components, the apparatus design, and experimental procedures.

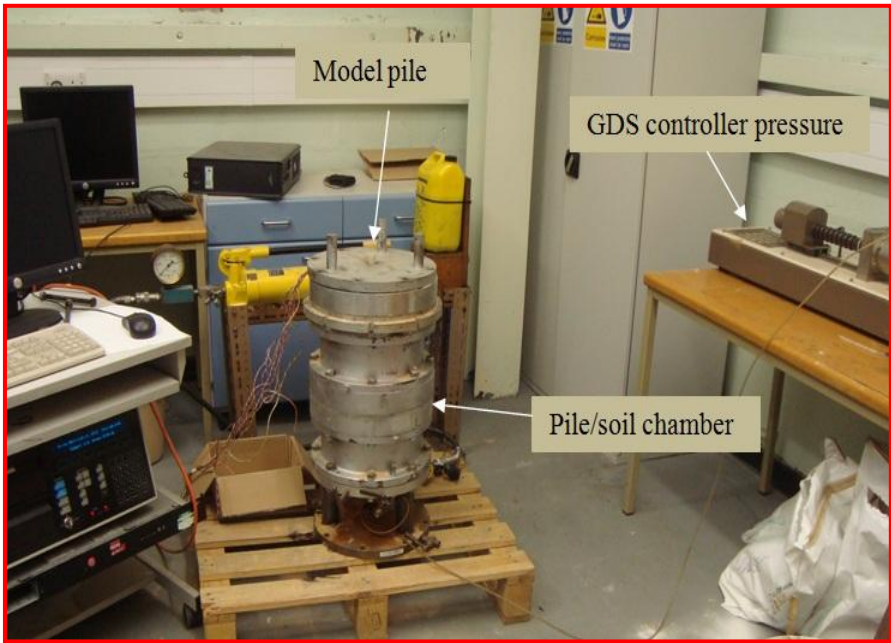
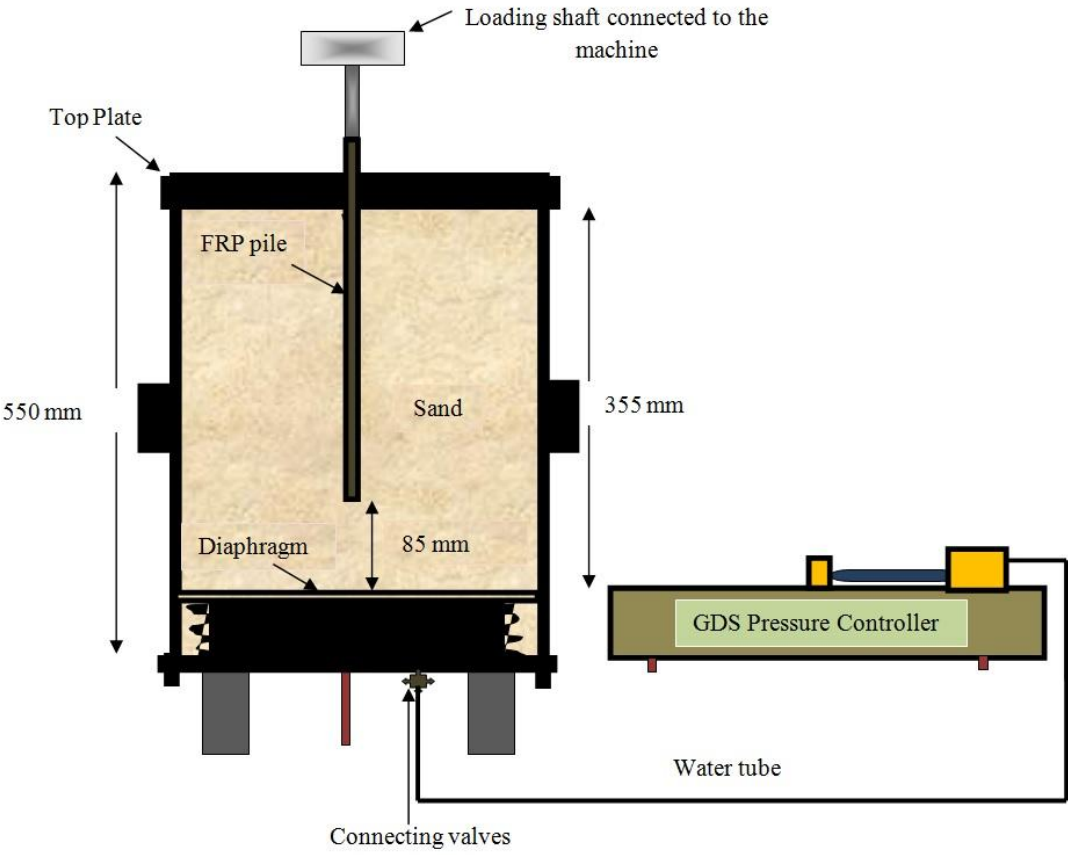


Figure 7.1: Description of FRP-pile/soil chamber test

7.1.2 Pressure Chamber

The pressure chamber was constructed and developed herein in order to simulate pile/soil system during loading process. The general configuration of a pressure chamber test is shown above in Figure 7.1. The following list and details of the basic components of a chamber pressure system:

Soil Cell: The soil cell used is 256 mm in inside diameter and 550 mm height. The cell was fabricated from mild steel with a wall thickness of 10 mm and a top plate thickness of 20 mm. In order to simulate various field stress conditions, the plastic diaphragm was fixed on the bottom of the soil cell which can be controlled independently. The pressure was applied to the plastic diaphragm by external pump through an input port. A suitable central hole was made in the top plate for the axial and lateral test as shown in Figure 7.2. These holes were made to allow the pile specimen motion during the test. However, the behaviour of axially and laterally loaded model piles can be adequately tested using this technique. The suggested top plate is used to confine the sand specimen under different vertical pressure. It was assumed to be insignificant effect on the behaviour of pile during the loading tests.

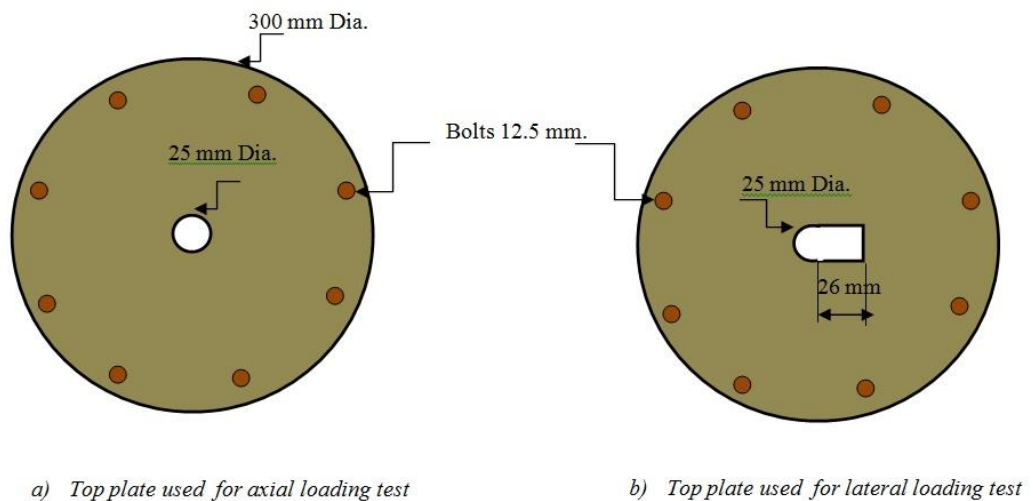


Figure 7.2: Top plates description

- **GDS Pump:** The pressure measurement and control system was achieved by using volume and pressure digital controlled made by GDS Instruments. A GDS advance pressure/volume controller was connected to the lower soil cell to supply a constant pressure throughout the test. The GDS controller instrument was flow regulated, with a capacity of 300 ml, which can be applied over a period of 30 min. The water quantity inside the GDS controller should be checked and filled after each test.

- **LVDT:** A linear variable differential transducer (LVDT) was installed horizontally at the top plate of the chamber pressure cell. High-accuracy LVDT (± 0.001 mm) was attached to measure pile model displacement during lateral loading tests. The LVDT was connected by one channel to acquisition system and the data were recorded during the lateral loading test.

- **Load Cell:** The load cell (2.5 kN) is placed atop of the pile head to measure the increment load during the lateral test. The preliminary calibration consisted of increasing the load in increments of 50 N up to a maximum of 2000 N.

7.1.3 Tested Materials

- **FRP Pile:** Two different FRP composite piles (CFRP and GFRP) were used in this study. Both CFRP and GFRP tubes have an average outer diameter of 20 mm and a wall thickness of 1.25 mm. The two FRP tube materials are referred as CFRP and GFRP. The dimensions of FRP piles used in this study were chosen to represent a pile shaft segment with total length of 300 mm and 270 mm embedment length inside the soil cell.

- **Mild Steel Pile:** Mild tube specimen is used as a reference material. The steel model pile used in this study was smooth steel pipe having a diameter of 20 mm and a wall thickness of 1.25 mm. A Photo of these three test piles is shown in Figure 7.3. For comparison purposes the mild steel pile was selected in this study.



Figure 7.3: GFRP, CFRP and Mild steel Piles

- **Mortar:** The FRP and mild steel tubes are filled with a mortar material using a small funnel. The same mortar batch as designed in chapter three was used to fill the FRP composite tubes and mild steel pipe. Details of the mortar mix proportion (M) are shown in Table 3.2 in Chapter three. The piles were filled by mortar due to this material can be flow easily without need any mechanical vibration and thus assures the structural integrity of tubes and eliminates air pockets.
- **Sand Material:** Congleton sand was used in this study for all model pile tests. The properties and grain size distribution for this sand were presented in Chapter four. The sand specimen was prepared using a special technique (raining method) to obtain good-quality samples of sand that are very homogeneous and a uniform soil distribution inside the sand cell as shown in Figure 7.4. Sand is dropped in a hand controlled on a diffuser, composed of two diffuser sieves. The diffuser 5 and 2.5 mm sieves were bolted to the frame of sand raining device. The height of diffuser sieves can be controlled

by adjusting the location of the raining device with respect to the sand cell. Sand raining was terminated temporarily after the height of the sand in the tank was 85-90 mm, where the pile specimen was held vertically in place at the sand cell of the testing pressure chamber where its tip was in contact with the underlying sand. Thereafter, the sand raining was resumed until the specified height of the sand in the pressure chamber was reached, at which the raining was terminated and the sand surface was levelled. The raining of sand was stopped when the sand rained in pressure chamber was about 10-15 mm thicker than required. The sand surface was levelled, extra sand was removed and the top steel plate was placed on the top.

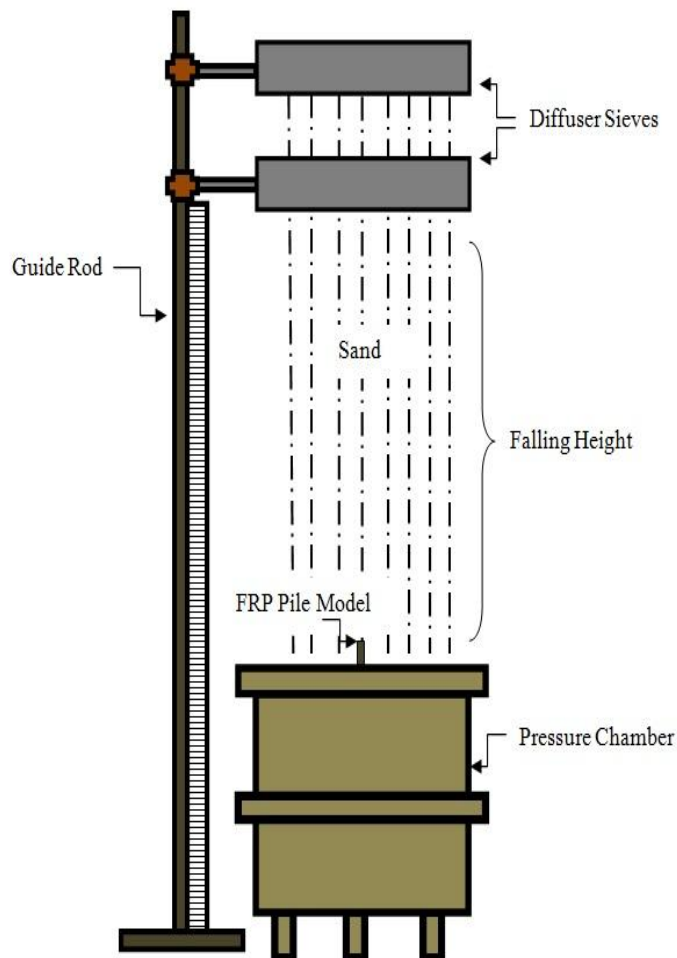


Figure 7.4: Principle of sand raining device

The sand specimen was weighed and raining from the different levels to achieve the desired relative density. The sand sample were raining at four different locations in the pressure chamber to measure and monitor the uniformity of relative density of the sand inside the pressure chamber. At each 150 mm of soil deposition, the sand raining process was resumed until the specified height of the sand in the pressure chamber was reached. Figure 7.5 shows the density versus height for the sand sample. It is clear that the soil density was reasonably uniform.

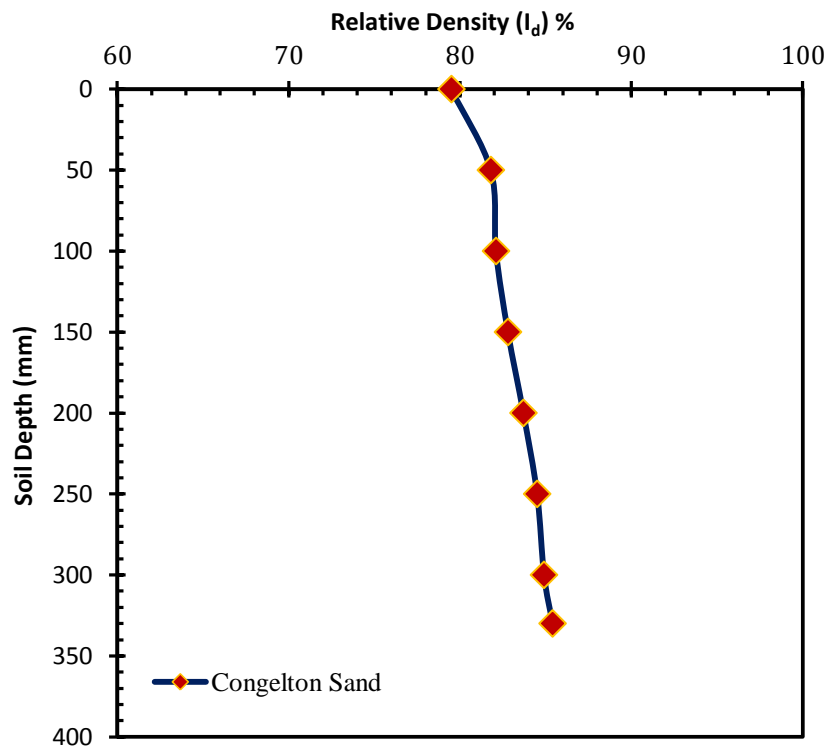


Figure 7.5: Average sand relative density distribution along the depth of the sand sample

7.1.4 FRP pile/sand Preparation

The principal FRP pile and sand preparation technique is illustrated in Figure 7.6.

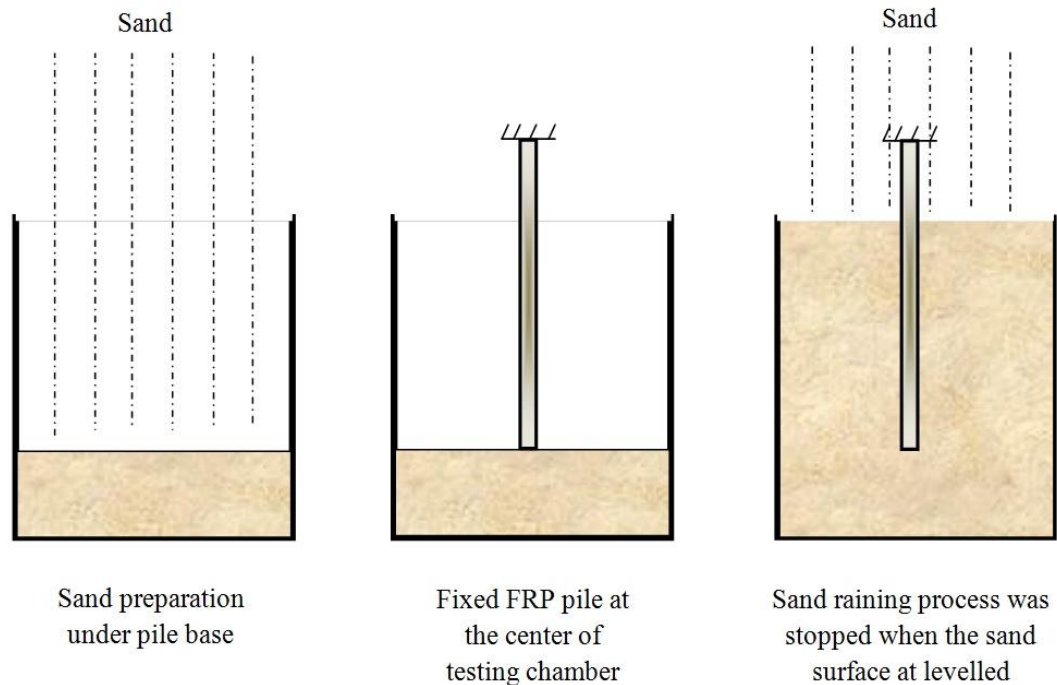
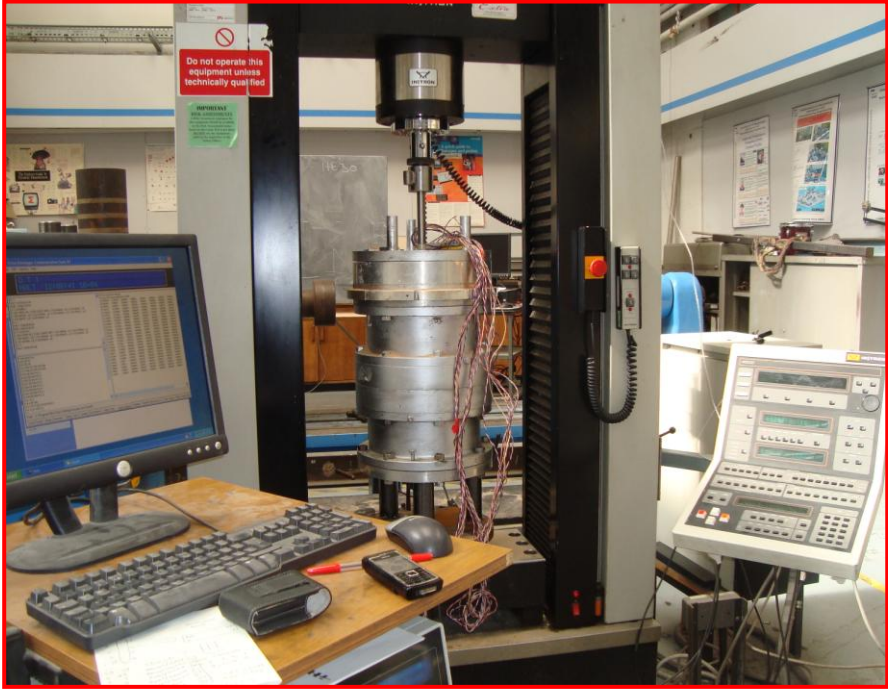


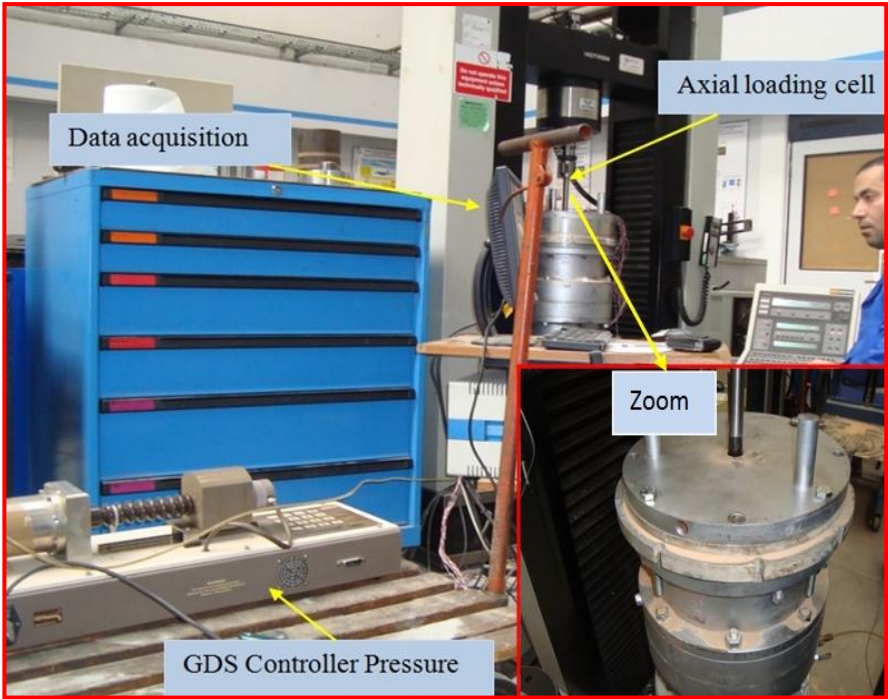
Figure 7.6: Sand and FRP preparation

7.1.5 Loading System

- **Axial Loading System:** The instrumentation of the piles for static axial loading test consisted of a loading rod placed atop the pile (at the pile head) and connected to load cell fixed on the machine to measure the static axial loading during the test. The load cell is connected to the electronic data acquisition system and the data were recorded every the settlement at every loading test. Figure 7.7 shows the experimental test setup used in this study during the axial tests.



a) Front view



b) Side view

Figure 7.7: Axial loading set-up

- **Lateral Loading System:** The test set-up for the lateral load tests was carried out using the same setup chamber. As mentioned earlier, another top plate was placed on the soil surface to measure the lateral load capacity for the model pile. The test set-up for the lateral load tests consisted of a steel frame fixed on top of the top plate and a hydraulic jack placed horizontally at the pile head level. A 2.5 kN load cell was attached between the reaction frame and the hydraulic jack to measure the applied lateral load at the pile head. A linear displacement transducer (LVDT) was attached to the reaction frame near the soil surface to measure the lateral displacement and rotation close to the ground surface. Figure 7.8 shows a schematic details and photograph of the lateral experimental set-up test using in this study.

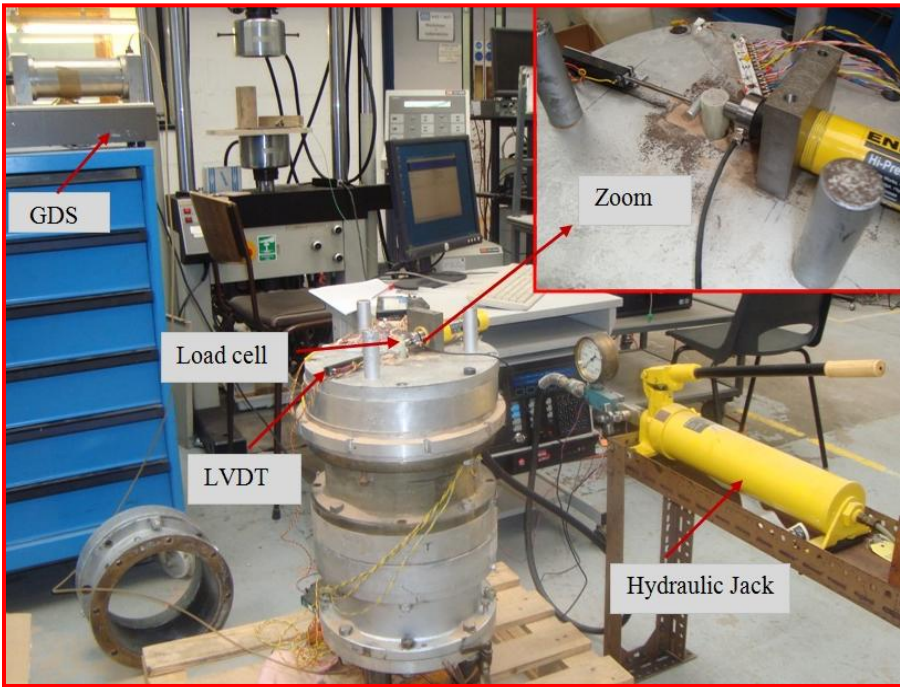
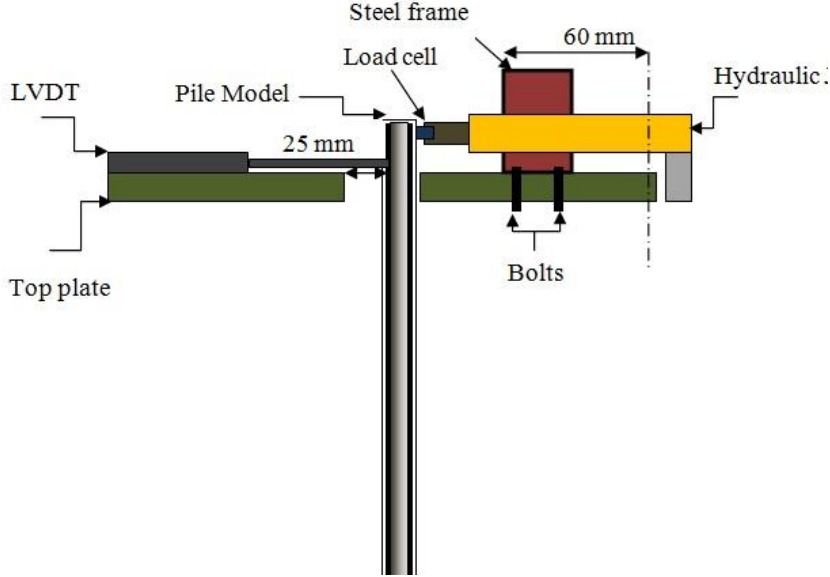


Figure 7.8: Lateral loading set-up

7.2 Experimental program

Table 7.1 and 7.2 present the experimental testing program that conducted to investigate the effect various important parameters on the FRP pile during static axial and lateral loading tests.

Table 7.1: Axial loading program

No.	Effect of study	Pile type and ID	No. Of tests	Vertical Pressure (kPa)	Relative density index %
1	Surface roughness	GFRP	3	250	80
		CFRP			
		Mild steel			
2	Loading rate	CFRP	3	250	82
3	Vertical pressure	GFRP	2	100	80
				250	
4	Relative density	GFRP	2	250	80
					60
Total of Tests			10		

Table 7.2: Lateral loading program

No.	Effect of study	Pile type and ID	No. Of tests	Vertical Pressure (kPa)	Relative density index %
1	FRP pile type	GFRP	2	120	80
		CFRP			
2	Pile diameter	CFRP	2	120	78
3	Aging environment (PH=2)	GFRP	2	120	80
		CFRP			
4	Aging environment (PH=12)	GFRP	2	120	80
		CFRP			80
Total of Tests			8		

7.3 Discussion of Results

7.3.1 Axial Load Results

In order to understand the behaviour of two FRP composite and compare its response to mild steel pile specimens, the axial load tests conducted in this study include the following influence factors:

- FRP pile surface roughness
- Rate of axial loading
- Vertical pressure
- Sand relative density

7.3.1.1 Influence of Pile Surface Roughness

To study the effect of roughness of the pile on axial load capacity, the surface roughness of GFRP, CFRP and mild steel piles were measured using a Taylor Hobson Profilometer as shown in Figure 7.9.



Figure 7.9: Surface roughness measurements

A number of surface roughness measurements were performed on each pile specimens. The roughness parameters for these three pile models are summarized in Table 7.3.

Table 7.3: Surface roughness parameters

Pile Type	R_t (μm)
GFRP	27.3
GFRP	18.1
Mild Steel	7.8

However, the axial load test was carried out by increasing the axial load using constant load increments of 50 N. After each load increment, the applied load on the pile was held constant for a time interval of 2.5 minutes. Then, the pile head settlement was measured and the output data was recorded. Figure 7.10 shows the measured axial load versus pile head settlement diagrams for all three test piles. These tests were conducted under confined pressure 250 kPa.

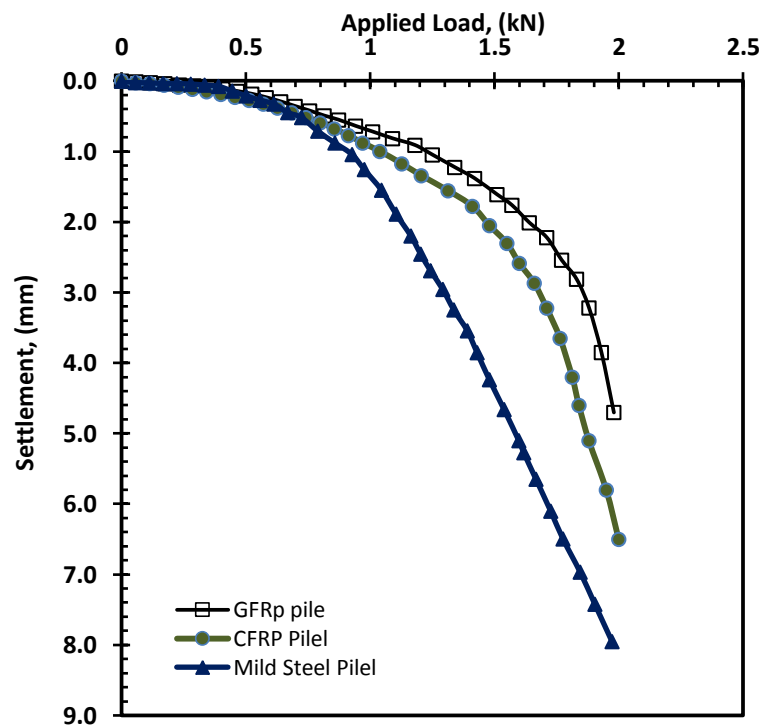


Figure 7.10: Influence of Surface roughness on FRP pile response

The axial bearing capacity of piles was evaluated as the load required for displacing the pile head by 10% of the pile diameter (De Nicola and Randolph, 1999). Based on this chart, it can be seen from Figure 7.10 that the both FRP piles exhibit higher bearing capacity compared to mild steel pile. About 30 % and 27% increase is seen in cases of GFRP and CFRP piles respectively.

It can be seen that the responses plotted in Figure 7.10 have a general pattern as shown in Figure 7.11. This pattern consists of three main zones AB, BC and CD. In most tests, up to point A, that includes elastic displacement, variations of surface roughness slightly affect the pile shaft resistance and the resistance due to increase of roughness is mobilized after this point has been achieved. In zone AB elasto-plastic behaviour dominates. Furthermore in this zone a linear relation between shaft resistance and displacement of pile may be adopted. From point B up to point C behaviour becomes nonlinear. At point C flow process manifests itself and then develops. Finally at point D, soil surrounding the pile fails and the pile settles rapidly.

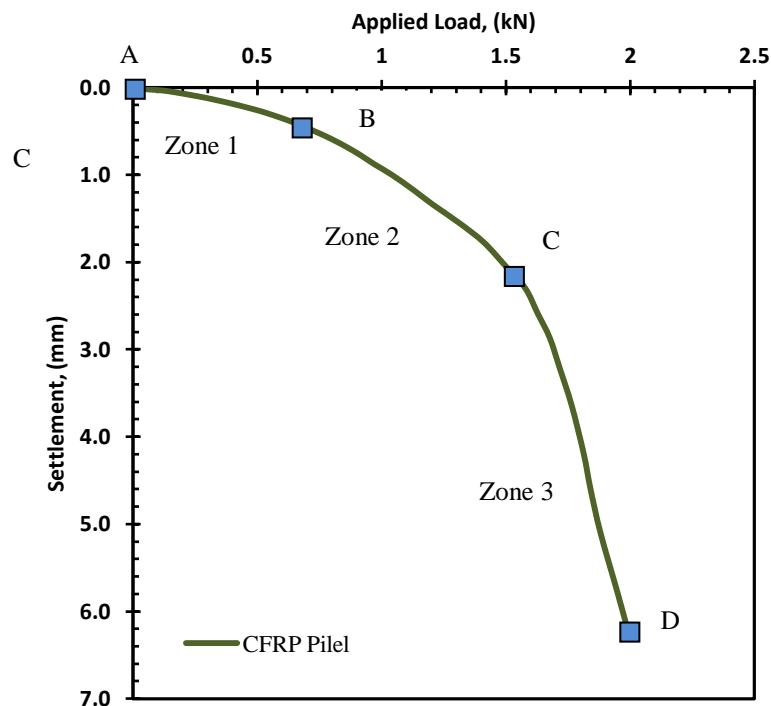


Figure 7.11: General pattern of test results

In the middle of elasto-plastic zone AB, for a defined increase of stress rate, the pile settlement rate decreases as the surface roughness increases and causes the shaft resistance to increase. The pile/soil interface mechanism is presented schematically in Figure 7.12. It is seen that when surface of pile is rougher, (high R_t) and consequently interlocking between such as GFRP pile and soil increases. On the other hand, the mechanism of shear transfer between sand/mild steel involved particle rolling which was evidenced by lack interlocking (small R_t).

Thus the load required to overcome the surface resistance due to interlocking, increases and thus the rate of pile settlement decreases as the surface roughness increases. As the load is increased the interface soil dilates due to shear strain growth. This, in turn, increases lateral stress and causes the shaft resistance to increase. It seems that as settlement proceeds due to load increment the specific volume of the sand intimate to the pile surface finally reaches to its critical state and then the pile settles rapidly.

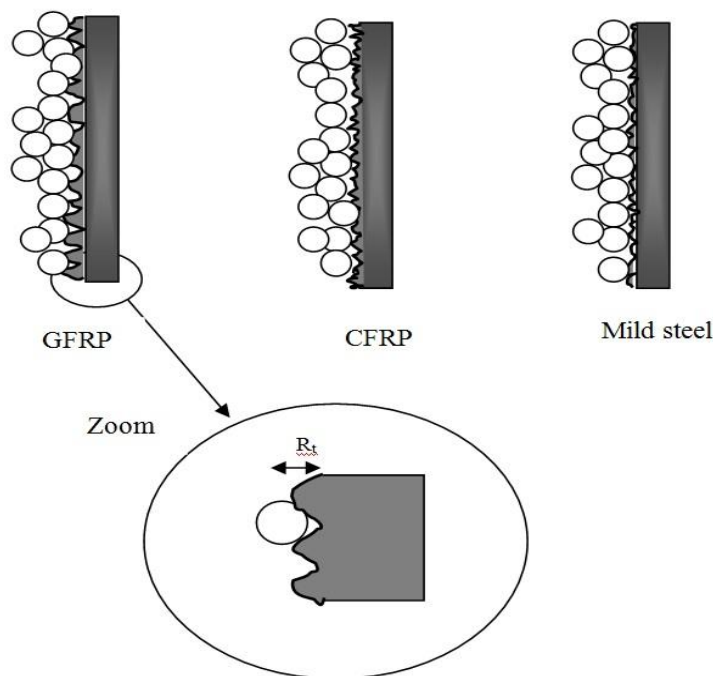


Figure 7.12: Pile surface and soil interface

The pile load capacity curves obtained from tests versus surface roughness is shown in Figure 7.13. It is observed that the relation between average surface roughness and pile load capacity is acceptably linear.

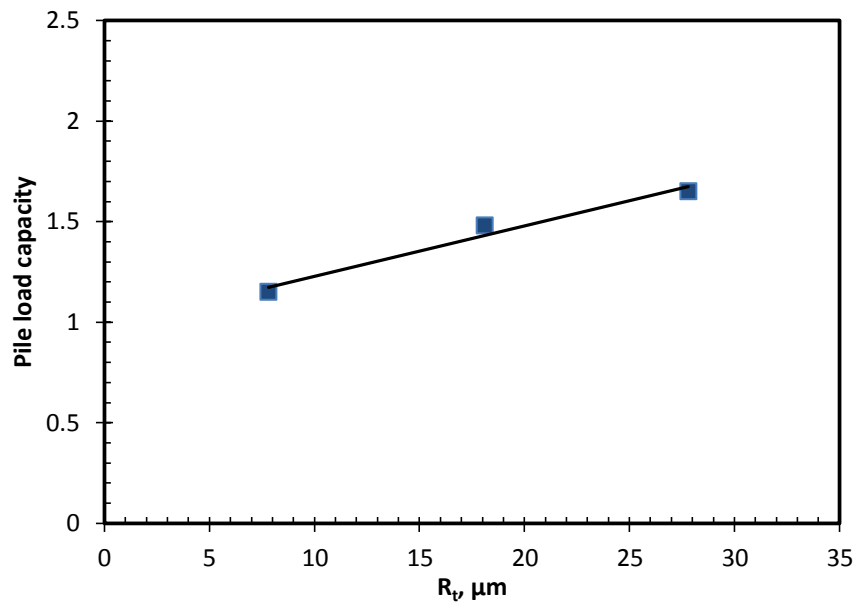


Figure 7.13: Variations of pile load capacity against surface roughness

7.3.1.2 Rate of Axial Loading

The rate of loading is increased the maximum bearing capacity can affect on the bearing capacity of the pile in sand [(Horvath, 1995) and (Dijkstra, 2004)], whereas (Dayal and Allen, 1975) have shown insignificant behaviour. It is important to investigate the possible influence of loading rate on bearing capacity of FRP pile. Therefore, three axial static load tests were conducted using the CFRP pile. The axial load was applied to the CFRP pile using a loading machine, which provides a constant rate of vertical displacement. The CFRP model piles were loaded at three different velocities (0.5, 1.5, and, 5 mm/min). Each test was conducted under confined pressure 250 kPa and the relative density of Congleton sand 80%. The surface roughness R_t for tested CFRP pile model was 17.6 μm . Figure 7.14 presents the load-displacement curves for three loading tests. It can be seen from these responses that effects of loading rate on the load-displacement are less significant for

FRP pile embedded in cohesionless soils. However, such behaviour is in agreement with the observation made by (Dayal and Allen, 1975).

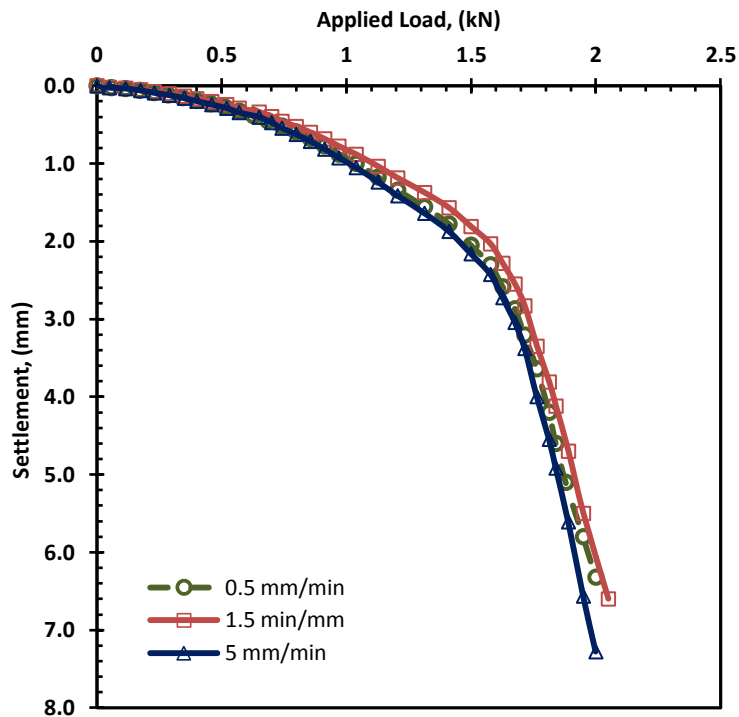


Figure 7.14: influence of loading rate on bearing capacity of the FRP Pile

7.3.1.3 Vertical Pressure

In this section, the effect of vertical pressure on the response of FRP axial bearing capacity was investigated by conducting additional pile load tests at two vertical pressure levels of 100 and 250 kPa. In order to consider the effects of vertical pressure levels on the bearing capacity behaviour of FRP piles under axial loads applied at the pile head. Two tests were performed using CFRP installed at Congleton sand at an average relative density of 80%. The results of these tests are presented in Figure 7.15.

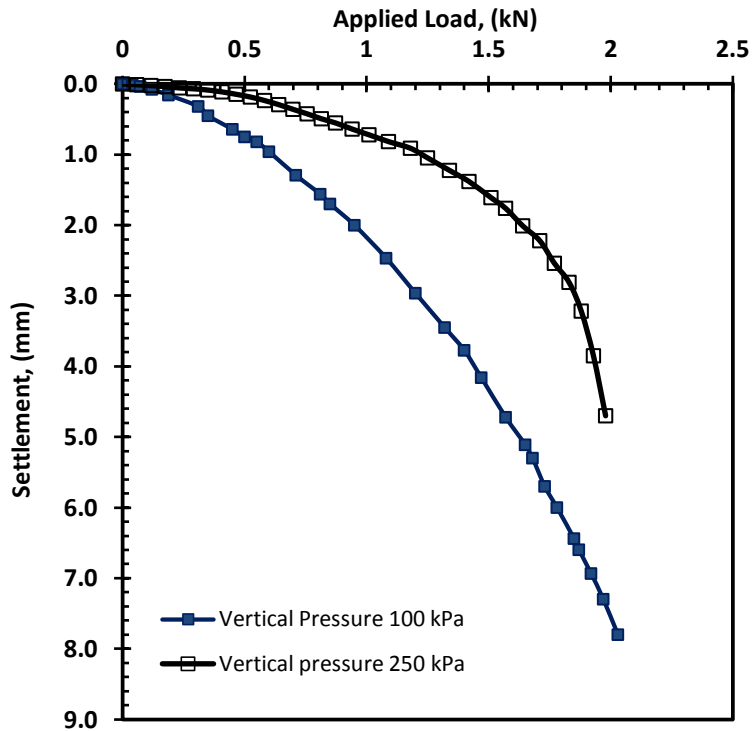


Figure 7.15: Influence of vertical pressure on the bearing capacity of FRP pile

From this curves, it can be seen axial load capacity of pile increases with increase in confined pressure of the sand for same FRP pile. When the pile is loaded, such pressure confinement resists the axial displacements of soil particles around the pile shaft confined pressure leading to a significant decrease in the axial settlement and hence improving the bearing capacity.

7.3.1.4 Relative Density of Sand

To study the effect of density of sand on the axial load capacity in case of FRP pile, tests were done on two densities using Congleton sand. Figure 7.16 shows the influence of relative density on the axial bearing capacity of FRP pile.

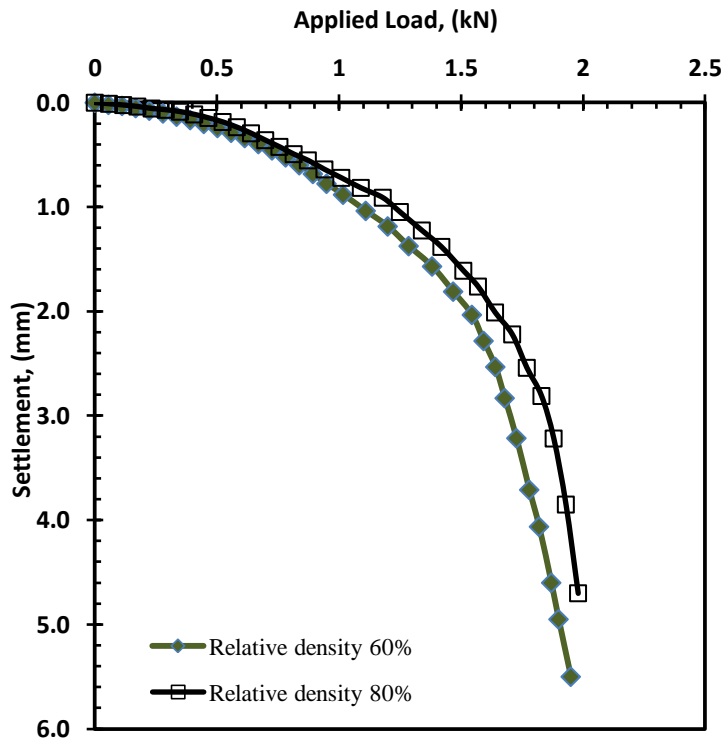


Figure 7.16: Influence of relative density on the bearing capacity of FRP pile

From the results, it can be observed that axial load capacity of the FRP pile increases with increase in the density of sand i.e. at $I_d = 80\%$ the FRP pile was exhibited higher bearing load than at $I_d = 60\%$ and this increase is nearly 8%. This is because the shear strength of sand increases as it becomes denser. This is attributed to higher interlocking of sand particles at higher relative densities, which causes a higher bearing capacity.

7.3.2 Lateral Load Results

The behaviour of piles subjected to lateral loads is governed by many parameters, such as pile properties, including pile stiffness and geometry, the pile soil interaction, and sand density. In this study, the effect of FRP tube configuration (FRP type) and FRP tube diameter of pile will be investigated. In addition, it is also important to understand the behaviour of these materials under environment

conditions. However, the effects of these important parameters on the FRP pile are explored following sub-sections.

7.3.2.1 Influence of FRP Pile Type

Two tests were conducted with a 20 mm diameter FRP piles to study the effect of pile type and configuration using Congleton. The applied pressure was 120 kPa provided by GDS controller pressure. Both FRP composite piles have identical dimensions and wall thickness. Figure 7.17 shows the deflection response of the both CFRP and GFRP piles subjected to the lateral load. The behaviour indicates that the lateral load capacity of CFRP pile is relatively higher than that of beam GFRP pile. As shown in the Figure 3.24 in Chapter three that CFRP piles has higher flexural stiffness compared to GFRP pile of the same diameter and thickness. Lateral bearing capacity of FRP piles is governed by the laminate structure of the FRP tube in terms of the effective elastic modulus in the longitudinal direction (0 degree angle).

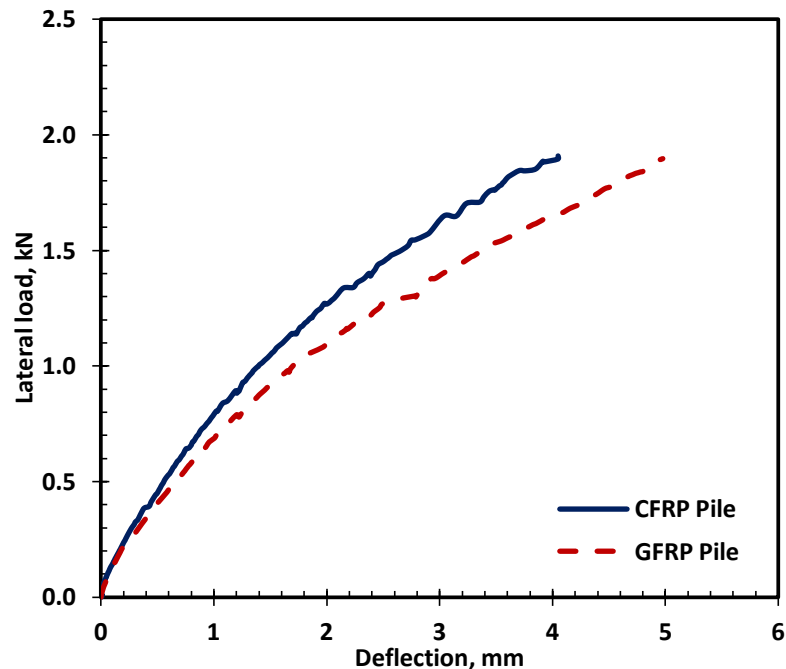


Figure 7.17: Influence of FRP Pile Configuration on the lateral capacity

7.3.2.2 Influence of FRP Pile Diameter

To study the effect of diameter on lateral load capacity, two CFRP model piles of different diameters such as 20 mm, and 12.5 mm were tested. The tests carried out using Congleton sand at relative density 78% and confined pressure 120 kPa. Figure 7.18 shows the effect of FRP diameter of the pile on lateral load capacity. From the results, it can be observed that lateral load capacity increases with increase in diameter of the pile. This is due to the effect of changing in pile surface area. In general increasing surface area will increase the lateral bearing capacity. Also the FRP pile stiffness, EI , increases with increase in moment of inertia which depends on the diameter of pile. This is in agreement with the observation of (Salini and Girish, 2009).

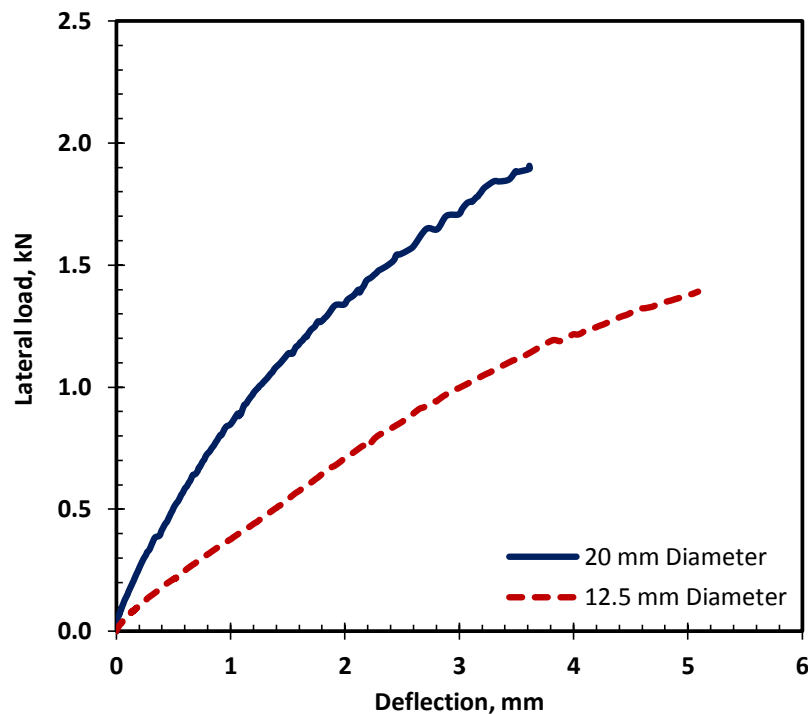


Figure 7.18: Influence of FRP pile diameter on lateral load capacity

7.3.3 Influence of Ageing Environment

One of most important in this research project is to determine the long-term environmental influence on FRP pile bearing capacity. Although composites piling have been used in marine and waterfront applications, they are still fairly new compared to the traditional materials. Therefore, it is imperative to carry out an independent study to examine the long-term performance of the FRP composites in aggressive environments. This study was providing link to long-term program which presented in Chapter four. The FRP's piles were prepared have been subjected to two aggressive environments: acidic and alkaline solution for 180 days. The aging was accelerated at 45°C elevated temperatures. The following subsections describe the long-term assessment on the axial and lateral bearing capacity of the FRP piles using different aggressive environment.

The CFRP and GFRP piles specimens were removed from the acceleration containers after 180 days. Immediately after the aggressive solutions on the surface of the specimens were wiped away and left to dry at laboratory temperature. The surface roughness was carried out on the both CFRP and GFRP specimens before and after aging. After long-term aging it was clear that aggressive media at the surface only had observed along the FRP pile shaft in both acid and alkali solutions at acceleration temperature 45°C. An acceleration of the chemical reactions using higher temperatures thereby enables long-term strength predictions (Riebel and Keller, 2007). The surface roughness measurements for both CFRP and GFRP piles used in the long-term laboratory experimental program are summarized in Table 7.4.

Table 7.4: Surface roughness measurements (T=45°C)

FRP Pile Material		CFRP		GFRP	
Aggressive solutions		pH=2	pH=12	pH=2	pH=12
R _t	Before aging	17.2	18.8	26.2	27.7
	After aging	23.6	25.4	31.1	33.4

The lateral test procedure was conducted to estimate the long-term capacity of FRP pile. The same experimental apparatus and procedure was adopted for conducting the lateral capacity test on FRP piles which described in this chapter. Figure 7.19 and 7.20 show the typical pile head deflection responses for both GFRP and CFRP piles which immersed in acid and alkali solutions. For the GFRP pile, it can be seen that the lateral capacity for specimen which aged in alkaline solution is relatively lower than these aged in acid solution. Small cracks are occurred at the tension side of the GFRP pile which exposed in alkali solution. Then, a serious damage is occurred in the range from pile depth levels -30 mm to -45 mm as shown in Figure 7.19b. The cracks run almost in the same direction along the tension side and directly crossing the matrix between the fibres. As already discussed in Chapter three section 3.5.2, The loss of matrix stiffness due to microcracking, fibre/matrix debonding and plasticization led to a first rapid and significant drop of element strength especially with specimen exposed to pH=12. However, the generation of microcracking during the ageing process could explain the decrease in the FRP tube stiffness of the testing FRP specimens after subjected to the different aging environments.

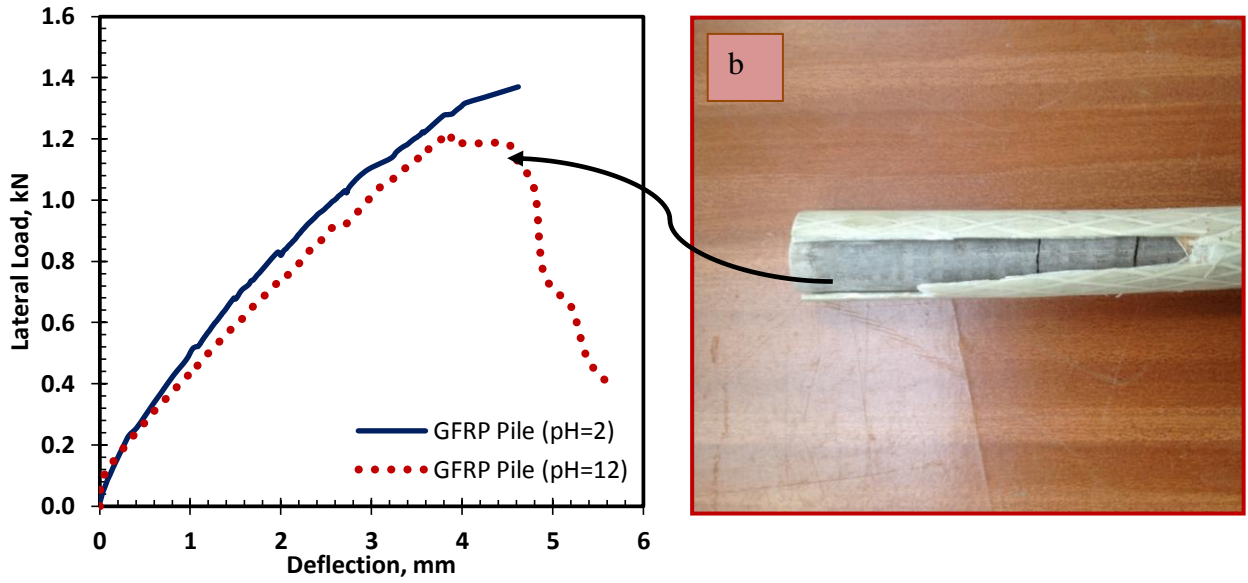


Figure 7.19: Lateral load behaviour for GFRP in long term at different condition

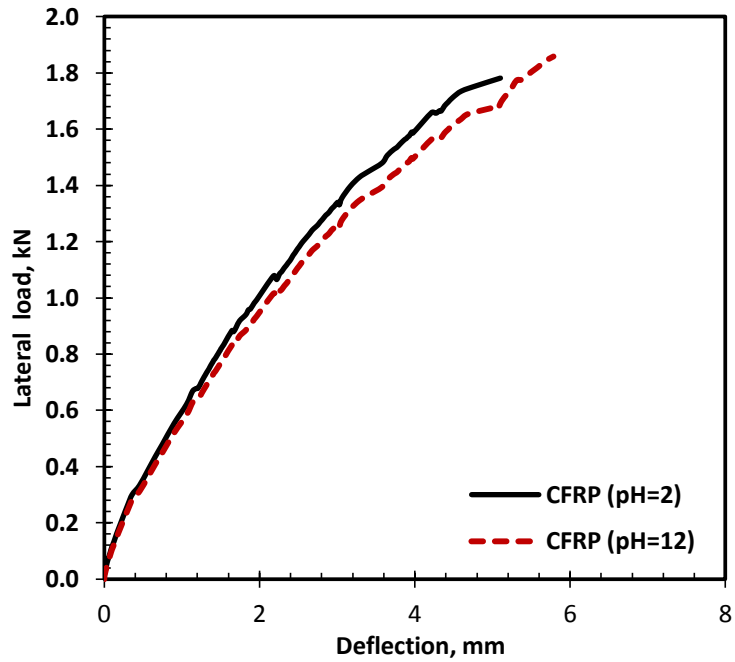


Figure 7.20: Lateral load behaviour for CFRP in long term at different condition

On the other hand, the acid aging environment was found to have less on effect on CFRP pile tube than alkaline with presence of small cracks on tube surface after immersion as shown in Figure 7.21. Although the presence of epoxy resins in FRP composite around the fibre filaments can be expected to protect the fibres from attack, the alkaline solutions can accelerate the degradation of fibre/matrix bond and dissolve some of the resins and it might be diffused into FRP/matrix leading to be more degradation than acid. The similar behaviour of CFRP pile under lateral load was observed exposed in both aggressive solutions. This is probably that the lateral load was not reached to the high capacity at this limit. The aging environment effect on the CFRP pile response is expected at the high lateral loading.

Based on the above discussion, the results in suggest that the alkaline aging environment (pH=12) promotes better curing reaction properties than the acidic aging environment. In fact, this difference can be attributed to the difference in the amount of liquid that could diffuse into GFRP and CFRP tubes which is function of aggressive environments (chemical solution) and the affinity of the diffusing molecule to specific groups present in the epoxy (Diamant et al., 1981)

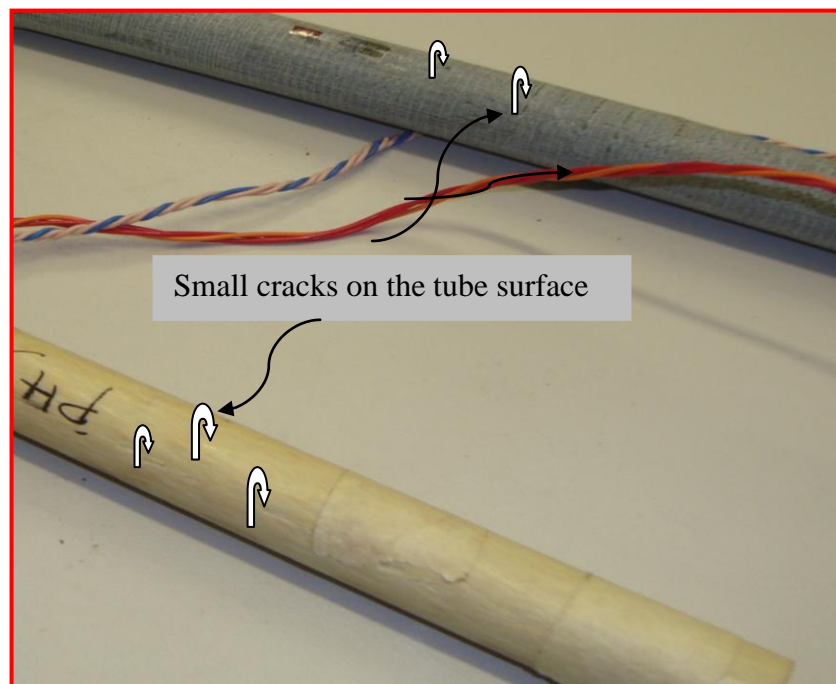


Figure 7.21: FRP piles after exposure to alkaline solutions

7.3.4 Model Scale Size

Pile load capacities measured in a calibration chamber are different from those measured in the field due to chamber size effects. In order to use the calibration chamber test results for computation of pile load capacity in the field, corrections for chamber size effects were performed for every chamber test. In the estimation of chamber size effects, the ratio of the chamber to the equivalent diameter of the model pile used in the tests is required. Many researchers have attempted to estimate the chamber size needed for boundary effects on pile bearing capacity or cone resistance to become negligible. Parkin and Lunne, (1982) suggested 50 times the cone diameter as the minimum chamber diameter for chamber size effect on cone penetration resistance to become acceptably small. Diameters of the chamber and test pile used in this study are 256 and 20 mm, respectively. Considering the results of the research on chamber size effects mentioned above, the size of the chamber used in this study is not sufficiently large for chamber size effects on pile bearing capacity to be neglected.

7.3.5 Slenderness Ratio

As mentioned in Chapter two, the pile slenderness is defined as the ratio between the pile length and diameter (L/D). The pile behaviour is also influenced by pile slenderness ratio (L/D) during loading. Abbas et al., (Abbas et al., 2008) mentioned that the pile deformation due the lateral load is also influenced by pile slenderness ratio (L/B). The short pile ($L/D=8.3$) give a small amount of lateral tip deflection for the same amount of loading than the piles have the slenderness (L/D) ratio more than 8.3. However, the slenderness is not studied herein considering that a much smaller database exists for these pile models.

7.4 Summary

An experimental test pile program was conducted to permit direct comparison of the axial and lateral load behaviour of three test piles. Two composite (GFRP and CFRP) and one mild steel piles were examined under axial and lateral loads in term of some important parameters. The tested piles were installed in dense sand using specially designed chamber. The laboratory testing program included static axial load tests, and static lateral load tests. Furthermore, the FRP composite piles were also selected to be used to assess the lateral load capacity under different aging environment. The testing program involves immersing the GFRP and CFRP testing piles in two different aqueous solutions; NaOH (pH=12), and HCl (pH=2) which represent acidic and alkaline soil environments, respectively, for 24 weeks at temperature 45 °C. The following conclusions can be drawn from the test program:

- From the load-settlement curves, it was observed that variation of the total load capacity with different pile types was relatively significant in term of pile shaft surface roughness.
- The axial loading rate has insignificant effect on the behaviour of pile subjected to the axial load. On the other hand, the confined pressure had more significant effect.
- The CFRP pile has greater lateral load carrying capacity and remarkably lower deflection due to high stiffness moduli compared to GFRP pile.
- The accelerated GFRP pile which immersed in alkaline solution was failed rapidly under lateral load compared to CFRP. The alkaline solutions can accelerate the degradation of fibre/matrix bond and dissolve some of the resins and it might be diffused into FRP/matrix leading to be more degradation than acid solution.

CHAPTER EIGHT: NUMERICAL SIMULATION OF FRP PILE/SAND

8.1 Introduction

Finite element method (FEM) is a common tool within the field of geotechnical engineering. In the last two decades, there is a growing number of mature FEM commercial software in the international market (e.g. DIANA, ABAQUS, PLAXIS and FLAC). Among them, ABAQUS and PLAXIS are widely used FEM software in the geotechnical engineering and ABAQUS is excellent in dealing with contact problem (Bing-can et al., 2010). Therefore, ABAQUS software (6.11) is adopted by this research and is used to simulate the experimental FRP pile model subjected to different loading mode. FEM modelling approach is used to generate numerical data which then provides a basis for validating experimental analyses.

The ultimate aim of this work is to provide structural and geotechnical engineers with an efficient, accurate and robust information of FRP pile simulation. This chapter is conducted using FEM numerical simulations to generate comprehensive database to guide the development of experimental work which presented in chapter six. Additional analyses were performed to investigate the influence of various important parameters on the FRP piles response during loading test. The basis of back-calculation technique for material properties was used to minimizing the differences between numerically simulated and experimental results.

8.2 Pile/Soil Analysis Using FEM

In general, several numerical studies have been performed by various researchers to investigate the behaviour of traditional piles in various soil profiles subjected to axial and lateral loads. Torchanis et al., (1991) attempted to study the response of concrete pile under combined vertical and lateral loads based on 3-dimensional finite element method. The emphasis was mainly focused on the influence of lateral load on the axial response of a pile rather than the influence of vertical load on the lateral

response of piles. Feng et al., (2012) used the ABAQUS finite element software to calculate the vertical bearing capacity of single piles in Tianjin and through the comparison of the data gained through the in-situ static load pile foundation tests and the finite element results. They found that the Young's modulus of the soil at the bottom of the pile could have important role in improving the vertical bearing capacity of single piles.

Pile foundations are frequently used in situations where large lateral forces and movements must be resisted. Examples include high-rise buildings subjected to wind loads, and bridge abutments. Therefore, the evaluation lateral load capacity of FRP pile is considered an important object of this study in order to confidently confirm the applicability of using FRP as piling foundation. A number of FE studies have been proposed to assess the pile response to lateral load. Goh et al., (1997) presented a simplified numerical procedure based on the FEM for analysing the response of single piles to lateral soil movements with assumed soil displacement profiles. Hsueh et al., (2004) investigate the response and performance of reinforced concrete pile shaft subjected to lateral loading using the numerical finite-element program ABAQUS, and considered both soil and pile nonlinearity. Unfortunately, To date, research work related to the performance of FRP piles and their behaviour subjected to lateral loading conditions using FEM is however very limited. This chapter will be described in details the geometrical, material and loading application parameters used to model the problem of FRP pile/soil system under different loading modes.

8.3 FE Commercial Code ABAQUS

ABAQUS is a set of finite element analytical programs originally developed by Hibbitt, Karlsson & Sorensen, Inc. and currently maintained by SIMULIA Corp. ABAQUS is a general purpose finite element package which has been used extensively by many to simulate a wide range of problems including pile structure response under loading. Numerous of geotechnical studies and examples have been solved from numerical methods by using many FEM programs. This software is used worldwide by educators and engineers to solve various types of civil engineering.

However, ABAQUS version (6.11) was used in this research due to its availability and capable of predicting the behaviour of the pile under different loading.

8.4 Constitutive Model of Materials:

- **Elasticity Model:** The elasticity-based models are those models whose constitutive relations are deduced from the elasticity theory which is governed by the Hooke's law. It is suitable for isotropic, linear elastic materials. Hooke's law relates the stresses and strains through two constants, Young's modulus (E) and Poisson's ratio (ν).
- **Mohr Coulomb Constitutive Model:** Elasto-perfectly plastic model with Mohr-Coulomb failure criterion, usually named as Mohr-Coulomb model, is widely used in finite element analysis of geotechnical engineering, due to its simplicity and sufficiently accuracy (Chen and Saleeb, 1982). This elastic perfectly-plastic model requires five basic input parameters, namely a Young's Modulus, (E), a Poisson's ratio, (ν), a cohesion, (C), a friction angle, ϕ and a dilatancy angle, ψ was used in this study.
- **Pile Soil Interaction:** In order to verify the numerical model results with those obtained from experimental model, the FRP pile/sand model was simulated using the contact property technique in term of interface friction. The interaction relationship between the FRP pile and the soil around and bottom FRP pile can simulate the penalty contact-type (Pan et al., 2011). This type of interface friction is capable of simulating the interface friction between the pile surface and the soil in contact (Sam, 2007). The FRP external surface, FRP pile tip are contacted with the sand as shown in Figure 8.1.

8.6 Model Characteristics

Pile/soil simulation behaviour requires careful selection of the modelling parameters so as to produce accurate results that are as close as possible to the actual behaviour of the loaded members. The general characteristics of the model are as follows:

- **Element type:** Eight-noded linear brick element type C3D8R with reduced integration was utilised for the model. This type of elements suffers from hour-glassing problem, therefore ABAQUS introduces hourglass control to overcome this numerical problem and enhance the solution convergence.
- **Finite element mesh:** The finite element mesh of half of the pile and the surrounding soil is considered as shown in Figure 8.2. The three-dimensional finite element mesh (Figure 8.2) comprises three parts: the FRP tube, pile with and the soil. It is noted that the mesh is finer in the vicinity of the pile since that zone is the zone of stress concentration. No mesh convergence studies have been performed. Generally, seed, mesh and assign are three basic steps for mesh module. The different size of mesh will result in the different accuracy of results and running time. However, the nature of FE model and the element size that used in this study in order to get best fitting results with the experimental results.

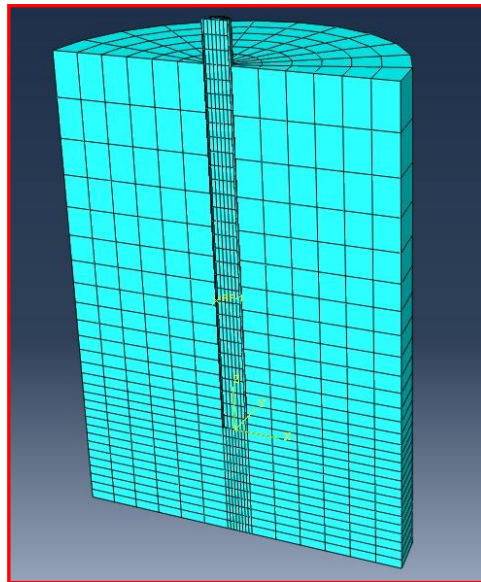


Figure 8.2: Three-dimensional FE mesh

➤ **Modelling parameters:** The material behaviour of the pile was assumed to be linear elastic. The properties of materials of pile material are determined from compression test on the mortar cylinder using the typical stress-strain curve as shown earlier in Figure (3.12) in Chapter three. The elastic approach is used to estimate the response of pile subjected to working loads assuming that the pile behave as elastic materials. The sand was modelled as elastic-perfectly plastic model based on the Mohr-Coulomb failure criterion. The interface experimental results were used to simulate the coefficient of friction between pile and sand material. In addition, the equations (8.1 and 8.2) suggested by other researchers [(Chae et al., 2004) and (Al-Defae et al., 2013)] were used to simulate the sand properties. Table 8.1 summarises the typical material properties used in this analysis.

$$E_{\text{sand}} = 25I_d + 20.22 \text{ MPa} \tag{8.1}$$

$$\psi_{\text{sand}} \approx \phi - 30 \tag{8.2}$$

Table 8.1: Material properties used in the analysis

Material	Model	Young Modulus, E (MPa)	Poisson's Ratio ν	ϕ°	ψ°
Pile	Elastic	28000	0.22	----	----
Sand	Mohr-Coulomb	41.5	0.31	33	4

The material behaviour of FRP and sand in general is very complex. In this study, the FRP tube composite material is modelled as unidirectional orthotropic. The three principle directions (direction 1 along the fibre direction and directions 2 and 3 perpendicular to the fibre direction) are orthogonal to each other. The material properties of both carbon and glass fibre composites are shown in Table 8.2.

Table 8.2: Properties of CFRP and GFRP tubes

Property	Symbol	Unit	CFRP	GFRP
Density	ρ	g/cm ³	1.6	2.0
Longitudinal Modulus*	E_{11}	MPa	135000	50000
Transverse in-Plane Modulus*	E_{22}	MPa	10000	40000
Transverse out-Plane Modulus*	E_{33}	MPa	10000	8500
In-plane Shear Modulus**	G_{12}	MPa	5000	4300
Out-of-Plane Shear Modulus**	G_{23}	MPa	1900	3500
Out-of-Plane Shear Modulus**	G_{13}	MPa	5000	4300
Major in-Plane Poisson's ratio**	ν_{12}	----	0.3	0.27
Out-of-Plane Poisson's Ratio**	ν_{23}	----	0.5	0.50
Out-of-Plane Poisson's Ratio**	ν_{13}	----	0.3	0.27

*: provided by manufacture:

** : Ref. ¹⁵²,

In ABAQUS, Linear elasticity in an orthotropic material can also be defined by giving the nine independent elastic stiffness parameters. In this case the stress-strain relations are of the form:

$$\begin{bmatrix} \sigma_1 \\ \sigma_2 \\ \sigma_3 \\ \tau_{12} \\ \tau_{13} \\ \tau_{23} \end{bmatrix} = \begin{bmatrix} D_{1111} & D_{1122} & D_{1133} & 0 & 0 & 0 \\ & D_{2222} & D_{2233} & 0 & 0 & 0 \\ & & D_{3333} & 0 & 0 & 0 \\ & & & D_{1212} & 0 & 0 \\ & \text{Sym} & & & D_{1313} & 0 \\ & & & & & D_{2323} \end{bmatrix} \begin{bmatrix} \epsilon_{11} \\ \epsilon_{22} \\ \epsilon_{33} \\ \gamma_{12} \\ \gamma_{13} \\ \gamma_{23} \end{bmatrix} \quad 8.3$$

For an orthotropic material the Abaqus engineering properties are calculated and listed Table 8.3 based on Eq's. 2.14 and 2.15 which described in Chapter two.

Table 8.3: FRP material stiffness matrix

ABAQUS Parameters	Matrix Parameter (Eq's. 2.14 and 2.15)	Orthotropic Parameter Values	
		CFRP (MPa)	GFRP (MPa)
D ₁₁₁₁	C ₁₁	138660	53279
D ₂₂₂₂	C ₂₂	13604	55957
D ₃₃₃₃	C ₃₃	13604	55957
D ₁₁₂₂	C ₁₁	6101	6073
D ₁₁₃₃	C ₁₃	6101	6073
D ₂₂₃₃	C ₂₃	6937	29290
D ₁₂₁₂	C ₁₂	5000	4300
D ₁₃₁₃	C ₁₃	5000	4300
D ₂₃₂₃	C ₂₃	1940	3500

8.7 Validation of Axial Load Results

The static axial load was applied at constant increment and increased gradually until the required maximum loads are reached. The pile/settlement response was evaluated in term of its interface friction coefficient. The coefficients of interface friction GFRP, CFRP and steel pile models were 0.55, 0.45 and 0.27 respectively based on the interface shear tests as described in chapter four (see Tables 4.4, 4.5 and 4.6). The comparison results, in term of pile/settlement response between the numerical and experimental showed good agreement using as illustrated in Figure 8.3. These coefficients were used to model the interaction behaviour between the pile and sand. However, the numerical analysis was shown be able to predict the pile/settlement results, illustrating the ability of three dimensional ABAQUS program to model the behaviour of pile subjected to axial load.

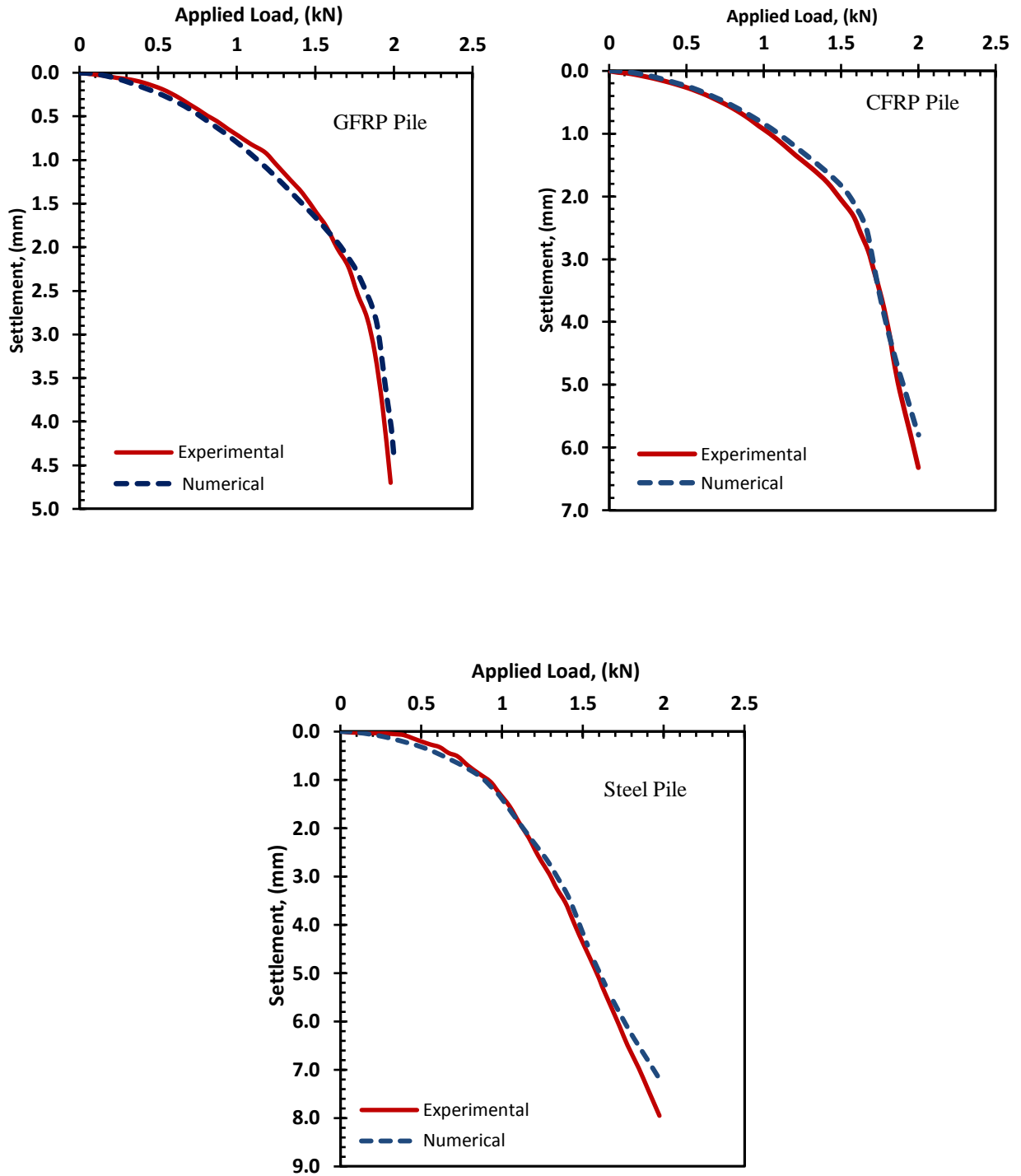


Figure 8.3: Pile load versus settlement curves for testing piles

8.8 Influence of Important Parameters on FRP Pile Response Subjected to Axial Load

The effects of a number parameters on FRP pile response including, FRP type and configuration, vertical pressure and sand dilation angle were investigated in this part. The FRP pile response was presented in term of the FRP shaft settlement. The effect of these parameters on the FRP pile response is explored in the following subsections.

8.8.1 Effect of FRP Tube Configuration

As mentioned in chapter two, fibre composite materials are generally used as a stack of multiple layers in a form of a laminate. Each layer is assumed to have different fibre orientation than the adjacent one. The laminate has a total thickness of and number of layers. To investigate the effect of FRP tube configuration on the pile behaviours subjected to axial load, the composite element technique provided by ABAQUS was selected for these analyses. The CFRP types, the first, third and fifth layers of the composite tube were modelled with the material properties of unidirectional layers in longitudinal orientation (0°). The second and fourth layers were modelled in the hoop direction (90°). Figure 8.4 shows the FEM modelling of configuration of both CFRP and GFRP laminate. In this study, the interaction between each FRP pile and the sand is simulated using a penalty-type interface with a friction factor of 0.50 for both analyses. Each pile was subjected to axial load under confined pressure 250 kPa. The typical pile/settlement curves using the finite element analysis are shown in Figure 8.5.

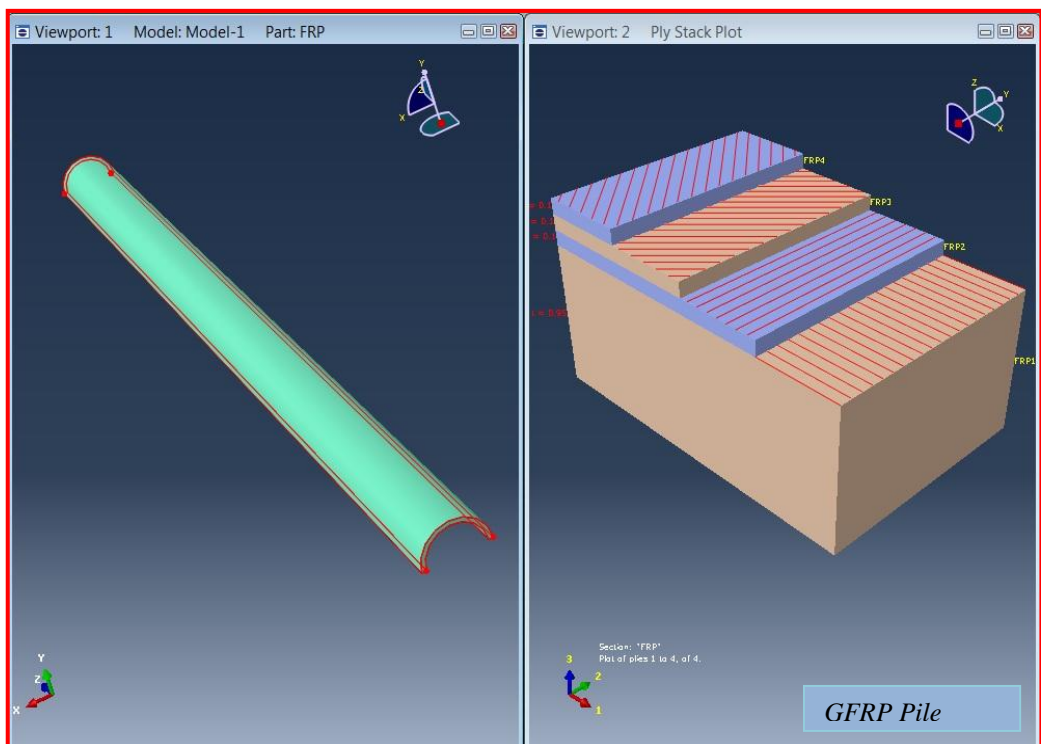
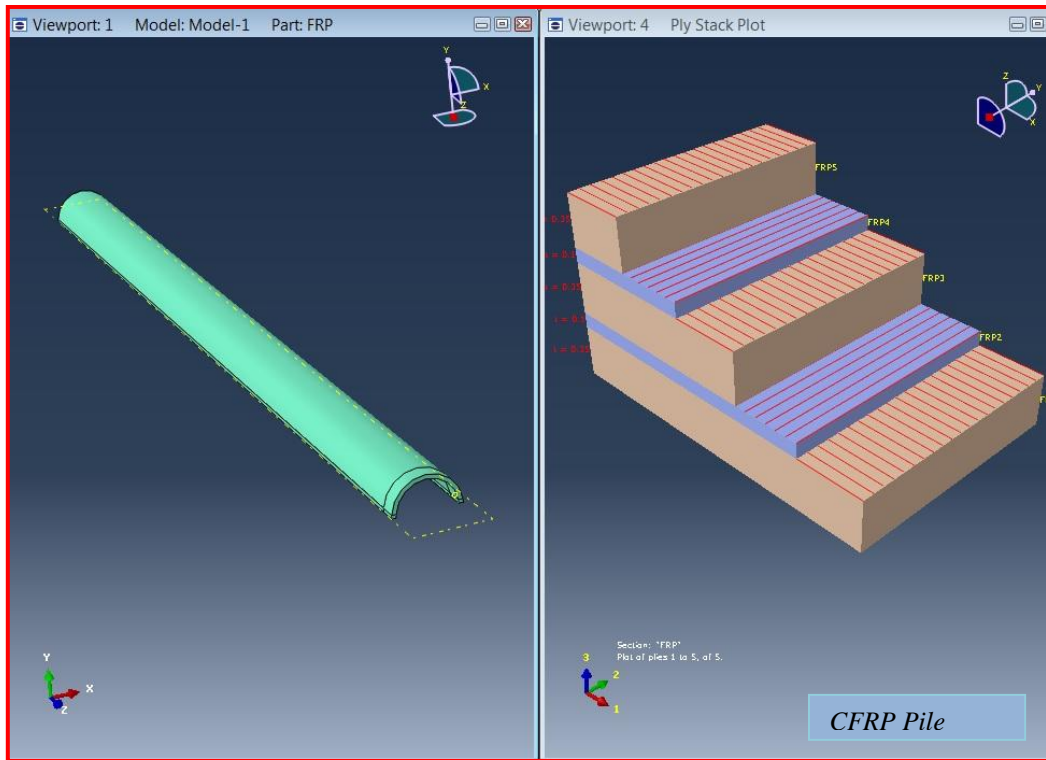


Figure 8.4: The FRP lube laminate structure

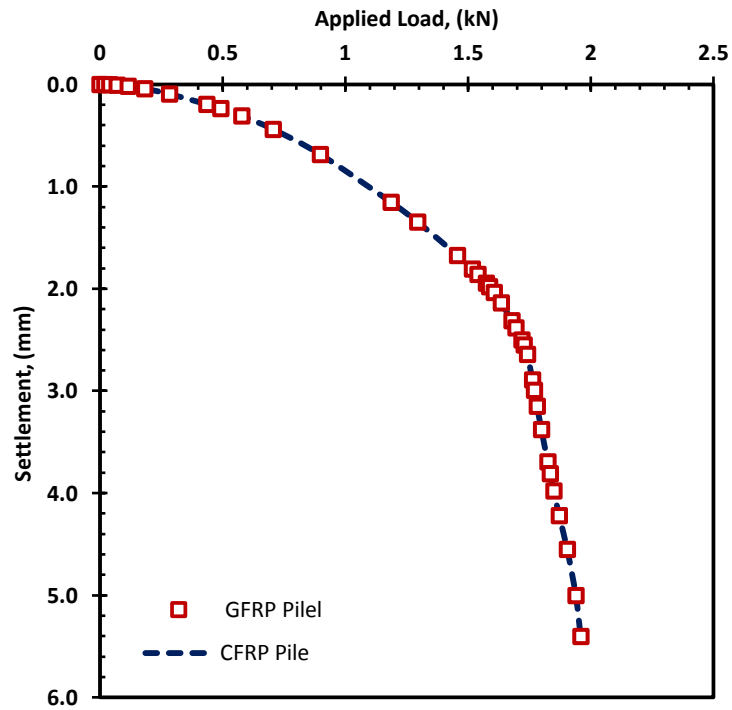


Figure 8.5: Effect of FRP material on axial load settlement response

It can be observed that the load settlement for both CFRP and GFRP exhibited similar response. The measured axial load/settlement behaviour showed that the FRP pile configuration insignificant influence on the FRP pile response. However, the FRP pile bearing capacity is controlled by the mechanism of FRP tube interaction with surrounding soil.

8.8.2 Effect of Vertical Pressure

To study the effect of varying vertical pressure on axial load capacity in case of GFRP pile, FEM analysis were performed under three different pressure (50, 100, and 250 kPa). Figure 8.6 shows the results of GFRP pile axial load-settlement obtained by FEM analysis. It appears that the GFRP composite pile performance is highly influenced by the soil pressure. However, the pile settlement for the soil pressure 100 kPa was approximately 2 times greater than that obtained from 250 kPa. This is because the shear strength of bottom sand increases as it becomes high

dense. This indicates that the pile performance in the axial mode is controlled by applied pressure on the pile/soil.

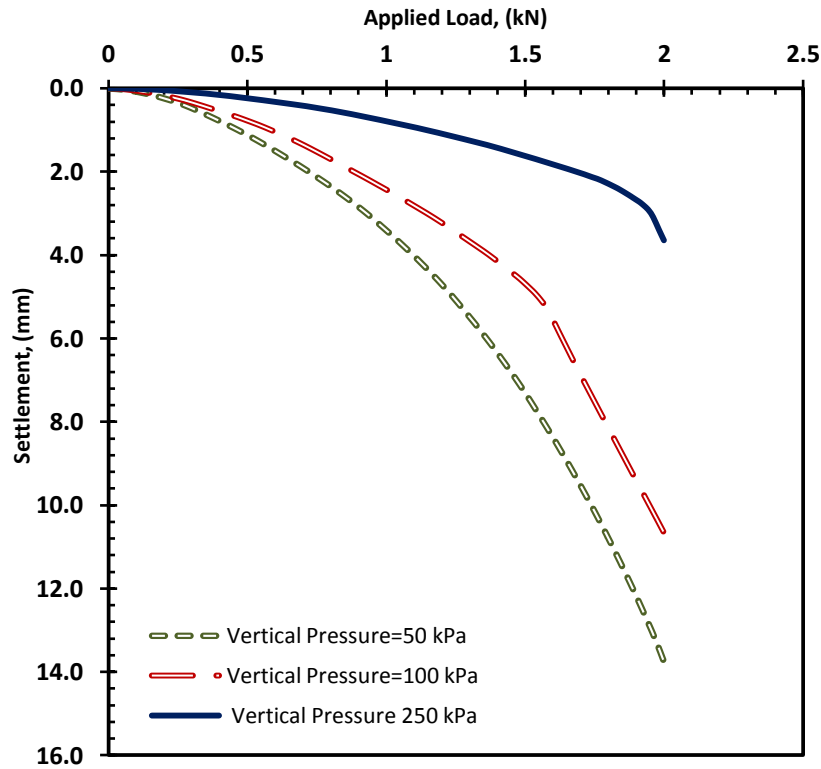


Figure 8.6: Effect of sand pressure on FRP pile response

8.8.3 Effect of Sand Dilation Angle

Three dilation angles of $\psi=0$, 4, and 15 were investigated for the effect of dilation angle of the sand on the FRP behaviour subjected to axial load. The computed results, using the GFRP pile model, are shown in the Figure 8.7 . It can be seen that FRP pile system response is shown very sensitive to the choice of dilation angle. Pile capacity reached its yielding apparently in the non-dilatation soil ($\psi=0^\circ$), while at the higher dilation angle ($\psi=15^\circ$), predicted a nearly elastic response and was overly unconservative. In general, the different pile responses show that, as the sand dilation angel increase, the soil pressure increase. Indeed, the dilation angle of sand has greater influence on the FRP composite pile/settlement response during axial static load.

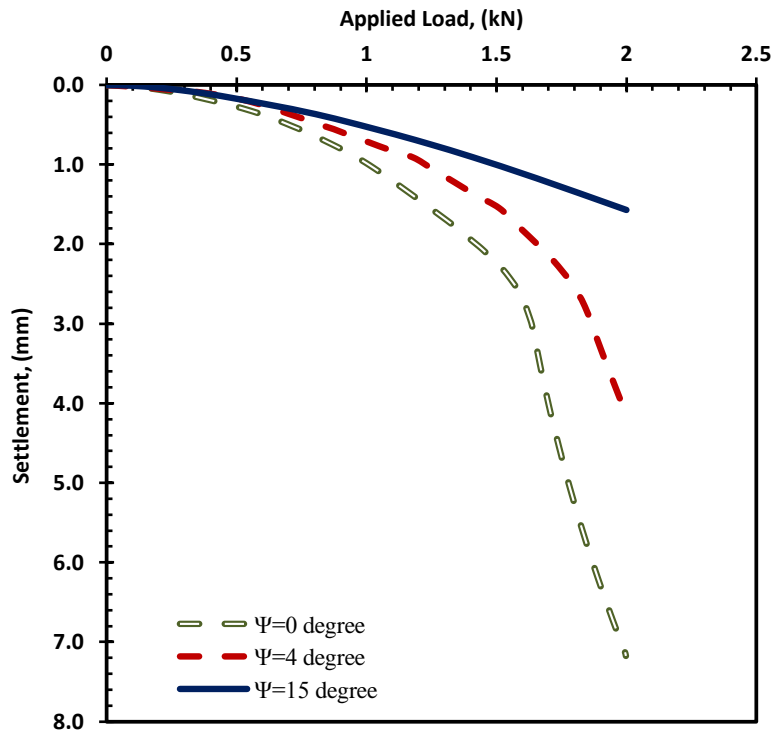


Figure 8.7: effect of sand dilation angle on the FRP pile response

8.9 Lateral Load Modelling

FEM analysis of laterally loaded piles is similar to that of axially loaded piles except for loads that are applied in the horizontal direction at or above the ground level as shown in Figure 8.8. The FRP pile/soil model is modelled using the ABAQUS analysis package based on experimental setup to evaluate the lateral load-deflection response of the FRP pile. The FEM analyses were performed to verify/validate the results from the experimental test described in previous chapter. To provide insight into the mechanism of FRP tube, and gain a greater understanding of the behaviour of the FRP pile under the lateral loading using numerical method, additional analyses were conducted to examine the effect of some important parameters e.g. (coefficient of interface friction between pile and soil, vertical pressure, sand young's modulus, and FRP tube configuration). The FEM comparison between two FRP piles and traditional pile (concrete and mild steel) was conducted in this study.

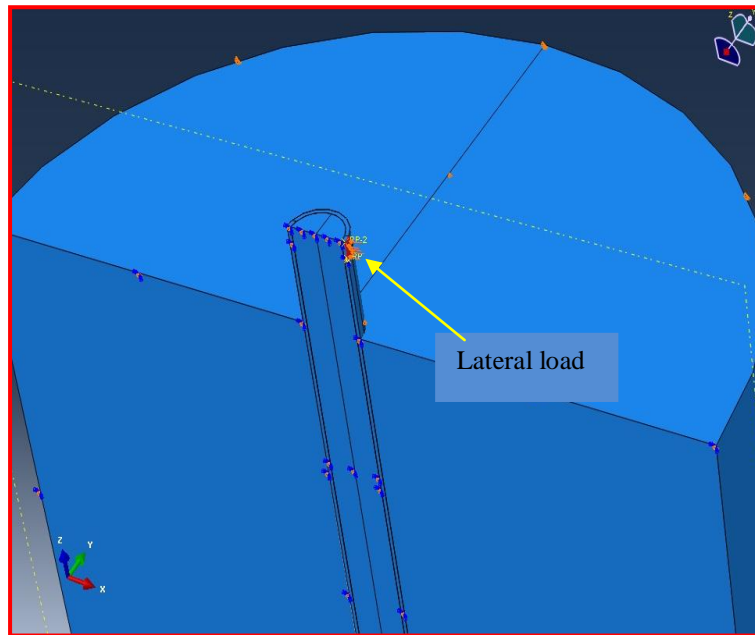


Figure 8.8: Simulation of FRP pile/soil under lateral load

8.10 Validation of Lateral Load Results

The experimental model is simulated in this study to provide an important understanding of the behaviour of FRP pile and soil during the testing of lateral load. Experimental results were used to verify the three dimensional finite element model (FEM) in term of lateral deflection response. The comparison between experimental test and numerical analysis for the pile load-deflection results is shown in Figure 8.9. The pile deflection was measured from the displacement at the pile head. It can be seen that the behaviour of the load-deflection from FEM simulation agreed reasonably well with experimental load test result for both FRP piles. It is apparent that for a given load the pile deflection of the CFRP composite pile is considerably lower than GFRP pile. This is primarily due to the CFRP tube laminate configuration. The fibres have oriented in the longitudinal axis and having a higher stiffness than the GFRP piles. It is a quite clear that the FRP pile deflection depend on the FRP laminate, and fibre configuration relative to the longitudinal direction of FRP tube. However, the FRP pile deflection is governed by elastic modulus of the

tube in the axial direction. The magnitude of the FRP piles and sand displacements contours as shown in the Figure 8.10.

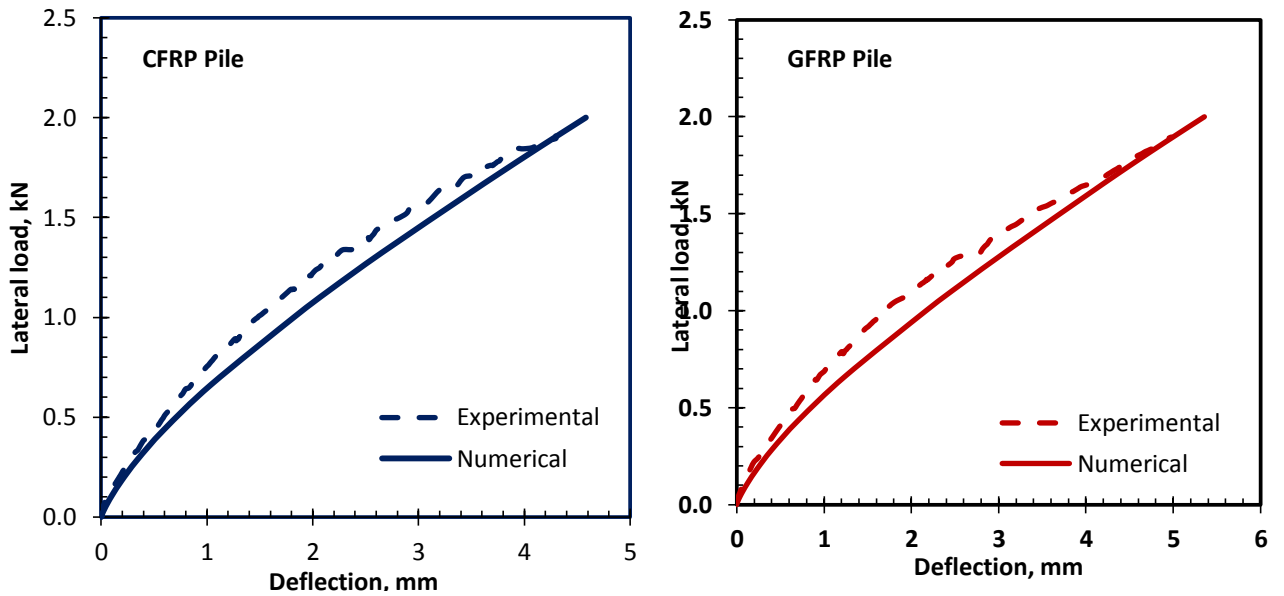


Figure 8.9: Comparison between experimental and FE results for both FRP piles

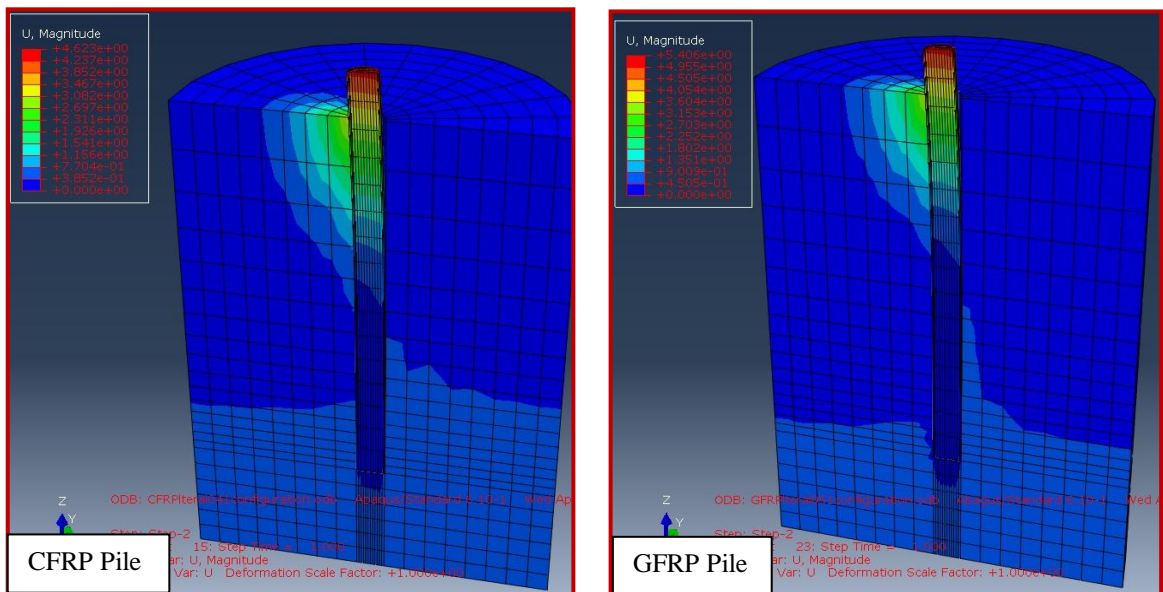


Figure 8.10: Contours showing the magnitude of both FRP piles and sand displacement

8.11 Influence of Important Parameters on FRP Pile Response Subjected to Lateral Load

Additional analyses were undertaken as part of this section to investigate the effect of some important parameters on the FRP pile subjected to lateral load. The interface friction coefficient, vertical pressure, sand Young’s modulus, and FRP tube configuration were studied in the following sub-sections.

8.11.1 Effect of FRP Pile/Soil Interface

Three FE analyses were conducted to investigate the effect of interface friction coefficient on the FRP pile response subjected to the lateral loading under vertical pressure 120 kPa. These analyses were conducted using two different interface friction coefficients (0.22, 0.35, and 0.57) respectively. The comparison, in term of the pile load deflection was presented in Figure 8.11. As a result it can be seen that that both analysis behaved in a similar manner between three analyses. Therefore, the interface relationship between FRP pile and sand used in this study has a minor effect on the pile response when subjected to lateral load.

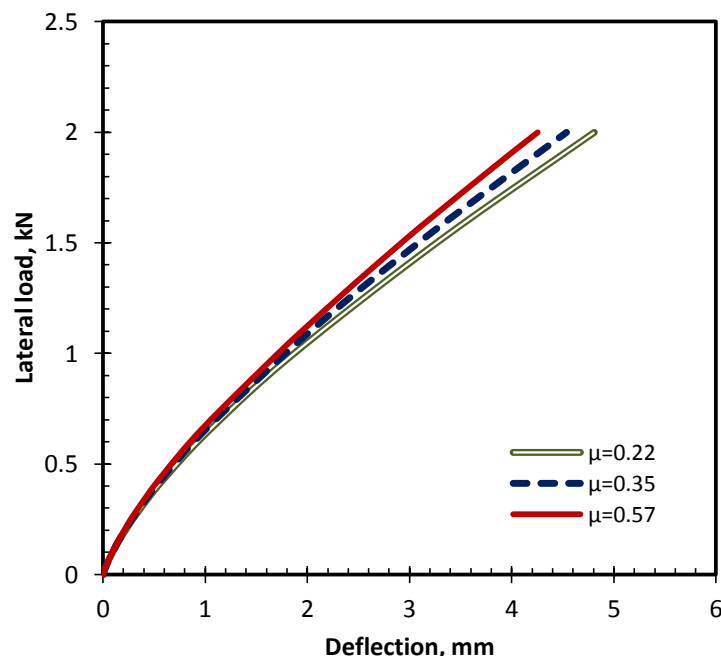


Figure 8.11: Effect of FRP material on lateral load deflection response

8.11.2 Influence of Vertical Pressure

In order to study the effect of vertical pressure on the FRP pile response, when examined to a lateral load, two FEM analyses were performed on the GFRP pile with three different vertical pressure values. The modelling of GFRP pile/soil system was subjected to the pressure 120, 250 and 400 kPa respectively. As noted earlier, the sand specimen is become denser when the pressure increased. Figure 8.12 shows the lateral load deflection curves of the GFRP pile subjected to the different soil pressure. It can be seen that lateral load capacity increases with increase in the pressure of sand. It can be seen that the lateral load capacity of the pile was increased as the soil pressure increased. This is due to the fact that shear strength of sand specimen increases as it become high denser.

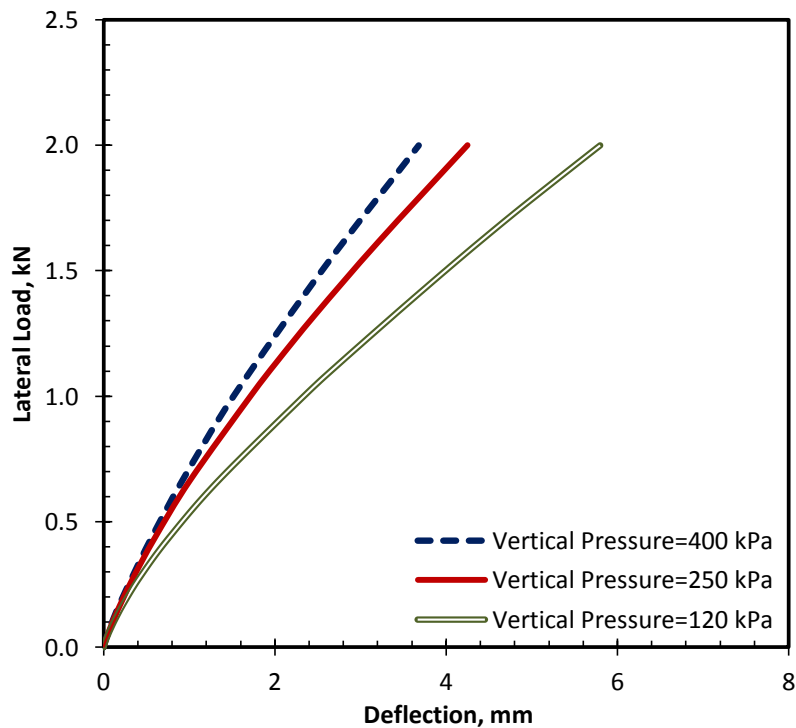


Figure 8.12: Effect of sand pressure on the lateral load deflection response

8.11.3 Influence of Young's Modulus of the Sand

The sensitivity of the Young's modulus of the sand on the FRP pile model was investigated using three values. The standard CFRP model was studied using three Young's modulus E_{sand} (20, 41.6 and 65 MPa). The lateral load and pile model deflection curves for all three cases are plotted in Figure 8.13. The curves responses show that, by decreasing the E_{sand} of the model to 10 times, the deflection on the CFRP pile increase most notably at the pile head. As expected, when the pile is embedded in a loose sand soil, the deflection of the pile increase to approximately 4.25 times at the maximum load from that obtained from the dense sand soil ($E_{sand}=65$). In between, the sand with ($E_{sand}=41.6$ MPa), the CFRP pile deflection was 1.5 times higher than obtained from ($E_{sand}=65$ MPa). Indeed, the Yong's modulus of sand has greater influence on the pile lateral response.

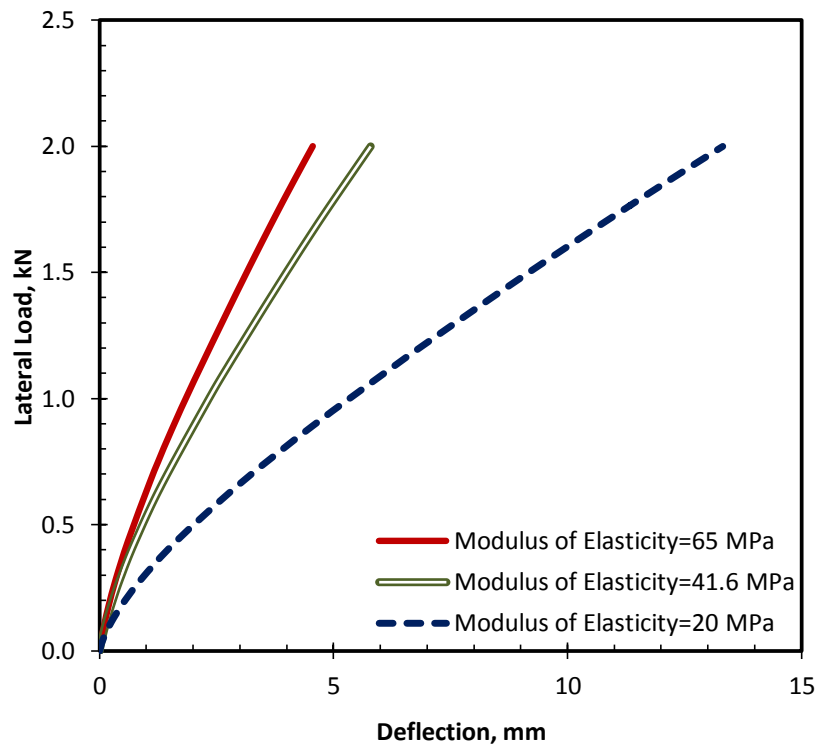


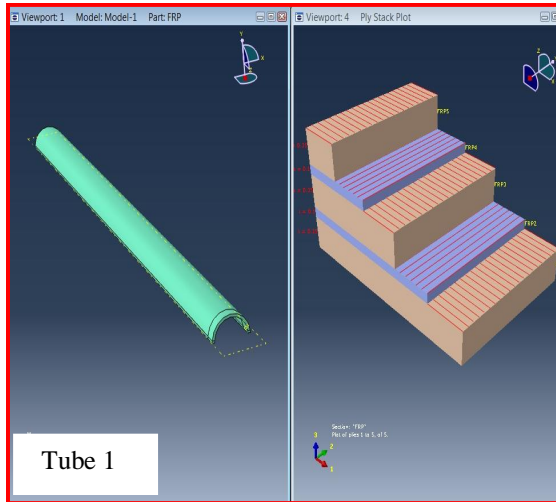
Figure 8.13: The effect of Young's modulus on the FRP pile response under lateral load

8.12 Influence of FRP tube configuration

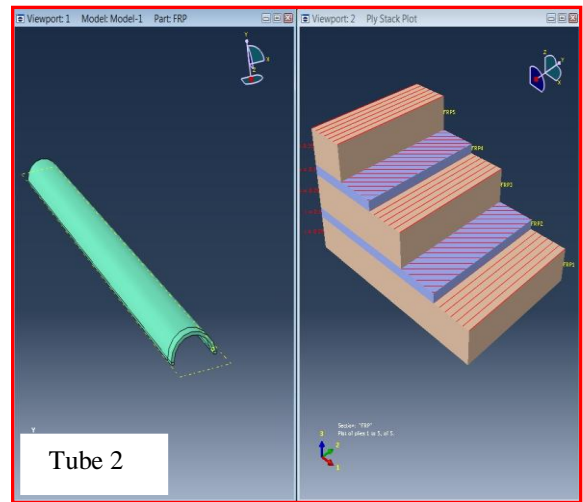
The CFRP pile was used in this study to investigate the effect of FRP laminate configuration on the FRP pile lateral load. Four different laminate configuration cases were studied as described:

1. Case 1: tube $(0^\circ, 90^\circ, 0^\circ, 90^\circ, 0^\circ)$ is representing to the control tube.
2. Case 2: tube $(90^\circ, 45^\circ, 90^\circ, 45^\circ, 90^\circ)$.
3. Case 3: tube (0°) .
4. Case 4: tube (90°) .

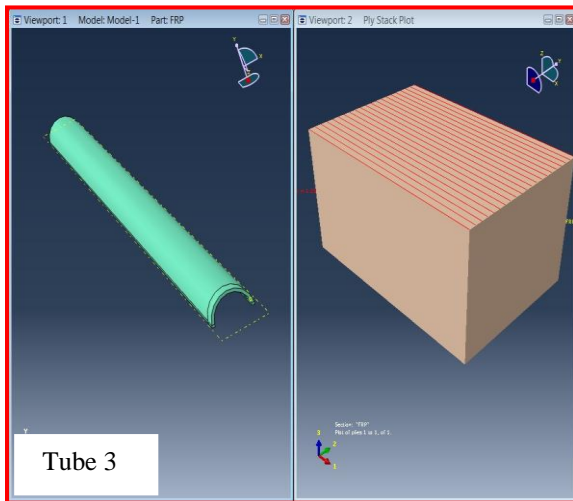
Figure 8.14 shows the laminate configuration for these FRP tubes laminates.



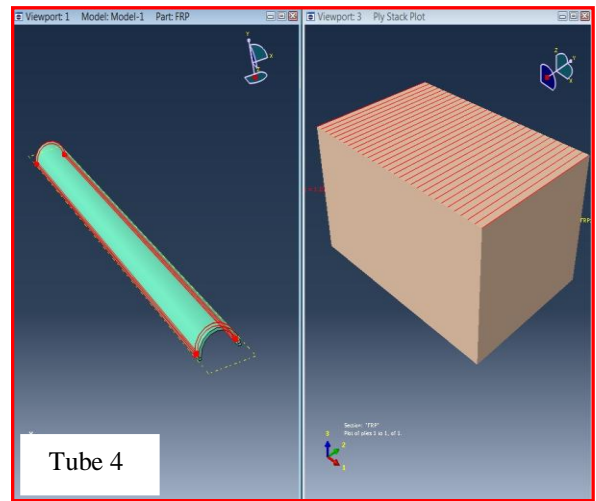
Tube laminate: $(0^\circ, 90^\circ, 0^\circ, 90^\circ, 0^\circ)$



Tube laminate: $(90^\circ, 45^\circ, 90^\circ, 45^\circ, 90^\circ)$



Tube laminate: (0°)



Tube laminate: (90°)

Figure 8.14: Different FRP tubes laminate configuration

The FE model has been developed to investigate the effect laminate configuration using these four types of tubes. Figure 8.15 illustrates the normalized load-deflection in term of laminate FRP laminate configuration. The observed variation in the FRP responses after subjected to lateral load is due to the fact of laminate configuration

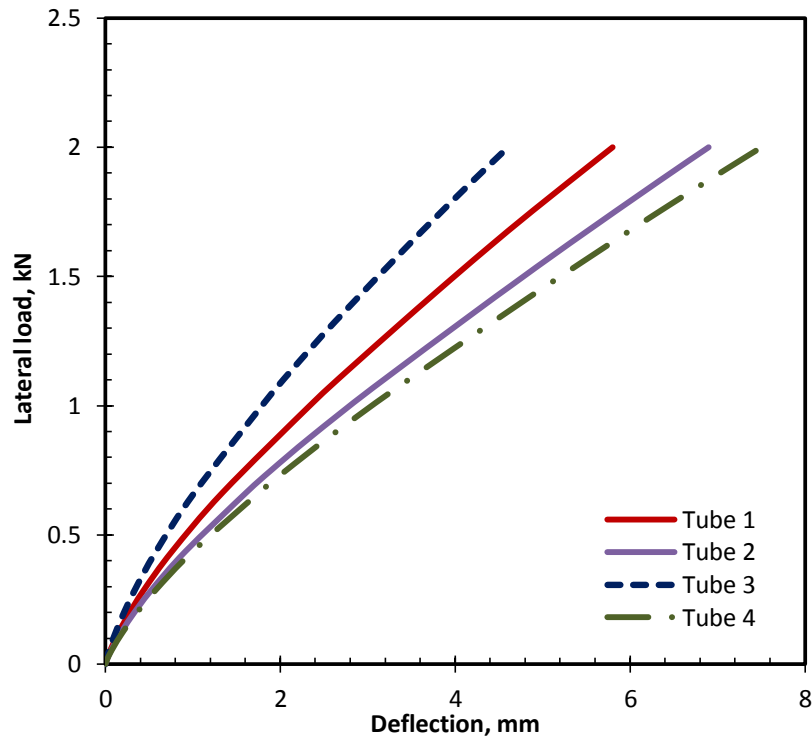


Figure 8.15: Effect of FRP tube laminate configuration

The four tubes have comparable stiffnesses. However, tube 3 achieved a 25 percent higher strength. This is attributed to the difference in tensile strength of the tubes as indicated by the ultimate tensile strains. On the other hand, the tube 3 response is exhibited high capacity than tube 4. This behaviour confirms that tube 4 has no reinforcement oriented in the longitudinal. This is attributed to the lack of stiffness in the longitudinal direction. However, the response behaviour of FRP tubes subjected to lateral load have shown that FRP laminate configuration is one of the main factor in the development of FRP pile capacity.

8.13 Comparison between FRP and Traditional Piles

The normal concrete pile under later load was modelled and simulated for comparison purposes. The similar numerical model was used for the FRP piles simulation.

The comparison of the four sets of results for mild steel, concrete and both FRP composite pile is shown in Figure 8.16. It is apparent that for a given load deflection response of the mild steel and FRP composite piles is considerably lower than concrete pile. This is primarily due to that mild steel and FRP piles having a stiffness of higher than the concrete piles. Again CFRP pile showed higher capacity and stiffness due to the higher reinforcement ratio in tube laminate at the longitudinal direction. In fact, the stiffness was almost directly proportional to the reinforcement ratio.

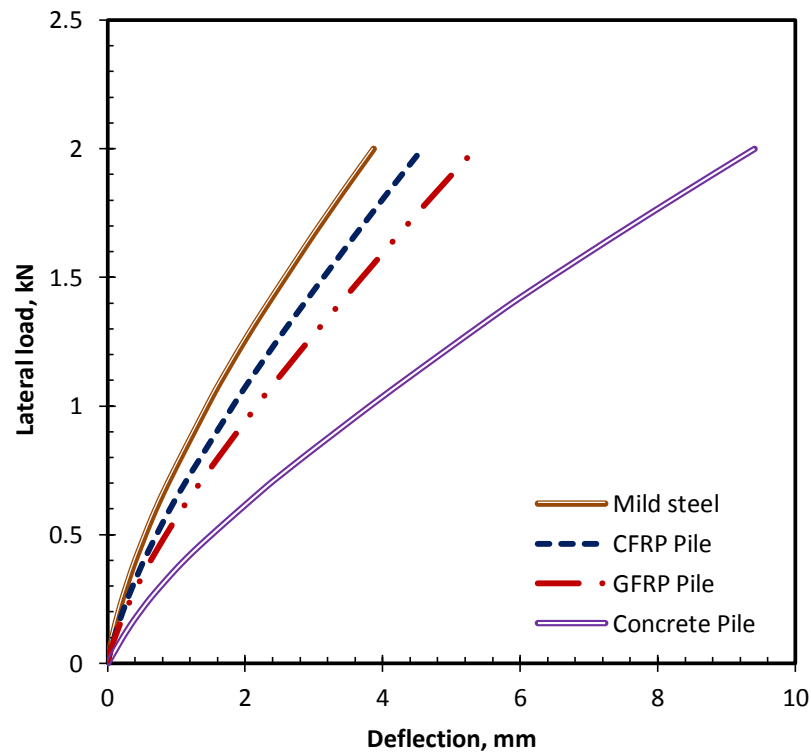


Figure 8.16: Load deflection comparison between FRP and traditional piles

8.14 Summary

ABAQUS program was successfully used to model the results from the FRP pile model tests subjected to the axial and lateral loads. The solid element was used to simulate the model structures (FRP, mortar, and sand). The results from the analyses show the following key findings:

- The shapes of the axial curves from the ABAQUS were in good agreement to that obtained from the experimental.
- The lateral load-deformation response agreed reasonably well between the measured and FEM predicted results.
- Interface friction coefficients between FRP and sand had a significant effect on the behaviour of the FRP pile subjected to axial load.
- Interface friction coefficient has a minor effect on the behaviour of FRP pile subjected to the lateral load.
- FRP laminate and configuration, vertical pressure, and sand Young's modulus have a significant effect on the FRP pile response subjected to the lateral load.
- It was found that the deflection response of the mild steel and FRP piles are considerably lower than concrete pile.

CHAPTER NINE: SUMMARY AND CONCLUSIONS

9.1 Introduction

Traditional piles are generally made of steel, concrete, and timber materials. These pile materials have limited service life and high maintenance costs when used in aggressive environments. In the construction industry, an alternative material is needed to eliminate some problems associated with the use of traditional materials due to the change of environmental and social requirements. Nowadays, one of the more common composite material systems that has found widespread application in structural and geotechnical engineering projects is those involving FRP composite tubes confined concrete. FRP composite materials such as CFRP and GFRP composite have become attractive alternative materials in many construction industries. These materials has superior corrosion resistance, limited service life and high maintenance costs when used in aggressive environments [(Lampo et al., 1998), (Pando et al., 2003) and (Park et al., 2010)].

The performance of FRP composite systems during their service lifetime in terms of structural and geotechnical properties is of major importance in selection of FRP composite materials for certain deep foundation applications. As discussed earlier, few studies have investigated the structural and geotechnical behaviour on FRP tube confined concrete. Furthermore, the possible degradation of FRP under different aging environments should be assessed especially in terms of geotechnical engineering such as interface shear behaviour. To the authors' knowledge, this subject is not yet covered in the existing literature of FRP-geotechnology.

However, in order to confidently confirm the applicability of using FRP composite materials for piling foundation systems, more experimental and numerical data are presented in important issues of structural and geotechnical behaviour in short and long-term conditions. The overall objective of this research project was to establish the potential of using composite materials in pile substructures. The objective outlines summaries of this research are described in Table 9.1.

Table 9.1: Research objectives and outlines

No.	Objective	Evidence of objective completion
1-	<ul style="list-style-type: none"> ➤ The performance of the FRP-tube confined concrete under compression load was evaluated. ➤ Evaluation of the stress-strain response of two FRP tubes (CFRP and GFRP) confined with different concrete batches. ➤ The experimental results and extensive database from previous literatures were assembled. A new topographic chart to predict the enhancement strength based on concrete strength and FRP confinement pressure. ➤ Evaluation experimentally the influence of ageing environment on FRP tube subjected to the flexural load. 	<ul style="list-style-type: none"> ➤ An experimental program including a total of 32 cylindrical specimens, 24 of which were FRP-tube filled to concrete and the remaining 8 were unconfined (control) specimens. The specimens were tested using compression loading conditions. ➤ The results of 138 specimens conducted by 17 different researchers and 24 specimens from the current study are collected in addition to the present study to predict the strength enhancement for FRP confined concrete considering different concrete grades and different confining pressure. ➤ An experimental program was also conducted in this study to assess the effect of different ageing environment conditions on FRP specimen under flexural load.
2-	<ul style="list-style-type: none"> ➤ Evaluation of the interface friction behaviour between two FRP's (CFRP and GFRP) against granular materials. ➤ Evaluation the change in surface roughness and interface shear coefficient of two different FRP counterface surfaces that sheared against two different types of sand under increased normal stress levels. 	<ul style="list-style-type: none"> ➤ An extensive laboratory study was undertaken in an effort to investigate the interface shear behaviour between two FRP materials against different granular materials (four British sand and three glass beads). ➤ Laboratory tests were conducted in this study quantify the interface shear induced surface roughness changes under increased normal stress levels for FRP materials.

No.	Objective	Evidence of objective completion
3-	<ul style="list-style-type: none"> ➤ Evaluation the ageing induced changes in (FRP)/Granular interface shear behaviour under different aging environments. The experimental program involves assessing the ageing effect on the testing FRP materials in terms of the changes in their hardness and surface roughness properties. 	<ul style="list-style-type: none"> ➤ The testing program involves immersing the GFRP and CFRP testing sheets in two different aqueous solutions; NaOH (pH=12), and HCl (pH=2) which represent acidic and alkaline soil environments, respectively, for 24 weeks.
4-	<ul style="list-style-type: none"> ➤ The constitutive interface shear surface (CISS) in the three dimensional domain of surface roughness, surface hardness, and interface shear coefficient. 	<ul style="list-style-type: none"> ➤ The testing program was designed to characterize the geometric features of the constitutive interface shear surface (CISS) within HV-R_n-μ domain. For this purpose, the testing granular and counterface continuum materials in this study were selected to measure the evolution of μ as R_n changes at different six HV values.
5-	<ul style="list-style-type: none"> ➤ Evaluation of the response of FRP piles under axial and lateral loading. The piles behaviour under axial and lateral loading condition was explored in terms of different parameter such as: FRP pile surface, FRP configuration, sand density and sand pressure. 	<ul style="list-style-type: none"> ➤ Small-scale FRP system was tested under axial and lateral loads using soil chamber facility.
6-	<ul style="list-style-type: none"> ➤ FEM model to be developed to validate the experimental model piles. An additional analysis to be examined a few important parameters such as FRP tube configuration, interface friction coefficients and confining pressure. 	<p>Numerical study was presented using the ABAQUS FEM package (6.11).</p>

9.2 Activities Summary and Conclusions

The following sections provide a summary as well as conclusions of the findings from this research.

9.2.1 Literature Review

The research literature review provided an overview of two different FRP composite materials which used as piling foundation system. The gap knowledge has been identified in the literature which urgently needs more studies and information to develop piles structure using FRP composite materials.

9.2.2 Structural Behaviour of FRP-Tubes Confined Concrete Study

The following conclusions of this research study are drawn as a result of axial and flexural experimental testing:

1. Strength enhancements of FRP-tubes filled to concrete tend to decrease with an increase of the unconfined concrete strength.
2. The stress-strain responses in the axial and lateral directions of FRP-tubes filled to concrete are bilinear. The first slope of the response depends basically on the concrete core, while the second slope depends mainly on the hoop stiffness of the FRP tube.
3. The failure modes of FRP specimens were characterized mainly by FRP tubes rupture in the longitudinal direction.
4. Based on the experimental and previous literature database, a new topographic chart was proposed to predict the enhancement strength based on concrete strength and FRP confinement pressure.

5. For the flexural behaviour, CFRP tubes achieved higher strength than GFRP tube due to the high tensile strength and modulus in the axial direction.
6. The effect of the aggressive solution on flexural strength was much more pronounced in pH=12 than that pH=2.

9.2.3 Interface Characteristics of FRP/granular Materials Study

From the results of the interface friction laboratory study, the following conclusions and observations can be drawn:

1. Interface friction tests showed that the interface behaviour between FRP materials and sand depended on the FRP surface roughness, mean particle and relative density.
2. The peak interface friction coefficient values obtained for the sand and glass beads tested against the GFRP and CFRP composite were higher than the values obtained for the mild steel.
3. The test results indicated that quantifiable surface roughness and interface resistance changes could be induced by the interface shearing process under increased normal stress levels. Finally, a conceptual explanation is provided in this study to interpret the observed behaviour.

9.2.4 Long-Term Interface between FRP/granular Materials Study

From the results of the long-term interface laboratory study, the following conclusions and observations can be drawn:

1. Both aggressive solutions were caused the degradation of composite resins surface leading to increase the surface roughness.

2. The peak interface friction coefficient was increased with the acceleration of temperature at the same aggressive solution.
3. The interface results of this study indicated that although aging under the adopted environments in this study could have detrimental effects on the structural mechanical properties of FRP, it improves the FRP interface shear property as it is a matrix-dominated property.

9.2.5 Effect of Surface Roughness and Hardness on the Interface Shear Strength

Based on the conducted experimental program in this study, the following conclusions and observations were made:

- 1- A CISS was proposed which introduces a new understanding for the effect of HV and R_n on μ .
- 2- The results of this study were exploited to define schematically the constitutive interface shear surface (CISS) in the three dimensional domain of surface roughness, surface hardness, and interface shear coefficient.
- 3- The proposed CISS in this study provides a robust mean to: (i) understand the coupling effect of continuum surface roughness and hardness on the interface shear behaviour, (ii) interpret the observed different results in the literature.

9.2.6 Performance of FRP Piles under Different Loading

Based on the experimental testing and analysis the following conclusions and observations were made:

1. Both FRP composites exhibited relatively higher bearing capacity compared to mild steel in terms of coefficient interface.

2. Axial load tests showed that the behaviour of model pile depended on the FRP pile surface roughness, and confined pressure.
 - The axial loading rate has insignificant effect on the behaviour of pile subjected to the axial load. On the other hand, the confined pressure had more significant effect.
 - The CFRP pile has greater lateral load carrying capacity and remarkably lower deflection due to high stiffness moduli compared to GFRP pile.
 - The accelerated GFRP pile which immersed in alkaline solution was failed rapidly under lateral load compared to CFRP.

9.2.7 Simulation FRP Piles Using ABAQUS Package

Based on the FEM numerical results the following conclusions can be drawn:

1. The interface friction between FRP pile and soil was more significant on the FRP pile during axial loading test.
2. The vertical pressure was affected on the FRP pile response during axial and lateral static tests.
3. Vertical pressure, sand dilation angle and sand Young's modulus had a significant effect on the FRP pile response.
4. The mild steel and FRP piles have greater load carrying capacity and remarkably lower displacement compared to concrete piles.

9.3 Conclusions and Final Remarks

Pile foundation has historically involved the use of traditional materials such as concrete, steel and timber. However, these materials suffer from strength degradation and their repair cost is significant, especially if they install in harsh marine/aggressive environments. A relatively new trend in the piling industry is to use FRP composites as substitute materials. The current study was undertaken to investigate the structural and geotechnical behaviour of FRP composite piles.

As regards in the structural study in this project, the experimental program has been conducted to evaluate the axial strength enhancement of FRP tubes confined concrete. Despite a large amount of previous research effort, a proper model to predict the axial strength enhancement of FRP tubes confined concrete has not yet been established. Most of the previous models are empirical in nature and have been calibrated against their own sets of experimental results to predict the axial strength enhancement of the FRP tubes confined to concrete. The experimental results of the present study are combined with other results reported in the previous literature on the behaviour of FRP tubes confined concrete subjected to the axial compression load. From these, a new design chart is proposed to predict the strength enhancement based on the concrete strength and FRP lateral confinement.

As regards in the geotechnical study, extensive research programs have been conducted to investigate the engineering performance of the FRP piles as interface friction and load bearing applications. The small number of previous studies on the FRP composites as piling materials gave some indications which encouraged the author to proceed with further study in that field. The geotechnical study investigation was subdivided into four main pillars:

- The interface friction study was conducted between FRP and particulate materials. The interface tests were carried out using a modified direct shear box. The tests were conducted using different particulate material (i.e. sand and glass beads) with two FRP composite materials (i.e. GFRP and CFRP).

Several factors including polymeric material physical/mechanical properties (e.g. Surface roughness and hardness), granular soil particle shape (i.e. angularity /roundness), density, and normal stress levels were examined and discussed in this study.

- Long-term interface friction under different aggressive environments was investigated. To the author knowledge, there is no evidence in the existing literature of FRP/soil of this subject having been studied. Therefore, the interface tests were conducted using an aged FRP material to evaluate the effect of aggressive environments on the FRP/ particulate interface shear behaviour.
- The effect of FRP hardness and roughness of a continuum surface on its interface shear behaviour against granular material was also investigated. This study was exploited to define schematically the constitutive interface shear surface (CISS) in the three dimensional domain of surface roughness, surface hardness, and interface shear coefficient. The proposed CISS in this study provides a robust means to understand the coupling effect of continuum surface roughness and hardness on the interface shear behaviour. These studies will guide the geotechnical practitioner's and academic researchers to understand the behaviour of FRP pile/soil during the interaction load process.
- Small scale laboratory pile loading tests were carried out to assess the FRP pile behaviour under axial and lateral loads. The laboratory test results were used to verify/validate a numerical model developed by the commercial finite element package ABAQUS (6.11). The obtained results was gathered, analyzed, and disseminated to help contribute to the current state of knowledge of the behaviour of new FRP composite piles.

In view of the limited extent of the previous studies in this field, the current study could be considered a good attempt to better understand the structural and geotechnical behaviour of FRP composites in piling foundations.

9.4 Recommendations for Future Works

Based on the findings from this investigation, there are a number of areas where are not carried in this research that permit future work to be carried out. The following subsections are recommended for future work on FRP composite piles:

9.4.1 Experimental Study

1. Only small numbers of tests are available for FRP-tubes confined concrete with different laminate configuration. However, more tests are needed to enlarge this database.
2. Additional FRP pile/soil models are recommended to extend the conclusions of this study to other FRP composite piles with different soil types.
3. Full-scale field load test programs are recommended using different FRP pile with different soil. It would be useful to extend the present investigation to a large scale field study in the UK.
4. The response of FRP piles to extreme loading conditions such as impact load and seismic should be evaluated.
5. The response of FRP pile under soil movement should be evaluated.

9.4.2 Numerical Study

1. Assess the FRP pile response and damage after driving and impact loads.
2. The study of FRP pile group is recommended.
3. The modelling of FRP pile in different type of soil is recommended.

4. The driving mechanism should be modelled to evaluate the FRP pile during installation.
5. Modelling the influence of axial loads on the lateral response of the FRP pile is recommended.

REFERENCES

1. Abbas, J. M. et al. (2008). Single pile simulation and analysis subjected to lateral load. *Electronic Journal of Geotechnical Engineering*, **13**, 1-15.
2. Al-Defae, A. et al. (2013). Aftershocks and the whole-life seismic performance of granular slopes.
3. Alampalli, S. et al. (1999). FRPs for bridge construction and rehabilitation in New York. *Materials and construction: Exploring the connection*, ASCE, Reston, VA, 345-350.
4. Alavdeen, A. et al. (2006). A Textbook of Engineering Materials and Metallurgy, Firewall Media.
5. Amini, F. and Chakravrtty, A. (2004). Liquefaction testing of layered sand-gravel composites. *ASTM geotechnical testing journal*, **27**(1), 36-46.
6. ASTM D2240-05 (2005). ASTM D2240 - 05(2010) Standard Test Method for Rubber Property—Durometer
7. Aysen, A. (2005). Soil mechanics: Basic concepts and engineering applications, Taylor & Francis.
8. Bandyopadhyay, A. and Odegard, G. (2012). Molecular modeling of crosslink distribution in epoxy polymers. *Modelling and Simulation in Materials Science and Engineering*, **20**(4), 045018.
9. Barney, D. K. (2004). Identification mapping and evaluation of timber bridges in the Wide Bay District.
10. Basu, D. et al. (2008). Analysis of Laterally Loaded Piles in Multilayered Soil Deposits. *Joint Transportation Research Program*, 330.
11. Bernard Potyrala, P. (2011). Use of fibre reinforced polymer composites in bridge construction. State of the art in hybrid and all-composite structures.
12. Berthet, J. et al. (2005). Compressive behavior of concrete externally confined by composite jackets. Part A: experimental study. *Construction and Building Materials*, **19**(3), 223-232.
13. Bing-can, H. et al. (2010). Nonlinear FEM analysis of bearing capacity and sedimentation of single pile in multi-layered soils. *Proc., Computing in Civil Engineering and Building Engineering*.

14. Bisby, L. A. (2006). Durability of FRP composites for construction, ISIS Educational Module No. 8.
15. Bolton, M. (1986). Strength and dilatancy of sands. *Geotechnique*, **36**(1), 65-78.
16. Bowden, F. and Tabor, D. (1966). Friction, lubrication and wear: a survey of work during the last decade. *British Journal of Applied Physics*, **17**(12), 1521.
17. Bowden, F. and Tabor, D. (1954). Mechanism of friction and lubrication in metal-working. *J Inst. Petroleum*, **40**, 243-253.
18. Broms, B. B. (1964). Lateral resistance of piles in cohesionless soils. *Journal of the Soil Mechanics and Foundation Division*, **90**(SM3), 123-158.
19. Brumund, W. and Leonards, G. (1973). Experimental study of static and dynamic friction between sand and typical construction materials. *Journal of Testing and Evaluation*, **1**(2), 162-165.
20. Caceres, P. G. (2002). Effect of microstructure on the abrasive wear properties of infiltrated tungsten alloys. *Materials characterization*, **49**(1), 1-9.
21. Cairns, S. W. (2001). Circular concrete columns externally reinforced with pre-fabricated carbon polymer shells.
22. Chae, K. et al. (2004). Lateral resistance of short single piles and pile groups located near slopes. *International Journal of Geomechanics*, **4**(2), 93-103.
23. Chen, W.-F. and Saleeb, A. F. (1982). Constitutive equations for engineering materials, Wiley New York.
24. Childs, T. (1992). Deformation and flow of metals in sliding friction. *Fundamentals of Friction: Macroscopic and Microscopic Processes*, Springer, 209-225.
25. Daniel, I. M. and Ishai, O. (1994). Engineering mechanics of composite materials. *New York, USA*.
26. Dayal, U. and Allen, J. H. (1975). The effect of penetration rate on the strength of remolded clay and sand samples. *Canadian Geotechnical Journal*, **12**(3), 336-348.

27. De'Nève, B. and Shanahan, M. (1993). Water absorption by an epoxy resin and its effect on the mechanical properties and infra-red spectra. *Polymer*, **34**(24), 5099-5105.
28. De Nicola, A. and Randolph, M. (1999). Centrifuge modelling of pipe piles in sand under axial loads. *Geotechnique*, **49**(3), 295-318.
29. DeJong, J. T. and Westgate, Z. J. (2009). Role of Initial State, Material Properties, and Confinement Condition on Local and Global Soil-Structure Interface Behavior. *Journal of geotechnical and geoenvironmental engineering*, **135**(11), 1646-1660.
30. Demers, M. and Neale, K. (1999). Confinement of reinforced concrete columns with fibre-reinforced composite sheets-an experimental study. *Canadian Journal of Civil Engineering*, **26**(2), 226-241.
31. Desai, C. et al. (1985). Cyclic testing and modeling of interfaces. *Journal of geotechnical engineering*, **111**, 793.
32. Diamant, Y. et al. (1981). The effect of network structure on moisture absorption of epoxy resins. *Journal of applied polymer science*, **26**(9), 3015-3025.
33. Dijkstra, J. (2004). Influence of loading rate on pile capacity in unsaturated sand. Master's thesis, Faculty of Civil Engineering and Geosciences, TU Delft.
34. Dove, J. et al. (2006). Particle-scale surface interactions of non-dilative interface systems. *Geotextiles and Geomembranes*, **24**(3), 156-168.
35. Dove, J. and Frost, J. (1996). A method for measuring geomembrane surface roughness. *Geosynthetics International*, **3**, 369-392.
36. Dove, J. et al. (1996). Geomembrane Microtopography by Atomic Force Microscopy. *Geosynthetics International*, **3**, 227-245.
37. Dove, J. E. and Frost, J. D. (1999). Peak friction behavior of smooth geomembrane-particle interfaces. *Journal of geotechnical and geoenvironmental engineering*, **125**(7), 544-555.
38. El Naggar, M. H. and Sakr, M. (2000). Evaluation of axial performance of tapered piles from centrifuge tests. *Canadian Geotechnical Journal*, **37**(6), 1295-1308.

39. El Naggar, M. H. and Wei, J. Q. (1999). Response of tapered piles subjected to lateral loading. *Canadian Geotechnical Journal*, **36**(1), 52-71.
40. Fakirov, S. and Bhattacharyya, D. (2007). Handbook of engineering biopolymers: homopolymers, blends and composites, Hanser Gardner Pubns.
41. Fam, A. et al. (2003). Precast piles for Route 40 bridge in Virginia using concrete filled FRP tubes. *PCI journal*, **48**(3), 32-45.
42. Fam, A. and Rizkalla, S. (2001). Confinement model for axially loaded concrete confined by circular fiber-reinforced polymer tubes. *ACI Structural Journal*, **98**(4).
43. Fam, A. and Rizkalla, S. (2003). Large scale testing and analysis of hybrid concrete/composite tubes for circular beam-column applications. *Construction and Building Materials*, **17**(6), 507-516.
44. Fam, A. Z. and Rizkalla, S. H. (2002). Flexural behavior of concrete-filled fiber-reinforced polymer circular tubes. *Journal of Composites for Construction*, **6**(2), 123-132.
45. Fardis, M. N. and Khalili, H. Concrete encased in fiberglass-reinforced plastic. ACI.
46. Feng, S. L. et al. (2012). Finite Element Analysis of the Vertical Bearing Capacity of Single Piles in Tianjin Soft Soil Areas. *Advanced Materials Research*, **446**, 1387-1390.
47. Fleming, K. and Elson, K. (2008). Piling engineering, Taylor & Francis Group.
48. Fleming, K. et al. (2008). Piling engineering, Taylor & Francis Group.
49. Flores, S. E. et al. (2008). Scratching of elastic/plastic materials with hard spherical indenters. *Journal of Applied Mechanics*, **75**(6), 1021.
50. Frost, J. et al. (2002). Shear failure behavior of granular–continuum interfaces. *Engineering Fracture Mechanics*, **69**(17), 2029-2048.
51. Frost, J. and Han, J. (1999). Behavior of interfaces between fiber-reinforced polymers and sands. *Journal of geotechnical and geoenvironmental engineering*, **125**(8), 633-640.
52. Frost, J. and Han, J. (1999). Behavior of interfaces between fiber-reinforced polymers and sands. *Journal of geotechnical and geoenvironmental engineering*, **125**, 633.

53. Frost, J. et al. The evolution of sand structure adjacent to geomembranes. *Proc., Proceedings of Geosynthetics*, 559-573.
54. Fuggle, A. R. et al. Quantification of Shear-Induced Wear on Curved Surfaces. *Proc., GeoCongress 2006@ sGeotechnical Engineering in the Information Technology Age*, ASCE, 1-6.
55. Gadelmawla, E. et al. (2002). Roughness parameters. *Journal of Materials Processing Technology*, **123**(1), 133-145.
56. GangaRao, H. and Vijay, P. (2010). Feasibility Review Of Frp Materials For Structural Applications. *Report Submitted to (CEERD-CT-T)-US Army Corps of Engineers*.
57. Gee, M. (2001). Low load multiple scratch tests of ceramics and hard metals. *Wear*, **250**(1), 264-281.
58. Gindy, M. et al. (2005). Integrity Assessment of Composite and Timber Piles in the Marine Environment Using Nondestructive Testing.
59. Goh, A. et al. (1997). Analysis of piles subjected to embankment induced lateral soil movements. *Journal of geotechnical and geoenvironmental engineering*, **123**(9), 792-801.
60. Guades, E. et al. Driveability of composite piles. *Proc., Proceedings of the First International Postgraduate Conference on Engineering, Designing and Developing the Built Environment for Sustainable Wellbeing (eddBE2011)*, Queensland University of Technology, Faculty of Built Environment and Engineering, 237-242.
61. Gupta, V. et al. (1985). The temperature-dependence of some mechanical properties of a cured epoxy resin system. *Polymer Engineering & Science*, **25**(13), 812-823.
62. Han, J. (1997). An experimental and analytical study of the behavior of fiber-reinforced polymer piles and pile-sand interactions. *Dissertation Abstracts International Part B: Science and Engineering*, **58**(3), 1420.
63. Han, J. and Frost, J. D. (1999). Buckling of vertically loaded fiber-reinforced polymer piles. *Journal of reinforced plastics and composites*, **18**(4), 290-318.
64. Han, J. et al. (2003). Design of fiber-reinforced polymer composite piles under vertical and lateral loads. *Transportation Research Record: Journal of the Transportation Research Board*, **1849**(1), 71-80.

65. Hanna, S. (2002). ENGINEERING PERFORMANCE OF FRP COMPOSITE PILING.
66. Harris, B. (1986). Engineering composite materials, Institute of Metals UK.
67. Horeczko, G. Marine application of recycled plastics. *Proc., Restructuring@ sAmerica and Beyond*, ASCE, 834-837.
68. Horvath, R. G. (1995). Influence of loading rate on the capacity of a model pile in clay. *Canadian Geotechnical Journal*, **32**(2), 364-368.
69. Howie, I. and Karbhari, V. Effect of materials architecture on strengthening efficiency of composite wraps for deteriorating columns in the North-East. *Proc., Infrastructure@ sNew Materials and Methods of Repair*, ASCE, 199-206.
70. Hsueh, C. K. et al. (2004). Lateral performance of drilled shaft considering nonlinear soil and structure material behavior. *Journal of Marine Science and Technology*, **12**(1), 62-70.
71. Iskander, M. et al. (2001). Driveability of FRP composite piling. *Journal of Geotechnical and Geoenvironmental Engineering*, **127**(2), 169-176.
72. Iskander, M. and Hassan, M. (1998). State of the practice review in FRP composite piling. *Journal of Composites for Construction*, **2**, 116.
73. Iskander, M. G. and Hassan, M. (2001). Accelerated degradation of recycled plastic piling in aggressive soils. *Journal of Composites for Construction*, **5**(3), 179-187.
74. ISO-Standards (1997). ISO 4287 Geometrical Product Specifications (GPS)-Surface texture: Profile method-Terms, definitions and surface texture parameters. *Geneve: International Organization for Standardization*, 1-25.
75. Jaffry, S. A. D. (2001). Concrete filled glass fibre reinforced polymer (GFRP) shells under concentric compression.
76. Juran, I. (2001). Durability of Recycled Plastic Piles in Aggressive Soils.
77. Kajorncheappunngam, S. et al. (2002). Effect of aging environment on degradation of glass-reinforced epoxy. *Journal of Composites for Construction*, **6**(1), 61-69.
78. Karbhari, V. and Gao, Y. (1997). Composite jacketed concrete under uniaxial compression-verification of simple design equations. *Journal of Materials in Civil Engineering*, **9**(4), 185-193.

79. Katsuki, F. 11 PREDICTION OF DETERIORATION OF FRP RODS DUE TO ALKALI ATTACK. *Proc., Non-Metallic (FRP) Reinforcement for Concrete Structures: Proceedings of the Second International RILEM Symposium*, Taylor & Francis, 82.
80. Kaw, A. K. (2006). *Mechanics of composite materials*, CRC press.
81. Keller, T. (2003). Use of fibre reinforced polymers in bridge construction, Iabse.
82. Khodair, Y. A. and Hassiotis, S. (2005). Analysis of soil–pile interaction in integral abutment. *Computers and Geotechnics*, **32**(3), 201-209.
83. Kishida, H. and Uesugi, M. (1987). Tests of the interface between sand and steel in the simple shear apparatus. *Geotechnique*, **37**(1), 45-52.
84. Lam, L. and Teng, J. (2003). Design-oriented stress–strain model for FRP-confined concrete. *Construction and Building Materials*, **17**(6), 471-489.
85. Lam, L. and Teng, J. (2004). Ultimate condition of fiber reinforced polymer-confined concrete. *Journal of Composites for Construction*, **8**(6), 539-548.
86. Lam, L. et al. (2006). FRP-confined concrete under axial cyclic compression. *Cement and Concrete Composites*, **28**(10), 949-958.
87. Lampo, R. et al. (1998). Development and Demonstration of FRP Composite Fender, Loadbearing, and Sheet Piling Systems. *Soils and foundations*, Champaign, III, US Army Corps of Engineers Construction Engineering Research Laboratories, .
88. Lee, M. C. and Peppas, N. A. (1993). Water transport in graphite/epoxy composites. *Journal of applied polymer science*, **47**(8), 1349-1359.
89. Lehane, B. et al. (1993). Mechanisms of shaft friction in sand from instrumented pile tests. *Journal of geotechnical engineering*, **119**(1), 19-35.
90. Lemos, L. J. L. (1986). The effect of rate on residual strength of soil, University of London.
91. Li, G. (2006). Experimental study of FRP confined concrete cylinders. *Engineering structures*, **28**(7), 1001-1008.
92. Lopez-Anido, R. A. et al. (2000). Emerging materials for civil infrastructure: state of the art, Amer Society of Civil Engineers.
93. Mahmoud, M. and Burley, E. (1994). Lateral load capacity of single piles in sand. *Proceedings of the ICE-Geotechnical Engineering*, **107**(3), 155-162.

94. Meyerhof, G. (1995). Behaviour of pile foundations under special loading conditions: 1994 RM Hardy keynote address. *Canadian Geotechnical Journal*, **32**(2), 204-222.
95. Meyerhof, G. et al. (1988). Lateral resistance and deflection of flexible piles. *Canadian Geotechnical Journal*, **25**(3), 511-522.
96. Mirmiran, A. (1997). Behavior of concrete columns confined by fiber composites. *Journal of Structural Engineering*, **123**, 583.
97. Mirmiran, A. and Shahawy, M. (2003). Composite pile: A successful drive. *Concrete international*, **25**(3), 89-94.
98. Mirmiran, A. and Shahawy, M. (1996). A new concrete-filled hollow FRP composite column. *Composites Part B: Engineering*, **27**(3), 263-268.
99. Mirmiran, A. et al. (1998). Effect of column parameters on FRP-confined concrete. *Journal of Composites for Construction*, **2**(4), 175-185.
100. Miyauchi, K. et al. (1997). Estimation of strengthening effects with carbon fiber sheet for concrete column. *Non-Metallic (FRP) Reinforcement for Concrete Structures*, **1**, 217-224.
101. Mohamed, H. M. and Masmoudi, R. (2012). Effect of test parameters on flexural strength of circular fiber-reinforced polymer-confined concrete beams. *Journal of reinforced plastics and composites*, **31**(13), 897-914.
102. Moore, D. F. (1972). *The friction and lubrication of elastomers*, Pergamon Press Oxford, etc., 288p.
103. Murphy, K. et al. (1999). Effect of concrete based alkaline solutions on short term response of composites. *Society for the Advancement of Material and Process Engineering, Evolving and Revolutionary Technologies for the New Millenium*, **44**, 2222-2230.
104. Nanni, A. and Bradford, N. M. (1995). FRP jacketed concrete under uniaxial compression. *Construction and Building Materials*, **9**(2), 115-124.
105. O'rouke, T. et al. (1990). Shear strength characteristics of sand-polymer interfaces. *Journal of geotechnical engineering*, **116**(3), 451-469.
106. O'Rourke, T. et al. (1990). Shear strength characteristics of sand-polymer interfaces. *Journal of geotechnical engineering*, **116**(3), 451-469.

107. Oda, M. et al. (1982). Experimental micromechanical evaluation of strength of granular materials: effects of particle rolling. *Mechanics of materials*, **1**(4), 269-283.
108. Paikowsky, S. et al. (1995). A dual interface apparatus for testing unrestricted friction of soil along solid surfaces. *ASTM geotechnical testing journal*, **18**(2), 168-193.
109. Pan, W. D. et al. (2011). Finite Element Analysis about the Properties of CFG-Pile Composite Foundation Based on Parametric Language PYTHON. *Advanced Materials Research*, **320**, 20-25.
110. Pando, M. et al. (2003). Axial and lateral load performance of two composite piles and one prestressed concrete pile. *Transportation Research Record: Journal of the Transportation Research Board*, **1849**(-1), 61-70.
111. Pando, M. et al. Performance of a composite pile in a full scale Statnamic load testing program. 909-916.
112. Pando, M. A. et al. (2006). A laboratory and field study of composite piles for bridge substructures.
113. Pando, M. A. et al. Interface shear tests on FRP composite piles. ASCE.
114. Pando, M. A. et al. Durability of concrete-filled tubular FRP piles. *Proc., The 3rd Int. Conf. on Composites in Infrastructure, ICCI*, 10-12.
115. Park, J. S. et al. An Experimental Investigation on the Structural Behavior of FRP-Concrete Composite Compression Members. *Proc., Materials Science Forum*, Trans Tech Publ, 2644-2647.
116. Parkin, A. and Lunne, T. (1982). Boundary effects in the laboratory calibration of a cone penetrometer for sand. *Norwegian Geotechnical Institute Publication*(138).
117. Perrin, F. et al. (2009). Water transport in epoxy-aliphatic amine networks—Influence of curing cycles. *European Polymer Journal*, **45**(5), 1524-1534.
118. Potyondy, J. (1961). Skin friction between various soils and construction materials. *Geotechnique*, **11**(4), 339-353.
119. Purba, B. K. and Mufti, A. A. (1999). Investigation of the behavior of circular concrete columns reinforced with carbon fiber reinforced polymer (CFRP) jackets. *Canadian Journal of Civil Engineering*, **26**(5), 590-596.

120. Reddy, J. N. (2004). *Mechanics of laminated composite plates and shells: theory and analysis*, CRC.
121. Renard, F. et al. (2012). Surface roughness evolution on experimentally simulated faults. *Journal of Structural Geology*.
122. Richart, F. et al. (1929). The failure of plain and spirally reinforced concrete in compression. *Bulletin*, **190**.
123. Riebel, F. and Keller, T. (2007). Long-term compression performance of a pultruded GFRP element exposed to concrete pore water solution. *Journal of Composites for Construction*, **11**(4), 437-447.
124. Rowe, P. W. (1961). The stress-dilatancy relation for static equilibrium of an assembly of particles in contact. *Proceedings of the Royal Society of London. Series A. Mathematical and Physical Sciences*, **269**(1339), 500.
125. Rowe, P. W. (1962). The stress-dilatancy relation for static equilibrium of an assembly of particles in contact. *Proceedings of the Royal Society of London. Series A. Mathematical and Physical Sciences*, **269**(1339), 500.
126. Saadatmanesh, H. et al. (1994). Strength and ductility of concrete columns externally reinforced with fiber composite straps. *ACI Structural Journal*, **91**(4), 434-447.
127. Saafi, M. et al. (1999). Behavior of concrete columns confined with fiber reinforced polymer tubes. *ACI Materials Journal*, **96**(4), 500-509.
128. Sakr, M. et al. (2005). Interface Characteristics and Laboratory Constructability Tests of Novel Fiber-Reinforced Polymer/Concrete Piles. *Journal of Composites for Construction*, **9**(3), 274-283.
129. Salini, U. and Girish, M. (2009). Lateral Load Capacity of Model Piles on Cohesionless Soil. *The Electronic Journal of e-Government*.
130. Sam, H. (2007). *Applied Soil Mechanics with ABAQUS Applications* [Book].-[sl]. John Wiley & Sons, Inc.
131. Samaan, M. and Shahawy, M. (1998). Model of concrete confined by fiber composites. *Journal of Structural Engineering*, **124**, 1025.
132. Scholz, C. and Engelder, J. The role of asperity indentation and ploughing in rock friction—I: Asperity creep and stick-slip. *Proc., International Journal of Rock Mechanics and Mining Sciences & Geomechanics Abstracts*, Elsevier, 149-154.

133. Siddique, R. (2008). Waste materials and by-products in concrete, Springer.
134. Stachowiak, G. and Batchelor, A. (1993). 1993, Engineering tribology, Elsevier.
135. Tabor, D. (1954). Mohs's hardness scale-a physical interpretation. *Proceedings of the Physical Society. Section B*, **67**(3), 249.
136. Taylor, R. B. (1995). New developments in marine fendering. *Dredging & Port Construction*, **22**(3), 4.
137. Teng, J. et al. (2007). Theoretical model for fiber-reinforced polymer-confined concrete. *Journal of Composites for Construction*, **11**, 201.
138. Theriault, M. and Claude, S. (2004). Fiber-reinforced polymer-confined circular concrete columns: investigation of size and slenderness effects. *Journal of Composites for Construction*, **8**(4), 323-331.
139. Thomason, J. (1995). The interface region in glass fibre-reinforced epoxy resin composites: 2. Water absorption, voids and the interface. *Composites*, **26**(7), 477-485.
140. Tomlinson, M. (1994). Pile design and construction practice, Taylor & Francis.
141. Toutanji, H. (1999). Stress-strain characteristics of concrete columns externally confined with advanced fiber composite sheets. *ACI Materials Journal*, **96**(3).
142. Toutanji, H. and Deng, Y. (2002). Strength and durability performance of concrete axially loaded members confined with AFRP composite sheets. *Composites Part B: Engineering*, **33**(4), 255-261.
143. Trochanis, A. M. et al. (1991). Three-dimensional nonlinear study of piles. *Journal of geotechnical engineering*, **117**(3), 429-447.
144. Tuakta, C. (2005). Use of fiber reinforced polymer composite in bridge structures. Massachusetts Institute of Technology.
145. Uesugi, M. and Kishida, H. (1986). Frictional resistance at yield between dry sand and mild steel. *Soils and foundations*, **26**(4), 139-149.
146. Uesugi, M. and Kishida, H. (1986). Influential factors of friction between steel and dry sands. *Soils and foundations*, **26**(2), 33-46.
147. Uesugi, M. et al. (1990). Friction between dry sand and concrete under monotonic and repeated loading. *Soils and foundations*, **30**(1), 115-128.

148. Vaid, Y. et al. (1990). Stress path and steady state. *Canadian Geotechnical Journal*, **27**(1), 1-7.
149. Watanabe, K. et al. (1997). Confinement effect of FRP sheet on strength and ductility of concrete cylinders under uniaxial compression. *Non-Metallic (FRP) Reinforcement for Concrete Structures*, **1**, 233-240.
150. Wei, J. and El Naggar, M. H. (1998). Experimental study of axial behaviour of tapered piles. *Canadian Geotechnical Journal*, **35**(4), 641-654.
151. Whitehouse, D. J. (2010). Handbook of surface and nanometrology, CRC.
152. Wu, S. (2011). Finite Element Analysis and Theoretical Study on FRP Wrap Concrete Cylinders. Master, The University of Manchester.
153. Xiao, Y. and Wu, H. (2000). Compressive behavior of concrete confined by carbon fiber composite jackets. *Journal of Materials in Civil Engineering*, **12**, 139.
154. Xu, J. et al. (2009). Curing Process Simulation of Fiberglass-Reinforced Plastic (FRP) Pipes. *Materials and Manufacturing Processes*, **24**(6), 657-666.
155. Yoshimi, Y. and Kishida, T. (1981). A ring torsion apparatus for evaluating friction between soil and metal surfaces. *ASTM geotechnical testing journal*, **4**(4).
156. Zettler, T. et al. (2000). Shear-induced changes in smooth HDPE geomembrane surface topography. *Geosynthetics International*, **7**(3), 243-267.
157. Zhan, Y.-g. et al. (2012). Numerical Study on Load Capacity Behavior of Tapered Pile Foundations.
158. Zhang, S. et al. (2000). A study on polymer composite strengthening systems for concrete columns. *Applied Composite Materials*, **7**(2), 125-138.
159. Zobel, H. et al. (2005). Kompozyty polimerowe w mostownictwie. *Materiały Budowlane*.

Table A-1: Comparison of peak stress predictions by various models

Model No.	1	2	3	4	5	6	7	8	9
	Fardis and Khalili	Saadatmanesh et al.,	Karbhari and Gao	Mirmiran and Shahawy	Samaan et al.	Saafi et al.	Toutanji	Lam and Teng	Teng et al.
Sum. Error	5.49	8.39	2.07	0.28	3.87	2.82	7.02	3.51	4.00
AE%	22.88	35.00	9.00	1.15	16.14	11.77	29.23	14.62	16.69
SE%	8.00	8.00	4.22	4.37	3.69	4.44	7.28	5.51	6.00

APPENDIX

FRP-Confined Concrete
Specimens Tested by Other Researchers

The following table summarizes the FRP-confined concrete specimens tested by other researchers. The data are presented in the alphabetical order of the researchers' names.

Table A-2 FRP-confined concrete specimens tested by other researchers

Author	f_c	f_l	f'_c	f'_c/f_c
(Berthet et al., 2005)	25	6.6	42.8	1.712
	25	6.6	42.3	1.512
	25	6.6	43.1	1.832
	40.1	11.8	89.6	2.268
	40.1	7.9	66	1.66
	40.1	3.7	51	1.29
	52	8.9	80	1.59
	52	5.8	75	1.45
(Cairns, 2001)	29.8	5	43.9	1.47
	29.8	5	43.4	1.45
	29.8	9.9	59.3	1.98
	29.8	9.9	59.3	1.98
	29.8	9.9	57	1.91
(Demers and Neale, 1999)	32.2	3	32.2	1.02
	32.2	3	32	1.04
	32.2	9.1	48.3	1.50
	32.2	9.1	48.3	1.50
	32.2	4.9	41.1	1.27
	47.3	4.9	48.4	1.11
	47.3	14.8	75.2	1.70
	47.3	14.8	73.4	1.68

(Howie and Karbhari, 1994)	38.6	3.0	45.5	1.18
	38.6	3.0	41.9	1.08
	38.6	3.0	47.2	1.22
	38.6	8.4	56.5	1.46
	38.6	8.4	60.6	1.57
	38.6	8.4	61.9	1.60
	38.6	13.1	80	2.1
	38.6	13.1	76.4	1.98
	38.6	13.1	75.8	1.96
	38.6	21.6	89.5	2.32
	38.6	21.6	89.9	2.33
	38.6	21.6	89	2.31
	38.6	5.4	47.1	1.22
	38.6	5.4	47.7	1.24
	38.6	5.4	50	1.3
	38.6	10.0	68.3	1.77
	38.6	10.0	67.3	1.74
	38.6	10.0	64.7	1.68
	38.6	6.1	52.7	1.36
	38.6	6.1	49.3	1.28
38.6	6.1	52.3	1.36	
(Jaffry, 2001)	29.8	3	34.8	1.16
	29.8	3	32.4	1.08
	29.8	3	37.2	1.24
	29.8	6	44.8	1.50
	29.8	6	49.3	1.65
(Lam et al., 2006)	41.1	8.2	52.6	1.28
	41.1	8.2	57	1.39
	38.9	16.4	76.8	1.97
	38.9	16.4	79.1	2.03
(Lam and Teng, 2004)	35.9	8.2	50.4	1.4
	35.9	16.3	69.9	1.95
	34.3	24.5	90.4	2.62

	38.5	8.1	58.3	1.51
(Mastrapa, 1997)	29.8	4.5	33.7	1.13
	29.8	4.5	35.6	1.19
	31.2	13.5	91	2.07
	31.2	22.5	96.9	2.92
(Mirmiran et al., 1998)	30.4	9.7	53.7	1.74
	30.4	9.7	56.5	1.83
	30.4	16.4	72.9	2.36
	30.4	16.4	65.7	2.13
	30.4	16.4	78.0	2.52
	30.4	10.3	67.1	2.27
	29.6	10.0	55.3	1.87
	29.6	10.0	60.2	2.03
	29.6	16.8	74.6	2.52
	29.6	16.8	93.0	3.14
(Miyachi et al., 1997)	45.2	5.1	59.4	1.31
	45.2	10.2	79.4	1.76
	31.2	5.1	52.4	1.68
	31.2	10.3	67.4	2.16
	31.2	15.3	81.7	2.62
	51.9	7.7	75.2	1.45
	23.6	10.2	36.0	2.15
	33.7	7.7	50.0	2.07
	33.7	15.3	69.0	2.61
	33.7	23.0	88.0	3.26
	26.3	7.7	50.0	1.93
26.3	15.3	79.0	2.7	
(Saafi et al., 1999)	35.0	4.8	55.0	1.57
	35.0	10.2	68.0	1.94
	35.0	16.0	97.0	2.7
	35.0	4.7	52.0	1.51
	35.0	10.6	66.0	1.89
	35.0	17.6	83.0	2.37

(Theriault and Claude, 2004)	36.0	14.4	64.0	1.78
	36.0	25.3	90.0	2.50
	35.0	14.4	66.0	1.89
	39.0	14.4	70.0	1.79
(Teng et al., 2007)	39.6	4.1	41.5	1.04
	39.6	4.1	40.8	1.03
	39.6	8.2	56.6	1.37
	39.6	8.2	56.3	1.42
	39.6	12.3	60.9	1.45
	39.6	12.3	62.2	1.53
(Watanabe et al., 1997)	1.54	30.2	46.6	5.8
	2.80	30.2	87.6	11.4
	3.40	30.2	104.6	22.7
	1.30	30.2	41.7	2.8
	1.80	30.2	56.0	6.5
	2.10	30.2	63.3	6.9
	1.29	30.2	39.0	4.8
	2.27	30.2	68.0	10
	3.05	30.2	92.1	14.8
(Xiao and Wu, 2000)	33.7	7.9	47.9	1.42
	33.7	7.9	49.7	1.47
	33.7	7.9	49.4	1.47
	33.7	15.8	64.6	1.92
	33.7	15.8	75.2	2.23
	33.7	15.8	71.8	2.13
	33.7	23.7	82.9	2.46
	33.7	23.7	86.2	2.56
	33.7	23.7	95.4	2.83
	43.8	7.9	54.7	1.25
	43.8	7.9	52.1	1.19
	43.8	7.9	48.7	1.11
	43.8	15.8	84.0	1.92
	43.8	15.8	79.2	1.81

(Xiao and Wu, 2000)	43.8	15.8	85.0	1.94
	43.8	23.7	96.5	2.2
	43.8	23.7	92.6	2.11
	43.8	23.7	94.0	2.15
	55.2	7.9	57.9	1.05
	55.2	7.9	62.1	1.14
	55.2	7.9	58.1	1.05
	55.2	15.8	74.6	1.35
	55.2	15.8	77.6	1.41
	55.2	15.8	77.0	1.39
	55.2	23.7	106.5	1.93
	55.2	23.7	108.0	1.96
	55.2	23.7	103.0	1.87
	(Zhang et al., 2000)	34.3	12.0	62.1
34.3		12.0	62.5	1.82
34.3		5.4	44.2	1.29
34.3		6.1	47.5	1.38
34.3		9.9	62.0	1.73